UNIVERSITY OF CALIFORNIA, SAN DIEGO

A Proposed Mechanism for Control of Capillary Network Perfusion: the Role of Endothelial Mechanotransduction Through Nitric Oxide Signaling and the Glycocalyx

A dissertation submitted in partial satisfaction of the
requirements for the degree
Doctor of Philosophy
in
Bioengineering

by

Nicholas Michael Scheidler

Committee in charge:

Professor Geert W. Schmid-Schönbein, Chair
Professor Shu Chien
Professor Alan Hargens
Professor Marcos Intaglietta
Professor Peter Wagner

2007

The dissertation of Nicholas Michael Scheidler is approved, and it is acceptable in quality and form for publication on microfilm:

_____

_____

_____

_____

_____

Chair

University of California, San Diego

2007

DEDICATION

To my parents, the original inspiration

and

my dearest Giovanna, the most recent one

that I might make them proud...

EPIGRAPH

IT is the great prerogative of Mankind above other Creatures, that we are not only able to behold the works of Nature, or barely to sustein our lives by them, but we have also the power of considering, comparing, altering, assisting, and improving them to various uses. And as this is the peculiar priviledge of humane Nature in general, so is it capable of being so far advanced by the helps of Art, and Experience, as to make some Men excel others in their Observations, and Deductions, almost as much as they do Beasts. By the addition of such artificial Instruments and methods, there may be, in some manner, a reparation made for the mischiefs, and imperfection, mankind has drawn upon it self, by negligence, and intemperance, and a wilful and superstitious deserting the Prescripts and Rules of Nature, whereby every man, both from a deriv'd corruption, innate and born with him, and from his breeding and converse with men, Is very subject to slip into all sorts of errors.

The only way which now remains for us to recover some degree of those former perfections, seems to be, by rectifying the operations of the Sense, the Memory, and Reason, since upon the evidence, the strength, the integrity, and the right correspondence of all these, all the light, by which our actions are to be guided, is to be renewed, and all our command over things is to be establisht.

Robert Hooke, excerpt from Preface to Micrographia, 1665

TABLE OF CONTENTS

LIST OF FIGURES

LIST OF TABLES

ACKNOWLEDGMENTS

I would like to first acknowledge the support of my advisor, Dr. Schmid-Schönbein, without whom I would not have the project, the funding, or the inspiration to study microvascular phenomena. His patronage has been requisite; and his knowledge exemplary. My only regret is that I did not learn more than a small fraction of what he could have taught me. The studies that he has directed will result in three publications, listed below with full acknowledgments:

- The work described in Chapter 2 has been included in part as a paper entitled "Endothelial control of capillary perfusion", in preparation for submission. The authors include myself, Namgyun Lee, Frank DeLano, Christopher Bertram, and Geert Schmid-Schönbein.

- The work described in Chapters 3 and 4 has been summarized as a paper in preparation for submission that will be titled "The impact of endothelial mechanotransduction on capillary network perfusion". The authors include myself, Namgyun Lee, Frank DeLano, and Geert Schmid-Schönbein.

- Studies outlined in Chapter 5 are also in preparation for publication entitled "Disruption of endothelial mechanisms for capillary flow control in hypertension". The authors will include myself, Namgyun Lee, Frank DeLano, and Geert Schmid-Schönbein.

I would also like to acknowledge the efforts of another — but no lesser — advisor, Dr. Frank DeLano. His daily advice, companionship, knowledge of practical matters, and linkage to another great researcher has been a light in dark times. He taught me the surgical methods that I utilize herein, some of which he learned from a great researcher, Dr. Ben Zweifach, others that he developed himself. His qualities of honesty and faithfulness have been a shining example of what a researcher should be. Frank was the greatest asset I could have asked for as I journeyed from the lowly questioning beginnings to becoming a talented and knowledgeable researcher myself.

My compatriot in graduate studies, Patrick Lynch, was also a person I often looked to for advice or distraction from the day to day struggles in research. They were available for constant support when experiments or surgical preparations went awry. Without Pat

and Frank, I honestly think the stressors of the research process might have broken me down beyond repair.

My undergraduate assistant, Namgyun Lee, has also been a great asset in the completion of my research. His untiring energy and passion for research will take him far in his studies; his help was crucial for the completion of data analysis and for inspiring me to elevate my own standards of quality.

The individuals whom I have studied with, either in the lab or outside the lab, since starting at UCSD have also been no minor assistance to the process. My friends and fellow researchers, I thank you.

My love, my fianceé, Giovanna has been there through it all. When I made a decision to be all that I could be, she was there by my side, supporting me. Without her, very little of this would have been possible.

Finally, UCSD as an institution should be commended for it's high level of research - both facilities and minds. Again, my only regret is that I didn't learn more than a small fraction of what it seems the university has to offer. Sometimes when standing on the shoulders of giants, you can hit your head on the ceiling of your own mind. At that point, one must expand their mind while keeping focused on the objective. No goal is too lofty when a willing mind applies the full extent of its cognitive abilities toward achievement.

VITA

2001	Bachelor of Science, Chemical engineering Rose-Hulman Institute of Technology
2002-2006	Teaching assistant, Bioengineering department University of California, San Diego
2002-2007	Graduate student researcher Microcirculation laboratory, Bioengineering, University of California, San Diego
2005	Master of Science, Bioengineering University of California, San Diego
2007	Doctor of Philosophy, Bioengineering University of California, San Diego

PUBLICATIONS

Scheidler NM, Lee N, Shin SH, Bertram CD, DeLano FA, and Schmid-Schönbein GW, "An Endothelial Mechanism for Chronic Control of Capillary Flow Spee", in preparation.

Scheidler NM, Lee N, DeLano FA, and Schmid-Schönbein GW, "Impact of Endothelial Mechanotransduction on Capillary Network Perfusion", in preparation.

Scheidler NM, Lee N, DeLano FA, and Schmid-Schönbein GW. "Novel Assessment of Capillary Dysfunction in Hypertension", in preparation.

FIELDS OF STUDY

Major field: Bioengineering

Professor G.W. Schmid-Schönbein	Study of Microcirculation
	Study of Biomechanics
	Teaching of Continuum mechanics
	Teaching of Biomechanics
Professor R. Nelson	Teaching of Biomedical imaging
Professor X. Huang	Teaching of Molecular biotechnology

ABSTRACT OF THE DISSERTATION

A Proposed Mechanism for Control of Capillary Network Perfusion: the Role of Endothelial Mechanotransduction Through Nitric Oxide Signaling and the Glycocalyx

by

Nicholas Michael Scheidler

Doctor of Philosophy in Bioengineering

University of California, San Diego, 2007

Professor Geert Schmid-Schönbein, Chair

Extensive evidence displays that vascular endothelium from arteries and veins respond to fluid shear stress. But the fluid shear response in capillary endothelium is unexplored. In this thesis, I hypothesize that the capillary endothelium can control capillary network velocity through modification of individual capillary dimensions in a shear stress-dependent mechanism. The effect of the hypothetical capillary-level control is a capillary network that exhibits similar perfusion velocities inside each capillary despite heterogeneity in capillary length, diameter, and network connectivity.

I developed a new method to determine red cell velocity simultaneously in all the capillaries of a capillary network by utilizing intravital microscopy and state-of-the-art imaging software. A highly sensitive camera recorded the passage of fluorescently labeled blood cells through the capillaries and this information is processed to determine capillary velocity. I investigated the effect of topology and rheology on capillary network velocity in

control tissue. I found that rheology does not appear to contribute significant variation to the overall capillary network velocity variation. Topological effects may create the baseline heterogeneity. Any system for control of topology may cause modified capillary velocity variation.

I investigated the involvement of shear-sensitive aspects of endothelial structure and function in a capillary velocity control system. I examined the contributions of nitric oxide signaling and the endothelial glycocalyx to the maintenance of capillary hemodynamics. These particular components of endothelial signaling pathways have been shown to affect the endothelial fluid shear response. Nitric oxide attenuation caused an elevation of capillary velocity variation, while enzymatic reduction of the glycocalyx reduced the variation. The studies served to determine that capillary endothelium may be capable of sensing and responding to local shear-stresses.

I applied the analysis outlined above to the specific endothelial dysfunction in a chronic hypertension model. Disruption of nitric oxide signaling and glycocalyx have been previously determined in hypertension, but a functional relationship to perfusion homeostasis and capillary network resistance has not been established. Herein I measure velocity in distinct capillaries of the same network to study the effects of endothelial dysfunction intrinsic to hypertension on capillary network perfusion.

Chapter 1

Introduction

Microvascular research focuses analysis on the function of living tissues, in both the normal physiological and diseased states. Examining small vessels allows fundamental analysis of the etiology of pathology — the first manifestations of disease exist on the scale of the microcirculation. My overall goal is to understand these fundamental mechanisms that may exist in healthy microvascular networks as a basis for detecting disruption in disease or tissue damage.

1.1 Introducing the hypothesis

Microvessels possess a number of mechanisms that serve to locally control perfusion. In this thesis, my primary interest is *mechanotransduction*, which is classically characterized by arteriolar and venular endothelial cells transmitting hemodynamic stimuli to smooth muscle cells. The smooth muscle cells are then responsible for local control of the perfusion through vascular architectural or tonic modifications. The classic endothelial function is to sense pressure and shear stress, but little attention has been given to endothelium as a potential modulator of local perfusion. In capillaries, the small dimensions suggest that even minor adjustments in endothelial structure or phenotype may serve to alter local capillary perfusion. In the following, I will focus on the hemodynamic control of the capillary network perfusion independent of the upstream arterioles.

I hypothesize that a control system exists that maintains local capillary perfusion in capillary networks. The capillaries supplied by a single arteriole-venule pair have identical upstream fluid pressure; but capillary lengths measured from node to node, diameters, and bifurcation angles are non-homogeneous within any capillary network. Network topology

creates a highly variable environment, but because blood is a non-Newtonian fluid with viscosity that depends on local hematocrit [32], the fluid itself also creates a stochastic pressure-flow relationship in the vascular network. The non-uniform resistances lead to different volumetric flow rates from capillary to capillary unless there is a mechanism that serves to adjust the capillary diameters designed to homogenize the capillary velocities within a network. We hypothesize the mean velocity in a capillary may be regulated by a shear stress-dependent mechanism that modifies the capillary lumen dimensions.

Any control system depends primarily on sensors and actuators to determine set-points and modulate parameters to meet them. This should be no different in biology, and we presume capillaries contain the necessary components for local control. The endothelium presents a boundary layer between static tissue and dynamic fluid flow, and is apparently the primary sensor of fluid shear stress in classical endothelial-smooth muscle mechanotransduction mechanisms. Although there is sparse evidence for contraction of endothelial cells in a manner similar to muscular actuation, at the scale of the capillary, minute changes could have large effects due to small capillary dimensions. Since small changes in small quantities like capillary diameter are at the visible detection limit, we study the microcirculation *in vivo* which allows rapid detection of small changes in tissue parameters such as erythrocyte velocity.

Therefore, I will measure and analyze red cell velocity as a measure for the degree to which capillary networks and their endothelium is capable of locally controlling the rate of capillary perfusion. I will also methodically decouple the effects of hemodynamics, microvascular topology, and smooth muscle interaction to rigorously define the effects on the level of the capillary network.

1.2 Previous research

There have been many scientific giants whose research into microvascular structure and function must be presented to build the case for capillary network control. Important aspects of microvascular biology will be introduced, including the structure and function of microvasculature, especially in skeletal muscle, along with focused portions of endothelial cell biology.

1.2.1 Blood flow in microvascular networks

Capillaries are vessels that are predominant numerically in the body, and they provide the interface between blood and tissue. There are on the order of 10^9 total capillaries in the adult human, distributed in every tissue and organ. The structure of a capillary differs between organs, but the typically accepted "true" capillaries exist in skeletal muscle, retina, and mesentery among many organs. A typical capillary vessel is approximately 200 microns in length and ranging from about 4 to 8 microns in diameter [31, 133]. The vessel microstructure consists of a thin basement membrane intraluminally lined by endothelial cells and occasional pericytes. The smooth muscle layer that surrounds arterial and arteriolar endothelial cells terminates prior to the pre-capillary bifurcations. There is also smooth muscle in venules, but smooth muscle effects in microvascular networks occur primarily at the arterial and arteriolar level [125].

The microvascular network structure in skeletal muscle is arranged into modular bundles of capillaries [133]. These capillary networks are perfused by terminal arterioles and collecting venules. They are positioned downstream of a system of arcade and transverse arterioles that regulate perfusion on an organ level [126, 142]. The arteriolar network serves to provide inlet pressure to the capillary networks at a relatively uniform level throughout a skeletal muscle [17]. The capillaries themselves are predominantly oriented parallel to the longitudinal direction of the muscle fibers, with several cross-connections between capillaries. The capillary connections to the arteriole and venule tend to be non-uniform. These variations in network structure may provide insight into the small deviations in capillary network velocity.

Despite decades of research, many aspects of microcirculatory perfusion, particularly with respect to hypertension, inflammation, atherosclerosis, and other pathophysiologies, remain poorly understood. Much of this research has focused on flow in individual vessels, especially on rheological and hemodynamic aspects. Therefore, fundamental hemodynamics in individual microvessels have been well characterized. Individual microvessel perfusion is highly dependent on the local hematocrit due to the Fåhræus-Lindqvist effect [32, 33]. The cell-cell and cell-vessel interactions are modified as the scale of vessel decreases; in fact, the Fåhræus effect at the capillary level is inverted — there is an elevation of hematocrit and resistance to flow as the size of vessel decreases beyond 5 μm [23, 181]. Furthermore, the particulate nature of blood along with active leukocyte-endothelial inter-

actions cause the resistance to flow to not only be non-Newtonian but stochastic as well.

These non-Newtonian properties of whole blood are accounted for through the use of the "apparent viscosity" [86]. Apparent viscosity and biomechanics approaches have allowed generation of empirical formulae for mean velocity in capillaries [182], but more detailed solutions have been conducted more recently. The stochastic distribution of hematocrit in individual vessels of the microvasculature has been modeled with limited success [108, 113]. An iterative approach to modeling the microcirculation has created larger and more complex models that attempt to explain the circulating cell biology and cell-cell interactions that dominate hemodynamic resistance *in vivo*, but only recently has the full particulate nature of blood on rheology been effectively modeled with a 2D lattice Boltzmann approach [141].

Current models take into consideration a variety of microvascular phenomena, including blood rheological and viscoelastic properties of microvessels. Furthermore, some models have predicted the need for mechanisms locally controlling perfusion. Pries et al. have shown that control of microvascular networks requires a vascular shear stress response, but specifically the shear must be in proportion to individual vessels' transmural pressure [111]. This contrasts Murray's famous "minimum cost hypothesis" [98] that suggests that wall shear stress is uniformly distributed throughout the microcirculation. Due to arcade arteriolar function, the pressure at the entry to capillary networks is relatively homogeneous [17]. Uniform wall shear stress and Pries' hypothetical shear relationship may be similar predictions if inlet capillary network pressure is maintained.

1.2.2 Control of microvascular perfusion

The importance of capillary perfusion in nutrient exchange was first examined by Krogh [80], who concluded that the capillaries are the fundamental unit of perfusion control. This conclusion was challenged with the suggestion that arterioles — especially terminal arterioles — are the primary controlling factor of microvascular perfusion [146]. The arteriolar control has been found to provide heterogeneous perfusion to different capillary networks. But others have concluded that the capillary network has a contribution to perfusion control [28]. Elevation of overall perfusion rates increases the degree of homogeneity of perfusion between capillary vessels, which suggests that passive rheological effects such as hematocrit or the highly branched nature of capillary topology [124] may be the deciding

factor in capillary perfusion. Another group showed the opposite result, instead finding that modifications in upstream perfusion rates had little effect on heterogeneity of capillary perfusion [14]. Thus, there has never been conclusive evidence that proves or disproves the control of capillary vessel perfusion. One conclusion that can be made is that upstream flow control dominates effects at the capillary level.

Capillary vessels have the ability to signal to upstream locations suggesting that capillary-originating stimuli for perfusion control may exist. Vasoactive agents like adenosine and norepinephrine were directly applied to a capillary via micropipette delivery causes the arteriole directly upstream to dilate [21, 22, 135]. Pries *et al* simulated the requirement of a conducted signal from distal to proximal regions in a capillary network [112]. This hypothesis seems to be borne out by experimental results that show that capillary endothelial K^+-dependent depolarization along the endothelium can travel opposite the direction of flow and stimulate smooth muscle relaxation [161]. Acetylcholine and potassium ions can stimulate Ca^{2+} currents that travel bidirectionally along the arterioles [25]. Endothelial cells electrochemically communicate with neighboring cells through Ca^{2+} signaling in a connexin-gap junction mediated response [88]. Others have shown that a conducted response may be stimulated by receptor-ligand binding [129, 135]. Furthermore, a metabolic response to tissue oxygen levels is required in addition to those listed above (shear, pressure, conduction) in another network model [109]. Pries *et al* attempts to synthesize a model that adequately predicts the results outlined above and that completely describes the perfusion response to metabolic requirements. Predictions from the most complex models do provide a sound basis for further simulations into pathophysiology [110]. But these simulations do not account for the full scale of variation of capillary perfusion that exists *in vivo*.

1.2.3 Spatial and temporal variation in microvascular perfusion

The impact of a putative control system in capillary networks would be to reduce the variability of perfusion velocity between capillaries of the same network. But previous research has shown that there is a degree of variation as assessed by red blood cell (RBC) flux and velocity. A brief discussion of previous results will allow further enhancement of the hypothesis.

Vessel tone is one parameter that is often used to determine the health of microvasculature prior to perfusion studies [124]. Vasodilation in response to adenosine or

vasoconstriction in the presence of elevated oxygen tension are hallmark tests for functional vessels. The tonic changes are due to the smooth muscle cells in the media of the vessel responding to adrenergic or local stimulation. Tonic changes can alter the amount of blood that perfuses a whole organ, but even more, fine control systems function to deliver blood evenly throughout the tissue comprising an organ. The spatial and temporal variations in blood flow delivery can be the difference between a healthy, robust organ and a diseased, pathological organ. Finding the source of capillary variation is a central theme in this thesis research. First, I discuss the previous research focused on characterizing microvascular variation.

Previous assessment of spatial and temporal variation

Spatial variation in microvascular perfusion has been studied at the level of capillaries. One group including Drs. Tyml, Groom, and Ellis in particular published a series of papers throughout the 1980s that are of interest. They built on early velocimetry research from Johnson [174] and Intaglietta [68, 119] to try to understand the source of heterogeneity in blood flow measurements. The outline of their work below will introduce the concepts of spatial variation that I utilized for my work.

Studies on frog capillaries in which velocity recordings were made over a range of time scales revealed that temporal variation may be consistently correlated only with the heart rate. Velocity measurements from individual capillaries ranged from 60 seconds (at 10-15 measurements per second) to 50 minutes (filtered to data on a period of 3.3 minutes). The discrete time points were filtered with a Fourier series analysis that revealed important periodicity in the data. The shortest data with the highest temporal resolution revealed that heart rate correlates well with velocity fluctuations at the capillary level. A second source of temporal variation was significant on longer time scales, and was presumed to be due to vasomotor cycling or pre-capillary sphincter function [158]. Another study attempted to decouple spatial variation in capillaries from upstream temporal variation, but was largely unsuccessful. This study however remains the first time I have seen an attempt to separate red cell velocity into individual capillaries instead of combining velocity measurements from a number of capillaries [157]. Their conclusion was that the upstream temporal variation masked any spatial variation within the capillary network. Unfortunately, they also appeared to be more interested in comparing *network to network* variability rather than

within-network variability [157].

One interesting approach taken by the same group was to compare capillary velocities in only two capillaries of the same network. The velocity in two capillaries correlated with each other approximately 95%, which is an amazing display of capillary homogeneity. The conclusion they drew was that upstream control of perfusion maintains the same capillary velocity in the two vessels. Arterioles control pressure and flow to maintain a moderately constant capillary supply rate. But stochastic hematocrit and red blood cell delivery to the two blood vessels would vary as a function of the velocity. Small disturbances at the capillary level should reduce correlation between velocity profiles in neighboring capillaries. Furthermore, the capillary ultrastructure and topology would not be exactly equal regardless of close proximity, which would alter hemodynamics, if only on a small scale. The existence of a long-term capillary growth process may be supported by this result. In addition, they find that a large component of the velocity variation that cannot be explained by arteriolar function exists on the order of seconds. They conclude that any regulation of this variation would require active capillary function [159].

The development of a simultaneous method for velocity measurement in capillaries allowed investigation of the question of capillary recruitment. The assessment of capillary recruitment and the impact on heterogeneity of capillary perfusion required a sensitive velocimetry method. Early attempts to quantify recruitment include Krogh's seminal capillary efforts [80], but even much later, the methodology required a jump from no-flow capillaries to perfused capillaries. It was shown in rat spinotrapezius that the baseline perfusion levels were already above a threshold wherein recruitment due to stimulated muscle contraction was minimal [64]. But with simultaneous methods, the degree of capillary velocity homogeneity was used as an index for recruitment [153]. They showed that the coefficient of variation (CV) of velocity between capillaries was an index for both recruitment and blood flow homeostasis in capillary networks.

The interest in capillary recruitment in skeletal muscle also prompted further studies where the primary result was capillary velocity. It was concluded that rheological effects in red cell supply rate at the arteriole level can effect capillary homogeneity. That is, delivery of increased blood flow via chemical stimulus [155], electric stimulation, or hemodilution increased capillary velocity homogeneity [154]. They attributed this increased velocity similarity to a more even fractional distribution of blood at capillary bifurcations [28]. Con-

trasting results from another group calls this conclusion into question, but differences in muscle tissue utilized in the study may promote some differences found [14]. Finally, an early paper suggested that the path "selected" by cells as they pass through a network factors into the transit time. This result seems obvious in retrospect, but control of metabolic factors proportional to transit time could be under control at the capillary level [124]. The comparison of capillary blood flow at segmental levels with flow for an entire path has never been investigated.

Functional aspects controlling capillary blood flow at the level of the capillary beyond this point have focused increasingly on molecular aspects in the endothelium. Signaling pathways that can be construed as agonist-dependent and/or mechanosensitive continue to be areas of investigation at the capillary level, but the impacts on capillary perfusion assessed via velocity homogeneity have not been investigated. Most recent research focuses either on *in vitro*conditions or arteriolar control of capillary perfusion.

Vasoactive networks

One source of temporal variation that should be noted is due to changes in microvessel tone, or vasoactivity. Spontaneous modifications of vessel tone occur non-periodically at the level of the microcirculation — most notably in arterioles. Changes in vessel tone cause temporal variation in delivery of blood flow to a tissue region, something often seen in normal, healthy tissue. Indeed, many different organs display high degrees of temporal variation such as skeletal muscle and brain. In a hamster window model, spontaneous alterations in arteriolar diameters were seen in nearly 90% of the arterioles, with the largest percent constrictions occurring in the smallest vessels [46], and the effect of drastic vasoconstriction on microvascular resistance is significant. Small regions of an organ may receive reduced blood flow for periods of time. This kind of periodic difference in blood flow was designated "temporal variation".

It should be mentioned that except in extreme cases such as ischemia models or hemodilution, the impact of the temporal variation in blood flow is not severe, but may be a function of the microvasculature to keep tissue oxygen levels dispersed evenly despite reduced flow to the organ [67]. A model solution verifies this concept with the finding that skeletal muscle perfused with elevated vasoactivity will maintain at least 5 mmHg oxygen tension in a greater percentage of the tissue. So, temporal changes may aid in the efficient

distribution of flow to an entire organ, but the impact of temporal changes on capillary vessel perfusion has not been clearly stated. The capillary network functions downstream of a series of primary actuators in control of blood delivery, and signaling activity at the capillary level has not been linked to capillary endothelium.

The cause of spontaneous vasomotor cycling has been biochemically modeled. It has been shown that regular calcium currents undergo brief cycles in smooth muscle of the vascular wall. The sarcoplasmic reticulum in these cells release and re-uptake calcium regularly to cause depolarization and muscle contraction. The wave of depolarization in single cells separate from other cells is asynchronous, but via gap junction signaling, cells in communication with other smooth muscle cells will induce synchronized depolarization and subsequent muscle contraction [103]. There have been studies on connexin function in gap junctions in arterioles, capillaries, and venules that showed that endothelial signaling via calcium currents requires connexin function.

1.2.4 The molecular basis for mechanotransduction

Blood flow is under many levels of control, from the nervous control of the heart down to the local effects in the microvasculature. Mechanotransduction, or the signal transduction pathways responding to mechanical stimuli, is a local response to mechanical stimuli that classically involves a smooth muscle element serving to actuate vascular tone. Indeed, the function of the arterioles depends on smooth muscle vasoactivity, and is responsive to a number of tissue signals both chemical and mechanical. Many biochemical factors present in pathophysiological states such as inflammation have been shown to mediate vascular tone. But results have shown that shear stress mediates an endothelial cell-dependent smooth muscle relaxation while local pressure elevation causes increased vessel circumferential stress, which stimulates the myogenic response. These functions ensure that the inlet pressure to capillary vessels remains controlled to within 1-2 mmHg with the aforementioned temporal variations due to upstream arteriolar tone.

Capillary structure is often simplified by assumptions that the vessel is a straight, rigid tube with few surface characteristics. More complex models take two-dimensional variations in diameter into account [114], which increases the modeled vascular resistance, but still leaves predictions about 75% lower than observed *in vivo* vascular resistance [87]. This may be due to luminal shape variations, a nuclear "bulge", or active processes in

the capillaries themselves [82]. It has been shown that endothelial cells may also respond to low-flow perfusion states by modulating their thickness [91] or with the formation of pseudopodia [81]. Endothelial cells themselves have been shown to align their major axis to the direction of shear *in vivo* [20, 47]. This effect is replicated in vitro by restructuring of the actin cytoskeleton upon application of different shear profiles [47, 84, 99]. These effects suggest that endothelial cells in a capillary may be capable of modifying local perfusion and therefore local shear stress profiles on a short, biologically-relevant time scale.

Nitric oxide signaling

The discovery that nitric oxide was a mediator in signaling pathways in vascular dynamics was an important biological finding [66, 102]. While the actual shear stress sensing mechanism has not been fully identified, but the nitric oxide signal transduction pathway has been elucidated for many cell types.

Nitric oxide is produced enzymatically via nitric oxide synthase (NOS). Three isoforms of NOS exist and are expressed in various tissues: the endothelial subtype (eNOS), inducible (iNOS), and neuronal (nNOS). Active research has shown that each NOS may respond to different stimuli in contradictory roles, e.g., eNOS function has been linked to anti-inflammatory responses, whereas iNOS may be pro-inflammatory. Functionally, it appears that adenosine agonist-dependent eNOS activation occurs through upstream regulation by Src-tyrosine kinase phosphorylation through a PI3K/Akt-dependent pathway [44, 179]. Other agonists (estrogen, HDL, etc.) may activate similar upstream regulators. Nitric oxide is synthesized from L-arginine catalysis into L-citrulline in a Ca^{2+}-calmodulin dependent process by eNOS although one component of plasma membrane, a sphingolipid called ceramide, has also been shown to activate eNOS independent from calcium currents [65]. Burst production of NO activates smooth muscle soluble guanylyl cyclase (sGC) which generates cGMP *in situ* [152]. cGMP is an important second messenger in many pathways, but in particular, it causes smooth muscle relaxation and therefore a reduction in vascular tone.

NO release through eNOS has been shown to be tightly regulated through post-translational modifications and other allosteric interactions with caveolins and/or PECAM-1 [26, 48]. Furthermore, recent research has shown that eNOS expression may be affected by the cytoskeleton and the intracellular G-/F-actin ratio [128]. Inhibition of nitric oxide

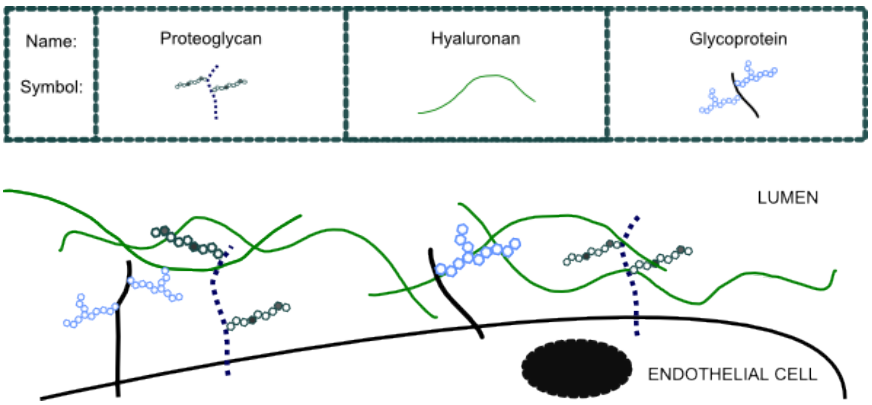

Figure 1.1: Schematic adapted from recent review [117] summarizing current theories regarding glycocalyx structure. The entire structure may extend up to 500 – 1000 nanometers into the lumen of the vessel and is composed of a mesh of proteoglycans and glycoproteins bound to the endothelial cell. Also, a set of soluble proteoglycans and glycosaminoglycans such as hyaluronan interact with the bound molecules to create the whole functional glycocalyx. Proteoglycans have long unbranched glycation groups added as post-translational modifications to a small set of core proteins, such as syndecan or glypican. Glycoproteins have shorter highly-branched glycation groups attached to a protein core. The two primary glycosaminoglycan groups are heparan sulfate (HS) and chondroitin sulfate (CS) that exist in approximately 4:1 and comprise approximately 90% of all glycations. An amazing variety of sugar moieties and sulfation patterns provide for protein selectivity and function. Schematic not to scale.

signaling through active site binding competitors has revealed the myriad effects of NOS proteins. Specific microcirculatory experiments conducted with the nitric oxide inhibitor L-NAME have shown leukocyte effects such as oxidative stress and adhesion in postcapillary venules may be important factors in microvascular network perfusion [92, 140].

Glycocalyx: structure and function

The glycocalyx also termed the endothelial surface layer (ESL) refers to a meshwork of glycoproteins, proteoglycans, and glycosaminoglycans that may be bound to the luminal surface of the endothelium in most vessels [117]. There have been estimates that are supported by experimental evidence that suggest that the length of the glycocalyx may be up to 500 – 1000 nanometers [19, 168], which corresponds to 20-50% of total plasma volume [114]! The glycocalyx has been shown to be involved in signaling pathways and in permeability control.

Structure of the glycocalyx

The structure of the glycocalyx starts at the endothelial cell surface with a series of proteoglycans that serve as the binding liaison between the majority of the endothelial surface layer and the plasma membrane. Among several proteoglycans, two that maintain direct interaction to the cell cytoskeleton are called syndecan and glypican. A simple schematic summarizes the current theory on the structure of the glycocalyx in Figure 1.1.

The generation of glycocalyx backbones such as proteoglycans starts with a core protein such as glypican or syndecan. Glypican and syndecan are two of several core proteins, but they are of particular interest because they are GPI-anchored and membrane spanning and may therefore interact with signaling proteins and cytosolic stress fibers. The core protein is translated normally, but a xylose (Xyl) monosaccharide is added to specific serine amino acid locations in the endoplasmic reticulum. Then in the *cis*-Golgi, two galactose (Gal) sugars are added to the xylose. A glucuronic acid (GlcA) group finishes construction of the GAG linker group, which in shorthand notation is GlcA-β3-Gal-β3-Gal-β4-Xylβ3-[Ser]. The next addition to the growing GAG chain will determine its type: an α4-glucosamine group would indicate a heparan sulfate whereas a β4-galactosamine would be a chondroitin sulfate. Following the first hexosamine is a series of glucuronic acids and glucosamines that form a long unbranched polymer. Enzymatic modifications in the Golgi include N-sulfations, O-sulfations, and epimerizations that change uronic acid groups. The number and variety of glycation and sulfation patterns allows an amazing quantity of discrete functions and disparate sensitivities. In contrast, the long GAG chain called hyaluronan is synthesized *in situ* on the cytosolic side of the plasma membrane via hyaluronan synthases. Therefore, there are no sulfations or modified sugar motifs on hyaluronan.

Function of the glycocalyx

Some have suggested that the various functions of the glycocalyx depend on synergistic interaction of proteoglycans, glycoproteins, hyaluronan, and other soluble components [148]. Therefore, of the several groups that have enzymatically digested component(s) of the glycocalyx and documented the results, it is difficult to determine which component is of primary importance. Hyaluronan digestion did not result in alterations in capillary endothelial cell thickness, but significantly reduced the overall glycocalyx thickness [165]. An-

other group found that hyaluronan reduction also reduced the nitric oxide production [93]. Heparinase treatment to remove the HS chains completely abrogated the shear-responsive NOx production in endothelial cells [37]. But, it has been hypothesized that hyaluronan serves to stabilize the meshwork interaction of the HS, CS, and proteoglycan backbones [59].

The hemodynamic effects of the glycocalyx must also be noted along with its contribution to shear-responsive signaling. The glycocalyx itself represents a significant structure with respect to the dimension of the capillary, and has been shown to be hemodynamically relevant [13, 134]. The glycocalyx forms a cellular exclusion zone in vessel lumens that may serve to regulate capillary hematocrit; heparinase disruption caused an increase in microvascular hematocrit that was not mirrored by reduced red cell velocity [19]. This may not be entirely explained by glycocalyx removal, however, since the authors also degrade other portions of the glycocalyx to little effect. Further, reduction (via enzymatic removal or oxidized LDL treatment) of the endothelial glycocalyx appears to allow increased leukocyte-endothelial interactions, especially rolling and firm adhesion [12, 95]. Similar results were seen during investigation of the inflammatory role of the glycocalyx [96].

The interplay of the glycocalyx with other mechanosignaling pathways remains an active research field. For example, nitric oxide synthase has been shown to be activated in response to adenosine [178], but adenosine reduces the exclusion properties of the glycocalyx and may cause arteriolar vasoconstriction [106]. Vink et al. showed that oxidized low-density lipoproteins (LDL) may also degrade the glycocalyx and allow increased platelet adhesion at PECAM [169]. The contribution of syndecan to signaling has been recently studied. In particular, it appears that syndecan-4 (out of -1, -2, -3, and -4) is the syndecan primarily expressed on vascular endothelium, but its involvement in shear-dependent signaling is unclear [150]. Finally, Thi et al. showed that heparinase pretreatment of endothelial cells *in vitro* reduced the actin restructuring apparent in control cells in response to shear [149]. All of these findings promote the hypothesis that the glycocalyx is an active participant in microvascular control phenomena.

1.2.5 Endothelial dysfunction in hypertension

The range of endothelial function that begins to go awry when considering hypertensive models is staggering. Important protein functions are altered and intracellular

communication is attenuated. Reactive oxygen species are produced at an enhanced level which can oxidize and damage cells and tissue. The vasculature is modified through capillary rarefaction and increased activity of resistance vessels. The effect of rarefaction on capillary network resistance and perfusion has not been established, but micropressure experiments have shown that capillary pressure differences in hypertensive rat skeletal muscle are insignificant. The amount of research into endothelial dysfunction in hypertension is staggering; a brief summary is provided below.

Endothelial derived factors

The impact of endothelial signaling in hypertension is multifaceted. Nitric oxide-mediated dilation of arterioles is reduced in the rat hypertensive model (spontaneously hypertensive rat, SHR) in response to stepped perfusion rates in isolated vessels [77]. The continued study of nitric oxide signaling displayed agonist-dependent activation via estrogen in hypertensive animals, which suggests that protein levels remain similarly expressed [61, 62], but eNOS is de-activated. Also, elevated reactive oxygen species may play a significant role in scavenging NO and therefore reducing NO bioavailability [15, 40]. Chronic nitric oxide inhibition has also been used as a model for hypertension [123].

Other important endothelial derived factors upregulated in hypertension are generally vasoconstrictive agents. In essential hypertension, increased endothelin-1, a powerful vasoactive agent, and decreased NO levels correlated with development of high blood pressure [72]. The function of the endothelin molecule depends on the expression level of endothelin receptor subtypes (ET-A or ET-B receptors) and can function as a constrictive, pro-inflammatory signal or a dilative, anti-inflammatory signal. The ratio of endothelin receptor subtypes has been investigated in hypertensive models recently [69, 101], but more functional results are still necessary. Reactive oxygen species are also produced at elevated levels in hypertensives, due in part to elevated levels of NADPH oxidase and xanthine oxidase [16, 145]. Nitric oxide signals are impacted by reactive oxygen species through oxidation of nitric oxide synthase and an important co-factor for NO synthesis [34].

Endothelial apoptosis leading to microvascular rarefaction

Microvascular length density in hypertensive rats is significantly decreased over normotensive animals [171]. Treatment with oxygen free radical scavengers such as su-

peroxide dismutase mimetics Tempol or Tiron reduced indexes of apoptosis and decreased rarefaction approximately 10 – 20% [75], which suggests reactive oxygen species play a role in development of rarefaction. The connection between rarefaction and NO bioavailability has also been examined. NO inhibition reduced constitutive angiogenesis in a wound-healing model, which suggests that NO bioavailability may play a role in rarefaction as well [73]. Finally, anti-hypertensive drugs such as ACE (angiotensin-converting enzyme) inhibitors have been shown induce angiogenesis, which may serve to enhance their efficacy in treating hypertension [8]. The matrix metalloproteinases (MMPs) that restructure vessels in rarefaction are linked to reactive oxygen species and also endothelin levels [2, 53]. Other chronic vasoactive treatments have enhanced MMP-9 expression in the microvasculature, which may be involved in angiogenesis [49].

The impact of rarefaction on microvascular resistance was investigated by a numerical simulation wherein capillaries were removed and network resistance was calculated. The network resistance increase was insignificant when 30% of capillaries were removed, but exponentially increased past this point. The model used in the study was simple, but as a first order approximation, leads to the conclusion that capillary rarefaction as seen in rat models of hypertension may not significantly elevate perfusion resistance in a time-invariant model [63]. Given higher order and random fluctuations such as the impact of blood cells or even metabolic requirements during exercise in microvascular perfusion, this model may be invalidated.

1.2.6 Summary of previous research

Endothelial function through nitric oxide-mediated mechanotransduction serves to stabilize microvascular perfusion. The glycocalyx is also viewed as a potential mediator of nitric oxide availability and the interactions of the glycocalyx with vascular function are still being determined. Vascular networks may require control at the capillary level for efficient perfusion delivery. The endothelial cell exists at the interface to respond to stimuli for microvascular perfusion control — whether through glycocalyx driven blood-endothelial interactions or communication upstream via gap junctional coupling. The interplay of endothelial mechanotransduction with capillary network perfusion exists on a length scale wherein random factors become significant events. The events at the scale of individual capillaries such as reduced glycocalyx or nitric oxide availability lead to symptoms of hy-

pertension. But molecular biology describes an incomplete system. A goal of my research was to determine capillary responses at the blood-tissue interface with a functional methodology to directly investigate responses in living tissues.

1.3 A hemodynamic analysis

Continuum mechanics applied to capillary vessels allows insight into laws governing blood flow. In this analysis, capillary level control on perfusion velocity in capillary networks is briefly discussed. The hemodynamics on the scale of capillaries are solved with assumptions that make closed-form solutions tractable. Deviations from the simple solutions are attributed to factors such as hematocrit, topology, and active cellular processes. For this reason, many of the following assumptions are made for first approximation, then the impact of realistic hemodynamics are determined by relaxing those assumptions.

1.3.1 Fundamental hemodynamics

At very low Reynolds numbers (0.001 and below), the flow of plasma in capillaries is governed by the Stokes approximation to the equations of motion which in index notation are

$$0 = -\frac{\partial P}{\partial x_i} + \mu \frac{\partial^2 v_i}{\partial x_j^2} \tag{1.1}$$

$$\frac{\partial v_i}{\partial x_i} = 0, \tag{1.2}$$

where v_i is the plasma velocity vector, P the pressure and x_i the spatial coordinates [125]. Due to the Fåhræus effect and blood cell separation at bifurcations, the hematocrit is reduced, and the non-Newtonian properties of the blood are ignored. The viscosity, μ, is constant with respect to shear rate. Integration of these equations in cylindrical coordinates (r, θ, z) across a circular cylindrical capillary cross-section (radius a) with predominantly axial velocity component v_z gives the parabolic velocity distribution

$$v_z = -\frac{1}{4\mu}\left(a^2 - r^2\right)\frac{\partial P}{\partial z}. \tag{1.3}$$

Dropping the subscript z for convenience, the mean (axial) flow velocity, $\overline{v}$, is

$$\overline{v} = \frac{Q}{\pi a^2} = -\frac{a^2}{8\mu}\frac{\partial P}{\partial z}, \tag{1.4}$$

where "mean" and the corresponding overbar in Equation 1.4 both denote a spatial average over the capillary cross-section. Q is the volumetric flow rate. The wall shear stress on the endothelium is

$$\tau_w = -\frac{a}{2}\frac{\partial P}{\partial z} = 4\mu\frac{\overline{v}}{a}. \tag{1.5}$$

Equation 1.4 shows that according to traditional hemodynamics the mean flow velocity depends on the pressure drop along the length of a capillary. Capillaries with different lengths would thus tend to have different mean speeds. This analysis neglects instantaneous elastic and viscoelastic features of the vessels, but may suffice for first approximation. In Equations 1.3 to 1.5, the vessels are assumed to have constant radius, a, throughout the length of the vessel. Again, the assumption is a simplification that reduces hemodynamic resistance when compared to in vivo vessel structures [114].

1.3.2 Hypothetical capillary endothelial shear stress response

We postulate that, by means of an active involvement of the endothelial cells, the lumen diameter of a capillary, $2a$, varies with wall shear stress, τ_w, such that an increase in shear stress over a limited physiological range causes a reduction of lumen diameter and vice versa, i.e. there will be an inverse relationship between shear stress and vessel radius. In first approximation this may be written as $\tau_w \sim \frac{1}{a^\alpha}$ In the following analysis we will examine the case for $\alpha = 1$.

We assume that there exists an optimal wall shear stress τ_o and an optimal lumen radius a_o such that

$$\tau_w = \frac{a_o \tau_o}{a}. \tag{1.6}$$

Note that we here consider only time-averaged quantities that neglect in vivo temporal variations due to leukocyte flow, hematocrit variations, upstream vasoactivity, or even cardiac output. However, it should be noted that Pries et al. have simulated that responses of microvascular networks on short time scales tend to mirror the long-term responses that have been observed [114]. Therefore, the flow distribution within a capillary network may adjust to this optimal shear stress through rapid restructuring of capillary endothelial structures such that the functional radius is optimized.

1.3.3 The mean capillary blood velocity

To examine this hypothesis we will first study a number of consequences predicted by Equation 1.6. Substitution of Equation 1.6 into Equation 1.5 yields a mean velocity after endothelial restructuring to optimal perfusion conditions

$$\overline{v_o} = \frac{a_o \tau_o}{8\mu} \tag{1.7}$$

This optimal mean velocity depends only on the optimal shear stress τ_o and associated optimal lumen radius a_o without dependence on the local pressure gradient, $\partial P/\partial z$, i.e. our hypothesis predicts that after adjustment of the capillary dimensions to an optimal state the mean velocity is uniform throughout a capillary network. This corollary to the above hypothesis may be tested *in vivo* through a thorough analysis of capillary network perfusion; conversely, in the case of homeostasis, small variations in vascular dimension may achieve vessel perfusion with reduced variability.

1.3.4 Impact of capillary network control on hemodynamics

The concept of a capillary network as a resistance model for extrapolation from a basic microvascular unit has been utilized to determine the pressure-flow relationship for a tissue or an organ. In muscle tissue, pressure-flow relationships have been rigorously determined in our laboratory for different perfusion suspensions [142–144]. But this methodology was highly invasive, and improved accuracy for hemodynamic models should allow calculation of vascular resistance based on increasingly detailed mechanics.

Linear conduction computations assuming no capillary level control

As above, for first approximations only, blood may be considered Newtonian in microvessels. Then, for a capillary network bundle a schematized topology and connectivity may be assumed from experimental measurements [132] as in Figure 1.2. While more complex networks have been modeled by Pries *et al*, again for a first approximation, this network contains many of the typical values for lengths and connectivity as is seen in spinotrapezius muscle *in vivo*. Then, a linear conduction model as utilized previously in our laboratory was able to solve a coupled set of linearized equations for flow rates and pressures in the schematized bundle [35]. For a simple network with simple rheology, the

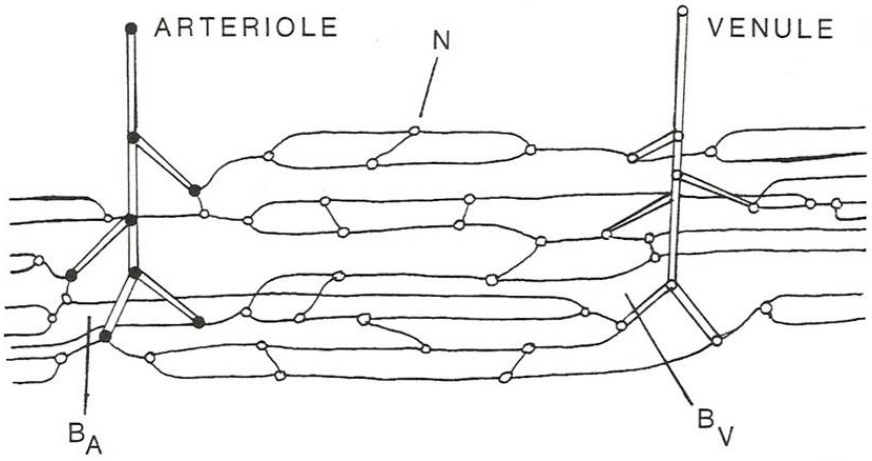

Figure 1.2: Schematic capillary network built from average spinotrapezius vascular measurements. The original network, published as part of T.C. Skalak's PhD thesis [132], has been utilized as modular network bundles to simulate blood flow in tissues.

predicted value for variability between perfusion velocity in the capillary vessels ranged between 60–120% as assessed by coefficient of variation.

This high variation in capillary network velocity has not been shown previously in living tissue. Therefore, living tissue may have mechanisms that reduce the level of variation between capillary velocity. The mechanism may be enacted either through active mechanical processes at the endothelial level or passive rheological or topological effects. At this time, the question of control over perfusion at the capillary level has been largely unexplored. The impact of capillary level responses on capillary velocity variation requires further exploration.

Computations of capillary velocity assuming strict control

Another set of computations were completed using the network topology seen in Figure 1.2 was recently conducted in the laboratory. The procedure for solution began with the network topology and applied conservation of mass and momentum as governing equations. Simplifying assumptions including Newtonian fluid and simple cross-sectional geometry of the vessels were applied to the conservation of momentum that allowed use of Poiseuille's equation. Then, one further assumption was made: a capillary level relationship exists that relates vessel radius and wall shear stress as shown above in Equation 1.6. This has the effect of simplifying Poiseuille's equation to provide constant mean velocity in all capillary vessels in the schematic network. The conservation of mass with modified

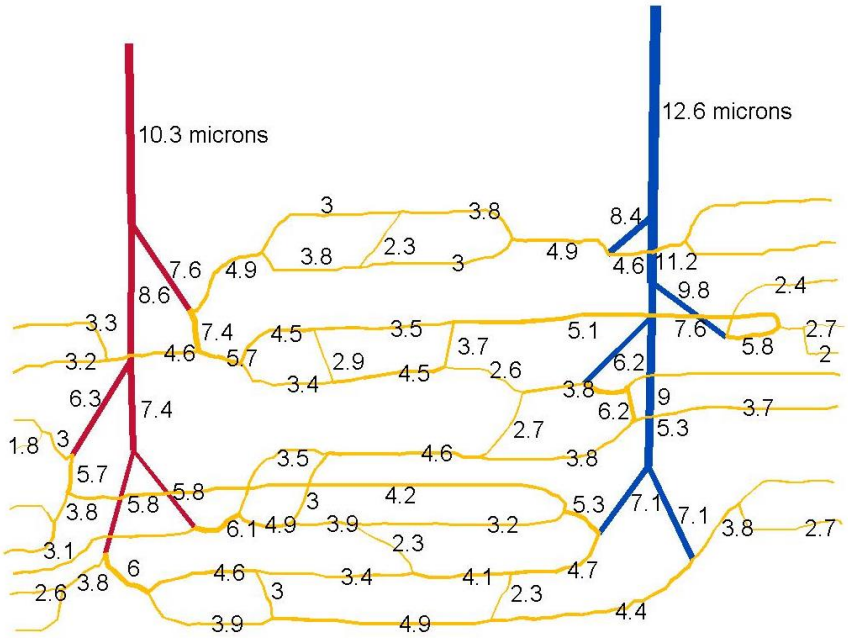

Figure 1.3: Vessel diameters are displayed for the steady-state solution found with the assumption of strict capillary level control over capillary velocity. The vessel diameters fall within a range established from experimental measurements. The velocity distribution in the vessels with these diameters has a coefficient of variation of 0%.

Poiseuille's law is then solved at each bifurcation in the network.

The steady-state solution of the set of nonlinear equations described above provides pressures at each bifurcation. The nodal pressures allow computation of the pressure drop through each vessel in the network and, therefore, the flow and velocity. The diameters of the vessels calculated and shown in Figure 1.3 were within experimentally determined ranges. The velocity distribution was assumed to be zero in this computation. The solution converges at stable solutions through a range of initial conditions. While the simulated diameter values are realistic, a coefficient of variation of capillary velocity of 0% has never been witnessed *in vivo*.

Computation versus intravital measurement

The results of the computations described above have not been verified *in vivo*. The level of variation in capillary velocity within capillary networks has never been rigorously established. Any control over capillary velocity at the capillary level may be responsible for a reduction in coefficient of variation between velocities. The extent to which this may occur has never been explored *in vivo*.

1.4 Specific aims

My thesis research is focused on probing the structure and function of capillary endothelium *in vivo*. Determination of the existence of a hypothetical system of control at the minute scale of capillary networks presented a novel challenge. Protocols were established to measure capillary velocity in microvascular networks in skeletal muscle. Then, experiments testing control of capillary velocity and the contribution of shear-sensitive endothelial structures were conducted.

1.4.1 Analysis of capillary networks

The question that I first asked was which hemodynamic parameters should be monitored to investigate perfusion of the capillary network. The putative control mechanism would modulate effective perfusion via some endothelial response: diameter regulation via cytoskeletal rearrangement, increased (or decreased) leukocyte-endothelial interactions, or some other effect. The result would be to modify the rate of perfusion of the capillary vessel. The type of modification from the endothelium may be varied, but the result is hypothetically similar.

Capillaries range from approximately 4–8 microns in diameter and while there are established methods for measurement of diameter, I would question whether capillary diameter can be measured *in vivo* with sufficient accuracy. A high degree of variability may exist in effective capillary diameter, since the impact of cell-free layers on hemodynamics has also been recently shown.

My preferred measurement then would be to analyze perfusion of many capillary vessels simultaneously. Additionally, by constraining the data collection to capillaries from the same network, the number of different hemodynamic factors such as upstream pressure or hematocrit effects may be reduced. The degree of variation between perfusion rates in capillary networks must first be established. Therefore, I study the *result* of capillary flow control: whether a minimization of variation in capillary velocity exists.

Protocols for data acquisition and analysis

The first step in the investigation required development of protocols to analyze the degree of variation in velocities between capillaries of the same network in control tissue. Previously described technologies for the recording of velocity information proved to

be inadequate for the determination of velocity in a number of capillaries simultaneously. Therefore, a novel intravital imaging and computational method was established for recording velocity in capillary networks. Subsequently, automated computer analysis for spatial and temporal variations in the velocity data was developed. This allows close attention to details of perfusion in the capillary networks while not becoming overwhelmed by mountains of data.

Establishment of evidence for hemodynamic control

Furthermore, two methods were used to probe capillary level control. The accepted hypothesis has been that capillaries are simply vessels for perfusion of blood. The impact of a capillary on its own perfusion has been studied, but never beyond the point of a capillary as a signaling component to standard vasomotor structures. Therefore, the hemodynamics of capillaries were assessed in one low-flow situation — occlusion of an upstream arteriole — and an increased flow situation — enhanced flow through electrically stimulated muscular activity. Flow rates in control tissue along with these different states were analyzed at the capillary level.

1.4.2 Investigate endothelial mechanotransduction pathways

Following the establishment of surgical, imaging, and computer protocols for the determination of capillary perfusion parameters in individual networks, it was possible to investigate the effect of endothelial mechanotransduction pathways on capillary network perfusion. Primarily, I analyzed the distribution of capillary velocity in a single network as two emergent components of endothelial mechanotransduction pathways were modulated.

Nitric oxide signaling

No molecular signal has been more heavily studied in the past twenty years than nitric oxide. The ubiquitous nature of the molecule in microvascular signaling made it an obvious choice for probing mechanosignaling in capillary networks. A primary endothelial response to shear stress is the production and release of nitric oxide signals. Nitric oxide stimulates smooth muscle relaxation and hence vasodilation in larger vessels, but additional responses to nitric oxide availability at the capillary level have not been investigated. Therefore, I completed a set of studies wherein the natural nitric oxide signal was abrogated with

an endothelial specific inhibitor of the enzyme responsible for the local synthesis of nitric oxide. The effect of nitric oxide inhibition on microvascular perfusion and distribution capillary network velocity was then analyzed. Furthermore, effects downstream of nitric oxide in the signaling cascade were probed with the phosphodiesterase inhibitor, papaverine.

Glycocalyx

Recent developments in research into mechanotransduction and endothelial structures have elucidated the potential impact of the glycocalyx. The classic paradigm in biomechanics was that the endothelial cell comprised the interface between blood and tissue. But the true interface between flowing blood and the surface of the endothelial cell may be a sub-endothelial structure. Capillaries are lined with a $0.5 - 1$ micron layer of glycoproteins both associated to the cell surface and the moving fluid layer. The hemodynamic impact of the glycocalyx is still being analyzed, but there can be little doubt that modifications to glycocalyx structure would alter fluid flow in the smallest vessels.

For this reason, I elected to enzymatically degrade a single component of the glycocalyx: heparan sulfate proteoglycan. Previous research into enzymatic removal of glycocalyx has shown that removal of this particular element within the glycocalyx had an effect on mechanosignaling in endothelial cells. Local application of heparinase to a tissue was achieved, and the impact of glycocalyx removal on capillary network perfusion was examined.

1.4.3 Examine impact of endothelial dysfunction in hypertension

Hypertension is a symptom of a greater disease afflicting millions of people today. The history of hypertension research has revealed that endothelial dysfunction is evident in the manifestation of the disease. Two specific endothelial roles are modified in hypertension: there is reduced nitric oxide availability and an attenuated glycocalyx. The impact of these changes on perfusion within capillary networks has not been studied in rigorous detail. But due to previous work showing the roles of both nitric oxide and the glycocalyx in mechanotransduction, this provides evidence of altered mechanosignaling in hypertension. Therefore, it was interesting to me to determine the capillary velocity distribution in hypertensive rats. The degree of glycocalyx expression in hypertensive animals was also analyzed. The interaction between glycocalyx expression and capillary network perfusion may provide insight into development of hypertension in a chronic animal model.

Chapter 2

Intravital methodology

Blood flow has been studied nearly as long as there has been microscopy. van Leeuwenhoek made some of the first microscopic observations of flowing fluids in living tissues and visualized capillaries to help confirm Harvey's theory of blood circulation [57]. Significant improvement in techniques have been made that have allowed more qualitative and even quantitative measurements in the microvasculature. In this chapter, I outline several major methods that have been utilized, and detail my own approach to developing new protocols for measuring velocity using intravital microscopy. The method allows simultaneous video acquisition of blood perfusion in an entire network of capillaries. The analysis of resulting images provides quantitative information about velocity in capillary networks, including from curved or visually-obstructed vessels. The image processing and velocity computations are presented with the aid of an example set of images. My overall objective is to expand the state-of-the-art of velocity measurements as a tool to uncover fundamental mechanisms that govern blood flow in capillary networks.

2.1 *In vivo* velocity measurement

Continuous and simultaneous *in vivo* approaches for characterization of capillary perfusion have been attempted. The researchers focused on single vessels through the use of the dual-slit correlation method [174] or multiple vessels with the flying spot method [156]. Methods that have been more recently developed are introduced and the applicability of their use for capillary network analysis is discussed. The rationale for development of an alternative method balanced reduced subjectivity and capability of whole network analysis.

2.1.1 Velocity measurement techniques

Prior approaches for velocity measurement in living tissue provide insight into the novelty of analyzing whole networks of capillaries simultaneously. Quantitative velocity measurements were first proposed historically with the dual-slit correlation method established by Wayland and Johnson [174]. The dual-slit method is utilized under brightfield conditions and takes advantage of the plasma gap between adjacent red cells in the circulation. A gate is placed at each of two locations separated by a known distance on a television monitor. The instantaneous light intensity through at the gate is monitored at both locations. As red cells pass the gate, the signal decreases. When plasma is present at the gate location, the light intensity increases. A tracing of the signals over a period of time is obtained at each location. The two signal tracings are cross-correlated to determine the time interval that maximizes the degree of correlation between the two signals. This time delay is utilized along with the known distance between the two gates to calculate the velocity in the microvessel. The reliance of this method on the plasma gap requires that only small vessels may be analyzed. Furthermore, the focal depth of the perfusion at the locations under both gates must be equivalent to deliver similar signals at each gate for correlation. This method provides accurate descriptions of single vessel flows, but high magnification and clear optical imaging of the vessel. This requirement makes imaging curved, tortuous capillaries and measuring velocity therein troublesome. Further, simultaneous acquisition of a capillary velocity in networks with the number of vessels on the order of 20 - would not be possible.

Few alternative techniques have been proposed to examine velocity in an entire network. The flying spot method utilizes a reduced magnification that allows recording of a network of capillaries, but is entirely subjective and cannot measure velocities in curved vessels [156]. As a video recording of blood cells in capillaries is replayed, a small spot can be transposed onto the television monitor. Linear motion of the spot is controlled by electronic manipulation. When the motion of the spot matches the motion of red cells in perfusion, the velocity of the spot is obtained from a readout. Multiple capillaries can be measured from the same video through sequential viewing of the tape. This method would allow simultaneous acquisition of capillary velocity, but is highly subjective and user-intensive. Furthermore, the flying spot is inappropriate for curved vessels since the motion of the spot is linear only, and visually obstructed capillaries are difficult to analyze. A method for

simultaneous recording and objective quantitative analysis of perfusion in capillary networks continuously over length scales on the order of minutes was required for my study.

Newer microscopic imaging methods, such as two-photon laser scanning microscopy, take advantage of higher wavelength light that penetrates farther into the tissue to analyze even three-dimensional vascular flows in thick tissues [74]. These methods take advantage of line scanning techniques similar to those utilized in dual-slit photometry. Two-photon microscopic methods have not been applied to simultaneous imaging of a network of capillaries.

Another method that has been developed to measure velocity in microvessels is called laser Doppler velocimetry (LDV) [85]. The Doppler effect describes that signals reflecting from a moving object return to the signal source with modified frequency correspond to the object's velocity. LDV takes advantage of the Doppler effect through utilization of coherent laser light impinging on moving blood particles and analyzing the backscattered light for changes in frequency. The advantages of this method are the reduced amount of preparation time and low level of invasive surgery required to provide access to surface muscles. Furthermore, it allows assessment of perfusion at varying levels of structure, from whole muscles or tissues down to large vessels and portions of capillaries. But the drawback — especially for capillary networks — is that the laser light impinges on a region of tissue proportional to the wavelength of the laser light, and illuminates the tissue area larger than the laser due to backscattering. Although the technique correlates with previous results determined directly with intravital microscopic methods for large microvessels [85], the accuracy and applicability to capillary vessels in close spatial alignment has not been explored.

Particle imaging velocimetry (PIV) or particle tracking velocimetry (PTV) is a technique with emphasis on computing and imaging components. Perfusion in vessels may be monitored by either manually or automatically tracking objects as they pass convectively with the flow in the vessel. Generally a tracer particle is introduced to the flow field, although in some applications (such as lymphology [24]) this is particularly difficult, and recent imaging technology makes tracers unnecessary through very high frame rates of image capture (>10,000 frames per second [185]). The tracer particle can be a fluorescent microbead, a rolling white cell, or another component of the blood labeled with a colored- or fluorescently-tagged molecule. The technique has been further developed to automate the

computational aspects of PTV — manually parsing through thousands of frames of video to find tracked object locations would be an extremely labor intensive enterprize [27].

Among these methods, the intravital techniques employed in the laboratory were the most natural selection. A manual PTV method had been attempted on a pilot basis by our colleague, Dr. Chris Bertram, prior to my matriculation at University of California. Therefore, I began my studies with a particle tracking method, and quickly determined that a semi-automatic method to analyze and parse the data would be necessary. Following in this chapter are detailed protocols for intravital velocimetry I utilized to pursue my research objectives.

2.1.2 Analysis of microvascular velocity

Many publications in the 1970's and early 1980's characterize the velocity in individual vessels — including capillary tubes of various dimensions and small blood vessels [6, 83, 105, 188]. The use of the two-slit method was analyzed and several correction factors constructed to correlate the measured blood cell velocities with actual mean flow velocities.

In narrow capillary vessels only, the ratio of cell diameter to vessel diameter is approximately one — therefore, the empirical relation between particle velocity and mean blood flow velocity is approximately 1.19 [182]. This parameter was tested over a range of simulated hematocrits from 10 to 30%, and found to be very consistent. This result suggests that at the scale of individual capillaries, the hematocrit may not be the primary determinant of blood flow velocity. Moreover, particle velocities determined in experiments conducted below could be correlated to mean velocity values with this 1.19 multiple. But I believed that small deviations in the tracking of individual cells that may or may not be associated with true "centerline" velocity values. Furthermore, the rationale of using a correction factor on measured particle velocities to find a "mean volumetric blood flow" can be debated with the simple fact that capillary cross-sections are not circular along the length of the vessel. This assumption has been widely used in the literature, but may not be valid at the length scale of the capillary.

Without simple assumptions like this, it is difficult to generate a continuum mechanics-based approach in capillaries. To illustrate, we can follow the flow path of a single red blood cell as it passes through a skeletal muscle. The cell exits arteries and arterioles and rapidly

decelerates as the vessel dimension becomes smaller. At the same time, the apparent viscosity decreases as fewer and fewer red cells are present alongside, until the red cell is in single file capillaries. The filamentous glycocalyx brushes up against the red cell, providing a softer buffer between cell membranes and protecting the endothelial cell and its nucleus. The capillary centerline follows a tortuous path through non-circular cross-sections and curved vasculature. Slight path changes are influenced by both the red cell membrane mechanics [183] and fluid mechanics reacting to small surface character such as the glycocalyx or nuclei on the endothelium. The red cell paths are repeatable at bifurcations but probably stochastic down the tortuous vessel length. The red cell finishes the trip to the venule but may encounter a white cell negotiating with an endothelial cell while it rolls along, but partially obstructing the available lumen. Despite the occurrence of these events, reducing capillary perfusion to simple velocity measurements allows simplification for studying fundamental aspects of network perfusion. In the following, I will focus on the motion of red cells as they perfuse single file capillaries.

2.2 Experimental and theoretical methods

The primary method utilized for the completion of this research required the surgical preparation of rat skeletal muscle tissue and subsequent intravital microscopy. The monitoring of blood flow in microvascular networks allowed the establishment of computer algorithms that provided the final indices for the functional status for the capillary networks. The analysis facilitates the separation of deviations of vascular perfusion into temporal and spatial components. The variability of red cell velocity can be further analyzed as a function of position in the capillary network and within each capillary itself.

2.2.1 Surgical methods for intravital microscopy

Tissue may be surgically extracted from anesthetized animals such that damage to the tissue is minimized and the perfusion to the muscle is similar to it's native state. Preparations of many tissues are outlined in the literature, but primarily I utilized the rat spinotrapezius muscle preparation [52] and the rat mesentery preparation [187]. Both of these surgical preparations were first developed with the founder of our laboratory and premiere microvascular researcher, Dr. B.W. Zweifach. I then optimized the general guidelines of the preparations for my own use.

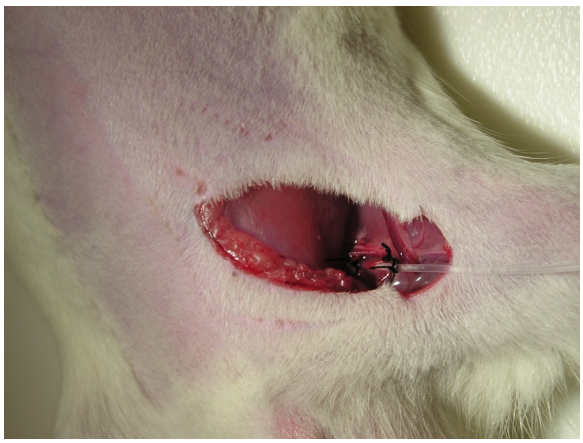

Figure 2.1: Anesthetized rat with femoral catheter inserted for maintenance of anesthetic state. The rat is initially anesthetized intraperitoneally or intramuscularly, then shaved and restrained prior to cannulation of the femoral vein.

All of the animal preparations were developed following guidelines set forth by the NIH for humane treatment of laboratory animals. Oversight was provided by UC San Diego's Animal Control Program in compliance with the Association for Assessment and Accreditation of Laboratory Animal Care (AAALAC) standards.

The preparation of the spinotrapezius muscle begins after delivery of general anesthesia is allowed by catheterization of the femoral vein as in Figure 2.1. A catheter is inserted following intraperitoneal injection of sodium pentobarbital (Nembutal, 50mg/kg animal). Further anesthesia is provided when necessary as determined by nerve stimulation in the toe or tail (5mg/kg).

Spinotrapezius muscle preparation

The spinotrapezius muscle is a skeletal muscle with muscle fibers aligned parallel to the spine; it contains a mixture of Type I and II fibers. The structure of the vasculature in the muscle has been well studied in a series of papers that outlined the arteriolar [31], capillary [133], and venular networks [29]. There is a fully developed system of arcade arterioles fed by two to three feed vessels, that will be designated *proximal*, *medial*, and *distal* feeders. Figure 2.2 schematizes the typical shape and vasculature of the spinotrapezius muscle. It should be noted that the tissue is significantly thinner near the proximal feeder on the dorsal aspect of the muscle — the tissue in this corner of the muscle consists of a single layer of muscle fibers. As the fibers approach the spine in this thin regional layer the fiber direction shifts from parallel to the spine to a 30° – 45° diagonal to the spine.

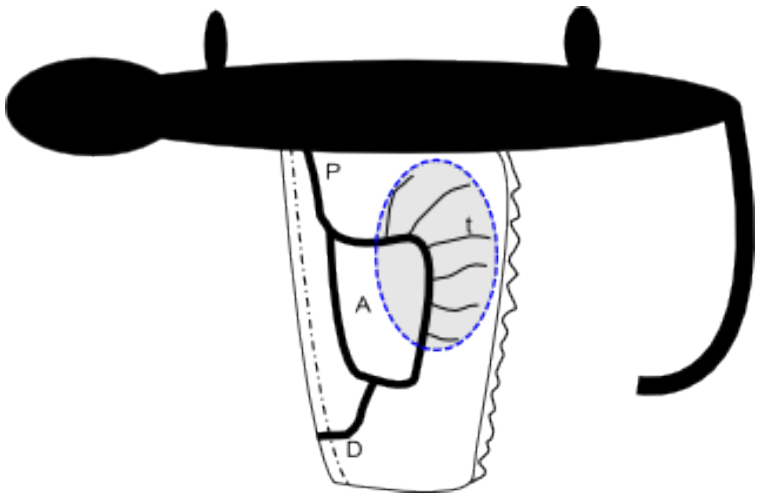

Figure 2.2: Schematized representation of a rat with enlarged spinotrapezius muscle. The arcade arteriole network ("A") is shown with feed vessels "P" (proximal) and "D" (distal). Examples of transverse arterioles extend from the arcade arterioles and end in terminal arterioles ("t"). The area inside dashed circle designates the thin region of muscle that is optimal for imaging. Also displayed are the dot-dashed area to the left of the muscle depicting the strip accessory muscle and the jagged line to the right of the muscle showing the spinal connective tissues.

The fibers are also observed to be discontinuously arranged into a "finger" pattern that is visible in the example shown later in Figure 2.6. Obtaining images of capillary network perfusion of this region of muscle tissue is especially preferred due to the extremely thin tissue offering low attenuation of light and simplified capillary network topology.

Following general anesthesia, the animal was shaved and placed on a heated stage fitted with a 22mm round window as in Figure 2.3. A dorsal midline incision was made from just below the neck extending down 4-5 cm to just above the hindlimbs. This exposes a layer of fascial tissue on back of the animal. Superfusion of Krebs-Henseleit solution allowed control of the tissue environment — temperature, osmolarity, pH and oxidation of the tissue must be maintained to minimize tissue damage. The solution contained sodium chloride, potassium chloride, magnesium sulfate, calcium chloride, and is buffered with sodium bicarbonate by a dissolved 95% nitrogen / 5% CO2 gas mixture. Krebs-Henseleit was maintained at 37 °C in a recirculating pump (Julabo West, Vista, CA) .

The fascia that covers the right spinotrapezius muscle was carefully removed with surgical scissors and forceps. A small superficial incision into the fat pad distal to the right shoulder was made. A tissue called the *strip accessory muscle* was then located, and used as a landmark to extend the incision through the fat pad and into the fascia. By lifting

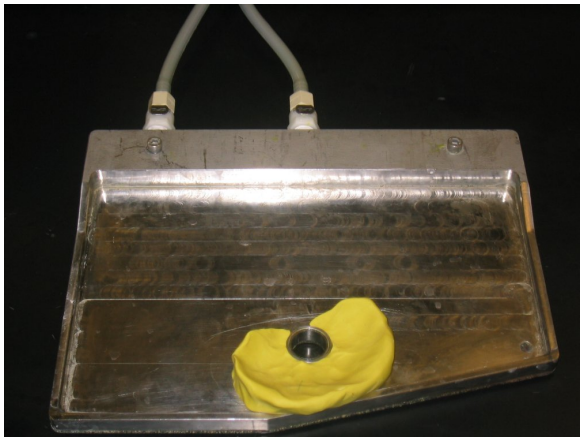

Figure 2.3: Heated metal stage with vacuum attachment provides body temperature control and simple superfusion of the tissue. The yellow clay surrounding the round window allows stabilization of the finished preparation.

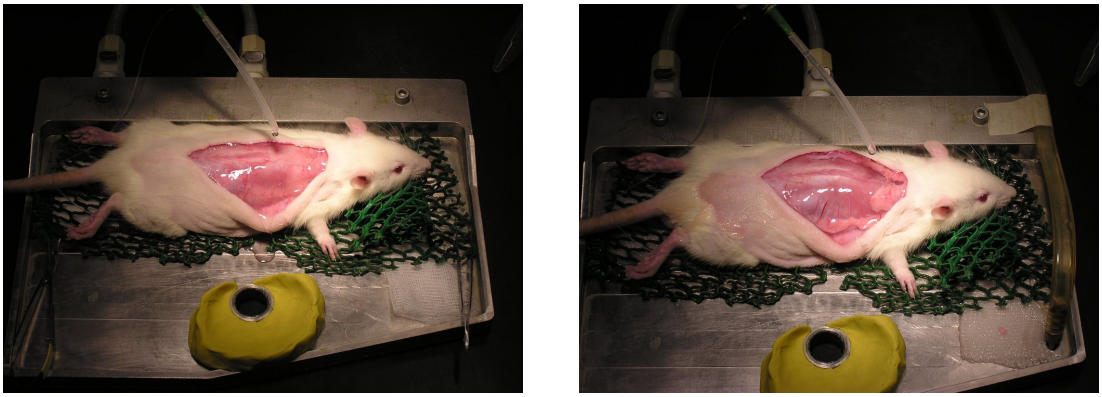

Figure 2.4: External aspect of the spinotrapezius muscle, shown with (A) and without (B) fascia tissue that lies between the muscle and the skin. Also, the subcutaneous fat pad has been removed up to the brown (highly vascularized) fat pad.

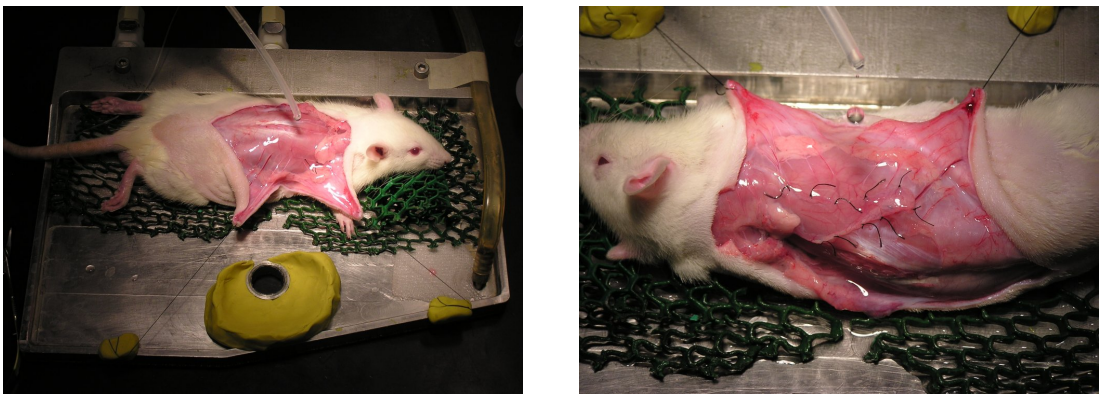

Figure 2.5: (A) Animal rotated 180° to continue separation of spinotrapezius muscle from underlying latissimus dorsi. The opposite spinotrapezius muscle — on the animal's left side — is separated from the spine. Two sutures are placed in the strip accessory muscle for grasping the muscle. Lastly, a perpendicular incision is made through the skin dorsal down to the abdomen with two sutures to maintain a clear working area. (B) The spinotrapezius muscle completely separated from the underlying latissimus dorsi and spinal connective tissue. A series of sutures are placed around the muscle for stabilization.

the fascia and/or fat pad and cutting the clear connective tissue between the fascia and the spinotrapezius muscle, the external aspect of the muscle was completely exposed as shown in Figure 2.4B. At this point, the flap of skin that covered the right side of the animal's back was dissected perpendicular to the first incision. Two lengths of suture were connected to the corners of the skin segments for holding the skin away from the surgical site. Two half-centimeter lengths of 6-0 suture were also tied to the strip accessory muscle to facilitate manipulation of the tissue. A dorsal incision along the *left* side of the spine severed the connective tissue that integrates the left and right spinotrapezius muscles into the spine. The animal was then rotated and placed on his opposite (left) side to improve access to the spinotrapezius (Figure 2.5A).

The spinotrapezius muscle was then surgically separated from the underlying latissimus dorsi muscle. There was another layer of connective tissue that was systematically separated by lightly pulling on the small 6-0 suture segments and trimming away exposed tissue connections. In some muscle preparations, there were medial feed vessels that extend into the spinotrapezius muscle from the latissimus dorsi. In this case, two ligatures were placed above and below an incision through the latissimus dorsi — blood flow in the muscle is better maintained by prevention of hemorrhage in this preparation. A series of 6-0 suture ties were placed first along the strip accessory muscle and then in thicker regions of muscle after the spinotrapezius begins to merge with latissimus dorsi. It was necessary to cut

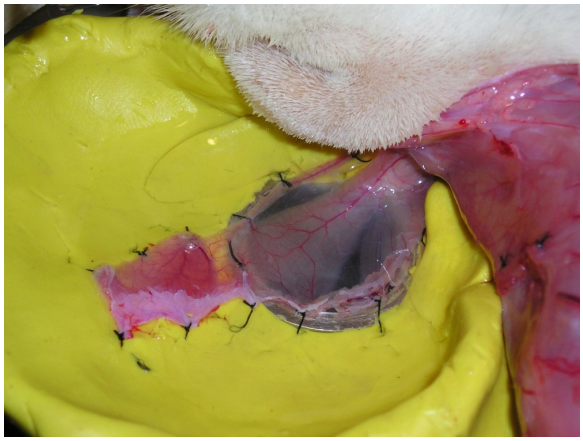

Figure 2.6: Spinotrapezius muscle completely prepared: tissue connected only at proximal feed point, muscle immobilized to clay, and animal motion minimized.

through a region of the latissimus dorsi at the distal end of the spinotrapezius muscle. The distal feed vessels are ligated similarly to the medial vessels. Ties are placed in the distal end of the muscle and then the connective tissue just distal to the muscle is dissected.

A series of suture ties are placed in the connective tissue along the spine, and the muscle is further freed from the spinal connective tissue. The caudal incision made just prior to flipping the animal around allows this simple final step to free the muscle completely from the spine. Special care must be made at the proximal end of the muscle. As mentioned, the thin region of the muscle that is of primary importance due to simplified microvascular structure adjacent to the final incision along the spine. Most previous descriptions of the spinotrapezius preparation neglect to extract this far under the fat pad to the insertion point of the muscle — to be able to properly image flow in the thinnest portion, the complete removal of the muscle from the spine is necessary. A completely excised image of the spinotrapezius muscle is shown in Figure 2.5B.

Stabilization of the muscle was required for completion of the preparation. Yellow clay was shaped around the stage window to allow pooling of Krebs-Henseleit on top of the muscle preparation (Figure 2.3). The shape of the clay formed a basin to maximize water retention for optimal imaging conditions with the water immersion objective (Leitz, 0.3 NA, 10x magnification). The animal was moved to rest next to the clay and window, with the muscle insertion point — below the right shoulder — directly adjacent to the stage window. The animal's right forepaw was manipulated to push the muscle insertion point closer to the stage window. A balance must be attained between water-layer retention and

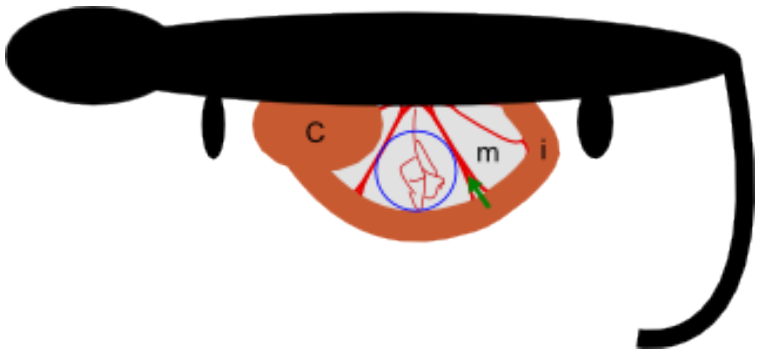

Figure 2.7: Schematic displaying the rat mesenteric tissue preparation. The cecum (**C**) is located and gently guided through the abdominal midline incision, pulling the small intestine (**i**) out of the peritoneal cavity. As the small intestine is guided out, mesentery sectors (**m**) are examined for small blood vessels at the limit of visual detection. When a suitable sector is located it is placed directly over the stage window (blue ◯). Stabilization of the intestine and mesenteric sector vessels (green →) is achieved through application of moistened gauze.

muscle proximity to the stage window — generally, a shorter vertical distance between the muscle insertion point and the window is preferred. When the correct body posture was found to minimize this distance, the right forepaw was taped in place. In some cases, it was also beneficial to immobilize the left forepaw across the body and next to the right paw for further reduction of the distance between the insertion point and the glass coverslip. The skin sutures as seen in Figure 2.5 were attached to clay pieces affixed to the stage; the skin was then pulled to minimize water siphoning away and further stabilize the appropriate animal posture. The small 6-0 sutures were then pressed into the yellow clay around the window such that the muscle was spread flat across the window. Tissue motion due to respiratory motion must be negated and the desired tissue locations must be accessible by the objective body. When all of the sutures were affixed in the clay, the spinotrapezius muscle preparation was complete.

Mesentery preparation

The mesentery is a thin tissue (∼100 microns) along the small intestine divided into sectors by large mesenteric sector vessels. A schematic displaying the proximity of a typical mesentery sector to the intestine is shown in Figure 2.7. Also shown is the typical microvasculature that perfuses a sector; although, it should be noted that many mesentery sectors spontaneously develop microvessels across the sector. Most sectors never show apparent, perfused vasculature. The number of vessels in mesentery sectors actually

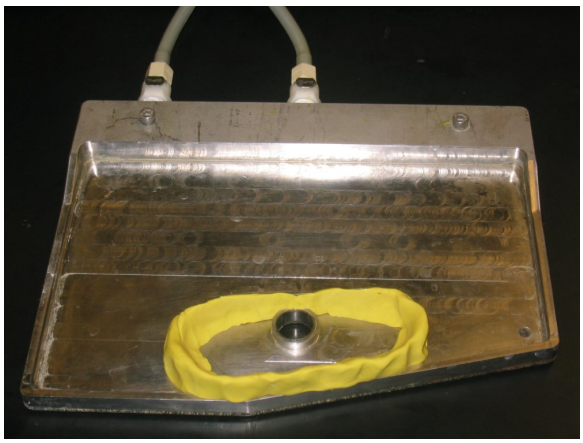

Figure 2.8: The stage is readied for a mesentery preparation by molding yellow clay in a ring to create a pool of Krebs-Henseleit. The intestine and mesentery is sensitive tissue, so extreme care must be used in alignment and stabilization.

varies from animal strain to animal strain, and generally increases with age of animal. In many ways, the mesentery is an uncharacterized tissue with little explanation as to its function. But also, few tissues have been examined as closely as the mesentery — at least under intravital microscopy — because the tissue lends itself to the requirements of intravital microscopy. Since the tissue is so thin, transmitted light microscopy may be easily achieved. Like many surgical preparations however, it is an easy tissue to image poorly; to achieve beautiful images requires artful preparation of the tissue as described below.

The preparation of the mesentery begins after delivery of general anesthesia is allowed by catheterization of the femoral vein. The cannula are placed following intramuscular injection of sodium pentobarbital in the hindlimb (Nembutal, 50mg/kg animal). Further anesthesia is provided intravenously when necessary as determined by nerve stimulation in the toe or tail (5mg/kg).

A stage was prepared similar to the spinotrapezius preparation, but the clay was shaped to form a pool (see Figure 2.8); the animal was rested on his back with its head aligned to the left of the stage. The animal was further prepared by shaving the hair from a region of about 8 cm^2 on his abdomen. Then, the preparation began with a 1-2cm long abdominal midline incision through both the skin and the abdominal wall, taking care to avoid cutting any vital organs as shown in left panel of Figure 2.9. Two long, wooden cotton swabs were doused in Krebs-Henseleit solution, and the peritoneal cavity was then probed for the cecum. When the cecum was located — usually right below the skin — it was pulled through the incision as the animal is placed on its side. The Krebs-Henseleit solution

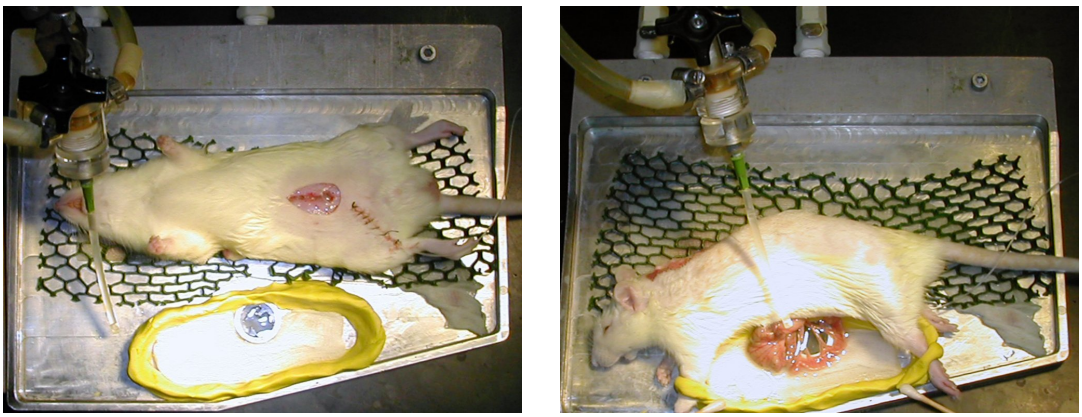

Figure 2.9: *Left:* Rat abdomen shaved and cleaned for mesentery preparation. A 1–2 cm midline incision is made in the abdominal skin and muscle to allow access to the vital organs. *Right:* Rat placed near moistened clay pool, while focusing on intestinal and mesentery tissue. The tissue is gently pulled through the abdominal incision, then arrayed over the window to find a mesentery sector containing vasculature.

was constantly superfused directly on the cecum and the attached intestines to avoid any tissue drying. These tissues were pulled through the incision to examine the sectors for microvasculature by eye as shown in the right panel of Figure 2.9. If a vessel crossing the sector was apparent by eye, there was a high probability that a significant number of vessels were visible under the microscope.

After a sector was located with a large crossing vessel, which likely perfused significant microvasculature, the tissue was stabilized over the stage window. Mesenteric tissue is extremely fragile, and extreme care must be taken to avoid direct contact with the tissue at all times. The force was instead applied to the intestine that surrounded the particular sector of interest using moistened cotton swabs. Sterile cotton gauze pads were immersed in the Krebs-Henseleit solution and placed around the stage window contacting the stage (Figure 2.10). The cecum and intestines were placed on the gauze such that the sector was gently restrained by the contact with moist gauze. Then, another layer of moistened gauze was prepared and laid over the intestine and cecum. This ensured the tissue received constant contact with Krebs-Henseleit solution. Also, the weight of the moist gauze provided gentle pressure that reduces the effect of peristaltic motion on the image quality; any motion made proper imaging difficult. Another source of motion to eliminate was due to the high rate of blood flow through the sector vessels (green $\rightarrow$ in 2.7). Additional pieces of moist gauze were placed over the sector vessels to reduce this motion.

The final preparation as shown in Figure 2.10 is a typical mesentery preparation,

Figure 2.10: The mesentery tissue displaying vasculature is stabilized over the stage window. The intestine and/or cecum is covered in moistened cotton gauze both to maintain tissue viability and to preclude peristaltic motion. The Krebs-Henseleit is constantly superfused over the gauze and the selected mesenteric window.

but the application of each piece of gauze varied for each preparation. It was common to place a finished preparation under the microscope only to see that there is some small motion of the tissue. A slow arrhythmic motion suggested that peristaltic movements would require more gauze over the intestine. Slow, regular motion was caused by respiration of the animal, which was eliminated by slight postural modifications. Rapid motion indicated that the sector vessels needed further immobilization. This portion of the preparation was often frustrating, but successfully attenuating this source of disturbance improved the quality of the rest of the experiment.

2.2.2 Velocity measurement by intravital microscopy

As described above, to measure the perfusion velocity in capillary networks I selected a particle tracking velocimetry method. Several particles have been used to measure hemodynamics *in vivo* [134] and *in vitro* [181] including silica or polystyrene microspheres or even gelatin particles. Each particle has benefits and drawbacks regarding their use. Microspheres are rigid particles commercially available in a wide range of sizes, and pre-labeled with a range of fluorophores or markers. But because they are rigid, a sphere too large could plug a vessel and a sphere too small may flow in distinct streamlines in even the smallest capillary. Blood cell ghosts and latex particles are similar in that they properly reflect the red cells' ability to deform in response to flow disturbances.

An attractive approach is to apply a fluorophore to the animal's own blood cells, making them the particle of choice to track. This has the advantages of availability and uniquely appropriate hemodynamics: a single microliter of blood has approximately 1,000,000 red blood cells, each of which was designed to deform and respond naturally to flow disturbances. The only drawback is that I must obtain a blood sample, removing cells from their natural environment, and then apply a label to facilitate tracking.

Blood cell labeling

A sample of whole blood was obtained from the venous catheter and labeled with fluorescent membrane stain to enable tracking of cells as they travel through capillary networks. Approximately 6% of the animal's total weight was assumed to be blood, and the density of blood was assumed to be 1 g/mL. Then, for a 200 gram animal, the blood volume was approximately 12mL. A 200 μL sample is withdrawn, which was approximately 2% of the total blood volume. As the range of animal size included in my studies was approximately 200–400 grams, a 200μL sample of fluorescently labeled blood reflected an actual percentage ranging between 1-2% blood volume. The blood sample was diluted in Hank's Buffered Salt Solution (HBSS, Sigma, St. Louis, MO) and centrifuged for 10 minutes at 400g. The supernatant was discarded, and the cell pellet re-suspended in Diluent C solvent. An equal volume of Diluent C with PKH26 lipophilic membrane stain ($5x10^{-6}M$, Sigma) was prepared. Pretreatment of the PKH26 stock solution included 30min warming in 37 °C water bath followed by two-minutes sonication to remove any dye crystals. When the cells and dye solutions were ready, they were combined and incubated with the dye on a shaker for five minutes. The dye–cell insertion reaction was stopped by adding an equal volume of 1% albumin solution at precisely five minutes to avoid cell toxicity. After one minute of shaking with albumin to ensure total reaction inhibition, the cells were again separated by centrifugation for 10 minutes. Following three wash steps with HBSS, the cells were resuspended in heparinized saline and left on a shaker for the duration of the surgical preparation.

Network selection

When the surgical preparation was complete, the animal stage was moved to the intravital microscope. The dispensing head for the Krebs-Henseleit solution was magnetized

to the metal stage, and stage heat and vacuum were connected. The lamps for brightfield microscopy (100W) and epi-illumination (100W mercury lamp) were both powered on and the microscope focused on the tissue region of interest. The thin portion of muscle was trans-illuminated – brightfield – and networks were selected on following criteria:

- Networks in single layers of muscle fibers were preferred because the darkfield images would display minimal autofluorescence and no perfusion in other focal planes would confound particle tracking
- Networks must be supplied by only one terminal arteriole and drained by one collecting venule so that capillaries with different pressure-flow relationships were not compared
- Networks should be simply defined and have primarily straight capillaries

It should be noted that some of these criteria are difficult to assess under brightfield conditions, because every capillary vessel is not visible in skeletal muscle. The first criterion was important but also difficult to require: in a large muscle there are hundreds of networks, but only a few tens of networks in the thinnest portions. In some cases, networks may be utilized in moderately thicker portions while still minimizing autofluorescence. Additionally, the second and third criteria were rules that were applied to reduce variability between networks. There was also significant network selection after the cells had been returned to the general circulation and were visible with epi-illumination. After several networks were located, data acquisition was begun.

Image acquisition

Images were obtained of blood flowing the selected capillary networks for one minute periods. The cells labeled with the PKH26 fluorophore were excited by green light and emitted photons in the red range. See Figure 2.11 for exact fluorescence information of the fluorophore. A filter cube was utilized to modify the white mercury-generated light to the excitation-emission requirements (N2.1, excitation bandpass 515-560nm, emission longpass 590nm; Leica Microsystems, Bannockburn, IL). The light path through the intravital microscope (Leitz, Wetzlar, Germany) was directed to a silicone-intensified target (SIT) camera (MTI66, DAGE, Michigan City, IN) set on automatic gain and black levels. Preview of output was sent to a television monitor and minor changes to the setup such as camera angle or stage offset were made. At this time, a standard high-fidelity video cassette

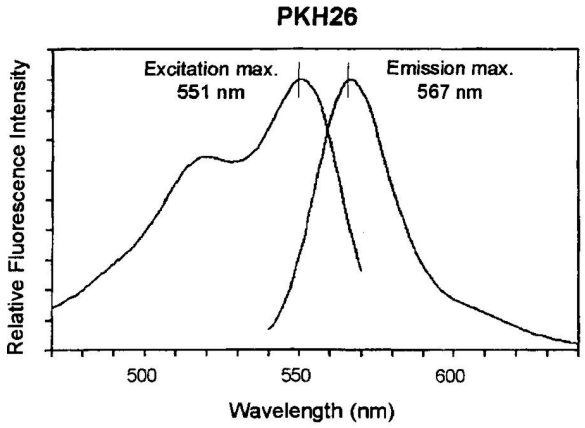

Figure 2.11: Excitation-emission spectra for PKH26, reproduced from Sigma product information sheet. To visualize cells labeled with PKH26, a filter cube standard for rhodamine fluorescence modifies incident white light, allowing only green light to pass through the excitation filter. The green light impinges on the PKH fluorophore which then emits a red-orange colored photon. A longpass filter allows only these red-orange photons to be viewed.

recorder (VCR) was prompted to record video of cellular transport through the network of interest. A timestamp was created on the videotape to facilitate future processing of the analog video. At least one minute was obtained: additional footage was generally recorded to ensure that one full minute of consecutive frames was available for analysis.

A one minute movie of cellular transits recorded onto videotape at video rate consisted of 1800 individual frames — that is, 60 seconds of 30 frames per second at video rate. Each frame on videotape reflected the state of the capillary network at a single instant in time, as shown in Figure 2.12. The cells are evident as the bright shapes in three consecutive frames (A, B, and C) and schematically represented (D) as a set of colored shapes.

2.2.3 Algorithms for automated analysis

A large amount of data was generated by the aforementioned image acquisition. The captured field of view at the magnification utilized was approximately $1mm^2$ and contained one to two muscle fibers. The muscle fiber(s) were perfused by one terminal arteriole and collecting venule — connected by an extensive capillary network of up to 50 distinct capillary segments. Each capillary segment was perfused by many fluorescent cells over the time period recorded in each movie. The analysis of a single movie is described below.

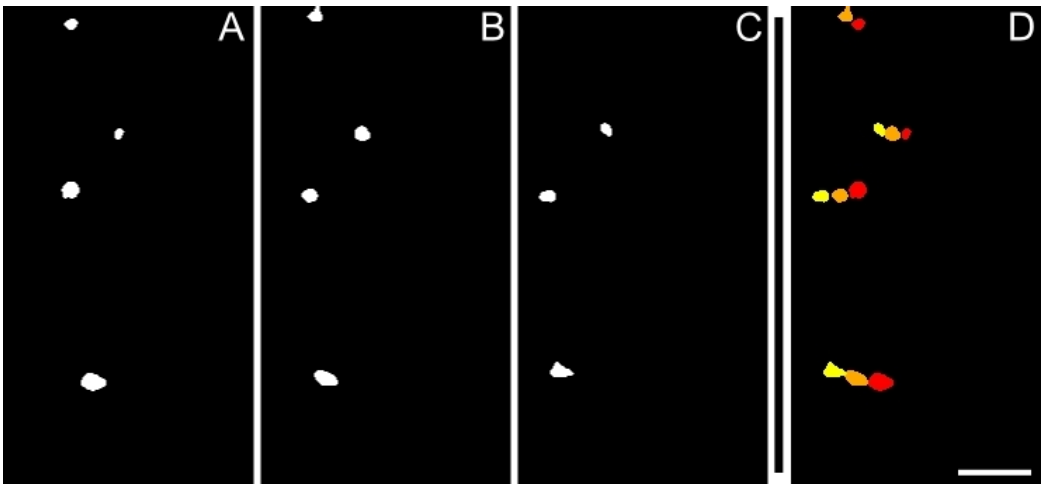

Figure 2.12: Individual image from one minute obtained via intravital microscopy (A) from frame n, (B) frame $n+1$, and (C) frame $n+2$, then processed and segmented. (D) A Schematic overlay of the images n, $n+1$, and $n+2$ to display the transmission of cells through the capillary network as time elapses. The scale bar shown in (D) represents 100μm and is applicable for (A)-(D)

Image digitization and deinterlacing

Images from the SIT camera were 8-bit grayscale — the photons emitted from PKH26 molecules on the passing blood cell were captured by the SIT camera and each pixel intensity in the final frame was assigned an intensity ranging from 0 to 255. The 8-bit signal was output via coaxial cable to be recorded to video tape with a standard video cassette recorder (VCR). The 8-bit signal is encoded via NTSC video protocols.

The video cassettes were then replayed in conjunction with a personal computer equipped with proprietary imaging software (StreamPix, v3.13, Norpix, Montreal, Québec). StreamPix allowed the capability of digitizing from videotape at video rate — 30 frames per second. Other software packages are very useful for digitizing still images from videotape, such as the freeware NIH Image or even commercial software like Image-Pro Plus, but they are incapable of video rate digitization. Also, it is possible to find cheaper hardware and software capable of converting analog video from cassette tapes into digital video on hard drives; these cheap alternatives should be avoided! In many cases, compression of video using popular MPEG codecs reduces the quality of each image. This is very enticing given the cost of additional hard drives, but compression degrades the video signal utilized for image analysis.

One minute sequences of video for digitization were found by following careful

cues recorded to the videotape; timestamps relative to the start of the experiment were also logged to allow re-digitization of the movie if necessary. The video was started and digitally acquired via StreamPix at the appropriate cue. The movie was digitized using the `1 minute` setting in StreamPix, which delivered 1799 frames of digitized footage. The minor discrepancy between the expected 1800 frames and delivered 1799 frames is explained by the *actual* frame rate digitized of 29.97 frames per second.

The StreamPix software required the use of modern hard disk drive capabilities and capacities. Unfortunately, the package was not equipped with a setting to define the dynamic range of the input signal. Therefore, the 8-bit signal output by the camera and recorded to tape was digitized as 24-bit RGB video (three 8-bit color channels). A single frame digitized under NTSC protocols contains 640 vertical lines by 480 horizontal lines for 307,200 pixels. An 8-bit image from video — 8 bits is one byte — required only 307,200 bytes of storage space. But the 24-bit image required 921,600 bytes. A single movie with 1799 frames needs approximately 1,658,000,000 bytes — about 1.5GB — hard disk space. Rapid data throughput was also required, since 30 fps of about 1MB equals 30 MBps (240Mbps). A rapid, high capacity disk drive was used to handle these requirements (Seagate, 300GB capacity, SATA2 [300MBps max] connection, 8MB cache).

Images generated with the NTSC standard were also interlaced. This means that on a 60Hz clock cycle (59.94Hz precisely), alternating *lines* of the frame were refreshed. For the n^{th} cycle, the odd lines 1, 3, 5, ... and 479 were all refreshed. Then, on the next clock cycle, n+1, the even lines 2, 4, 6, ... and 480 were updated. But StreamPix software only recognized half of the lines as valid, because it was locked into the video rate defined by the NTSC standard. An included option in StreamPix allowed the *deinterlacing* of each of 1799 frames of the movies. The lines of each movie that were valid (either odd *or* even) were duplicated in the place of the invalid lines. This created a smooth-playing movie for analysis. The movie was then exported as a multi-page `tiff` image. The image was imported into MATLAB as a `tiff` and the dynamic range reduced from 24-bit to 8-bit, using a custom conversion script. This had the effect of saving approximately 1GB of disk space per movie.

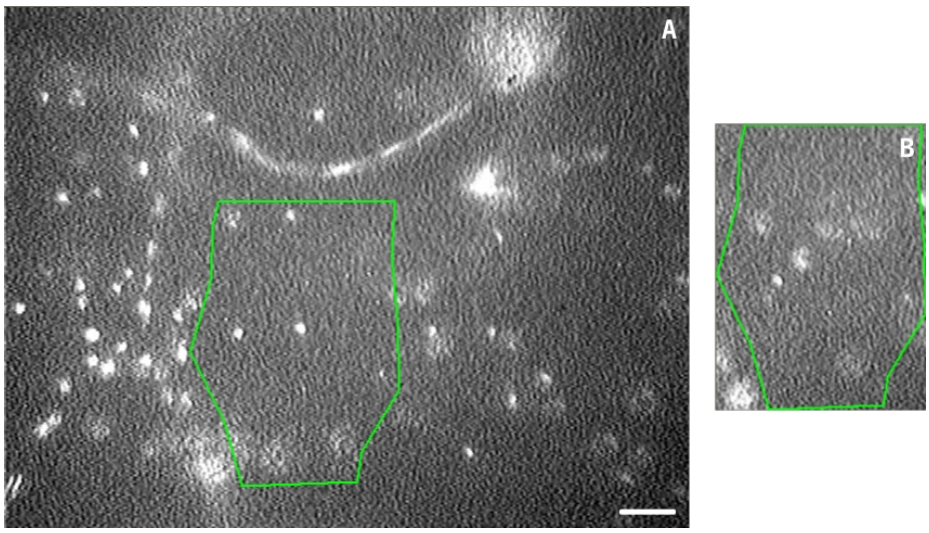

Figure 2.13: An example image with a region-of-interest constructed to focus processing on capillary vessels only before (A) and after cropping to size of ROI (B). A polygonal green line is drawn in the original 640 pixel by 480 pixel image using a series of mouse clicks as the movie is playing to exclude locations of arterioles and venules. The length bar in (A) is consistent for the following figures and represents 100 microns.

Image processing

The images recorded from a given network were processed to reduce noise and facilitate tracking of red cells. A rigorous period of trial and error established processing methods to apply to all image datasets equilaterally. The commercial imaging software Image Pro Plus (version 5.1, Media Cybernetics, Baltimore, MD) was used to construct the imaging protocol, but most of the functions are also applicable in MATLAB. But the task of finding the combination of several image processing techniques, each with different input parameters, was best solved with a commercial package like Image Pro Plus.

The first step of the image processing protocol was the establishment of a region-of-interest (ROI) as depicted in Figure 2.13. This step allowed a full frame image (640 pixels by 480 pixels) to be reduced to the minimum area that describes the capillary network. Since the capillary vessels were of primary interest, every effort was made to exclude areas of the full frame image that contain arterioles or venules. The differentiation between capillaries and arterioles or venules became difficult, especially at the transition between vessels. Bifurcations near the transverse arteriole and collecting venule were avoided, but some larger vessels may extend far into the capillary region. This portion of the image processing was subjective, but with experience the extraction of capillaries from arterioles

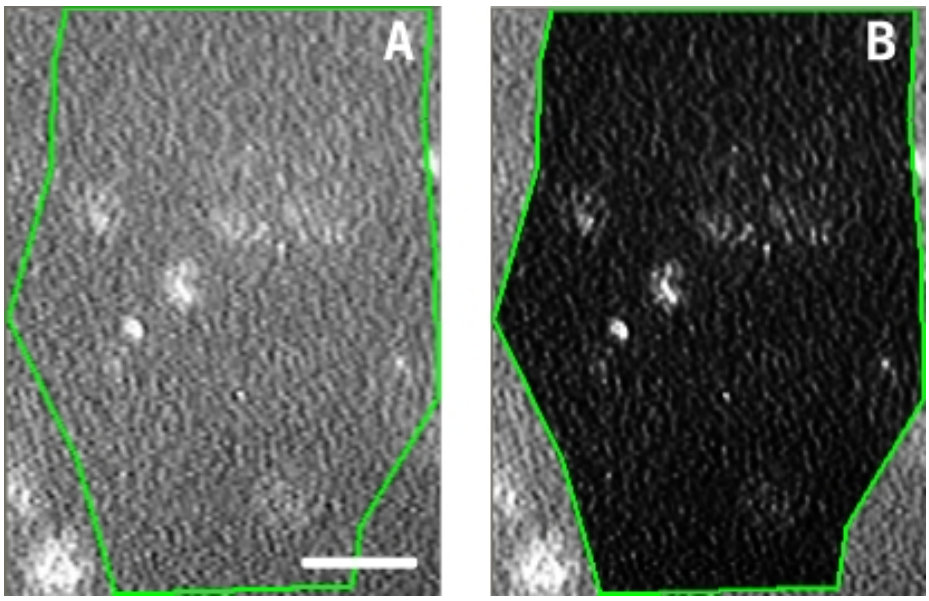

Figure 2.14: An example cropped image before (A) and after (B) a gamma transformation. A gamma transform of the images causes the dark background pixels inside the ROI to become darker, while increasing the intensity of the bright cell pixels. This enhances the effect of segmentation in the intermediate intensity range. The length bar in (A) represents 100 microns.

and venules was standardized.

One key feature of Image Pro that aids placement of the ROI is that the software allows human-computer interface (mouse clicks) while the sequence of frames was advancing. In this way, the region of interest was defined while visualizing the motion of fRBCs through the network. Cells that show high degrees of deceleration upon entering a vessel are deemed to be transferring into a capillary from an arteriole; conversely, cells accelerating upon leaving a vessel may be entering a venule. These two situations were avoided during construction of the ROI. Image Pro software also allowed the creation of a polygonal ROI which was optimal for defining capillary networks in various shapes. Following final ROI construction, the movie inside the ROI was duplicated as shown in Figure 2.13.

One drawback of high-sensitivity cameras, even with the latest electron-multiplication or back-thinned charge-coupled device (CCD) technology, is that gain settings create noisy images. The SIT camera was no different: the images recorded from the SIT camera were relatively noisy. As seen in Figure 2.14, the fluorescent cells were perceived as white regions rated at 255 on an 8-bit intensity scale — from 0 to 255 — in a field of grainy gray. The scale of the cells was inflated to the point where they were up to five times the actual cell

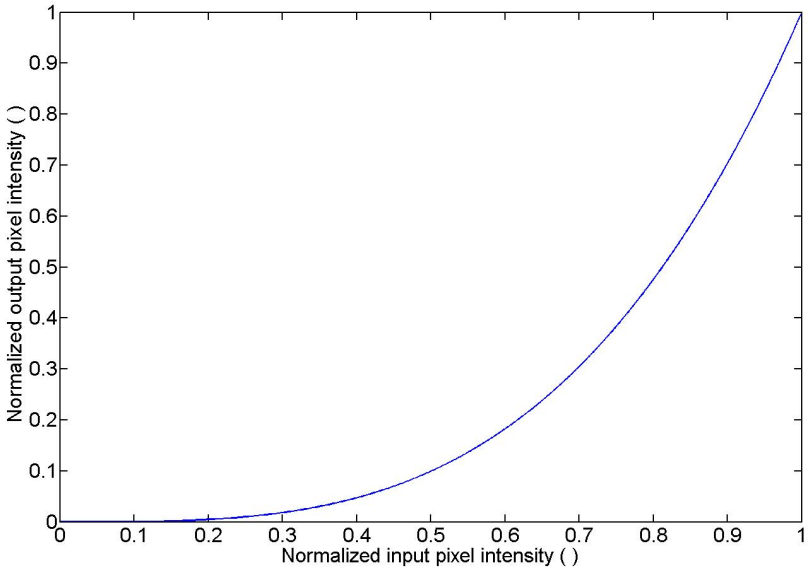

Figure 2.15: The gamma transform selected to modify the contrast between fRBCs in the foreground and tissue background. Gamma transforms operate on each pixel intensity by re-mapping the intensity profile according to the curve shown above. This causes gray levels in the middle range which are associated with background to have reduced intensity, while bright pixel intensities associated with fRBCs are unaffected.

size due to "blooming" effects in the camera. Additionally, some cells displayed a comet tail opposite the direction of their travel. This was due to decay of the signal that was slower than the cell transit time through the network. These phenomena were counteracted in part by reducing the background of the image. A 0.3 gamma transform was applied to the images (Figure 2.15). The output intensity was scaled based on the transform's effect on the input intensity. Pixels with low, black intensity were further reduced, and pixels with high, white intensity were unchanged. The strength of the nonlinear intensity transform redistributed pixel intensities such that only very white pixel intensities remained white pixels in the output image while the remaining gray pixels were reduced to black. Also note that the transform affected only the area inside the ROI as in panel B of Figure 2.14.

Noisy pixels that were very white were still prominent in a gamma transformed image. To eliminate this Gaussian noise, a 7x7 median filter was utilized. A box that was 7 pixels square was centered on every pixel, as schematized in Figure 2.16, and this box defined a neighborhood around the pixel. The intensity values in the neighborhood were listed, and the intensity of the center pixel was re-assigned to be the median value in the neighborhood. In this way, a large number of bright white pixels must be co-localized to maintain white intensity in the final image. Therefore, noisy pixels were eliminated,

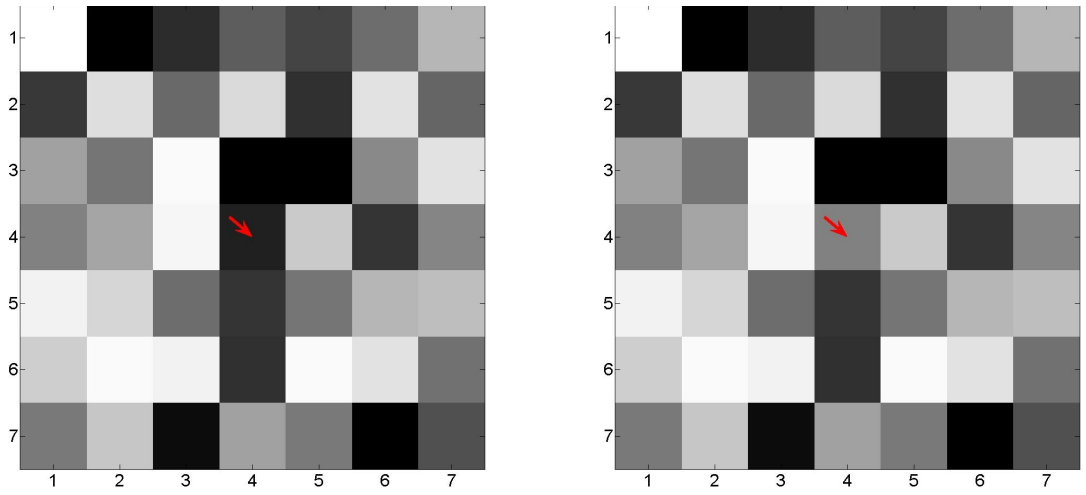

Figure 2.16: Schematized function of the median filter in imaging: the center pixel, shown with a red arrow, prior to the filtering process (A) and after (B). The pixel intensities in the 7x7 box are ranked and the center pixel is assigned a new value corresponding to the median of the ranked intensities. In this case, a dark center pixel with an intensity of 31 was replaced by a pixel with more average intensity, 123. The example was composed of $7x7 = 49$ random intensities, so it is natural that the replacement value would be near to the overall median, 128. This process is carried out for every pixel in the ROI.

as shown in the example in Figure 2.17. This also has a slight erosion effect on the cell outline, such that the final cell shapes are smoothed. The comet tails were also often seen to be diminished in intensity. These two side effects also allowed improved cell centroid estimation.

Calibration of each set of images was achieved using the Image Pro Plus spatial calibration wizard. An image of a micrometer was taken with the same objective and camera. Then, a series of lines of known pixel length were drawn on the micrometer image. The computer requires input of the number of microns that each line spans, from which the micron to pixel ratio is determined. For the system comprised by the SIT camera with the 10x water immersion objective, the approximate micron to pixel ratio is 1.95:1. This correction factor can be applied either before or after image tracking, but for consistency it was applied at this time in processing each set of images.

At this point, the images were ready for feature extraction. The critical problem that must be solved was selection of the *intensity segmentation* value, or the intensity value above which cells may be tracked and below which only noise exists. In practice, the selection of a single intensity value was often problematic. But each of the steps above had a single critical purpose to enhance the distinction between the foreground objects (the cells)

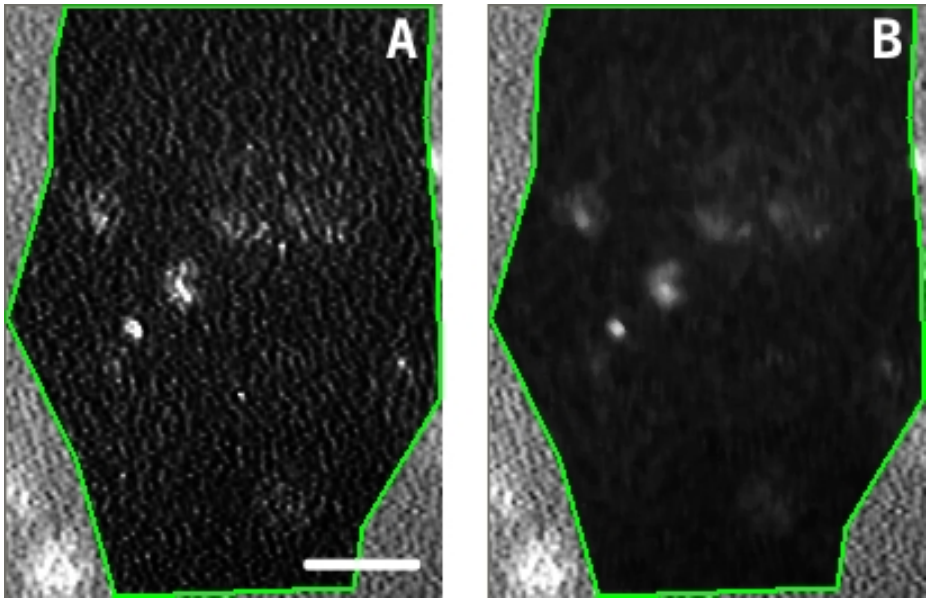

Figure 2.17: Example of the function of a median filter on the image region-of-interest. (A) Before the noise has been reduced and the edges of the cell objects have been smoothed and (B) after median filter has been applied. The length bar in (A) represents 100 microns.

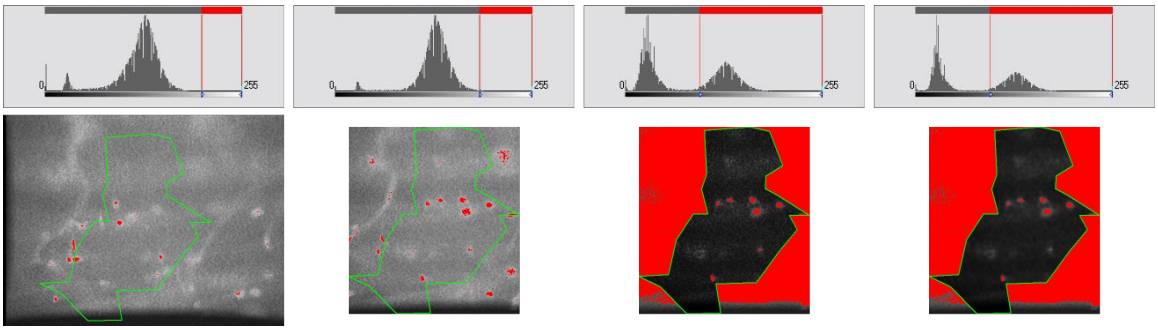

Figure 2.18: The histogram values above the images display the effect of the processing steps on the segmentation range. The uncropped image (far left) has a single large peak in the middle intensity range — the small peak at the lowest intensity reflects the dark portion at the bottom of the image which is a function of the parabolic intensity profile of the camera. The cropped image (middle left) has a similar histogram, but the peak width at half maximum is slightly reduced, as expected by the overall reduction in background pixels. The image after contrast enhancement (middle right) actually displays two intensity ranges, but there is a low level of noise between the two. The final image (far right) taken after median filtering shows very little noise between the intensity peaks, which is ideal for image segmentation and threshold selection.

and the gray background tissue. This process is illustrated in Figure 2.18 with a series of image histograms generated from Image Pro. The initial histogram and image in the top left was un-cropped, and was subsequently contrast-enhanced and median-filtered. The impact on the histogram shows power of the image processing for threshold application: initially, the large gray peak signified the noise and most of the cell signal mixed together. Some white pixels are colored red (above the threshold red line) but a computer cannot distinguish what is noise and what is cell — even the human eye requires some context like motion of the white pixels to segment vision. The white, intense pixels associated with cells were slowly unmixed from the noise peak to become a separate peak to the right of the overall histogram. By the end, even the noise bridging the two peaks is minimized; threshold levels selected at different locations between the two peaks will have marginal effect on cell tracking.

The actual threshold selection was performed in two ways. First, Image Pro provided one method called Automatic Bright Object (ABO) selection that was often appropriate for the datasets. An iterative thresholding process selected the segmentation value between 0 and 255 intensity that maximized the variance between the two classes (object and background, or white and black) for each image of the 1799 frame movie. Mathematically, the threshold level was iteratively altered until the maximum variance was achieved. ROIs with many perfused capillaries tend to always have a cell *on-screen* — that is, a bright object is present inside the ROI for each frame in the image set. When this is not the case, ABO selection provided a segmentation value that erroneously defined "noise" as "object". This caused problems for subsequent object tracking, and random objects become tracked.

A manual selection method was also utilized when ABO selection resulted in random cell tracks. The manual method started by selecting the ABO threshold applied to the first frame of a movie and performing the tracking using that threshold level for each frame (rather than a new threshold for each frame as in ABO). If random objects were still being tracked, the threshold level was moved up and down about 10 intensity values and tracking again performed. The threshold level that provided the best clarity for subsequent analysis of capillary structures was used. Another cue that was followed in final manual threshold selection was the acceptance/rejection of obvious cell objects — if a cell was rejected at a certain intensity level, the threshold was modified to bring "obvious" cells into tracking range.

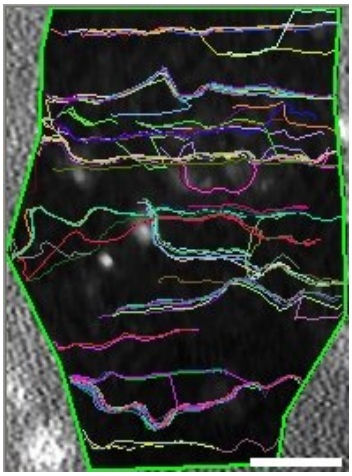

Figure 2.19: The Image Pro tracking module generated colored overlays of the track information on the processed image. The tracking was applied to the region of interest only. The highly dense portions of the image reflected the tracking of a large number of fluorescent cells. The white bar is 100 microns, as above.

The threshold level did have an effect on the tracking of some cells, most notably those cells that were out of focus. In-focus cells have a bright core of intensity surrounded by a darker ring, perhaps even followed by a tail of intensity generated from a lag in the camera's pixel decay time. So some cells were significantly larger in intensity than others. Another class of cells were those slightly out of focus, such that they did not exhibit a bright core. These cells may be excluded at selected threshold levels. Furthermore, some pixels of the cells may have existed over threshold, but noisy pixels may have also been present. To control noise from entering the final tracking step, another object classification threshold was established. The cell shapes had to consist of contiguous calibrated pixel areas in the range of 100 – 1000 μm^2. The red cell itself in its stress-free biconcave shape has a maximal visible cross-sectional area of πr^2 or about 30 μm^2. But due to the sensitivity of the camera, cells passing under the pixels appear larger due to the camera "blooming" effect. The largest cells could be white cells or cells that are slightly out of focus. The size exclusion thresholds were selected and applied equilaterally to all images.

The thresholding and object size exclusion processes were run on each frame in the movie sequence as part of the automatic tracking function built into Image Pro version 5.1. The cell tracking algorithm utilized several parameters to generate the cell tracks from the objects in each frame. First, a search radius was provided based on sample images obtained from cell tracking movies previously recorded during pilot experiments. A

value of 70 microns per frame was selected as a "window" inside which the tracking would commence on the subsequent frame — therefore, the program searched for objects up to 70 microns distant from a selected cell. If a cell was found, the program connected the two cell centroids as a track. Conversely, if an object was not found inside the search radius on the following frame, no track was generated. If multiple objects exist inside the search radius, the parameters for directionality of the tracks may be applied to select the most appropriate associable object. The tracks generated from blood traveling in capillaries is termed "directional", which lies between "straight" and "chaotic". Finally, the cells must be tracked for 5 consecutive frames to be included in the final output from the tracking module .

The tracking module generated a sparse matrix of velocity, and x,y-positions from the centroid values for each object in each track. The matrix dimensions were *number of tracks* which varied for each dataset by *number of frames* (1799). The tracking module also displayed the tracks in a multicolored overlay on the image (Figure 2.19), which allowed visual assessment of tracking quality. As explained above, if random objects were tracked, clearly defined capillary-associated clusters of data would not be visible, and thresholding was modified until the tracking was remedied.

Cell tracking data

The velocity data matrix was then exported into a text file. The tracking function tabulated the horizontal and vertical displacement of the cells' centroids relative to the upper left corner of the image. From this information, velocity and acceleration were calculated; for n positions, $n-1$ velocity *measurements* and $n-2$ acceleration measurements were determined. Mean and standard deviation of velocity measurements for each cell were also variables output to a text file. The text file was a tabulated list of values for each numbered cell, indexed by the frame number from which the data was obtained.

The velocity of cells' transmission through the capillary segments were used to define the velocity of the capillary segment. The output from the tracking function provided the information regarding a given cell's position in the frame. Every instantaneous *velocity measurement* was determined from the distance traveled and the time elapsed between

frames as

$$v_{meas,n} = \frac{\sqrt{(x_{n+1} - x_n)^2 + (y_{n+1} - y_n)^2}}{t_{n+1} - t_n}. \tag{2.1}$$

For each cell, a series of these measurements were was during the transmission through a capillary vessel. The mean *cell velocity* was determined by the following simple calculation,

$$\overline{v}_{cell,n} = \frac{\sum_{n=1}^{L} v_{meas,n}}{L}, \tag{2.2}$$

for a cell with $n = L$ velocity measurements. The cell velocity was simply an arithmetic mean of the individual velocity measurements obtained from the tracking module.

All the cells that pass through a capillary in a given time period — each cell with their own individual mean cell velocity — were used to calculate the mean *capillary velocity*. For C cells passing through the same capillary in a one-minute period, the capillary velocity was then

$$\overline{v}_{capillary} = \frac{\sum_{n=1}^{C} \overline{v}_{cell,n}}{C}. \tag{2.3}$$

Therefore, the *capillary velocity* was taken as a mean of the individual cell velocities obtained. An alternate calculation for the mean capillary velocity would be to average the individual measurements from the cells flowing in the capillary. The proposed calculation weighed each cell evenly, whereas a cell flowing slower through the network might be present for more frames, therefore slower cells would be weighed more than faster cells.

Finally, the *network velocity* may be computed as a mean of the capillary velocities recorded for a single network of capillaries present within the ROI. Each mean capillary velocity was — again — evenly weighted to reduce the effect of stochastic variation in hematocrit or cell staining. Network velocity was defined as

$$\overline{v}_{network} = \frac{\sum_{n=1}^{N} \overline{v}_{capillary,n}}{N}, \tag{2.4}$$

for a network with N capillaries. The velocities of the capillary segments that make up a capillary network are examined for similarity. The variable that was compared from network to network and from animal to animal was the coefficient of variation. The standard deviation of $\overline{v}_{capillary}$ is divided by the network velocity (mean of all $\overline{v}_{capillary}$ for a network) to find the coefficient of variation (CV) in capillary velocity. This variable will be described

as network CV or, simply, CV; CVs are often expressed as a percentage, and that convention will be followed in this thesis.

2.3 Analysis of cell velocity results

Utilizing the surgical, imaging, and computational methods outlined above, definitions for capillary velocities in single networks were constructed. The analysis of capillary networks was performed with a set of computer algorithms prepared to manipulate the data and determine the network CV as outlined above. Hundreds of cells were tracked simultaneously in each movie, but velocity data was obtained without a direct index that links a given cell to the capillary it flowed through. Therefore, the raw data was in a *pooled* form, and to generate the results as expressed in the equations above, the data must be in a *clustered* form. The process by which the data was manipulated is explained below.

2.3.1 Pooled variables

Computer processing of the data sets exported from Image Pro Plus tracking module allowed the analysis of large numbers of tracked cells. But I was completely responsible for the development of these computer algorithms. When I started my thesis work, attempts at analyzing capillary had been made on a small scale with a highly subjective and user-intensive image analysis approach. One of the first steps I took was to replace this system with the objective process developed above. Then, I developed a series of algorithms that processed each data set to deliver results to the user. All of the codes were developed in MATLAB and are reproduced in Appendix 6.4. The methods employed for the processing of a single example data set is outlined below for the edification of the reader.

The cell velocity data from the tracking module were transferred as a list of cell positions and velocity measurements indexed by the video frame in which the centroid location was determined. Without any processing then — only reading the data from the text file — a histogram of all cell velocity measurements across the whole network *pooled* together was created as in Figure 2.20. Furthermore, it was also easy to create a *pooled* representation of all cell velocities obtained in the network as in Figure 2.21.

The standard equations for the calculation of network CV were presented as Equations 2.1 to 2.4 above. Previous measurements of capillary velocity generally display capillary red blood cell velocity without regard to the vessel from which the cell came, as I

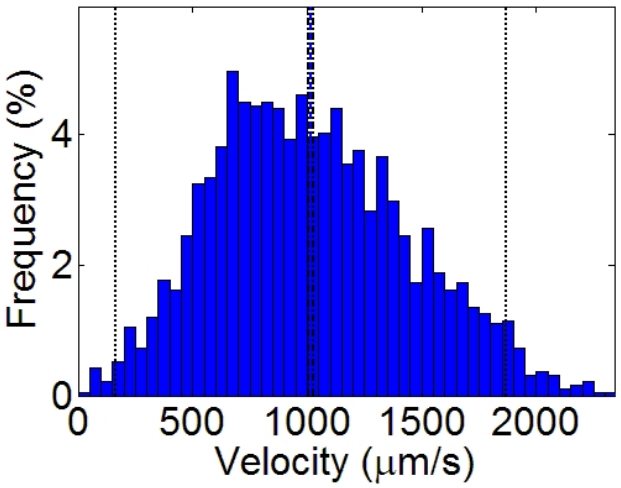

Figure 2.20: Histogram of all velocity measurements in the example data set pooled together. The pooled velocity measurements are the most basic measurements obtained from the video recordings. The coefficient of variation of velocity measurements is relatively high; the range is from approximately 50–150%. The velocity measurements reflect all of the possible sources of variation, including measurement error. The velocity measurements are immediately viewed as cell mean velocities to reduce the impact of error in individual velocity measurement acquisition. The velocity measurements are further processed to determine information regarding capillary velocity.

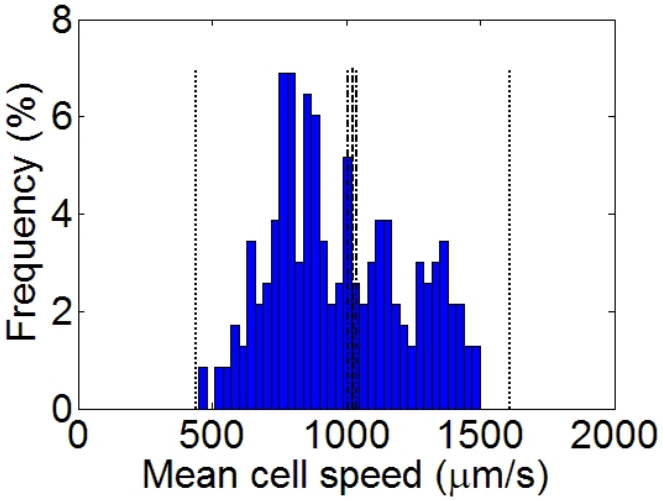

Figure 2.21: Histogram of all cell mean velocities in the example data set pooled together. As with the pooled velocity measurements in the Figure above, these cell mean velocities do not provide direct information regarding the capillary velocity. A clustering analysis is necessary to further compute capillary velocity from the cell mean velocities.

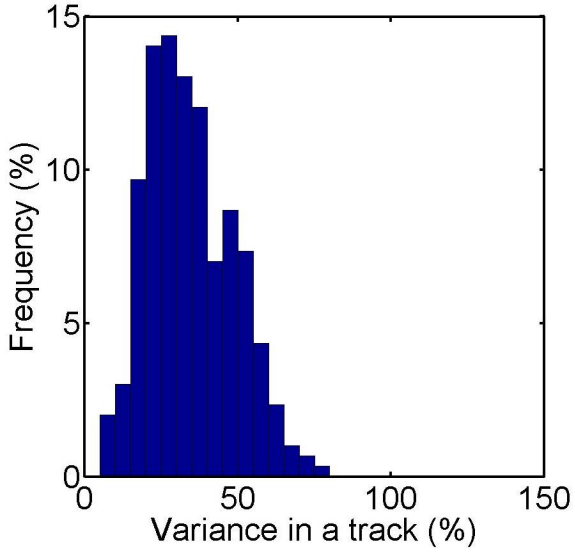

Figure 2.22: The coefficient of variation displayed for each track is computed from the individual velocity measurements. A mean cell velocity is computed from the velocity measurements as outlined in §2.2.3. The standard deviation of the velocity measurements for a track divided by the mean cell velocity is the *by track* coefficient of variation.

have termed *pooled*. Examples of velocity measurements in skeletal muscle capillaries from frog [153] and rat [154, 155] are available in the literature. Then to provide a comparison with their results, I developed a pooled representation for a *pooled network CV*. Without displaying rigorous mathematical equations, the standard deviation of all velocity measurements divided by the mean of all pooled velocity measurements was termed the *pooled measurements network CV*. Similarly, the standard deviation of all cell velocities divided by the mean of all pooled cell velocities was called the *pooled cells network CV*. These two variables for the example network were 41.9% and 25.2% respectively.

Note the difference between Figures 2.20 and 2.21. The overall number of velocity measurements was greater than the number of cell velocities, but there is a higher degree of variation associated with the tracking of a single cell. The variation inside individual tracks is shown in Figure 2.22. The example dataset showed that the plurality of tracks have from 0% to 50% CV due to individual velocity measurements. A small number of tracks displayed over 100% variation as well. This display does not provide any insight into the cause the of variation for each track. The analysis of velocity as a function of spatial position, discussed in 2.3.3 on page 61 offers a possible explanation. Additionally, measurement error associated with individual velocity calculations could contribute to this variation.

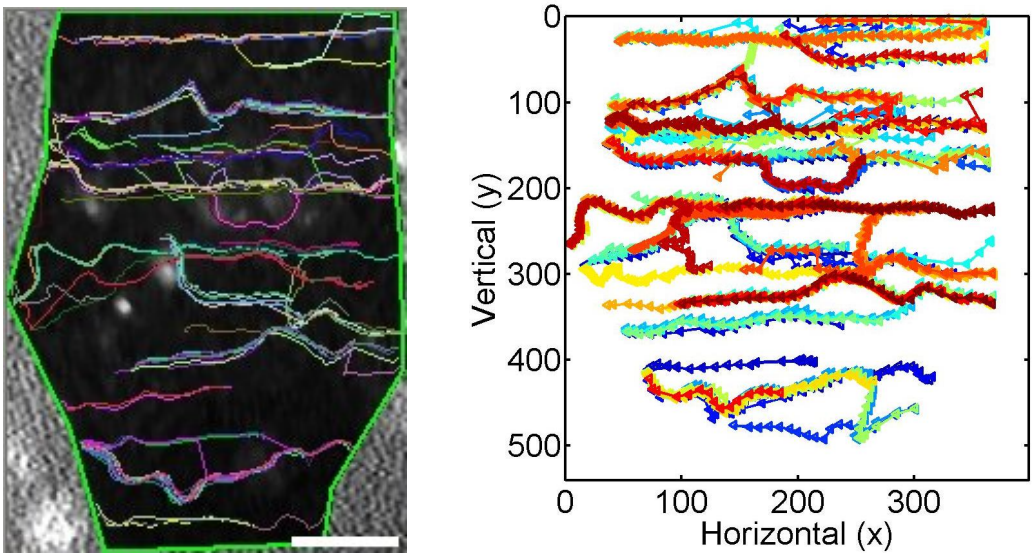

Figure 2.23: Example data set with all cells centroid positions overlayed. Each cell is presented with a different color, and each triangle is set at a given (x,y) point at which the position was recorded on a given frame. The direction of the triangle depicts whether the cell traveled from left-to-right or vice versa. Dense clusters of colored lines are visually interpreted as heavily perfused capillaries whereas few lines at a vertical position signifies either a lower flow vessel or a vessel that was slightly out-of-focus, and therefore harder to definitively image.

2.3.2 Clustered variables

Considerable effort was expended to define methods by which the cell track data would be *clustered* into capillaries. Since the data is recorded to video tape for a whole network of capillaries simultaneously, the resulting data set has no pre-defined order or index linking *cells* to *capillaries*. Four different methods were used to organize to the datasets; these methods will be outlined below, then the results obtained from their use will be presented and compared.

Clustering methods

The first step in clustering required presentation of the cell position data as a series of lines across the computer screen. This was generated by simply overlaying every cells' set of (x,y) positions as in Figure 2.23. The user then visually inspected the overlay with the intention of defining the "capillaries" by locations of clustered data line segments. The number of capillary *paths* was then input into the computer program (`vProcess.m` as in Appendix 6.4).

Clustering with k-means automatic and manual

The first two clustering algorithms required the *a priori* information regarding the number of capillaries in the overlay image. They were k-means clustering algorithms that utilize the number of clusters — k — for maximizing the squared Euclidean distance between clusters while minimizing the squared Euclidean distance within each cluster. Each cell track was represented by the average y-position (vertically on screen) along the track, because the SIT camera was rotated on its mount to record the cell transits primarily in the x-direction (horizontally on screen) within the capillary network. So clusters of the cell track y-positions were generated and were defined as *capillary clusters*. The first method — k-means automatic — utilized a randomly selected subset of data to "seed" each cluster, and then proceeded to automatically cluster the cells into capillary clusters. The second method required user input via MATLAB's `ginput` function to manually provide the starting seed position for each cluster. These two methods were designated the *k-means automatic* and *k-means manual* clustering methods.

Clustering by maximizing position correlation

The third clustering method, *correlation clustering*, relied on the (x,y) positions of each cell track in a one-minute video record. This method provided an improvement over the k-means clustering methods described above, because k-means analysis utilized only y-positional information. The *a priori* information regarding the number of user-perceived capillary clusters m was also utilized. A series of "reference tracks" was established using the `ginput` function: in locations of track density, the user clicked one reference track down the length of each perceived vessel. The path and direction of the vessel were the important pieces of information transcribed in this process. The actual number of user clicks was unimportant, but it was crucial that they were distributed down the vessel evenly. The program `ClusterByCorr.m` interpolated between points of the reference tracks such that there are 100 (x,y) values for each track. Similarly, the (x,y) positions of each cell centroid in a track were interpolated to contain 100 values. Then, the positions of the data track were correlated with each reference track's positional information according to the following formula:

$$r = \frac{\sum_{m=1}^{2}\sum_{n=1}^{100}(R_{mn}-\overline{R})(D_{mn}-\overline{D})}{\sqrt{(\sum_{m=1}^{2}\sum_{n=1}^{100}(R_{mn}-\overline{R})^2)(\sum_{m=1}^{2}\sum_{n=1}^{100}(D_{mn}-\overline{D})^2)}}, \tag{2.5}$$

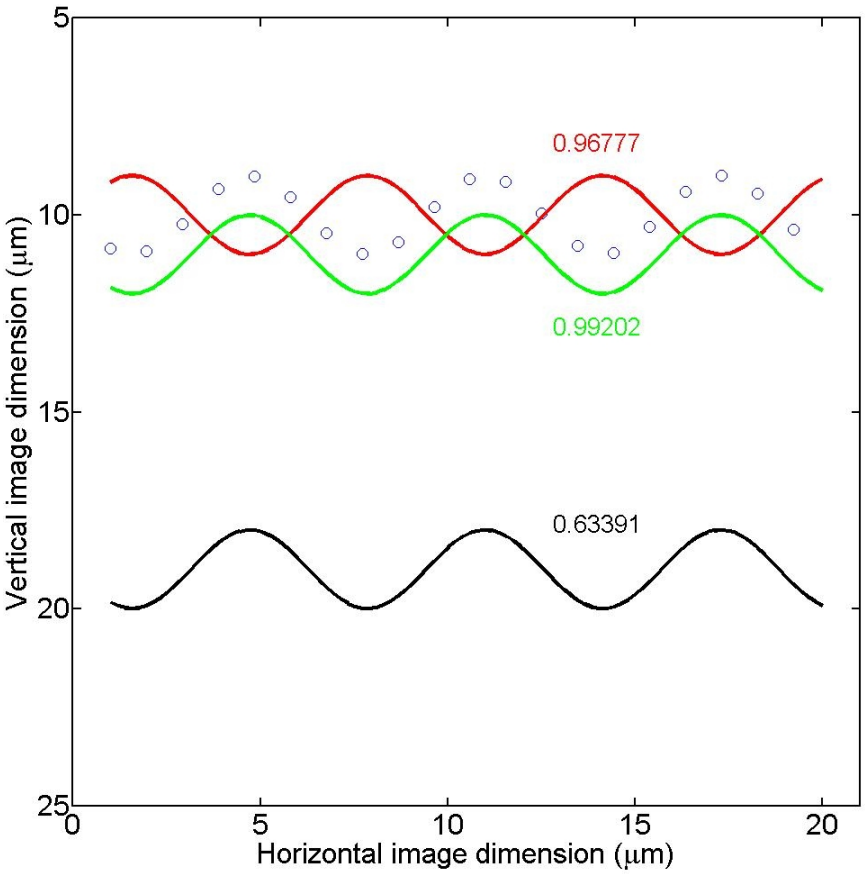

Figure 2.24: Example of 2D correlation used for correlation clustering. Shown is a series of blue circles representing the reference track clicked over the tracks in a capillary. The three sinusoids are simulated tracks, each colored differently and with the 2D correlation with the reference track shown in the same color code. The green line is in phase with but displaced away from the reference track by 1 μm and correlates best. The red line shows zero translation away from the reference but follows a path 180 $^\circ$ out of phase and shows reduced correlation. The black line is 10 μm distant from the reference track is displays the lowest correlation. For correlation clustering, a number of reference tracks are established and a given cell track is correlated with each reference; the cell track is assigned to the capillary to which it correlates best.

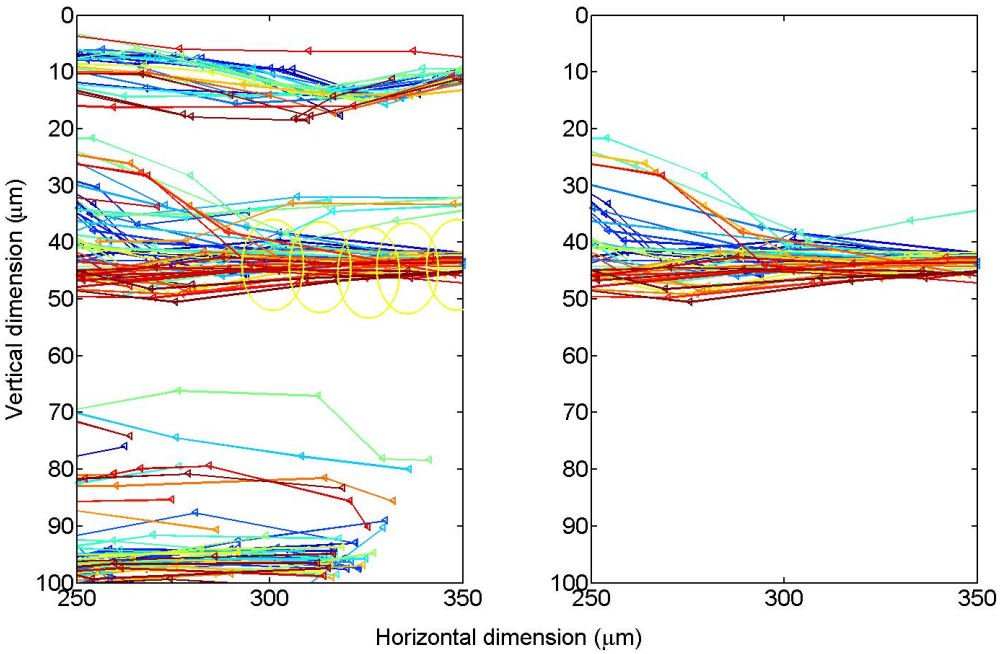

Figure 2.25: Example image containing track data (A) with zoomed focus on a single set of tracks and user-defined circle (B) displaying ability to select individual velocity measurements for node-to-node clustering scheme.

where $m = 1, 2$ represent x-coordinate and y-coordinate respectively. The deviation of each of the $n = 100$ points from the mean was calculated for both the reference track (R) and the data tracks (D). Then the summed deviation in (x,y) for the 100 points of data and reference was divided by the square root of the sum of the squared deviation. Figure 2.24 depicts an example of how three lines correlate in two-dimensional space with a simulated reference track. For n tracks in a dataset and reference tracks defined for each of m capillaries, an $n \times m$ matrix of 2D correlation coefficients was constructed. Then, for each of the n tracks, the cell track was assigned to the capillary for which the track-to-reference correlation coefficient was maximum. This established each capillary cluster as the set of all tracks that best correlates to the cluster's reference track.

Node-to-node clustering for capillary segments

The final clustering method required more user input for processing raw velocity measurement data. The method was designated as *node-to-node* clustering because it was used to break the track data into velocity measurements that describe a capillary segment from one bifurcation "node" to the next. The code written to handle this analysis is

`TrackVelocity.m` as found in Appendix 6.4 on page 160.

The cell track data were first plotted via MATLAB code (`PlotCluster.m`) as shown in Figure 2.25. Using the standard MATLAB plot interface, the data plot was zoomed in or out to view the data most accurately. Then, the user began to input a series of clicks on the tracks, taking care to click near to the actual triangles that depict a cell centroid as in Panel B of Figure 2.25. The program illustrated the impact of each click with a circle 10μm in radius around the clicked point as in Panel C. Cell centroids as depicted by the triangles that lie inside this circle were collected informatically. Each centroid was a placeholder for the velocity vector that extended from that centroid.

The collection of velocity measurements for a given cell were combined with those from other cells that have velocity measurements inside the series of user-placed circles. As the circles were carefully placed along a single capillary segment, only the velocity values for that segment were included in the calculations. The cell velocity, capillary velocity, and network velocity are computed as above in §2.2.3, with one minor caveat - when a cell has fewer than three velocity measurements in a given capillary segment, its mean velocity is not included as a cell velocity. Further, when a capillary was defined with fewer than three cell velocities, no capillary velocity was computed to include in the network velocity calculation. These steps ensured that the relatively high variability from the individual velocity measurements did not affect the capillary velocity calculation. Each of the four aforementioned clustering processes had its strengths and weaknesses; they traded off user-intensive decisions for each of hundreds of cells for some certainty that appropriate data clustering had been achieved. The fourth clustering process, node-to-node clustering, was much more user-intensive, but provided a deeper analysis into the network architecture. When the data was collected as described above, a cell track described the path each cell traveled through the capillary network; for this reason, the first three clustering methods was termed *by-path* methods. Node-to-node clustering allowed an analysis of each capillary segment in a path as a separate entity; it was called a *by-segment* clustering strategy. The distinction must be made in this way because the results that the two types of clustering methods yield are somewhat different.

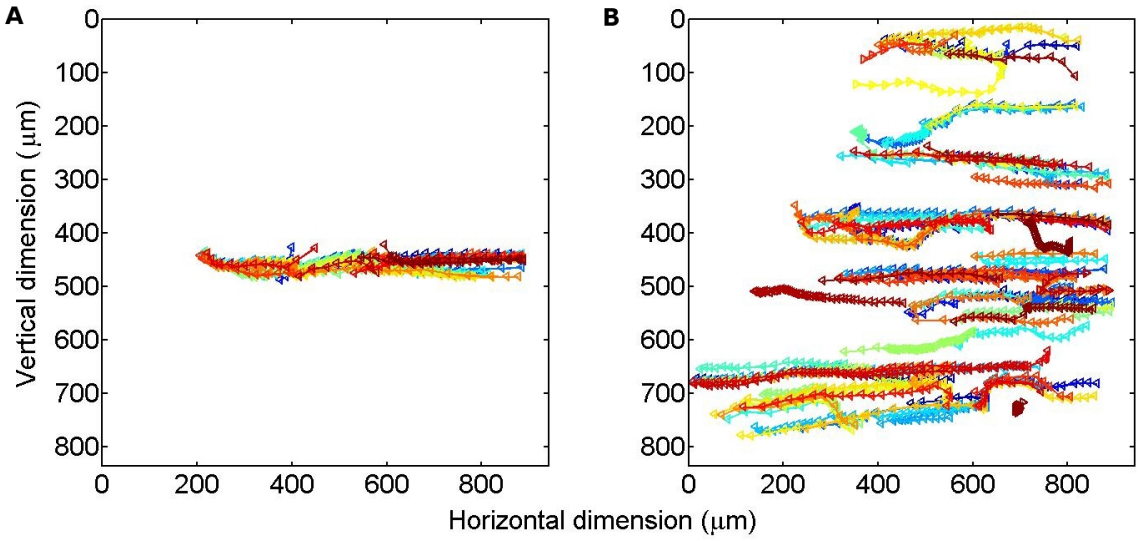

Figure 2.26: Data tracks may be clustered (A) or drawn from the whole dataset at random (B). For both cases, the code `DataCorrelator` determines the quality of clustering by performing a two-dimensional correlation of each data track in the cluster with *every* other track in the cluster. The mean of all the average scores for all tracks is then computed and taken as the correlation for that capillary cluster. As seen in the example, the clustered tracks have a correlation coefficient of 0.979, whereas the set of tracks selected randomly display only 0.316 correlation.

Assessing quality of clustering

With four different clustering methodologies, it was important to develop an objective method to determine which resulting coefficient of variation was best suited for the current analysis. For that reason, I computed the overall degree of correlation *within* a capillary cluster. The computation was illustrated in Figure 2.26 for the case of a sample of clustered data (A) and randomly-selected, un-clustered data (B). The positional information for a single track was correlated with every other track in the cluster. The average score for all the tracks in the capillary cluster was found; then, each capillary cluster correlation score was averaged across the network. An overall correlation score can be compared for each of the first three clustering methods. The correlation scores of four complete datasets from control tissue for each of the three clustering methods are also tabulated in Table 2.1 on page 61. Cluster correlations for networks from control spinotrapezius muscles in Wistar animals (weights 400-440g) are averaged. The correlation scores were computed from the velocity data for each network with the first three data clustering methods: *automatic k-means*, *manual k-means*, and *correlation* clustering. The correlation score was assessed as the average of the two dimensional (x- and y-coordinates) correlation of every track in

Table 2.1: Cluster correlation scores from Wistar animals for each clustering method

Animal	**Automatic k-means**	**Manual k-means**	**Correlation**
1	0.881	0.863	0.960
2	0.901	0.887	0.927
3	0.974	0.977	0.985
4	0.972	0.969	0.987
Mean	0.932	0.924	0.965
StDev	0.048	0.057	0.028

a cluster with each other track in each capillary cluster of a network. The intra-capillary correlation averaged across the network of capillaries was the final *correlation score*. The correlation clustering scheme tended to outperform the k-means clustering methods by this metric, as can be readily seen from these correlation results.

Objective scoring also allowed selection of a single best method for clustering a velocity dataset. Differential clustering of the cell tracks also affected the network CVs computed from the velocity data because one method may have assigned different cells to different clusters than another. The influence of this fact on final results was mitigated by comparing data from one clustering method only to other data clustered by the same method. Henceforth, any data that was presented will also contain a reference to the method which was used to cluster.

No correlation score was assigned to node-to-node clustered data. By defining the capillary segment based on the velocity measurements included inside a series of circular regions, individual capillary segment clusters were very highly correlated positionally. Therefore, assigning a score to node-to-node clustered data would be redundant. The MATLAB code that handled node-to-node clustering was called `DataCorrelator` and can be found in Appendix 6.4 on page 158.

2.3.3 Spatial and temporal data analysis

In addition to the definition of mean capillary velocities, clustering the data allowed further analysis of the velocity data spatially within the network and within the vessel. Clustered data was first and foremost expressed in terms of the network CV, as defined above in §2.2.3. Network CV was a parameter that was computed from the cell velocities

over a one minute period, and from a whole network of capillaries; the aggregate nature of this variable cannot be ignored. Over a one-minute period, changes in vasomotor tone or even heart rate could have occurred. Two interesting analyses of the data were developed to add insight into the capillary velocity measurements and to account for sources of variation present in the velocity data.

Spatial display of velocity

The spatial display of velocity can extend beyond division of the entire network of information into individual capillaries. The measured cell velocity was comprised of many individual velocity measurements which were themselves based on instantaneous cell centroid positions regularly recorded (Equations 2.1 and 2.2. Therefore, the velocity measurements were combined into alternative averages that allowed analysis of velocity patterns along the length of the capillary vessels.

To perform the subdivision of the velocity information, a MATLAB code called `SpatialDisplay` was written (Appendix 6.4 on 166). The pre-clustered cell velocity information was first parsed by absolute x-position for the entire capillary cluster. Recall that every attempt was made during image acquisition to ensure that flow is primarily horizontally directed. Therefore, the y-position was similar for measurements from within each individual capillary. This requirement may not be valid for every vessel, but was assumed for division of velocity measurements in this analysis. Then, a series of "bins" for velocity measurements were made at regular intervals for each capillary cluster. The absolute distance that the bin spanned was selected to be 50 μm. If a velocity measurement originated inside the bin — that was, if the centroid x-position was inside the bin — then the velocity measurement was assigned to the bin. As the cell passes down the capillary cluster, the velocity measurements were placed in the series of bins corresponding to the proper x-position. After all the cells that make up a capillary cluster were parsed in this way, the bin velocity was averaged. If the bin contained fewer than three velocity measurements, the bin velocity was not included to reduce the effect of measurement error. The capillary velocity plotted as a function of x-position for four capillaries of the same network is shown as Figure 2.27.

The display for the four capillary vessels offers an example of the information that may be shown for all capillaries in a network. Velocity information for each segment of the

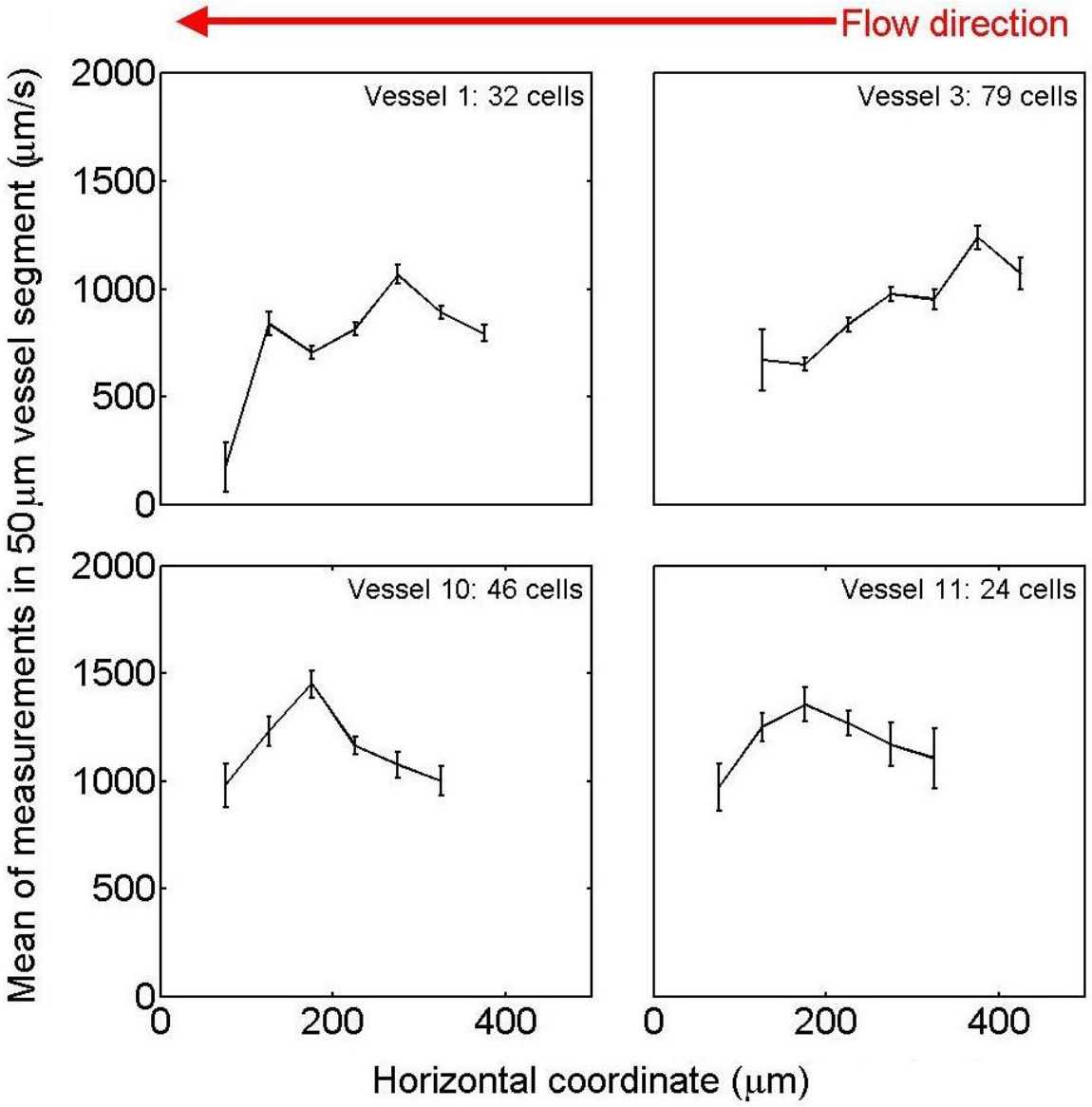

Figure 2.27: Spatial display of velocity as a function of horizontal position for four capillaries of the same network. The velocity information from each cell of a capillary is parsed into 50 μm segments down the length of the vessel. Velocity information for each segment of the vessel is then averaged. Most vessels display velocity within a range of 100–200 μm/s down the length of the vessel (as top-right and bottom-right), but some show reduced velocity as they enter or exit the capillary vessel (top-left). The entrance or exit regions of the vessel may be larger to provide less resistance to flow, but the cell may travel in an off-center streamline with increased drag along the vessel wall. Also, vessels sometimes display points of elevated or very low velocity in the center of the vessel (bottom-left). This may be viewed as either a pinch point in the vessel, such as a bulging endothelial cell or adherent leukocyte, or perhaps following a turn in a vessel, the red cell may roll off of the center streamline into a slower path through the vessel or against the wall.

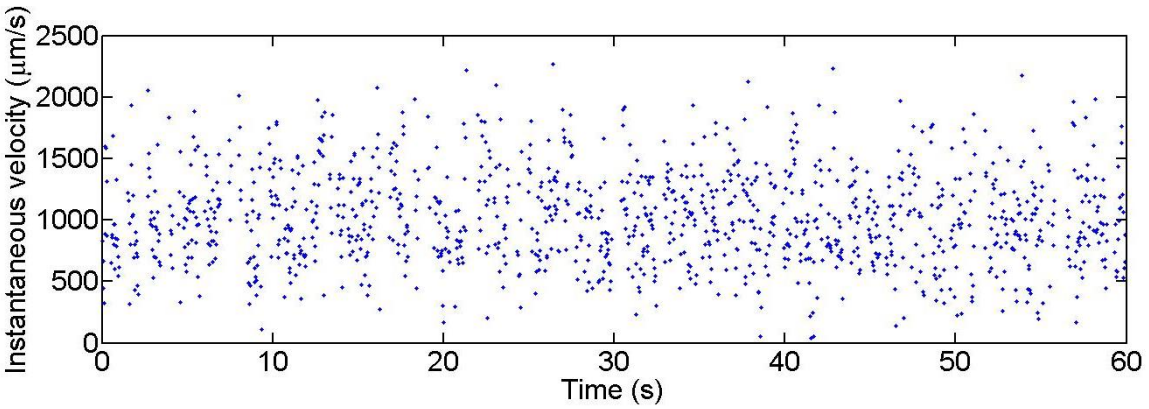

Figure 2.28: Velocity plotted for the entire network as a function of time. The velocity computed from a single frame — that is, each cell present and tracked on a given frame — was averaged. A large amount of variation is present when using instantaneous velocity measurements, therefore only extreme changes in upstream perfusion may be discriminated via this display. A more sensitive display is developed below, the temporally-averaged spatial variation.

vessel was relatively constant down the length of the vessel (as top-left and top-right), but some capillaries showed elevated velocity at the entrance and exit regions of the capillary vessel (bottom-left). The entrance or exit regions of the vessel may be larger to provide less resistance to flow. Also, vessels sometimes displayed points of elevated or very low velocity in the center of the vessel (bottom-right). This may be viewed as either a pinch point in the vessel, such as a bulging endothelial cell or adherent leukocyte, or perhaps following a turn in a vessel, the red cell may have rolled off of the center streamline into a slower path through the vessel or against the wall.

Temporal variation

The perfusion control functions at the arteriolar level to deliver different flow rates to the capillary networks being imaged at any given time. The degree of temporal variation viewed in the capillary networks was a concern, since any differences in upstream perfusion may be coupled to spatial variations between capillaries. It was important to determine a method to display and informatically decouple the temporal variations at the arteriolar level from capillary perfusion. Two standard plots were generated to view temporal variations. One method was used globally across the network and the other sought to understand the temporal variation inside individual capillary vessels.

The global network variation was constructed as a simple *by frame* average of all

instantaneous velocity measurements. Therefore, the velocity associated with each cell on a single frame were averaged together at that instant. Figure 2.28 simply displayed whether a high degree of velocity variation was present as a function of time. Each frame elapsed provides a different number of cells tracked, so the instantaneous velocity was not a reliable measure for comparison. But if upstream perfusion was suddenly reduced or modified, this display was a simple and rapid telltale.

Another display allowed a check of temporal variation within each capillary from the individual cells that make up the capillary velocity. After the cells were clustered into capillaries, each cells' mean velocity was plotted at the first instant in time when the measurement was made. A series of points may be plotted, with cell velocity as a function of time for each capillary vessel in the network. A subset of four capillary temporal plots are shown in Figure 2.29. The information provided in this display allows visual inspection of the perfusion of each capillary. In the case of drastic perfusion differences within a single capillary, a clustering error may have occurred and was repeated for accuracy.

Temporally-averaged spatial variation

Further analysis of temporal variation as a network variable was still necessary, because the instantaneous temporal plot contained too much variability and the individual capillary plots did not display enough temporal resolution. For this reason, a temporal average of the network CV was constructed using `TemporalCV` as found in Appendix 6.4 on page 161. In summary, the capillary velocity information was parsed as a function of time into one second segments. The cells that were present for a given one second period were identified, and the corresponding mean cell velocity values were compiled for each capillary perfused during that brief time period. Then, the network CV was computed for *only the capillaries perfused* during that one second segment. The process was repeated for each of 60 one-second segments in a movie. The temporally-averaged spatial variation allowed analysis of the spatial variation as a function of time.

The velocity measurements in the same given one second period were also displayed independent of the network CV calculation. The velocity values for the 60 segments of a given movie along with the temporally-averaged spatial variation are shown in Figure 2.30. The average velocity in the one-second segments are displayed (top) and the corresponding network CV as a function of time is also shown (bottom).

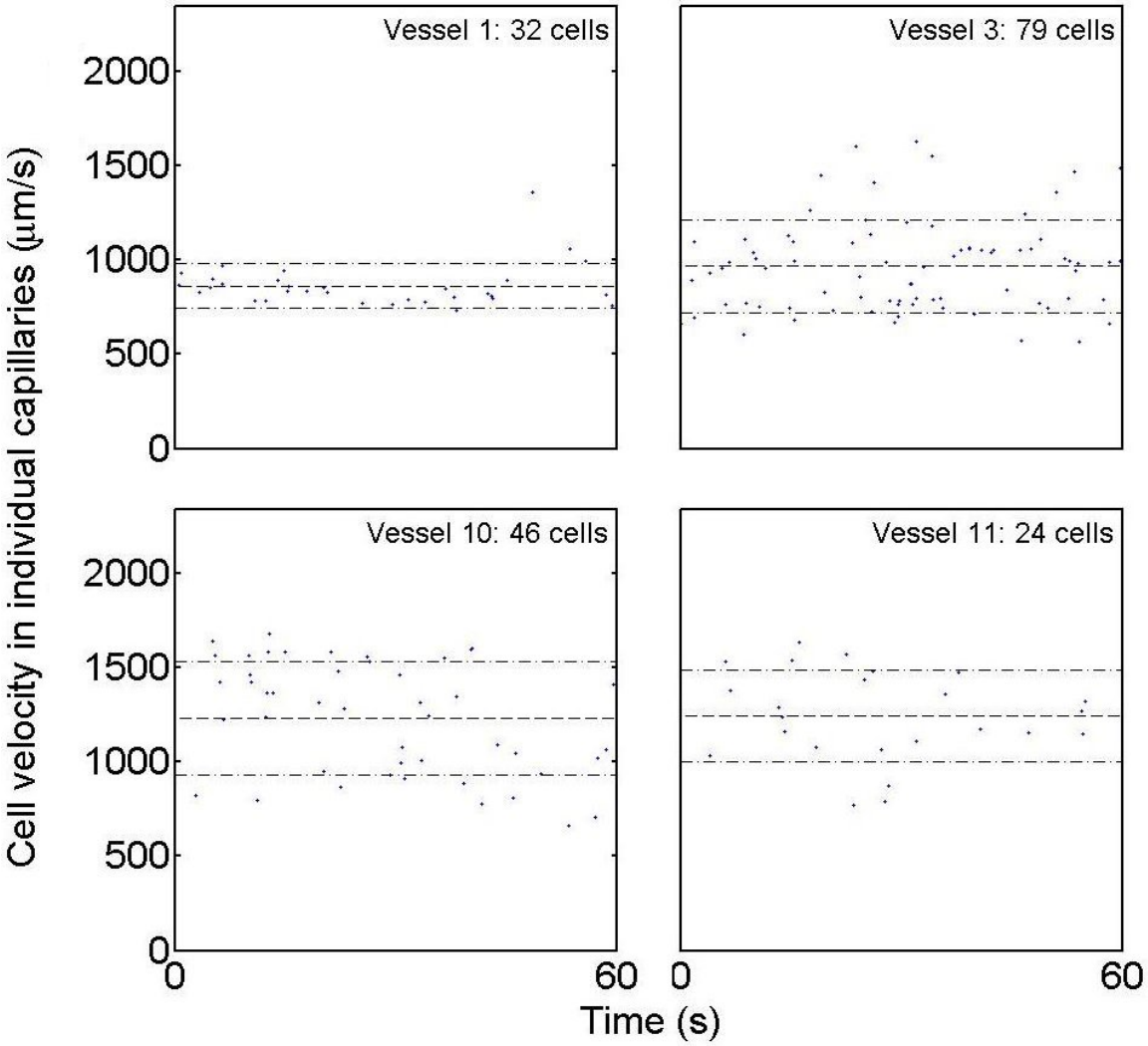

Figure 2.29: Individual capillary velocities were computed from mean cell velocities and each cell velocity was recorded at a certain time in the recorded image. The cell velocities that comprised a capillary are plotted as a function of time to visually inspect the values that were incorporated into the capillary velocity. The dashed lines represent mean capillary velocity and plus or minus one standard deviation.

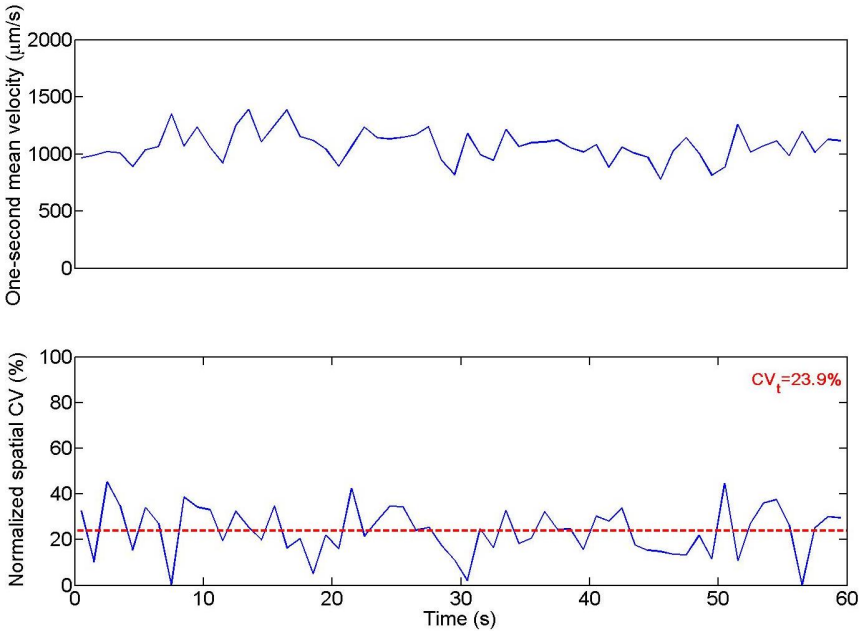

Figure 2.30: A temporal average of the network velocity and network CV was developed as a parametric measure of network temporal variation. The instantaneous temporal plot contains too much variability and the individual capillary plots do not display enough temporal resolution. The network temporal plot also allows computation of the network temporal CV from the one-second mean velocities.

A final variable assessing the degree of temporal variation was also computed from the one-second segments of velocity. Through determination of the mean velocity of each one-second segment, 60 time-dependent mean velocities were found. The average of these 60 one-second mean velocities was computed along with the corresponding sample standard deviation. The *temporal CV* was computed as the standard deviation divided by the mean for the 60 segment velocities. The temporal CV for the movie displayed in the temporal figure above was 23.9%. Further analysis and discussion of elevated or reduced flow may be found later in §3.4 and §3.3 on pages 96 and 85 respectively.

2.4 Method validation

A large amount of work went into the development of the object tracking system. To ensure that results from the system were dependable, two methods were utilized to validate the use of video footage to track cells for establishment of capillary velocity. The first method relied on an apparatus used for calibration of the older two-slit photometric velocimeter. The second method required the use of a fabricated set of microchannels. The

Figure 2.31: Picture of the spinning disk setup used to validate the Image Pro tracking of fluorescent blood cells. Fluorescent microspheres were placed on the surface of the plastic disk which spins at a constant rate determined by the potentiometer setting. A single revolution was timed and recorded simultaneously. With the distance from the center to the optical viewing location, the linear velocity may be calculated. The calculated linear velocity is then compared to the output from the Image Pro tracking module.

results from the two sets of validation trials are displayed below.

2.4.1 Spinning disk

The first method of validation was aimed to determine the quality with which cell tracking methods described the actual velocity. The imaging equipment and image processing each have limitations, and it was crucial to determine the deviations that the velocity tracking setup were generating. A calibration method for a two-slit photometric velocimeter was slightly modified to generate "control" velocity values to which the tracking method results were compared.

Spinning disk methods

The spinning disk setup was comprised of a disk mounted on a small electric motor controlled by a potentiometer as shown in Figure 2.31. The disk was spun at a constant rate that could be reproducibly quantified with a stop watch. By determining the distance between the center of the disk and the location under the microscope light path, it was possible to convert the angular velocity to linear velocity. A dilute suspension of AlexaFluor488-conjugated microspheres were placed on the surface of the spinning disk, such that as the disk spins, the path on which the microspheres travel was epi-illuminated under the microscope objective. One minute videotape acquisitions were made from images

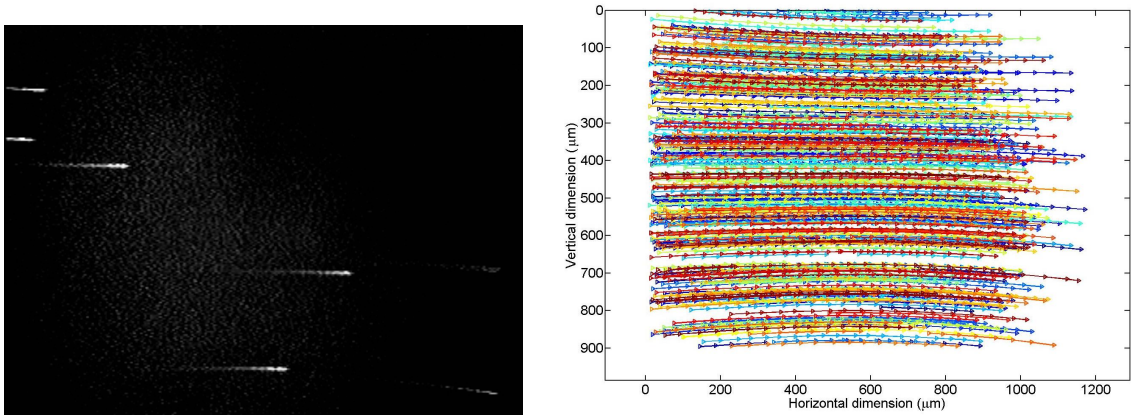

Figure 2.32: (*Left:* Photomicrograph of spinning disk with passage of fluorescent microspheres. The Image Pro processing of these images is simplified by negligible background intensity. *Right:* MATLAB data output of the spinning disk from tracking of fluorescent microspheres. The data are randomly arrayed across the height of the image since there is no vessel constraining their passage as in capillary object tracings. The mean of the cell velocities is calculated and used to compare the tracking velocity to the calculated rotational velocity.

Table 2.2: Velocity comparison for the spinning disk trials

Timed revolution (sec)	Actual linear velocity (μm/sec)	Pooled mean velocity (μm/sec)	Deviation (%)
42	2458.2	2336.1	4.97
79	1313.5	1288.4	1.91
93	1107.7	1192.5	7.66
			4.85

of the pseudo-linear transits of microspheres on the disk. The images were processed as explained above in Image-Pro, and the microspheres tracked as though they were cells in capillaries. The tracking module output was exported to MATLAB and analyzed.

Spinning disk validation results and discussion

The actual velocities for three trials at different speeds are shown in Table 2.2 along with the velocities computed from Image Pro tracking of one minute videos of fluorescent microspheres placed on the surface of the spinning disk. The individual microspheres as tracked across the viewing window are shown in Figure 2.32. Because the spheres were randomly dispersed across the surface of the disk, the image shown contains tracks across the

entire view field. For this reason, the tracking data from these trials are not clustered, and the Image Pro results in Table 2.2 are pooled mean velocity values. The average deviation of the Image Pro-generated pooled mean velocity from timed rotation linear velocity for each trial is also tabulated; the mean of this deviation over the three trials is 4.85%.

The deviation of the pooled mean velocity from actual velocity may represent a phenomena of object tracking from the images recorded from the SIT camera. There is some intrinsic uncertainty in the establishment of centroid position. The camera is set to use the automatic gain settings to maximize the difference between background and objects. But the cells or microspheres when moving quickly across the screen, will often display a comet tail opposite the direction of motion. This tail is a function of the decay rate of pixel excitation in the SIT camera itself. It is a technical liability inherent in the current setup of the system. A more sensitive camera with more rapid frame rate would reduce this effect significantly.

The coefficient of variation of the tracking data – that is, the standard deviation of the data divided by the pooled mean velocity – for the three trials is 11.5% on average. This may partially a function of slightly faster velocity on the outer edge of the spinning disk. The optical viewing center was measured by caliper to be 16.5 ± 0.3 mm from the center of the spinning disk. Then, since the viewing window is approximately $1mm^2$ vertically, cells at the bottom (closer to the center) portion of the field of view would be moving about 5.9% slower than the top of the field (farther from the center). But this effect was not seen in the data (not shown). The data had a slight slower slope on the order of 1%. This may again be due to deviations in centroid position generated automatically via threshold selection. The data averaged to a pooled mean velocity that is within measurement error for the center-viewing window distance. This result suggests that the tracking method should not be utilized via individually tracked measurements, but should instead be used as an average only. In all cases, the MATLAB processing of data takes this caveat into account. The cell-averaged velocity is used for all displays except for the intra-capillary spatial display (Figure 2.27), in which velocity measurements are averaged at each location temporally.

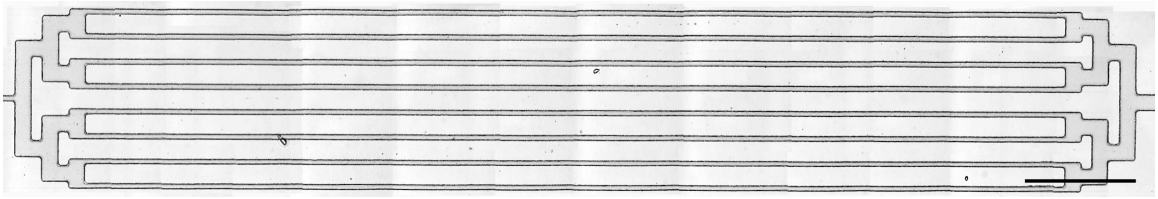

Figure 2.33: Photomontage of the microchannels fabricated from PDMS for validation of Image Pro tracking and MATLAB clustering. Fluorescent blood cells were delivered to the microchannels via syringe pump set for specific flow rates. The flow rates to each channel can be calculated from channel dimensions and pump settings. The black scale bar shown is 1mm.

Table 2.3: Results from the microchannel clustering validation trials

	Pooled mean	**Correlation method**		
Trial (#)	velocity (μm/sec)	Automatic k-means (%)	Manual k-means (%)	Correlation (%)
1	109	0.800	0.783	0.984
2	198	0.590	0.607	0.968
3	284	0.670	0.689	0.966
4	466	0.812	0.812	0.970
Mean		0.718	0.723	0.972
StDev		0.107	0.093	0.008

2.4.2 Microchannels

The aforementioned validation with a spinning disk tested the capabilities of the image tracking system to accurately measure cell velocity. But following Image Pro tracking, the velocity data was then output to MATLAB for clustering and data processing for display. Therefore, another series of trials were conducted to test the MATLAB clustering methods. This was accomplished with a set of microfabricated channels, or microchannels, constructed to allow the controlled transmission of fluorescently-labeled blood cells while being recorded via video microscopy. The microchannels that were used were a gift from a fellow graduate student, Lee Pang. A single set of channels is shown in Figure 2.33 as crafted from poly-dimethylsiloxane (PDMS) using standard microfabrication techniques. A set of rapid bifurcations at either end of the channel system leads into eight long, parallel channels of 1 cm in length, 50 microns wide, and 6 microns deep.

The microchannel system can be attached via PE50 tubing to a syringe pump (NE-1600, New Era Pump Systems, Wantagh, NY) that drives the flow at very minute quantities. Delivered flow rates are divided by the total cross sectional area of the 8 channels to determine the delivered axial velocities. The fRBCs were generated from a whole rat blood sample as discussed (§2.2.2). They were then pumped through the microchannels in a range of velocities similar to those found *in vivo*— approximately 100 – 500 μm/s. The image processing and cell tracking were performed as explained above. Finally, the MATLAB clustering processes were run on the microchannel velocity data. The results from this validation are shown in Table 2.3.

The MATLAB clustering methods were tested using a series of microchannel trials. Recordings were made as labeled cells passed through distinct channels and the results were clustered with *Automatic k-means*, Manual k-means, and the Correlation clustering methods. The correlation scores as outlined in §2.3.2 were assessed. The correlation method outperforms the k-means methods and is used as the primary *by-path* clustering method for future velocity recordings in capillary networks. The *by-segment* method of clustering was tested similarly, but the result is not shown above. By-segment analysis defines each capillary subjectively for a series of microchannels and assigning a correlation score is unnecessary.

2.5 Conclusions

A systematic process was established for particle tracking velocimetry in all capillaries of a capillary network. Surgical and intravital microscopy methods in two distinct tissues provided a platform for detailed measurement of red cell velocity *in vivo*. Digital image processing allowed images with high levels of background to be utilized for tracking and velocity measurement. Finally, standard algorithms allowed generation of capillary velocity values. The capillary velocities were then used to create a capillary *network CV* as an index for homogeneity in capillary networks. This index was utilized to compare velocity variation in many networks from a single animal — or to compare variation from animal to animal or between groups of animals. Also, individual networks can be probed before and after selected treatments to evaluate the effect on capillary network perfusion. Both of these experimental protocols are the basis for the measurements presented in the following chapters.

2.6 Acknowledgements

The work described in this chapter has been included in part as a paper entitled "Endothelial control of capillary perfusion", in preparation for submission. The authors were myself, Namgyun Lee, Samuel Shin, Frank DeLano, Christopher Bertram, and Geert Schmid-Schönbein.

Chapter 3

Hemodynamics in control tissue

3.1 Introduction

As mentioned in the previous chapters, capillary perfusion may be accurately monitored to examine hemodynamics lined to capillary network topology. Herein, I extend the analysis to decouple effects in arterioles from effects at the capillary level. Freshly prepared tissue is studied to determine the level of variation present in control conditions. Baseline levels of spatial and temporal variation are measured to provide comparison with perturbed capillary networks. Two methods I use to modify capillary perfusion are occlusion of an upstream arteriole and electrical stimulation of muscle contraction. By reducing or increasing flow to the capillary network, I will observe the dynamic flow control mechanisms present in capillary networks.

A control system at the capillary network level may act to adjust the variation in velocity of individual capillaries of the same network. Past evidence suggests that absolute velocity in a microvascular network may significantly impacted the coefficient of variation in capillary velocity. This result is re-examined below with the cell tracking velocimetry and analysis of spatial and temporal CV as discussed in the previous chapter. Furthermore, indications of central nervous system control of hemodynamics, such as systemic blood pressure and heart rate, will be recorded to determine their impact on the network CV. I will modify the input flow in arterioles upstream of the capillary network to examine the link between the absolute velocity and the capillary network variation.

3.2 Control establishment

In intravital experiments, a certain amount of subjectivity must be applied so that one muscle or mesentery preparation can be compared to another. This subjectivity can only be built through experience and hard work coupled with a desire to improve techniques. Even so, the surgical preparations for intravital microscopy require handling sensitive tissues with extreme care. So my approach has required many more animals and preparations to fully develop surgical skills and intravital microscopic technique such that the protocols are finely developed and timing issues are reduced. With honed experience in performing intravital animal studies, it was possible to delve into functional aspects of the microcirculation.

3.2.1 Methods for control studies

Experiments were conducted using one of two standard control rat strains: Wistar and Sprague-Dawley (Charles River Labs, Wilmington, MA and Harlan, Indianapolis, IN respectively). The majority of the studies included herein are from Wistar rats, but Sprague-Dawley experiments were performed for comparison in selected cases. The first problem encountered after development of the imaging and computational systems was establishing a true control.

To establish an untreated control, muscle tissue from Wistar animals in different weight ranges was prepared as outlined above (§2.2.1. The fluorescent red cells were prepared, re-introduced, and their passage through selected capillary networks was tracked as previously described (blood cell labeling: §2.2.2, page 38). One to three capillary networks from the muscle were imaged and the network mean velocity and network CV determined from velocity recordings for each network. Velocity recordings were drawn from control animals from three different age groups: adolescent (180–260 grams), young adult (260-380g), and adult (400-440g).

This method of establishing controls relied on accumulation of many velocity datasets from several animals. In the following experiments that follow, a control velocity dataset was recorded from a network, then a treatment was applied. Directly after the treatment, the network was again imaged and the velocity data was analyzed. Determination of network CV before and after a treatment allowed direct analysis of a particular treatment by comparison of velocities in a given capillary network. Additionally, a sham

treatment method was used to validate each experimental method.

Methods to correlate network CV with systemic hemodynamic factors

The spinotrapezius muscle was prepared in anesthetized and cannulated rats as described in §2.2.1 (n = 9 male Wistar, weights ranging from 180–260 grams). The animals also were cannulated in the femoral artery for determination of heart rate and systemic blood pressure with a computer strain-gauge interface (MacLab, ADInstruments, Colorado Springs, CO). Blood pressure recordings were continuously obtained during the image acquisition for the velocity analysis and an average value over the period of the velocity recording was used for the analysis.

The velocity data is processed as discussed in the previous chapter, and capillary velocities found for clustered tracks. Network mean velocity and spatial variation (network CV) was also found. The network mean velocity was used as an index for the upstream flow to the capillary network. A diameter measurement of this terminal arteriole in the skeletal muscle was not performed due to the requisite addition of further contrast agents. The network mean velocity was also correlated with network CV, systemic blood pressure, and heart rate.

Methods for vasoactive control

The methods used to study vasoactivity were as outlined above for other control experiments. While observing fluorescent blood cells flowing through the capillary networks, it was readily apparent from the acceleration and deceleration of the fRBCs in the capillary networks that vasoactive arterioles were spontaneously modifying blood flow to the network. The velocity recordings from the networks that were perfused by vasoactive arterioles were assigned to a separate group for analysis. The spatial and temporal variation in the capillary velocity was assessed through network CV and temporal CV, as previously discussed. These vasoactive networks provide an important positive control for my assessment of temporal variation, because a high level of temporal variation is readily apparent.

Table 3.1: Experimental parameters from Wistar animals of different ages

Animal age	**Weight range** (g)	**Network number** (#)	**Average velocity parameters**		
			Network $\overline{v}$ (μm/s)	**Network CV** (%CV)	**Correlation** (%)
Adolescent	180–260	9	360 ± 100	26.5 ± 11.7	96.7
Young adult	260–380	8	692 ± 465	29.3 ± 8.8	96.7
Adult	400–440	6	656 ± 192	26.2 ± 6.7	94.1

3.2.2 Results from control studies

Network mean velocity and network CV for control groups

The network mean velocity and network CV calculated for three groups of Wistar control animals of different ages indicate that capillary network perfusion does not vary with animal age (Table 3.1). The average of the network CV for each animal weight range is shown with network velocity and network CV values and the correlation score from the correlation clustering method. The velocity is drawn from varying numbers of networks in each group. Network mean velocity and network CV were compared with a one-way ANOVA and found to be not significantly different ($p > 0.05$). The age of the animal has no significant effect on observed CV of network velocity.

Effect of clustering analysis

As presented previously, the clustering analysis of the data parses the velocity information into individual capillaries to determine the distribution of perfusion in the capillary network. By-path clustering follows the path that each cell traced during its transit through the capillary network. As a first approximation, by-path clustering can accurately analyze most networks, but for cells following many bifurcations in highly branched networks, by-path clustering does not describe the flow field with the same accuracy as by-segment clustering.

In one set of control animals (Wistar, n = 4, wt. 400–440g), the same velocity data was parsed with both clustering methods. The baseline network CV for "path" to "segment" is elevated from approximately 25% to 35% respectively as in Figure 3.1. By-path clustering allows the division of cell velocity into individual velocity measurements and the

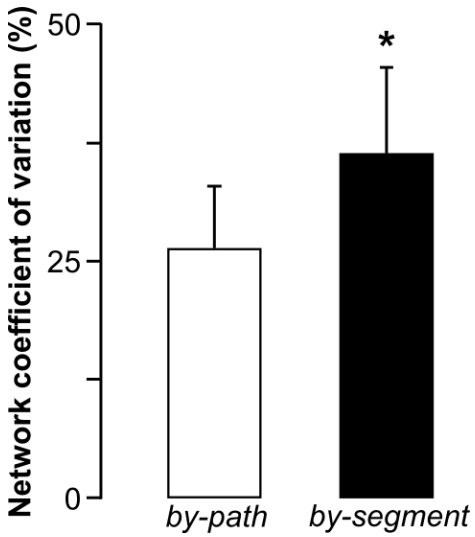

Figure 3.1: The effect of type of clustering method used on network CV. The same velocity data were analyzed with the two types of clustering utilized: *by-path* and *by-segment* clustering methods. The first method utilizes the cell velocity information from Image-Pro and performs no further manipulation, but instead simply parses the cell into an appropriate capillary cluster. The segment method requires user input to define a capillary segment as a collection of cell centroid locations, therefore manually constructing the capillary cluster. The final network CV calculated from the same data sets is significantly higher when by-segment clustering is used ($p < 0.05$). This reflects the intrinsic difference, that by-path methods cannot effectively cluster cells that flow in cross-connecting capillaries.

recombination into cell and capillary velocities for individual segments of the capillary flow path. This process adds capillary segments to the total number of clusters utilized from by-path clustering. A capillary path that previously included velocity measurements from a cross-connecting segment will be divided into three capillary segments — one mother capillary and two daughter capillaries at a bifurcation. The network velocity will be primarily unchanged, since the same velocity data is being analyzed with only minor differences, but, by addition of another separate low flow capillary segment — the cross-connecting capillary — there is an elevating effect on network CV. This difference is shown in Figure 3.1 as a significant effect — when comparing the same velocity data with by-path versus by-segment clustering a similar increase is always noted.

When velocity is modified by a treatment, by-path clustering can provide a quick and simple analysis of variation in the network. But, by-segment clustering does allow a deeper analysis of velocity data recorded. Unfortunately, as mentioned in the methods chapter, the method is time consuming and user intensive. A graphical user interface was designed to aid in cluster construction, but the program does not alleviate the need of a user.

For each group of animals, a consistent clustering method was applied. The selection of clustering method was based partially on when during the thesis research the group was completed. Early results were analyzed with "manual k-means" clustering only, whereas more recent animal groups were analyzed with all three by-path methods and the most recently developed by-segment method.

Control hemodynamics

A series of studies were first conducted to investigate the impact of hemodynamic factors such as heart rate, systemic blood pressure, and an index for capillary network for supply rate. The correlation between these parameters with capillary network velocity variation as assessed by network CV. The capillary network velocity data from 9 Wistar animals (one network each) were combined to examine the upstream factors.

Correlation between network CV and systemic hemodynamics

The correlations between both network CV and network mean velocity and the hemodynamic parameters were low. The network mean velocity shows weak positive corre-

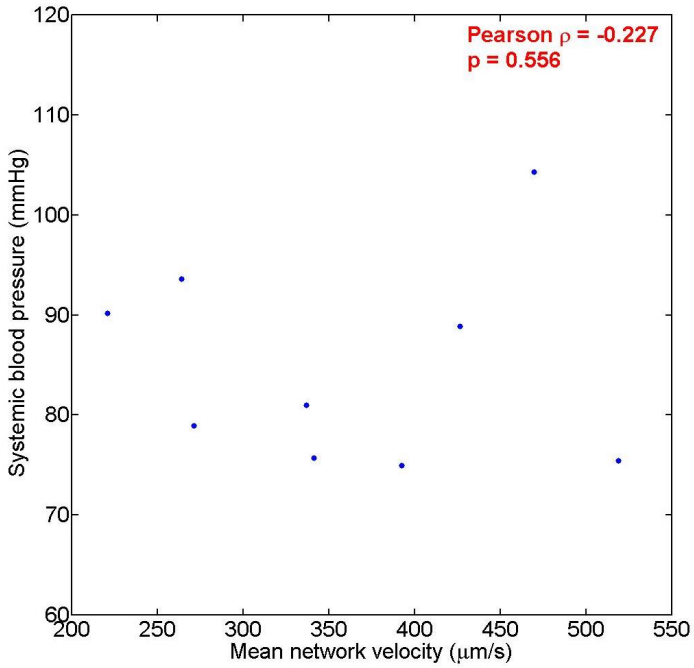

Figure 3.2: Display of network mean velocity correlation with systemic blood pressure for 9 capillary networks. The Pearson correlation coefficient was low (r = 0.227), and the high p-values suggests insignificance.

lation with the recorded systemic pressure (Pearson r = 0.335, p = 0.378) as in Figure 3.2 and non-significant positive correlation with heart rate (not shown, Pearson r = 0.542, p = 0.27). Both of these correlations of network mean velocity with whole animal hemodynamic parameters are insignificant.

Since the control capillary networks analyzed from the three age groups was not significantly different, the network velocities and network CVs were pooled. The network velocity and network CV for the 23 networks were compared by the Pearson correlation. The network CV shows no correlation with network mean velocity, as shown in Figure 3.3. The velocity data range from about 300 microns per second up to almost 1800 microns per second, but throughout that range, the coefficient of variation in velocity as assessed between capillaries of the same network — the network CV — did not depend on the velocity. The correlation coefficient found was 0.0865 (p = 0.68). If the single point at high velocity is neglected, the correlation decreases to r = -0.2165 but is still insignificant (p = 0.33).

The calculation of network coefficient of variation is the standard deviation of capillary mean velocities for the entire capillary network divided by the mean of capillary

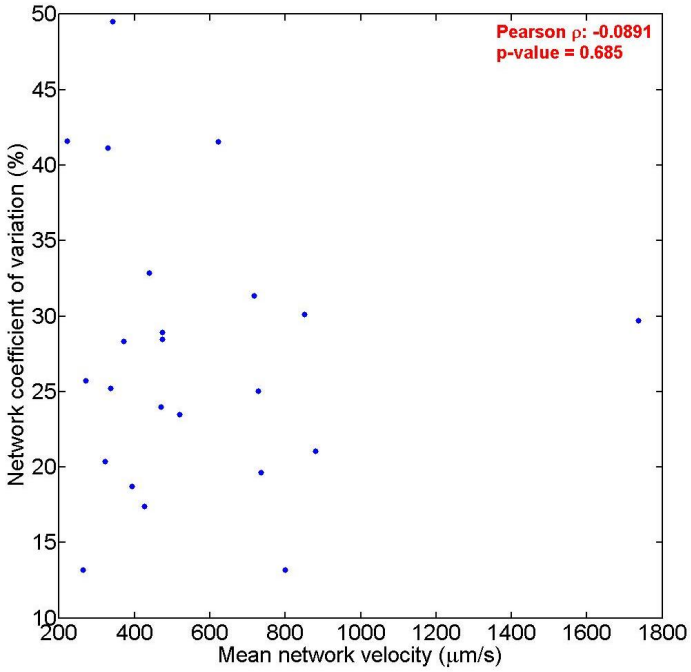

Figure 3.3: The correlation of network coefficient of variation with network velocity was found from 23 control networks from animals weighing from 180–440 grams. Recorded velocity and CV were similar by ANOVA from this range of animals. The velocity data range from approximately 300 microns/second to almost 1800 microns/second, but throughout that range of mean capillary network velocities, the network CV between capillaries of the same network did not appear to depend on velocity. The correlation coefficient was 0.0865 ($p > 0.6$). If the single point with highest velocity is neglected, an insignificant weak negative correlation exists (Pearson $r = -0.2165$, $p = 0.33$).

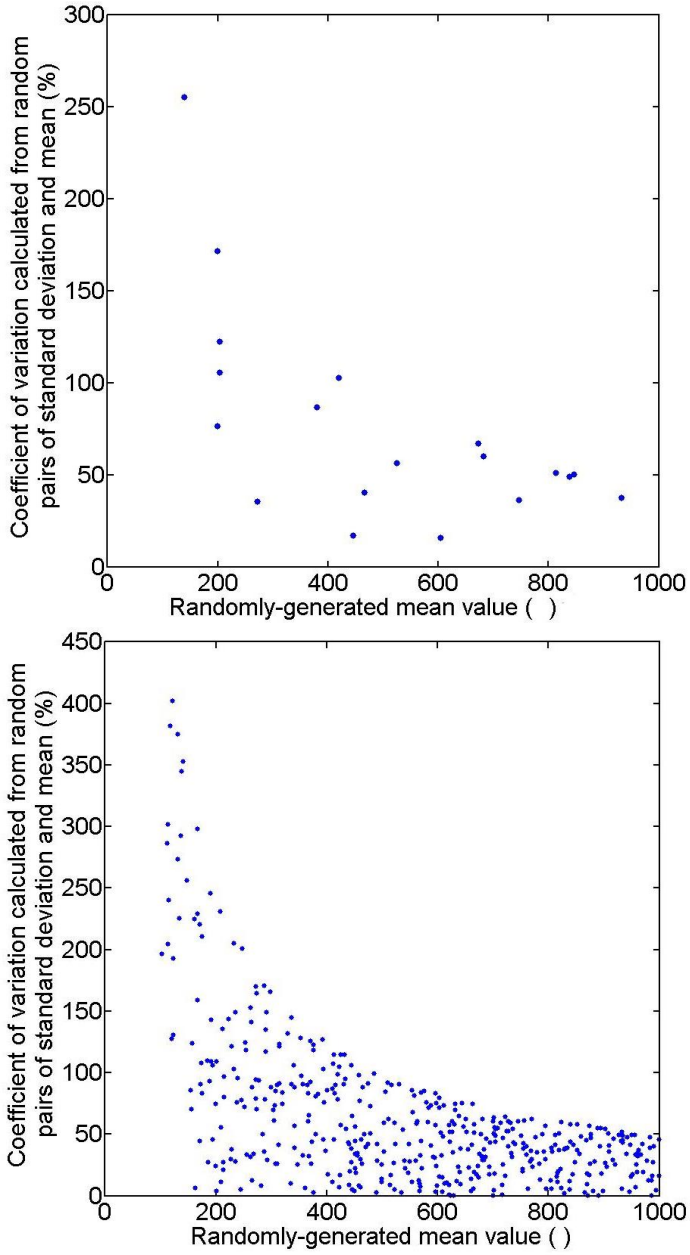

Figure 3.4: *Top:* Twenty randomly generated means and standard deviations were paired to generate coefficient of variation and view the correlation of CV with mean velocity. There is a significant autocorrelation introduced by calculating coefficient of variation and correlating with mean values (rho = -0.21, $p < 0.01$). *Bottom:* To further investigate this point, 500 standard deviation values and 500 mean values were randomly paired, and the CV was calculated. The CV asymptotically approaches 50% at higher mean values, but is unstable at lower mean values. This behavior is not witnessed from intravital velocity measurements displayed above in Figure 3.3.

mean velocities for the network (also called network mean velocity). By examining the correlation between network coefficient of variation and network mean velocity, a significant correlation should be introduced as a function of the calculation. To explore this point further, 20 values in the range between 0 and 1000 were randomly generated. Then, 20 values for standard deviation were randomly generated in the range between 0 and 500. This would allow for the calculation of coefficient of variation to be in a similar range as before - approximately 0 – 50%. These 20 pairs are plotted in the *top* panel of Figure 3.4. The correlation introduced into random data by comparing coefficient of variation to mean velocity is significant (ρ = -0.62, p < 0.01).

In further examination, 500 random points were similarly created. The randomly-generated CV plotted versus the mean asymptotically approaches infinity as mean approaches zero. This correlation is shown after discounting velocities under 100 microns/second in the *bottom* panel of Figure 3.4. The randomly-generated values display high coefficient of variation (>50%) in the range of mean velocity from 200 – 400 microns/second. The absolute values for CV found from the randomly generated numbers are dependent on the range selected. The trend is important: as mean value increases, the CV decreases with a negative correlation for the random data of rho = -0.57. The random data correlation suggests that the recorded velocity data were completely random, there would be a strong negative correlation. The actual result found was a *weak negative correlation* in the network CV versus network mean velocity. But finally, the asymptotic nature of the correlation was not witnessed in the *in vivo* results. While random numbers display instability at low mean values, the coefficients of variation from intravital velocity measurements are stable at mean velocities 200 – 400 microns/second.

Results from vasoactive networks

Velocity tracings from a control animal and a control animal exhibiting vasoactivity are displayed in Figure 3.5. The velocity tracings are averaged for one-second segments of the 60 second data set, and displayed for two experiments on the upper graphs: *left* for a control network and *right* for a vasoactive network. The bottom two graphs are the spatial variations calculated from the one-second segments of velocity data that has been parsed into individual capillaries. This displays second-to-second deviations in spatial variation over the minute-long data acquisition. The red dashed line is the temporally-averaged

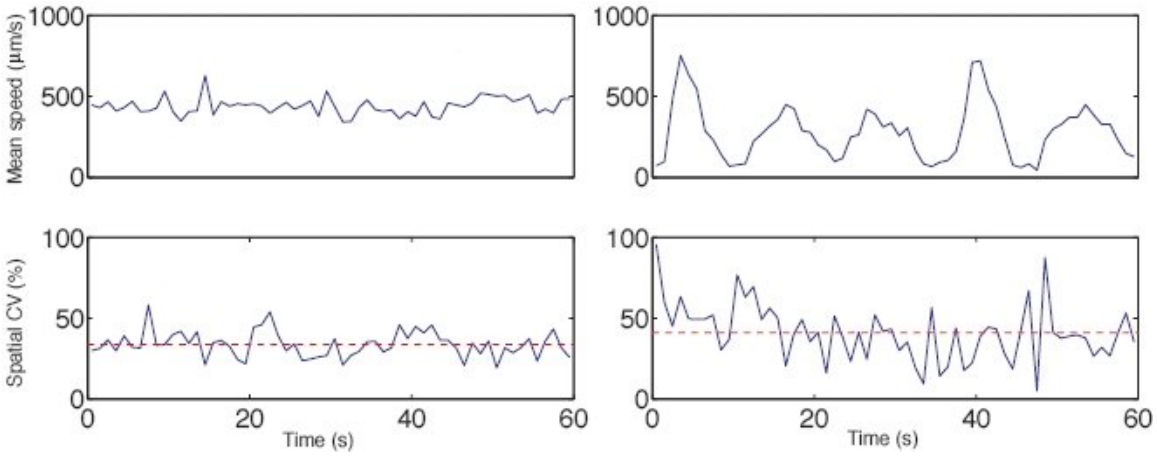

Figure 3.5: Instantaneous velocity tracings (*top-left, top-right*) and corresponding time-dependent network CV (*bottom-left, bottom-right*) from one minute acquisitions during a control experiment *left* and a vasoactive control *right*. While there is a degree of second-to-second temporal variation visually apparent in the control network, the obvious variability in vasoactive networks exists on approximately a 6–10 second time scale. This variability is consistent with previously described vasoactive velocity measurements. The red dashed line shown in the CV tracing displays the temporally-averaged spatial CV. The temporally-averaged spatial CV was 34% and 36% in these two cases. Overall, the vasoactive controls have similar spatial network CV despite the elevated temporal CV.

spatial variation. The final temporal variation assessed by averaging the velocity values for one-second segments was 47% for the displayed vasoactive network, but just 16% for the control network. The temporally-averaged spatial variations (as defined in §2.3.3) were 36% and 34% for vasoactive and control respectively.

The velocity recordings from other control and vasoactive networks were also analyzed for spatial and temporal variation. The spatial variation is assessed by network CV for each experiment, then combined as an average over each animal. The temporal CV was similarly combined. The summary of spatial and temporal CVs from selected and age matched animals is shown in Figure 3.6. The spatial variation for control and vasoactive tissues were both approximately 30% ($p = 0.76$), but the temporal variations were significantly different ($p < 0.01$). This may suggest that tissue can continue to control capillary velocities at very low and zero perfusion velocity.

A re-distribution of the one-second spatial CVs as a function of the one-second mean velocities provides further support for the hypothesis that velocity is not directly correlated to velocity variation. The velocity and corresponding spatial CV from the one-second segments in the temporal plot are re-plotted with CV as a function of velocity values.

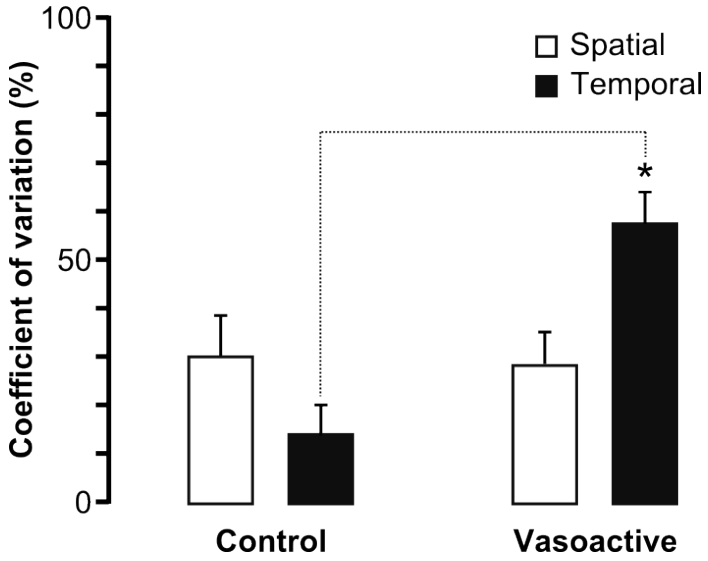

Figure 3.6: One-second averaged velocity *top* and temporally-averaged spatial CV *bottom* display the level of variation found in vasoactive networks. The mean of velocity measurements from one-second segments of the recording are taken as 60 separate second-to-second averages. Then, the standard deviation of one-second velocity divided by the mean of the one-second velocity is the temporal CV as shown as the red horizontal line. The temporal CV in the vasoactive network was approximately 47%, whereas the temporally-averaged spatial CV was 36%. The corresponding values from the plots for control tissue are temporal CV = 16% and temporally-averaged spatial CV = 34%.

Figure 3.7 clearly displays that there is no correlation between absolute velocity values and the corresponding one-second network CV (Pearson correlation r-value = 0.0035). For second-to-second variation inside individual networks, there also does not appear to be a relationship between CV and velocity.

3.3 Experimental approaches

To explore the hemodynamic interactions within the capillary networks, three experimental approaches were developed. First, a low-flow state was created via micropipette occlusion of an upstream arteriole. Then, enhanced flow was studied by application of two methods: electric stimulation of the muscle to "exercise" and maximal dilation of the muscle's arteriolar network via papaverine superfusion. These are experiments that have been conducted in the past, but capillary level results are either ambiguous or were analyzed with respect to *cell* rather than *capillary* velocity distribution. Furthermore, the level of detail achieved with the cell tracking method may allow deeper new assessment of the impact of hemodynamics on capillary network perfusion.

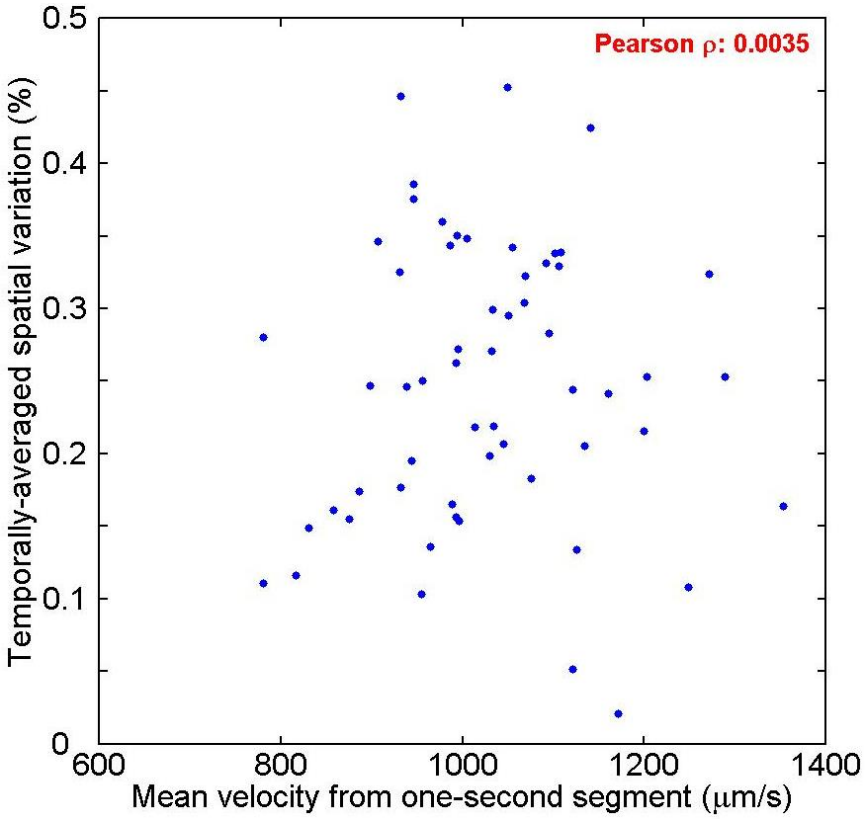

Figure 3.7: The one-second average parameters for network CV and velocity are plotted to determine the impact of absolute velocity value on CV. It was previously shown that increased absolute velocity values had a significant reducing effect on CV of velocity [160]. These data contradict that conclusion — the slight increasing trend shown by the red dashed line has only a 0.0035 Pearson r-value.

3.3.1 Impact of blood labeling on cell viability

During the compilation of Sprague-Dawley velocity recordings, a question arose concerning the viability of blood cells in suspension throughout the fluorescent labeling process. The labeling procedure described above in § 2.2.2 requires a series of centrifugation steps and insertion of a lipophilic membrane dye. Product descriptions suggest that the membrane dye can be cytotoxic at high concentrations, but the question whether the white cells in suspension could either be activated or the leukocyte fluid shear response attenuated is currently unanswered. Therefore, a series of Sprague-Dawley muscle preparations were performed to address the question whether white cell activation may have an impact on cell viability and network CV.

Methods for blood separation

The velocity recordings obtained with unseparated fluorescent blood cells were compared with those recordings with separated cell populations. Recordings from five muscle preparations were prepared in Sprague-Dawley animals with fluorescent whole blood (WBC+). Velocity recordings from muscles of two Sprague-Dawley rats were made with separated fluorescent cells (WBC-).

The protocol for labeling blood cell suspensions was modified to reduce white cell counts. The standard amount of blood (0.4mL) was withdrawn from the animal and a 10μL sample was taken for a white cell count (Unopette). A 200μL sample was then immediately layered on top of an equal volume of Histopaque-1077 (Sigma, St. Louis, MO) at room temperature. After 45 minutes of sedimentation, the relatively dense red cells had filtered through the layer of Histopaque, whereas white cells remained in the clear supernatant. The supernatant was manually removed from the red cell layer, and a 10μL sample was again taken for white cell counting. The remainder of the blood cell labeling protocol was followed as outlined above.

While the cells were separated, the Sprague-Dawley muscles were surgically excised for intravital microscopy as in §2.2.1. The cell labeling procedure and muscle preparation were both completed in similar times. The WBC-poor blood cells were re-introduced, and velocity recordings were obtained. The velocity datasets were analyzed as described in §2.2.3.

Table 3.2: White cell counts and separation efficiency for Sprague-Dawley animals

Animal (#)	**Before separation** (WBCs/μL)	**After separation** (WBCs/μL)	**Efficiency** (%)
1	5800	600	89.6%
2	4700	400	91.5%
3	3700	700	81.1%
4	3700	700	81.1%
5†	5100	1200	76.5%
5†	2700	500	81.5%
Average ± St. Dev.	4300 ± 1100	680 ± 280	84 ± 6%

†For the fifth animal, the white cell counting was performed twice. The separation procedure achieved $p < 1x10^{-4}$ statistical significance by Student's t-test.

Table 3.3: Impact of white cell labeling on network CV

WBCs	**Animals** (#)	**Networks** (#)	**Network** $\overline{v}$ (μm/s)	**Network CV** **by-path** (%CV)	**by-segment** (%CV)
+	5	21	621 ± 186	30.4 ± 6.1	39.0 ± 3.5
-	2	5	601 ± 185	22.3 ± 4.0	37.9 ± 6.9

Unseparated is shown as + WBCs, separated shown as - WBCs. Comparison of network CV insignificant via unpaired t-test (p = 0.76 by-segment, p = 0.17 by-path).

Results from blood separation studies

The results from five preparations with tracking of unseparated cell suspensions were compared with the results from two preparations with separated cell suspensions. Table 3.2 displays the white cell counts before and after the separation protocol and the achieved separation efficiency.

Selected results from velocity recordings with and without fluorescently labeled *white cells* are displayed in 3.3. The network CVs with and without separation of white cells were not significantly different (p = 0.76 when comparing by-segment network CV, p = 0.17 comparing by-path network CV). Therefore, it was concluded that the labeling procedure does not activate a quantity of white cells to significantly impact the CV results.

3.3.2 Occlusion of upstream arterioles

Control tissue provided a baseline for comparing variation between networks and between animals. The analysis was expanded by modification to the networks, first through manual occlusion of upstream arterioles to reduce flow rates to the capillary network. Second, the impact of rheological factors on the network CV during the occlusion periods allow changes to a small local region of the tissue, without upstream effects.

Methods for occlusion

A series of experiments in Wistar rats (260–380g) were conducted in which upstream arterioles were reversibly and partially occluded to reduce the perfusion rates in selected capillary networks. The muscle was prepared and an aliquot of blood cells were treated with fluorescent membrane dye as described above (§2.2.1 and §2.2.2 respectively). Then, video recordings were made prior to, during, and after (one minute each) occlusion with a blunt-ended micropipette directly applied on the abluminal surface of the arteriole feeding the capillary network. A micrograph of the pipette tip in place in relation to a network is shown in Figure 3.8. The perfusion in most capillary networks was reduced via occlusion at the level of the third-order arteriole, but logistically, the application of the micropipette varied between second- and fourth-order arterioles.

The micropipettes were prepared by pulling borosilicate glass capillary tubes (1mm OD $\times$ 0.5mm ID, 100mm length) in half with a Flaming/Brown style horizontal micropipette puller (Sutter Instruments, model P-87). The tip shape itself is unimportant, because prior to using a pipette, the tip is heated momentarily ($\sim$1s) in the flame of a match. This causes the tip to gently melt and seal closed. The size of the tip is rather large — approximately 50–100 microns in diameter. A smaller tip is not necessary and is certainly more robust against accidentally breakage during use. The rounded, "safe" tip minimizes tissue damage from the direct pressure application on the muscle.

After the muscle was prepared for intravital microscopy, the micromanipulator with needle holder was magnetically attached to the microscope stage, and the muscle visualized. The occlusion needle was brought into focus near a selected network. Proper placement of the pipette over the arteriole of interest was verified by slightly depressing the pipette onto the muscle and observing the capillary network flow through the eyepiece. When manipulation of the capillary flow was visually observed, the pipette was moved

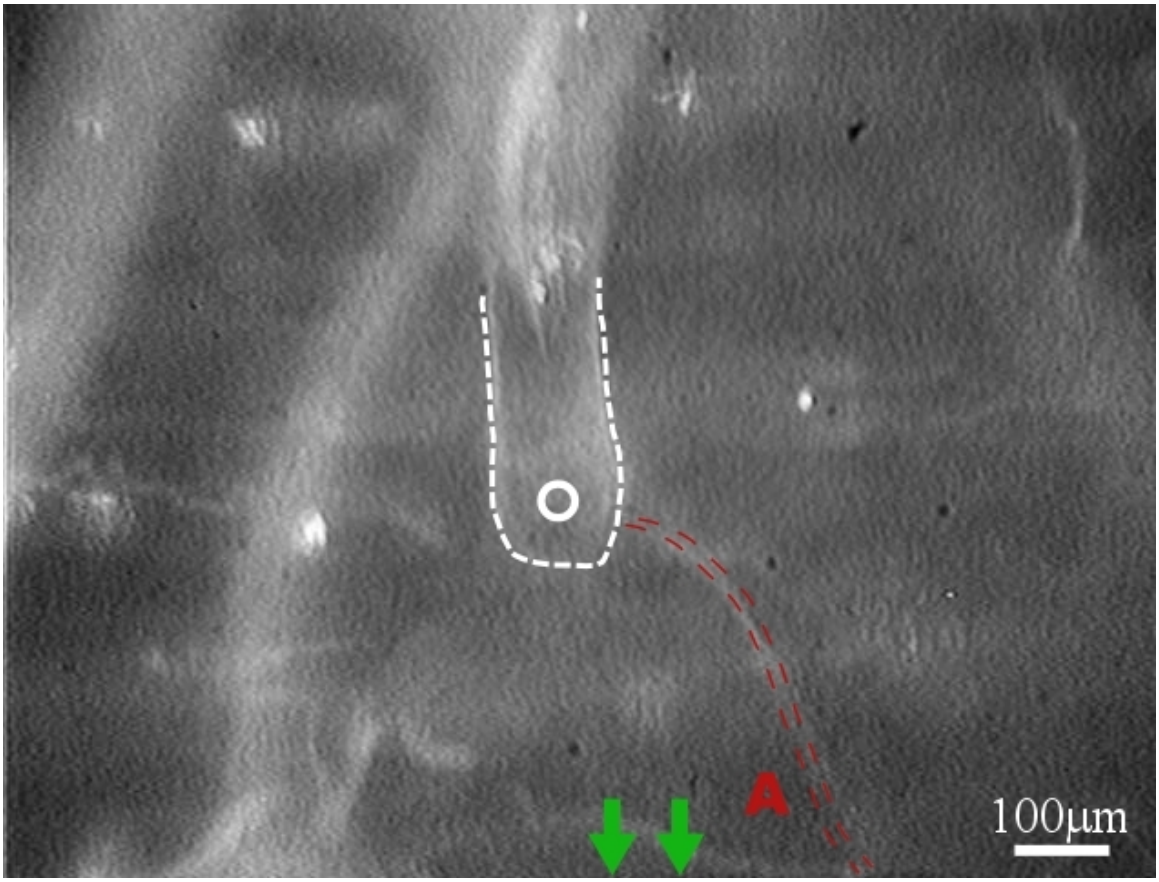

Figure 3.8: An *in vivo* micrograph with the tip of a micropipette shown surrounded by white-dashed line with an "O". The tip is placed to directly apply pressure for occlusion of the arteriole upstream of selected capillary networks. The location of the capillary network with respect to the needle placement was outside the field of view in the direction indicated by green arrows. The "A" and red dashed line highlights the arteriole. This partial occlusion was at the fourth-order arteriolar level, but in some cases the logistics of micropipette placement required second- or third-order occlusion.

vertically away from the tissue. This step ensured that occlusion could directly follow collection of images "prior to occlusion."

The fRBCs transit through the network was recorded for one minute. Then, the pipette was brought down on the tissue once more and flow was reduced. The initial pressure applied via micropipette often caused a transient period of reactive hyperemia as previously described [70]; additional forward translation served to compress the arteriole as needed. The flow rate was stabilized, and "during occlusion" images were obtained. Then, the tip was withdrawn from the tissue and a set of images "post-occlusion" were recorded. The three one-minute velocity recordings were analyzed as described in the previous chapter.

Results from arteriolar occlusion

The reduction of the blood flow in local areas of the microvasculature and even single capillary networks allowed analysis of function in a low flow state. Network mean velocity was calculated as the mean of the capillary mean velocities. Also, network CV was calculated for several networks from six animals. The manual k-means method was used to cluster the velocity data. The results for network mean velocity and network CV are summarized in Figure 3.9 for three cases: prior to, during, and post-occlusion. The data were analyzed for significance with the paired t-test compared with the "prior to occlusion" network CV and network velocity. The network velocity was significantly reduced by approximately 40% ($p < 0.01$, paired with pre-occlusion), but there was no concomitant increase in network CV during the occlusion ($p = 0.37$). Following the occlusion, the network velocity returned to within 2% of the original velocity ($p = 0.90$) and the network CV was also unchanged ($p = 0.59$).

3.3.3 Electric stimulation of muscle

Experiments were conducted to stimulate the muscle with electric pulses to generate contraction and "exercise" the muscle. The hypothetical result of the stimulation was that blood flow to the muscle would be enhanced following the simulated exercise. This principle is followed in everyday physical therapy and also by reports previously published in which muscles were stimulated and blood flow enhanced [14, 155]. The use of electric stimulation of muscle in my laboratory has been primarily in lymphology research — that is, muscle contractions to promote lymph flow and tissue/interstitial fluid uptake. There-

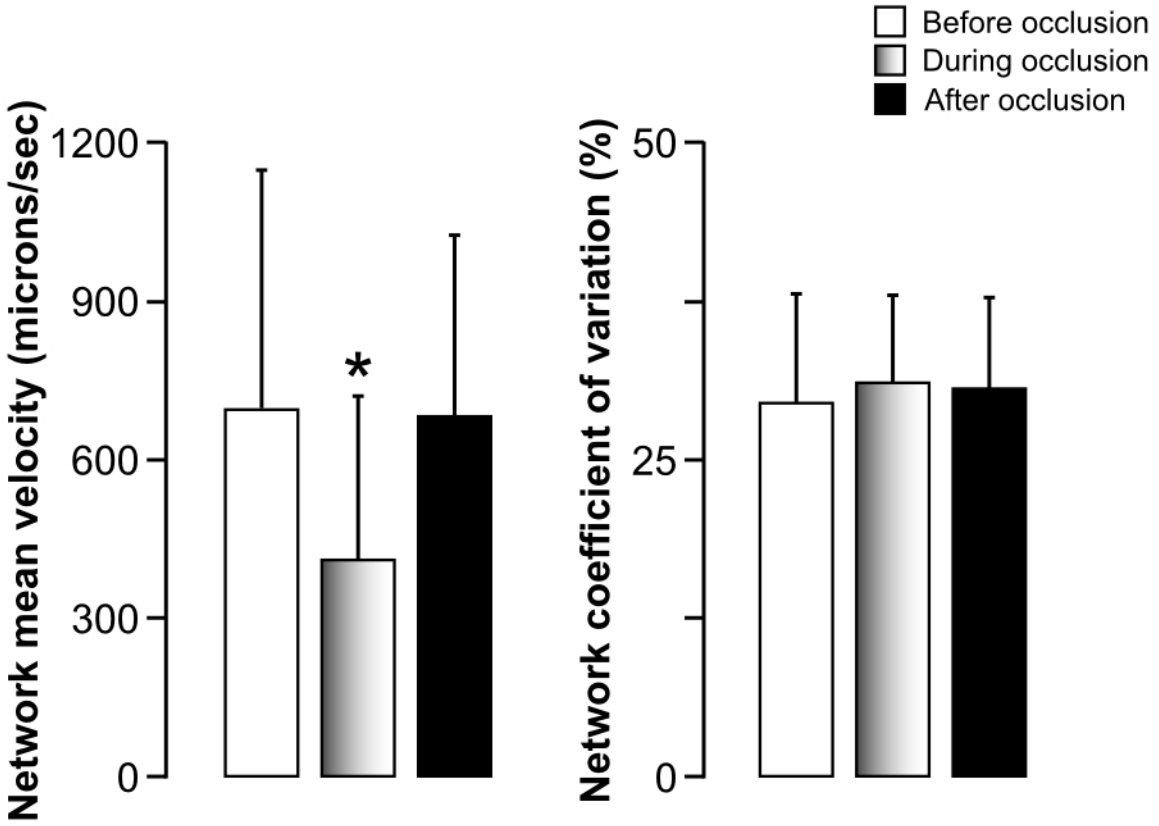

Figure 3.9: Network mean velocity *left* and network CVs *right* are displayed from eight capillary networks in five animals. Studies on occluded networks required the mechanical obstruction of upstream arterioles with a blunt-ended micropipette. The data is compiled for each network before, during, and after direct pressure application provided occlusion. The velocity was significantly decreased by over 40% (p ¡ 0.01) on average during the occlusion, but no impact on capillary network CV was shown (p = 0.37). After the occlusion, the velocities returned to within 2% of the original velocity (p = 0.90 compared to before occlusion) and the CV was also unchanged (p = 0.59 compared to before occlusion). Significance was assessed by the paired t-test.

fore, I utilized electrical values similar to those found in the literature [155]. The results are presented below followed by some basic questions and conclusions.

Methods for stimulation

The spinotrapezius muscle was prepared in young adult Wistar rats (n = 4, weight 260–380g). Prior to final stabilization of the muscle, one copper wire was buried in the yellow clay under the muscle preparation such that the wire would contact the underside of the muscle. The completed muscle preparation was placed over the top of the first wire, and a single capillary network was selected for intravital microscopy and acquisition of velocity measurements. The buried wire and a second copper wire were connected to a Grass stimulator (model 88) device to generate electric impulse sufficient to generate muscle contractions. The settings on the electric stimulator were as follows: 7V with 0.1 millisecond pulse duration and 1 Hz pulse frequency. The second wire was manually placed on top of the muscle to provide contact with the tissue. The stimulator was engaged and the voltage applied was visually capable of generating muscle contractions, and any reduction in voltage removed the visual muscle contraction.

The velocity measurements were determined from video records acquired before and after one minute of spinotrapezius muscle stimulation. A comparative analysis of the velocity in the capillary network was performed and the paired t-test was utilized to test for significant differences. The pooled cell mean velocity as computed from velocities measurements — the mean of the cell mean velocities for the entire network — was used as an index for the supply rate to the capillary network.

Results and initial conclusions from stimulation experiments

After stimulation I did not see the expected elevation of blood flow at the arteriolar level. The response to the exercise actually seemed to decrease the velocity in the capillary network in all trials performed. This initial observation was supported by the velocity results (Table 3.4). Brightfield images of the muscle (not shown) revealed that the muscle fibers appeared somewhat damaged and the autofluorescence under rhodamine epi-illumination was amplified. This effect of stimulating the muscle was unexpected, because of the positive results found from previously published electrical stimulation [14, 36, 155]. Due to lack of observed elevation in velocity, these velocity measurements were not further analyzed.

Table 3.4: Velocity results before and after stimulated muscle contraction

Animal	Pooled cell mean velocity	
	Before stimulation (μm/s)	**After stimulation** (μm/s)
1	458.8	404.3
2	340.4	348.3
3	514.2	495.0
Average	437.8	415.9†

† Not significantly altered by stimulated contractions (paired t-test, p = 0.35)

There are few differences between my protocols and previously published methods. I observe perfusion in entire networks of capillary vessels, which demands the utmost care during the muscle preparation. Furthermore, I study flow in a fragile, remote corner of the muscle, inside the thinnest portion. It is possible that by focusing my analysis in the thinnest portion rather than in thicker tissue that offers more support from muscle fibers and additional extracellular matrix, the networks were more sensitive to mechanical damage from forced contraction. The fascia layer surrounding the muscle was not dissected away from the tissue, which should provide some support to the tissue, but the contribution of the fascia for protection of the thin muscle layer has not been determined.

Another possibility arises due to pressure generation inside the muscle during contraction. It has been shown that pressure inside the human vastus medialis muscle during periodic voluntary contractions was elevated from pressures inside resting muscle [130]. In this study, it was found that the pressure elevation was dependent on tissue depth and degree of contraction. Thick muscles such as the human quadriceps were reported to generate intramuscular pressure of 700 mmHg during maximal contraction [147]. At intramuscular pressures of this magnitude, microvascular flow is reduced due to compression. Although the spinotrapezius muscle is thin, it may exhibit elevated pressure due to contraction. Intramuscular pressures were not recorded, nor was the degree of contraction in the rat spinotrapezius muscle measured. This mechanical explanation may partially explain the reduction in flow.

One further explanation for the lack of observed effect on capillary velocity is that capillary recruitment elevated the number of functional capillaries perfused in the network

rather than elevated velocity. It has been suggested that recruitment in spinotrapezius muscle is a minor effect following stimulated exercise perhaps due to the high basal rate of flow in this muscle [64]. The impact of capillary recruitment in these studies was not explored.

One final event that may have altered capillary hemodynamics following stimulated contraction was variability in sarcomere length. It has been shown that increased sarcomere length correlates with decreased capillary velocity [107]. I did not measure sarcomere length in my experiments, so the impact of increased or decreased muscle stretching is uncertain.

3.4 Discussion

A control system for capillary network perfusion requires rigorous analysis of capillary mean velocity distributions. Velocity is the variable under control of capillary diameter. Ideally, a study could be conducted wherein the velocity is obtained in a number of vessels simultaneously while diameters could also be determined. At this time, such a study is not feasible. At the microscopic magnification necessary to view a field of capillary vessels, recording consistent and accurate diameter measurements would be difficult. So instead, I observe velocity in a complete capillary network and observe the perfusion pattern as evidence of a control system.

The analysis of capillary perfusion with restriction of the comparison of perfusion between capillaries of the same network is novel. I have found previous research published wherein the measurement of velocity was made all in capillaries of the same network with the expressed intention to determine the source of variation in capillary perfusion [156]. But these researchers did not undertake a systematic analysis of velocity in a series of experiments. Other studies attempt to discuss capillary red cell velocity, but never approach a variable like the one computed for network CV. The coefficient of variation discussed in many of the previous works is comparable to the pooled red cell velocity. In one study, the red cell velocity histograms and corresponding CVs were displayed and appeared similar to those I constructed in §2.3.1.

The temporal and spatial variations in the capillary mean velocities are well captured by analysis of one minute records. Tyml and Groom studied variations in capillary flow over long time periods (5–20minutes), and concluded that 60 second acquisitions should be able to capture approximately 80% of the temporal variation [159]. The capillary network

pressure-flow relationship was simplified by restricting simultaneous velocity measurement acquisition to capillaries connected by same arteriole-venule pair. Therefore, the reported high level of network-to-network variation does not impact the network CV. The temporal variation present in capillary perfusion can be decoupled from spatial variation by averaging of cell mean velocities over the one-minute period. This reduces the impact of second-to-second variation on the final network CV calculation. The capillary level variation is still captured in metrics such as network CV and temporally-averaged spatial CV, since it is averaged, not filtered out as previously performed [158].

Vasoactivity and temporal variation

An interesting phenomena in vascular biology is the cyclic nature of vasomotor tone in arterioles. Although it was not viewed in all the preparations, approximately 1/3 of the muscles that were prepared displayed at least one network with vasomotor activity. As previously explained in §1.2.3, vasoactivity appears to be due to spontaneous cyclic Ca^{2+} currents in arteriolar smooth muscle cells. Although it has not been decisively linked to any particular dysfunction, in situations of reduced flow or ischemia, vasomotion hypothetically maintains minimal perfusion levels in all tissue regions of an organ [151].

Vasoactivity appears to be a natural response of the tissue, as previously concluded. It was witnessed spontaneously in tissue that was prepared under the same protocols as non-vasoactive tissue. Therefore, it was considered a variant of control tissue. The vasoactive data did show an elevated temporal variation on average, as computed by the temporal CV. But spatial variation as assessed by network CV was not elevated in vasoactive networks, nor was the temporally-averaged spatial CV different significantly different from control to vasoactive control. For these reasons, vasoactive networks were included in the rest of the thesis research as control networks.

The naturally occurring low flow states display spontaneous reductions in network mean velocity as a function of time. The reductions in network velocity did not correlate with any change in network CV in the same capillary network. The network mean velocity can be broken down into one-second segments to analyze temporal variation patterns, but still does display elevated capillary-to-capillary variation at low flow velocity. This evidence supports the hypothesis that capillary velocity is actively controlled by topological factors rather than being a function of passive rheological factors determined upstream of capillary

networks.

Temporal variation is naturally occurring in tissues under control conditions. The system developed can account for temporal variation, but the highly temporal variability in vasoactivity can be considered a natural state for tissue. Spatial and temporal variation (CVs) are reported above for vasoactive networks. The spatial network CV was similar to that reported for non-vasoactive tissue; therefore, despite clear differences in temporal variation (16% compared with 60% on average for vasoactive networks) for investigation of spatial variation, the temporal changes upstream may be neglected. The temporal CV was recorded for every experiment henceforth, but no further analysis was conducted to determine sources or impact on the network CV. Likewise, no significance between groups comparing temporal CVs was found above; "high" and "low" temporal CVs are found in the networks included in the animal subgroups.

Comparisons with previous capillary velocity measurements

The histograms and corresponding CV values correspond with previously reported values in the literature for *red blood cell velocities* [157]. The previous emphasis on pooled red blood cell velocity histograms and relatively high CVs suggested that flow was heterogeneous. Researchers did not take one step further and attempt to extract numbers for capillary velocity or network velocity from the RBC numbers. My work describes a method to complete the analysis, and shows a highly repeatable coefficient that might be used as an index for capillary network flow.

The basis for such a capillary network perfusion index required the completion of a number of muscle preparations to generate a baseline. In addition to the network velocity values determined from the capillary velocities, systemic measurements of heart rate and pressure were recorded. The capillary network mean velocities did not correlate with the systemic hemodynamic parameters. This finding is consistent with previous knowledge of capillary networks; the capillary networks are perfused by arcade arterioles that serve to control inlet pressures. Micropressure experiments were not conducted to verify this information, but could be a future elaboration on this study.

Control skeletal muscle perfusion provided repeatable network CVs at rest, and occlusion experiments also did not show elevated network CV, which suggests that reduced flow to the capillary network does not cause an increase in variation inside individual cap-

illary networks. Properties of blood associated with flow rate had been previously viewed as a source of variation in the capillary network, but may not be the primary factor determining network CV. At this point, the contribution of factors associated with flow rate to the variation as measured by network CV is small. I propose that vessel topology may be the primary contributor to the baseline variation measured by network CV, but active interactions between the endothelium or blood (leukocytes or platelets) may also comprise a considerable fraction of the total variation. Furthermore, capillary constituents may serve to reduce the overall variation from numerically-simulated levels.

Low range of recorded network CV

The range of network CV between 10–50% witnessed *in vivo* does not support existing computational models for capillary velocity. As mentioned in the introduction, computations for capillary velocity that did not presume any capillary level control over velocity displayed coefficients of variation ranging between 60–120%. A factor 3–4 difference between modelled and experimental parameters suggested that this model may be inaccurate. One other model that presumed strict control over capillary velocity at the capillary level provided a coefficient of variation of velocity of 0%. This model result was also not verified *in vivo*. The degree of variation between capillary velocities is created by rheological and topological factors — that may cause elevated coefficient of variations with *no control*. Any control over the variation in capillary velocity distribution may decrease the coefficient of variation.

Furthermore, the correlation between network CV and the network mean velocity was weak and insignificant. The calculations for network CV create a significant correlation as displayed from randomly-generated data above. This represents an inversion of the normal relationship: to show no correlation (i.e., random data distribution) between flow rate assessed by mean network velocity and the coefficient of variation between capillary mean velocities we should show a strong negative correlation as displayed by the randomly-generated numbers. The random numbers show such a strong, significant correlation because there are no bounds at low velocities on the degree of variation. But the asymptotic relationship at low velocities *in vivo* was not witnessed in the velocity recordings. The CV remained in a small range between 10–50% as mentioned above, even at very low network mean velocity. This may be a sign that the perfused vessels in any given

network are perfused at similar velocity despite overall low flow. From this we conclude that factors associated with overall rate of perfusion do not significantly impact network CV.

The issue of capillary recruitment in such networks must also be addressed. At low flow rates, a fraction of available capillary vessels are perfused. This fraction increases as flow rate increases. This is a variable that I did not determine due to technical limitations. The number of capillaries viewed in the network in a given time period depends on the passage of fluorescent blood cells. If a capillary is not perfused before *and* after a treatment, then the impact on the functional capillary density cannot be determined. In some cases, a fluorescent cell would become trapped in low flow vessels, but neither the cause of the entrapment nor whether plasma continued to flow in the vessel could be determined.

Study of capillary velocity in other tissues

Other muscles also have been shown to display approximately 30% CV from velocity measurements in the capillary network (unpublished results in rat cremaster muscle, Bertram *et al.*), but the question remains whether other tissues would show similar homogeneity. The study of other tissues would strengthen the case that the capillary endothelium responds to shear stress to control perfusion. Other organs would obviously require modification of methods, however, some work is being done in other tissues already, such as the brain [74]. Lung tissue has been previously examined and blood flow in the short highly branched structure has been termed "sheet flow" and the velocity therein is treated as a continuum [45]. So the vascular topology of different organs certainly impacts the degree of variation in capillary velocity. But the use of capillary velocity as an indication of disease has not been explored for most organs.

Leukocyte-endothelial interactions

The endothelial response to shear has been linked to anti-inflammatory cytokine release and gene expression profiles. In inflammation, the interaction of the leukocytes with the endothelium is viewed as elevated, but remains a stochastic probability. The impact of endothelial responses to shear that include nitric oxide release or dynamic modification of glycocalyx could be factors that provide the functional homeostatic rheological effects. Future efforts to investigate the impact of leukocytes on the capillary circulation could include

reduction of overall white cell counts. This could be accomplished through pretreatment with pentoxifylline, vinblastine, or an antibody to leukocyte membrane proteins (such as anti-CD18). The efficacy of each of these treatments for reduction of circulating leukocytes has been established. The network CV in animals with reduced circulating leukocytes would allow further assessment of whether active inflammatory processes impact the variation in blood flow at the capillary level.

3.5 Conclusions

In this chapter, I have found that the network CV is not directly correlated with the absolute velocity in the network. The variation described by the network CV can be decoupled from temporal variations, and does display the differences between capillary velocities in the same network. The baseline quantities for network CV established in this chapter can be used as a benchmark for future studies. The coefficient of variation was highly variable, as noted by previous researchers. More than even animal to animal results, network CV varies from network to network inside the same animal. This suggests that capillary network topology does contribute a significant portion of the variation that is present. But the question remains whether variation is minimized via a capillary-level control system.

Previous steady-state computations of capillary velocity showed a high coefficient of variation between capillaries when no systematic control over capillary velocity was presumed. As mentioned in the introduction, the CV ranged from 60 – 120% depending on initial and boundary conditions. But the variation *in vivo* was viewed to be lower than 50% in all networks. The fact that computations predict higher variation than measured quantities suggests that some elements of control over local velocity may exist at the capillary level.

The network CV has been established as an index for the control of capillary network variation. The evidence compiled thus far is primarily circumstantial, however, in that networks that were perfused at higher velocities did not display a lower CV. The independence of the CV with regard to velocity is an interesting result that suggests variation present may be controlled. The occlusion study wherein I reduced flow in capillary networks and did not see increased CV did show that rheology may not contribute additional variation. In the next chapter, I will investigate the possibility that mechanotransduction

mechanisms might contribute to minimization of capillary velocity variation.

3.6 Acknowledgements

The work described in this chapter will be summarized as a portion of a paper in preparation for submission that will be titled “The impact of endothelial mechanotransduction on capillary network perfusion”. The authors include myself, Namgyun Lee, Frank DeLano, and Geert Schmid-Schönbein.

Chapter 4

Capillary mechanotransduction

As discussed in previous chapters, the hypothetical control system for regulating perfusion in capillary networks relies upon mechanotransduction. In the second chapter, methods for analysis of capillary velocity were outlined. In the third chapter, control tissue was manipulated to determine the response to elevated and reduced flow in the same capillary network. In those studies, the function of the capillary endothelium was not probed since elevation and reduction of flow rates were attempted with mechanical methods. In the following chapter, experiments are described wherein the muscle endothelium was chemically treated with agents to modify perfusion. I chose to probe nitric oxide signaling and the glycocalyx as potential factors in a capillary level control system. Also, the interplay between these two fundamental endothelial functions was investigated.

Without constraining myself to a single hypothetical mechanism for capillary network perfusion control, I first aimed to disrupt a well-characterized endothelial response to fluid shear stress: nitric oxide production. The process of nitric oxide production and its effects on the microvasculature of many organs is currently a popular topic of research. Furthermore, there is wide acceptance that the typical endothelial cell response to shear stress is nitric oxide production.

The glycocalyx may also be a factor in capillary mechanotransduction mechanisms. The glycocalyx location and dimension at the interface between the endothelium and flowing blood could allow minute control over both hemodynamics and active signaling processes. Inflammatory interactions between the endothelium and leukocytes have been linked to glycocalyx removal. Molecules expressed in the glycocalyx or regulated by the glycocalyx are still being identified, but its ability to functionally control hemodynamics has already

been determined.

4.1 Nitric oxide inhibition

To investigate the impact of nitric oxide signaling on the putative mechanotransduction mechanism in the capillary networks of skeletal muscle, a non-specific inhibitor of nitric oxide synthases (NOS) was topically applied to the tissue preparation. The impact of inhibition on perfusion characteristics was studied as established in the previous chapter. The network CV was computed for single microvascular networks in skeletal muscle as an index for capillary network perfusion before and after inhibition. Mesenteric tissue was also prepared that served to verify the effects of nitric oxide inhibition through reaction with a fluorophore.

4.1.1 Methods for nitric oxide inhibition

Wistar rats weighing 180–260 grams were anesthetized and the spinotrapezius muscle was prepared as described previously in 2.2.1 on page 29. A sample of blood cells was removed and fluorescently labeled as before. Then, a single vascular network was selected for intravital microscopy and the passage of fRBCs was recorded. A topical superfusion of the potent, non-specific — that is, not specific to the endothelial subtype of nitric oxide synthase, but also an inhibitor of the neuronal and inducible subtypes — nitric oxide inhibitor L-NAME (N_ω-L-arginine methyl ester, 10mM, Sigma-Aldrich, St.Louis, MO) dissolved in Krebs-Henseleit solution was utilized to abrogate nitric oxide release. Two control experiments were conducted: first, a Krebs-Henseleit sham control was utilized, and second, the non-bioactive D- enantiomer of L-NAME (D-NAME, Sigma) was used as a 10mM addition to Krebs-Henseleit to verify that osmotic effects were not a factor. The images were digitized and processed as before, and the effects on capillary network perfusion were noted by the metrics previously described above. The results were compared for L-NAME treated animals (n = 6), sham control animals (n = 5), and D-NAME treated controls (n = 2) with the paired t-test to determine the effect of the treatment.

The inhibition of nitric oxide production was verified later in mesenteric microvessels through topical application of a molecule that fluoresces in the presence of nitric oxide, diaminofluorescein-2 diacetate (DAF2 DA). The DAF2 DA was incubated on the mesentery at a concentration of 3 μmol/L for 20 minutes prior to recording images under

FITC/fluorescein (L5 filter cube, bandpass 480/40nm excitation with 527/30nm emission; Leica Microsystems, Bannockburn, IL) conditions with the SIT camera set to the same manual gain settings for consistency. The same vessels were imaged before and after a 5-minute inhibition period with 10 mmol/L L-NAME to determine the degree to which DAF2 DA fluorescence had been reduced via attenuation of nitric oxide signaling.

Image analysis was required to determine final results from nitric oxide inhibition. Images from the spinotrapezius muscle were analyzed following the protocols set out previously. The images of DAF2 DA labeling in mesenteric vessels were analyzed by comparing intensity profiles in randomly selected vessels. The vessel was located under brightfield conditions and then the vessel was imaged under epi-illumination. The average pixel intensity was found inside a vessel-shaped region-of-interest (ROI) that was placed distant from the vessel to obtain a background intensity. Then, a segment of the vessel was selected with the same polygonal region of interest. The vascular intensity was recorded as the mean of intensity values inside the vessel ROI. As an example, see Figure 4.1.

4.1.2 Results from nitric oxide inhibition

Images acquired before and after nitric oxide inhibition were analyzed to determine how the reduction of the shear responsive signal impacted the capillary network perfusion in muscle. Also, mesenteric tissue was analyzed to determine the efficacy of 5-minute inhibition of nitric oxide with L-NAME.

Fluorescence verification of nitric oxide inhibition

Nitric oxide production was attenuated in the microvascular networks through superfusion with L-NAME. Verification of nitric oxide synthase (NOS) inhibition was performed with use of the fluorescent marker DAF. Micrographs (Figure 4.2) were recorded following DAF loading *before* and *after* topical application of L-NAME to inhibit NO production. The images depict reduced vascular labeling and also reduced mast cell labeling with DAF. This result suggests that the nitric oxide availability is impacted by the selected concentration and duration of L-NAME treatment. Intensity measurements inside and outside the microvessels were made from the micrographs. The reduction of NO availability in mesenteric microvasculature was significant ($n = 2$ animals, $p < 0.10$, paired t-test), but extravascular NO availability was not significantly modified (Figure 4.3).

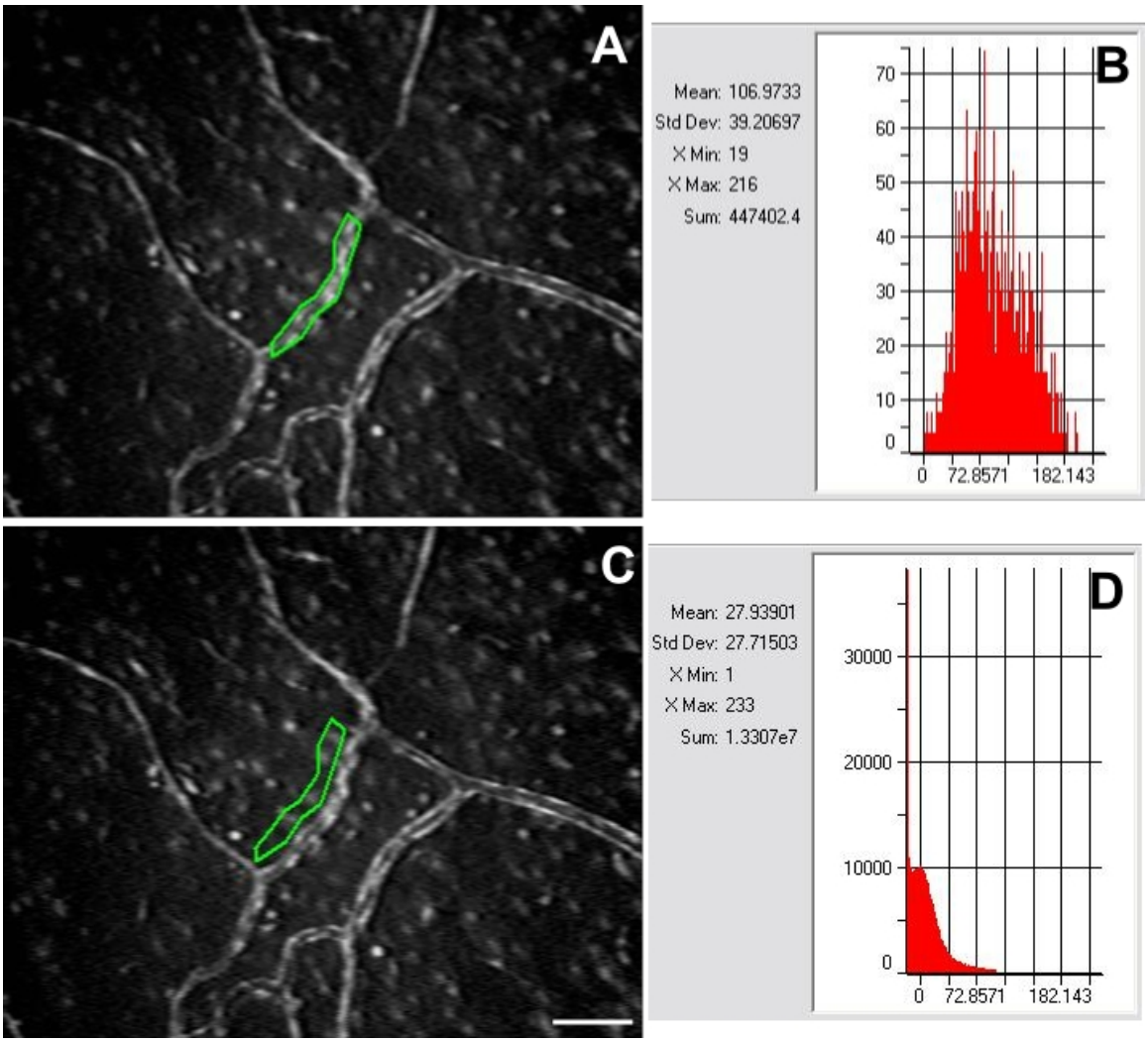

Figure 4.1: Vascular (*A,B*) and extravascular (*C,D*) intensity measurements allowed analysis of fluorescent intensity following DAF incubation on mesenteric vessels. A vessel-shaped ROI is placed over a vessel in a selected field (*A*) and the mean intensity is calculated from a histogram of pixel intensities (*B*). The same ROI is then moved adjacent to the vessel (*C*) and the mean intensity is again determined (*D*). The intensity measurements were performed on several vessels (*number of vessels:* from each mesentery preparation (*n=2*).

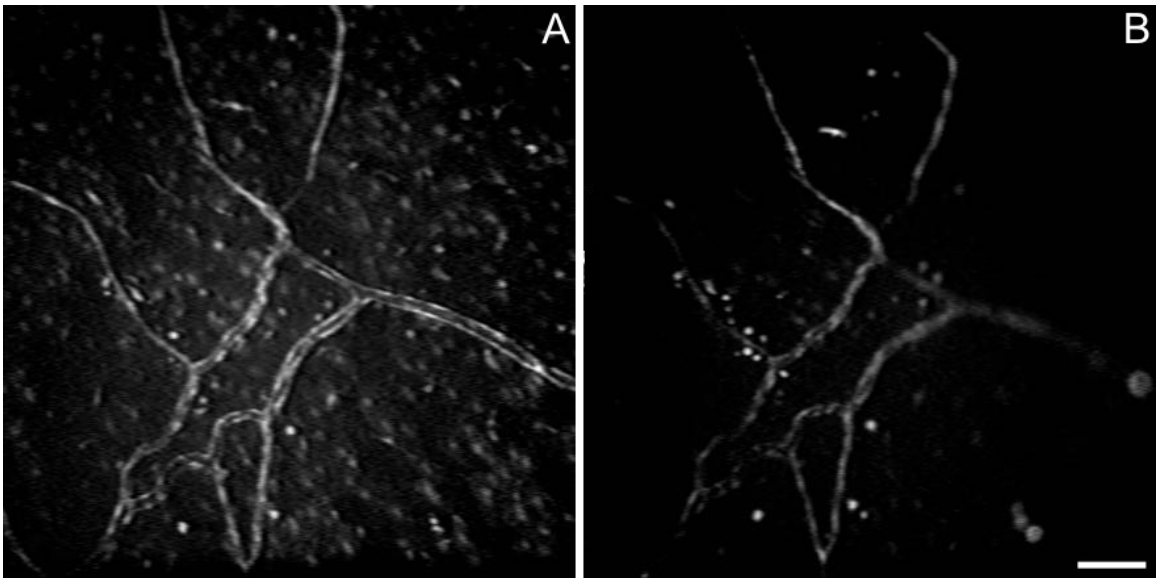

Figure 4.2: Intravital microscopy from mesenteric tissue provided images of DAF labeling in microvessels (A) before and (B) after nitric oxide inhibition. In this case, the same field is displayed before and after the treatment, but many images of vessels were taken both before and after the treatment for offline intensity analysis. Nitric oxide production was inhibited with topical superfusion of L-NAME (10mM for 5 minutes, 4mL/min). The scale bar is 100 microns.

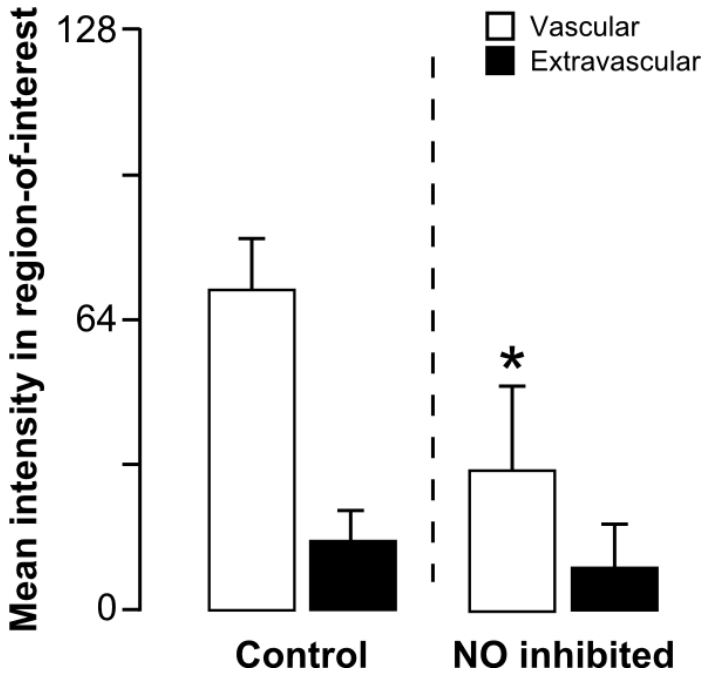

Figure 4.3: Intravascular and extravascular intensity measurements in mesenteric tissue labeled with DAF both before and after L-NAME treatment shows reduced microvascular NO availability. The vascular source of NO was significantly reduced by the L-NAME treatment ($p < 0.10$, n=2, paired t-test), but extravascular sources were not significantly reduced.

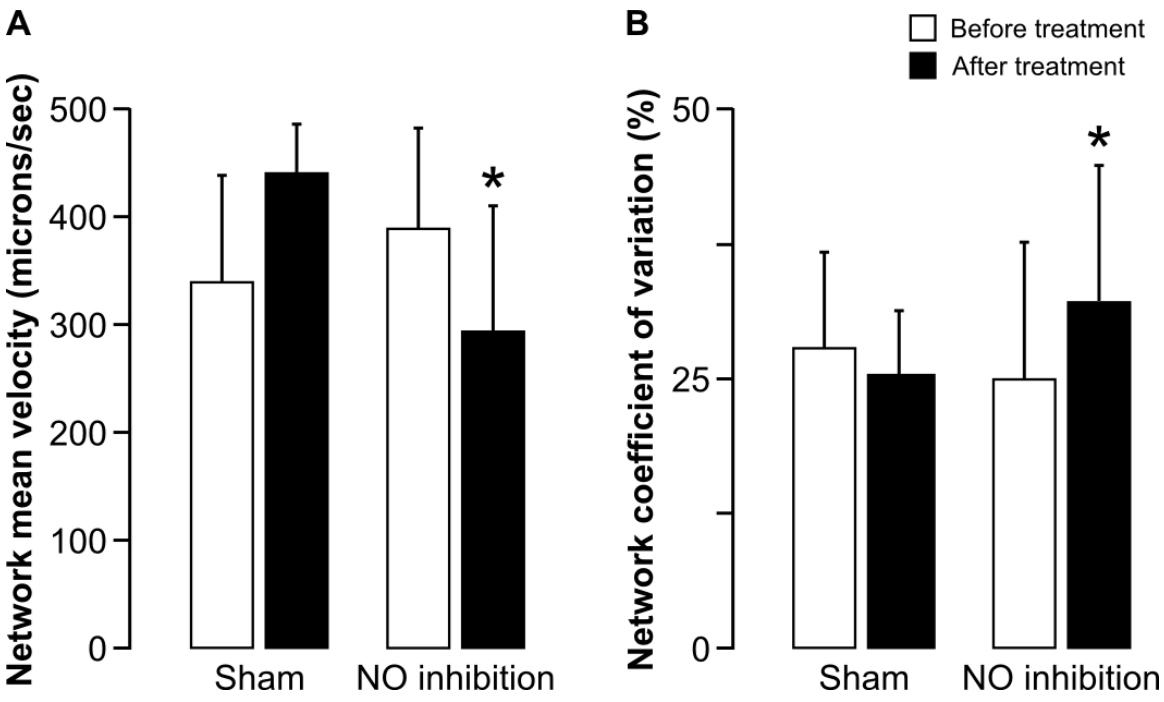

Figure 4.4: The impact of nitric oxide inhibition as assessed by measurement of variability in capillary network perfusion. Reduced nitric oxide bioavailability significantly elevated coefficient of variation between capillaries of the same network (spatial variation or *network CV*). The temporal effects were measured by the temporal average of spatial variation, but were not significantly changed by NO inhibition. Asterisk signifies $p < 0.05$ by paired t-test.

Capillary network velocity

The effects of nitric oxide inhibition on capillary network perfusion were noted by simultaneous acquisition of capillary velocities for all the capillaries of single networks. Similar control studies with either Krebs-Henseleit with no additional component or with D-NAME added were performed. The analysis of the velocity data was performed as described in the previous chapter. In brief, the spatial and temporal variations were reconstructed from clustered velocity data. The network CV was computed along with temporal CV. Figure 4.4 summarizes the effect of nitric oxide inhibition on both spatial variation as measured by the network CV and temporal variation as assessed by the temporal CV. With reduced nitric oxide availability, spatial variation was significantly elevated from 27% to 34% ($p < 0.05$ by paired t-test) — but temporal variation was not significantly modified. The tests with the non-bioactive D-NAME did not display any effect on either network mean velocity or network CV ($p = 0.41$ and $p = 0.55$, respectively). The studies with the sham control were also insignificant.

Table 4.1: Impact of slow cells in nitric oxide inhibition and corresponding controls

Group	**Average slow cells**		**Network CV with all cells**		**Network CV no slow cells**	
	(#)	(#)	(%CV)	(%CV)	(%CV)	(%CV)
	Prior	Post	Prior	Post	Prior	Post
CTL	10.4	7.8	27.7	26.6	25.3	25.4
L-NAME	3.6	14.5	25.7	24.2	32.2†	31.7†

† NO inhibition significantly increased network CV (paired t-test, $p < 0.05$)

The impact of nitric oxide inhibition on very slow or adherent cells was also analyzed. A custom MATLAB script for parsing velocity data called `Slowness` is reproduced in Appendix 6.4 on page 168. The code was used to locate cell tracks with cell velocity lower than 75 μm/sec. This allowed a cell to have a slow velocity at certain points, but not be pinpointed as a "slow" cell; only a cell that had a consistently slow rate of transmission was labeled *slow*. Table 4.1 summarizes the statistics for the incidence of slow cells in the capillary network after NO inhibition. The impact of the slow cells on the network velocity and network CV were also found. Approximately 1–2% differences were seen in the individual network CV measurements without slow cells, but the overall effect on the "control" and "NO inhibited" groups was minimal (less than 2%). A significant difference between the two groups was also present without slow cell velocities included ($p < 0.05$).

4.2 Dilated networks with papaverine

Control of capillary network perfusion at different arteriolar flow rates should allow analysis into the mechanisms that cause of velocity variation in the capillaries. If blood flow varies due to passive rheological effects, then modifications wherein the upstream flow is increased may have the effect of decreasing variation in capillaries, as was described above. To analyze a network with dilated arterioles, and hence elevated flow rates at the capillary network level, the alkaline opiate papaverine was topically superfused on the muscle preparations. The opiate functions as a phosphodiesterase inhibitor to increase levels of second-messengers such as cAMP and cGMP. As these messengers exist downstream of NO production, the papaverine treatment opposes nitric oxide inhibition by elevating the effects of dilatory signals and increasing blood flow.

4.2.1 Methods for papaverine application

The spinotrapezius muscle from adult Wistar rats (n = 4, weight 400 – 440g) was prepared for intravital microscopy as previously described above (§2.2.1). Also, the sample of blood was drawn from the venous catheter and fluorescently labeled with PKH26 as before (§2.2.2). When the muscle preparation had been completed, 1mg/mL papaverine (powder, Sigma, St. Louis, MO) was dissolved in 20mL Krebs-Henseleit superfusate buffer. With the papaverine solution prepared, the muscle was epi-illuminated at 545nm to visualize the fRBCs as before. Three to five networks were selected and perfusion through each recorded for a one minute period. After this period, the tissue was trans-illuminated and the objective placed over a larger (third- to fifth-order, or 20 to 40 microns in diameter) arteriole upstream of the networks of choice — the vessel was selected in a region with good tissue and vessel wall clarity to acquire diameter measurements. The papaverine solution was superfused over the tissue for a 5 minute period, during which the arteriole dimension change in response to the papaverine was recorded. After the 5 minutes, the tissue was again epi-illuminated and a network of choice was selected as representative for the capillary network perfusion response to papaverine and elevated flow.

The before- and after-papaverine recordings of capillary network perfusion were analyzed as above (§2.2.3). The network CV was used as a measure for spatial variation. Modifications of spatial variation inside individual capillaries were not viewed due to limitations in comparing the same capillary vessel before and after application. The diameter changes in large arterioles in response to papaverine were determined using calibrated digital length measurements (Image-Pro Plus). The relaxation response to papaverine treatment allowed verification of papaverine efficacy. The response was not uniform, and if the arteriole upstream did not dilate in response to papaverine treatment, the velocity measurement and network CV was removed from the final results.

4.2.2 Results from papaverine experiments

The effect of papaverine treatment on the muscle preparation was significant (Table 4.2). First, the vessel diameters did increase as expected, by 13.6% on average, following the 5 minute superfusion period. This vasodilation did not increase the capillary network velocity as hypothesized. I further hypothesized that elevated blood flow would significantly increase network velocity, but that the increase in network velocity would not have an effect

Table 4.2: Network velocity and network CV before and after papaverine treatment

Group	**Arteriole diameter** (μm)	**Network mean velocity** (μm/s)	**Network CV** (%CV)
Before papaverine	41.9 ± 15.7	656.7 ± 191.0	26.2 ± 6.7
After papaverine	47.3 ± 18.3†	597.3 ± 92.1	23.6 ± 8.2

† Significant increase in vessel diameter (13.6% on average, $p < 0.05$). ‡ The network mean velocity nor network CV were not significantly increased ($p = 0.14$ and $p = 0.41$ respectively).

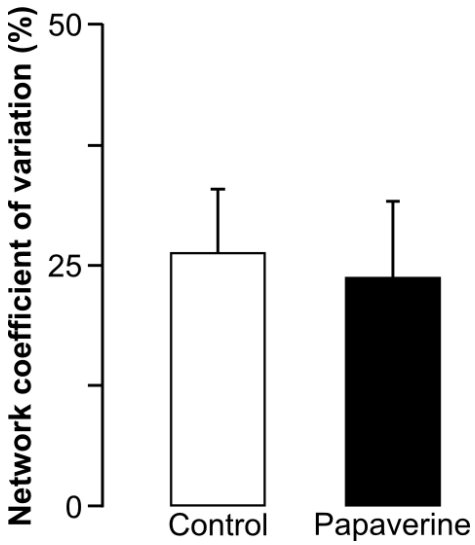

Figure 4.5: Summary of the effect of papaverine treatment on the network CV. Papaverine was superfused on the muscle for 5 minutes at 1mg/mL. This treatment has been shown to reduce vasomotor activity and dilate arterioles. While these effects were shown (see Table 4.2), the network CV was not significantly modified by the treatment.

on network CV. The observed effect of the papaverine treatment was no modification of network velocities ($p = 0.14$) and no effect on network CV in the six capillary networks ($p = 0.41$ by paired t-test from 4 animals). Final network CV calculations are summarized for all experiments in Figure 4.5. Additionally, an insignificant decrease in temporal CV accompanied the papaverine treatment (average, 33% → 22%), and the average data correlation score was found at 95.4%.

4.2.3 Discussion of papaverine treatment

The lack of increase in capillary network velocity was surprising. This may be due to control further upstream shunting flow away from the dilated spinotrapezius. Likewise, it may be due to other systems of control still functioning to maintain constant capillary inlet pressure. This response to papaverine was measured from a single network per muscle preparation, and network-to-network comparisons before and after papaverine were not attempted. The capillary network was also selected from a region far downstream in the thinnest tissue region. The elevated blood flow due to increased arteriolar diameter could have been directed primarily to networks proximal to the main feeding arterioles.

The papaverine treatment should inhibit phosphodiesterase activity, which would elevate levels of cGMP, the second messenger responsible for the dilatory response to nitric oxide in smooth muscle. This effect of papaverine likely predominates any further effect in arterioles. At the level of individual capillaries, the response to cGMP has been associated with permeability modulation, but no direct mechanotransduction effects. There has been a connection made between Ca^{2+} signaling and cGMP levels [167], and similarly, Ca^{2+} levels are directly related to the electrochemical connexin-dependent gap junction-mediated endothelial signaling known to be conducted from capillaries to arterioles [88]. Any mechanotransduction response that controls perfusion at the capillary level may not depend on cGMP. The cGMP elevation may also have had multiple effects that impact capillary perfusion. Further investigation of cGMP levels on capillary network perfusion would be necessary to decouple these effects.

4.3 Enzymatic removal of glycocalyx

Previous research probed the function of the glycocalyx *in vivo* and *in vitro* with delivery of various active enzymes that cleave one component from the structure. As out-

lined in the Introduction, the holistic structure of the glycocalyx may determine the complete function, but some individual enzymes were shown to have different effects (see page 11 for more details). It has been shown that mechanosignaling can be modified post-treatment with heparinase [37], an enzyme that degrades heparan sulfate proteoglycans. For this reason, the effect of heparinase delivery to muscle capillary networks was studied.

4.3.1 Methods for glycocalyx studies

The capillary velocity measurements were combined from four spinotrapezius muscles from Wistar animals (n = 4). The verification studies in mesentery were performed in additional Wistar animals. The images of lectin infusion were recorded in the mesentery of Wistar animals (n = 5). For this study, all animal weights ranged between 200 – 280 grams. Finally, a single ampule of heparinase III enzyme was aliquotted and used for the *in vitro*and all *in vivo*studies. Studies were performed with multiple lots of fluorescein- and AlexaFluor488-conjugated lectins. But images shown herein — and the corresponding intensity measurements — were all based on AlexaFluor-lectin labeling of the tissue.

4.3.2 Methods for heparinase delivery

The delivery of an active enzyme to the systemic circulation of a rat may have wide ranging effects, and therefore, it is difficult to decouple one result from another. For this reason, micropipette injection of the enzyme was performed. Microinjection has the benefit of providing minute quantities of active agents at relatively high concentrations directly to upstream arterioles such that when the dosage delivered finally reaches the general circulation, only minute quantities exist to further disrupt the animal. Therefore, microinjection represents a fine-tuned, tissue-oriented delivery technique that was optimal for the heparinase delivery.

Micropipette fabrication and utilization

The construction of micropipettes has been described many times in the literature (one such reference [104], and several commercial ventures have made technologies available for pulling capillary tubes into serviceable micropipettes. It was desirable to develop methods of my own for construction of pipettes that were both reproducible and effective. The Flaming/Brown P-87 micropipette puller (Sutter Instruments, Novato, CA) allowed

Table 4.3: Puller settings for construction of micropipettes for intravascular perfusion

Injection	**Puller stage settings**				**Pipette**
location	**Heat**	**Pull**	**Velocity**	**Time**	**tip shape**
Muscle	620	20	20	15	fat, with
	580	10	25	22	straight taper
	595	55	55	22	into 5–10μm tip
Mesentery	680	50	25	244	long, narrow
	650	30	15	50	barrel tapers slowly
	620	35	122	50	to 5–10μm, then
	650	25	25	55	closes at 2–3 micron tip

pipettes to be made for two applications — injection into muscle arterioles and injection into mesentery vessels. The pipette tips utilized for these two injections were somewhat different, simply because the tissues are somewhat different. The muscle pipette was constructed using a three-stage pulling process, and each row reflects the settings for a single stage. The mesentery pipettes were pulled using a four-stage process. After the final stage in both cases, the glass capillary tubing was drawn into two separate pipettes. Settings utilized for pipette construction on the pipette puller are included in Table 4.3.

Muscle tissue has a layer of relatively tough connective tissue that must be pierced and — in most cases — the arterioles which were selected for microinjection were large arcade vessels approximately 50 microns in size. The mesentery tissue is thin with little connective tissue on the vessel that generally is 20–30 microns in diameter. Mesenteric vessels never grow as large as an arcade arteriole until they are buried deep in the fatty tissue that surrounds sector vessels — making them poor candidates for microinjection. The tip of the micropipette was the primary difference between the pipette.

After micropipettes were constructed, it was necessary to ensure that the tips were open to allow transmission of fluid to the vessels. Visual inspection on a laboratory microscope first showed a closed tip as was desired — closed tips can be freshly fractured which yields a sharper and generally smaller tip for micropuncture. Then a small polystyrene weigh dish was filled with de-ionized water and the pipette carefully pulled backward away from the tip direction, barely touching the bottom of the dish surface. The pipette tip was broken open and water drawn into the micropipette by capillary action. The amount of

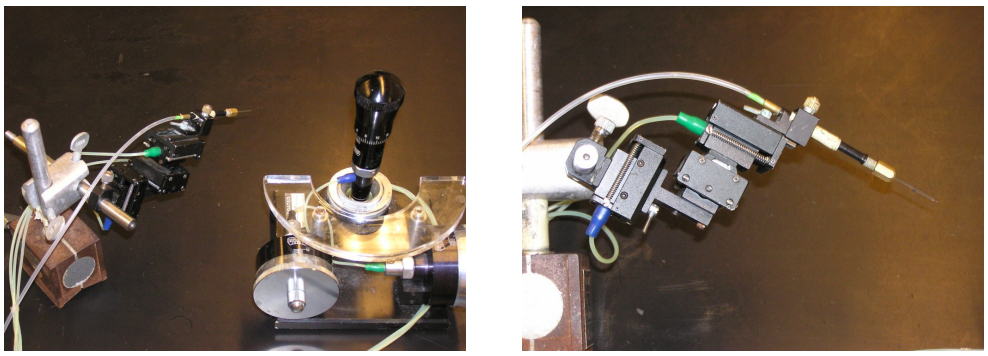

Figure 4.6: *Left:* Micropipette setup shown with pipette holder on magnetic stand and manipulator controls. *Right:* Needle holder in side view displays steep approach angle for microinjection studies.

water drawn up should be related to the size of the tip opening, which was easily viewed through the eyepieces. Pipette tips were freshly fractured just prior to the commencement of a surgical preparation.

The freshly fractured micropipette tips were backfilled with a long 30 gauge needle (Hamilton, Reno, NV) and placed in a custom needle holder with a single tubing (PE-90) channel attached to a glass syringe for pressure-driven fluid delivery. The needle holder was fixed on a micromanipulator (Narishige, East Meadow, NY) capable of articulated motion in three dimensions as shown in Figure 4.6 (*left*). The micromanipulator was then centered and ready for the experimental tissue preparation. The right picture shows the relatively steep approach angle assumed for the microinjection. This angle was assumed for clearance over the stage and, in mesentery preparations, the gauze that stabilizes the tissue. It should also be noted that the angle of approach altered the directionality of the manipulator controls significantly. *Forward* on the manipulator controls became forward-down, and *down* became down-backward. Left and right motions were not altered by the approach angle.

In vivo methods

Male Wistar rats weighing between 200 and 280g were anesthetized intramuscularly (sodium pentobarbital, 50mg/kg) and cannulated in the femoral vein for maintenance of anesthesia as needed (5mg/kg). An aliquot of blood cells was drawn into heparinized saline, and fluorescently labeled as outlined above. The right spinotrapezius muscle was prepared as previously described (§2.2.1 on page 29). One additional step was performed

with a surgical microscope: micro-forceps and micro-scissors were used to carefully trim connective tissue away from the surface of the muscle around the feed vessel and arcade arteriole proximal to the thin muscle region. This step facilitated access to selected vessels with the micropipette for infusion. Then the fRBCs were re-introduced and a series of 3–5 one minute movies were recorded that captured capillary network perfusion in selected networks downstream of the target arteriole. These movies provided a baseline level of capillary network perfusion in the same networks that were viewed after enzymatic degradation via heparinase treatment.

Following baseline image acquisition, a micropipette pre-filled with 1 U/mL heparinase (Sigma unit defined as amount of heparinase required to convert 1 mole of heparan sulfate into 1 mole of glucuronic acid in one hour) was aligned and placed proximal to the arteriole by the unaided eye. Under the microscope, the micropipette was carefully manipulated on top of the arteriole such that a small indentation into the arteriole was visible. In many cases, a small amount of connective tissue still covered the arteriole, and side-to-side motions with the pipette tip coaxed an opening to reach the vessel outer aspect. With the pipette tip firmly in place atop the arteriole, a sharp forward thrust of the manipulator with a slight concomitant downward motion pierced the vessel wall. In some cases, this final step had to be performed a number of times until finally the wall was pierced. Even when the pipette tip is in the lumen of the vessel, resolution of the tip location can be difficult. A slight pulse of pressure on the micropipette fluid served to effectively display the location of the tip. If the tip was pressing on the outer aspect of the vessel, a small amount of pipette fluid would bath the surface of the vessel. If, conversely, the pipette tip was in the vessel, a bolus of fluid would be visualized in the vessel replacing blood flow temporarily. A third case, which was often found, was that the tip was lodged in some location through which a pressure pulse could not push fluid — that is, in the vessel wall or up against the inner lumen or outer aspect of the vessel tissue. Small manipulations of the pipette were often necessary, even throughout the microinjection period to maintain flow out of the pipette tip.

After the tip containing heparinase was in position to deliver fluid to the arteriole, a timer was started and small pressure pulses were manually applied to a syringe connected to the micropipette fluid channel. Ten minutes of pulsed delivery alternating with the blood perfusion was visible. In some cases, the pipette tip would clog or clot inside the lumen of the

vessel, and fewer than ten minutes of delivery was achieved. These cases were not included in the results below. Following 10 minutes of heparinase delivery, the micropipette was withdrawn and moved distant from the muscle, and the circulation was again viewed under epi-illumination. The networks that were previously visualized and perfusion recorded were found once more and the flow after heparinase treatment was imaged. Generally, the same networks were visible and easily found, but in some cases, the effect of treatment changed the tissue "landscape", making re-visualization difficult. Flow in at least one capillary network was recorded both before and after heparinase treatment in each experiment included below.

Verification of heparinase function and delivery

In order to verify that an effective concentration and quantity of heparinase solution was deliverable via micropipette injection, two studies were completed. The first was an *in vitro* experiment that simply verified the heparinase activity in the purchased heparinase enzyme. The enzyme was reconstituted from lyophilized powder in a Tris-buffered saline solution at pH 7.0 as suggested (Sigma). The powder was solubilized at the final concentration of 1U/mL and 200μL was aliquotted into storage tubes and frozen at -20°C. A single tube of heparinase was later thawed and serially diluted to included 1x, 1:10x and 1:100x dilutions. A spectrophotometric assay was performed on the solutions to determine heparinase activity as follows: 20μL heparinase solution was combined with 0.1% heparan sulfate proteoglycan (Sigma) in a transparent cuvette for 30 minutes. After 30 minutes, the cuvette was placed in a spectrophotometer and the light absorbance at 235 nm wavelength — that of the heparan sulfate byproduct glucuronic acid — was determined. This information is directly correlated back to the unit (U) value for efficacy of the enzymatic cleavage.

The second experiment conducted to determine the delivery efficacy of the enzyme required the use of an *in vivo* marker for the glycocalyx. The goal of the study was to first label the glycocalyx, then apply the heparinase via micropipette and quantify the degree of removal of the glycocalyx. A number of techniques were attempted, both in the muscle and finally in the mesentery.

First, topical superfusion of lectin (GSI-B_4, AlexaFluor488-conjugated, 25mg/mL, Invitrogen, Carlsbad, CA) of the muscle was attempted following protocols previously described [54, 171]. This method of superfusion was seen to label all capillaries and small

arterioles and venules with diameter on the order of 20 microns with high efficiency, but also labeled lymphatic vessels and some larger microvessels. However, I hypothesized that primarily the external aspect of the vessel was labeled with topical lectin application. A series of micropipette injections of the lectin were conducted, with the pipette solution containing 25mg/mL lectin in 10U/mL heparinized saline to prevent tip clogging. This set of experiments achieved a much lower degree of labeling in the tissue, such that the vasculature was only sporadically visible over the muscle background fluorescence under 488nm excitation. This observation supported the hypothesis that external versus internal application stains different motifs in the vessel, but also revealed that muscle tissue would not be suitable for this verification step. The high background intensity and inability to selectively label capillary networks with lectin were obstacles difficult to overcome.

For this reason, mesenteric vessels were targeted for lectin application, first topically and then via micropipette infusion. This protocol had a number of advantages over the use of muscle tissue, but also some disadvantages. First, the mesentery tissue displayed an immeasurable background autofluorescence. Second, the stain intensity was relatively uniform when applied locally and the entire mesenteric sector circulation was accessible with lectin. An unfortunate side-effect of facilitated labeling and imaging was that the exact tissue utilized for velocity recordings was not usable for verification processes. This was a drawback that was weighed heavily, but it was assumed that the mesenteric microvessels would have similar glycoprotein moieties for intravascular labeling and would serve to verify that the heparinase treatment effectively reduced the glycocalyx.

Images from video recorded *in vivo* were digitized and intensity measurements were made that distinguished vascular lectin labeling from extravascular labeling. A polygonal region-of-interest (ROI) was created that included a single vessel, and the mean epi-illumination intensity value inside the ROI was obtained. The ROI was then moved adjacent to the vessel to obtain an extravascular intensity measurement. The extravascular measurement for lectin labeling performed a singular purpose of normalization to background intensity. The ROI was the same size and shape and was placed within 5–10 microns of the vessel to obtain an area-sensitive background reading. Intensity measurements were made on 101 vessels from 4 animals *before* and *after* heparinase treatment.

Impact of heparinase application on nitric oxide production

This study was performed once in a single Wistar animal as a pilot study. The rat mesentery was prepared as outlined above (§2.2.1 on page 34) following cannulation under general anesthesia. As above, micropipette tips approximately 1-3 microns in diameter were prepared. A pre-dispensed aliquot of heparinase enzyme (1U/mL concentration, 200μL total volume in Tris-buffered saline) was thawed from -20°C. The micropipette was backfilled with a long 30-gauge needle and mounted on the needle holder and micromanipulator. Mesentery sectors were selected that had large vessels crossing through the center of the sector. The main arteriole in the sector was pierced with the micropipette and heparinase was infused for 5 minutes. Following heparinase infusion, a DAF solution (3μmol/L DAF2-DA, 2mL/min rate) was topically superfused over the mesentery preparation for 20 minutes. After the DAF incubation period, brightfield and epi-illuminated (FITC wavelengths) images allowed visualization of NO production in the mesentery tissue.

4.3.3 Results from heparinase treatment

For the velocity measurements in muscle preparations, flow in 2–4 networks in each muscle was recorded. Then, heparinase was micro-infused for a period of 10 minutes. Immediately following infusion, the pipette was withdrawn, and the flow through the same 2–4 capillary networks was again recorded. The network velocity and CV were first averaged for each animal to reduce the network-to-network variation. The final velocity and CV numbers for each animal are reported.

The images obtained in mesentery preparations demonstrated lectin delivery and subsequent heparinase treatment. Again, the intensity measurements were made on a number of vessels and averaged for each animal. Then, the intensities of glycocalyx labeling are reported for each animal.

Capillary network velocity

Capillary velocity was significantly modified by treatment with heparinase. The network velocity was increased from 420μm/s to 773μm/s on average over the 4 animals (*p < 0.05). Furthermore, the distribution of velocity in the capillary networks was modified. The analysis was performed using both *by-path* and *by-segment* clustering methods, and differing results were found. The normalization process with the correlation by-path method

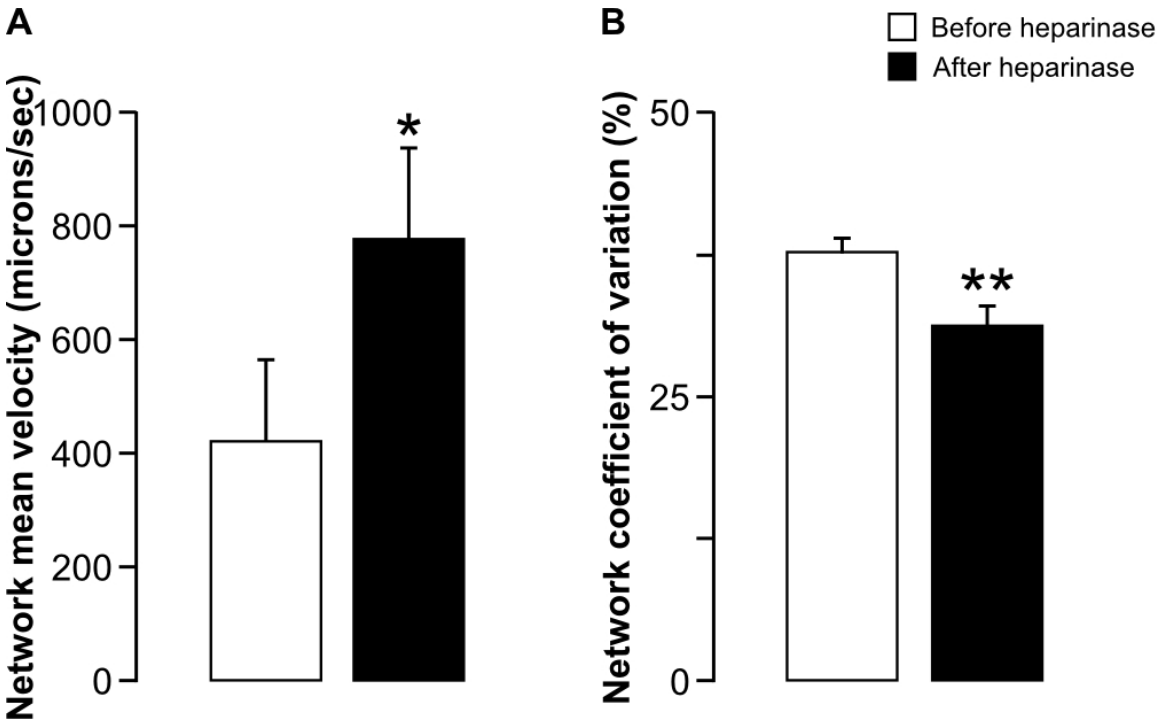

Figure 4.7: Heparinase treatment had significant effects on capillary network perfusion in 8 capillary networks from 4 animals. First, treatment caused an increase in network velocity. This increase was significant regardless of clustering method utilized ($p < 0.05$ by paired t-test). But in addition to the elevated velocity, in each network an overall reduction in network CV was assessed with the node-to-node by-segment clustering method ($p < 0.01$). This reduction was not significant with the by-path clustering methods (25.6% $\rightarrow$ 20.0%, $p = 0.29$). Temporal variation was not modified at the capillary level with heparinase treatment (not shown, $p = 0.71$).

did not yield different network velocity parameters when compared with the node-to-node by-segment clustering method as shown in Figure 4.7A. When the capillary velocities were clustered with by-path methods, the network CVs were not significantly changed as seen in Figure 4.7B ($p = 0.29$). But the reorganization of velocity and inclusion of cross-connections as distinct capillaries with by-segment clustering clearly shows reduced network CV following heparinase treatment (** $p < 0.01$). This change suggests that flow through the capillary cross-connections may be altered by an active mechanism dependent on functional glycocalyx.

In vitro heparinase assay

The *in vitro* assay was performed to verify the efficacy of the purchased enzyme for heparan sulfate degradation. The assay utilized did not produce measurable quantities of glucuronic acid. Biochemically, the product sold by Sigma should function as expected, but this was not verified by the spectrophotometric method. Many iterations were not attempted, because commercially available products *do* exist. This result was not critical for the completion of the project.

Image analysis of lectin labeling

The verification of heparinase efficacy was established *in vivo*with lectin binding and subsequent heparinase delivery. Images of lectin labeling *before* and *after* heparinase treatment are shown in Figure 4.8. In panels A and B, a field of view is shown *before* heparinase delivery under trans- and epi-illumination respectively. The same field of view is displayed 5 minute treatment with heparinase microinfusion in panels C and D. These micrographs display the typical reduction in lectin labeling on the microvessels following heparinase treatment.

The intensity measurements focused on microvessels in which lectin labeling was achieved via microinjection prior to the heparinase treatment. Therefore, two successful microinjections were necessary in the same vessel. A time period of approximately 10 minutes passed between the first and second injection due to re-loading the micropipette holder and other logistics. The lectin labeling reduction was not due to this time period, but was rather stable once labeled (not shown). Additionally, the fluorophore on the lectin was AlexaFluor488, a molecule designed to be resistant to quenching over short time spans

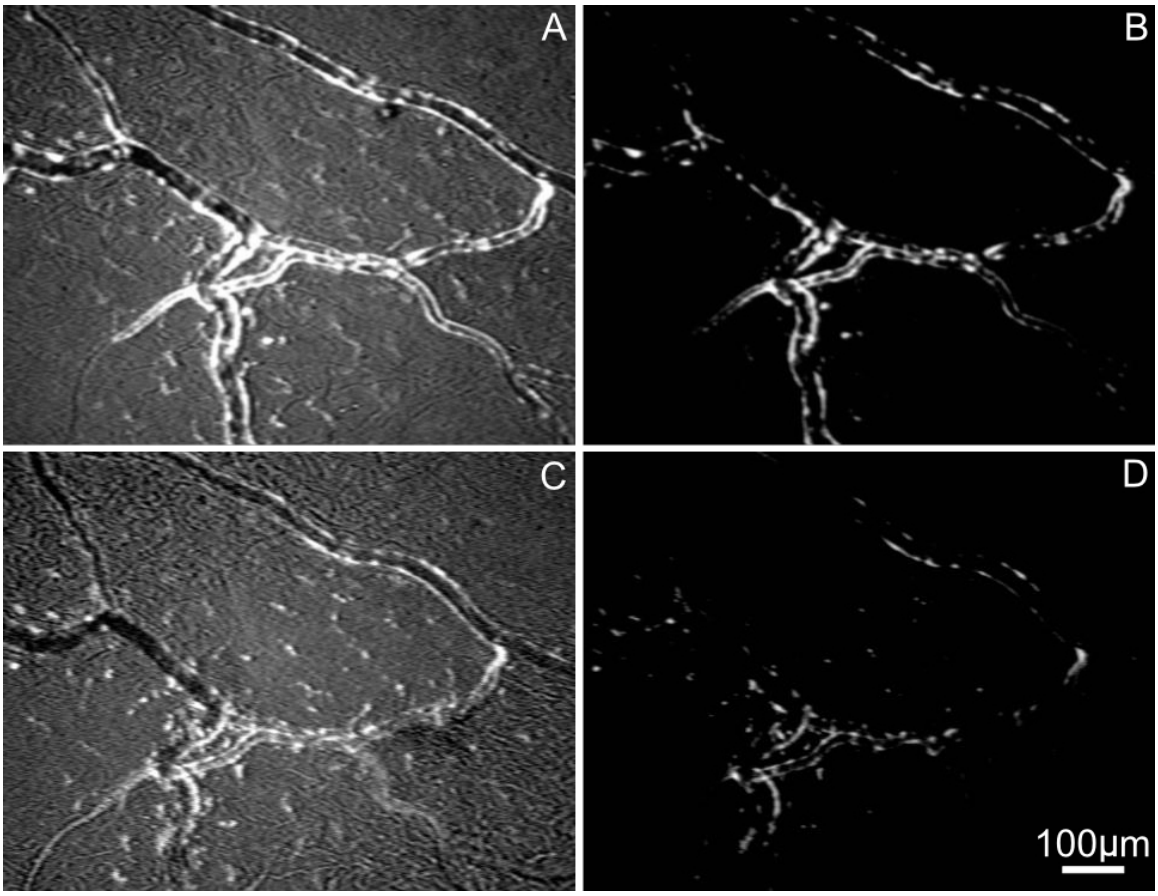

Figure 4.8: Brightfield and fluorescent micrographs from recordings made before (A,B) and after heparinase treatment (C,D). A brightfield/fluorescence overlay is shown in (A) with only fluorescence shown in (B). Then the same field is examined following a 5 minute microinfusion with 1U/mL heparinase enzyme (C,D). The fluorescent micrograph following treatment (D) can be directly compared to the image before the treatment (B). The intensity measurements are made similar to before for DAF labeling. In this case, the vascular measurement was normalized by the extravascular "background" intensity. The ratio for many vessels from a number of animals is reported below.

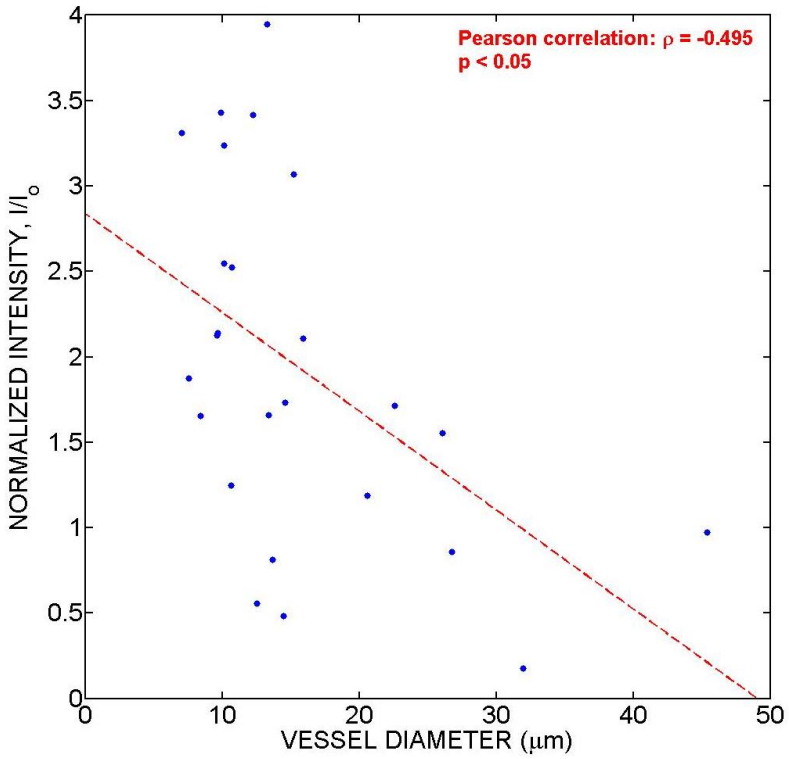

Figure 4.9: Correlation between fluorescent intensity measurements due to lectin labeling of the glycocalyx and vessel diameter. This correlation was made on the basis of diameter measurements made on epi-illuminated images with corresponding intensity averages. The correlation coefficient of -0.495 was significant ($p < 0.05$).

(minutes). The microvessels that did bind lectin were generally smaller, capillary vessels, but in some cases, the larger vessels did bind some lectin. Measurements across a range of vessel sizes showed that, in general, larger vessels did not display the same intensity that larger vessels showed. The correlation between vessel diameter and intensity is significant (ρ = -0.495, $p < 0.05$).

The larger vessels could be different for a number of reasons outside the scope of this study. My reasoning was to generate an *in vivo* method by which I could verify the impact of the heparinase enzyme in tissue with excellent optical characteristics. But a range of lectins that bind different sulfated glycoprotein motifs would be required to determine whether the larger vessels do, in fact, have reduced glycocalyx. Alternatively, the larger vessels may see more constant doses of lectin than smaller vessels due to the pulsed nature of the manual delivery. This variability in delivery is unavoidable, but still preferable when considering the alternative is whole-body delivery of the lectin and/or enzyme.

The measurements of fluorescent intensity showed that there was a significant effect

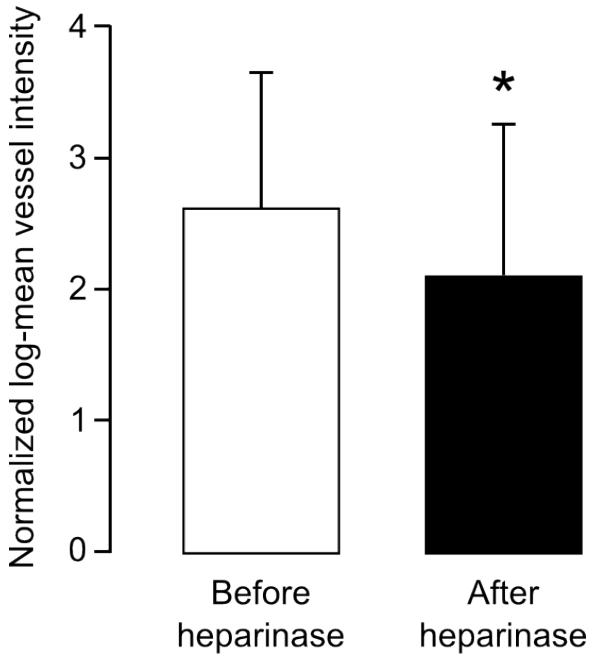

Figure 4.10: The average vascular intensity measurements for lectin binding before (white bar) and after (black bar) treatment with heparinase (1U/mL) for 5 minutes. The enzyme was microinjected following a previous microinjection with lectin conjugated with AlexaFluor488 (25μg/mL). The effect of the heparinase microinjection was significant ($p < 0.05$).

of heparinase delivery on lectin binding (Figure 4.10). The intensity inside the vessel was normalized by the extravascular region with the same shape and area as the vessel region. This normalization makes the measurement "area-insensitive", in that larger vessels cover more pixels, but the normalization covers the same pixel number. The intensity before treatment is significantly different than after treatment ($p < 0.05$ by paired t-test).

Nitric oxide production after glycocalyx degradation

Nitric oxide production as assessed by DAF2-DA labeling of mesentery tissue is shown in Figure 4.11. The images depict microvessels that received 5 minutes of direct heparinase treatment via micropipette infusion followed by 20 minutes of DAF loading. The intensity of vessel DAF labeling is reduced after heparinase treatment, such that the interstitial cells appear much brighter than the vessel. This treatment was performed on only one tissue, so no vessel intensity measurements were performed. The results were promising on a pilot basis, but further experimentation would be necessary to rigorously determine the effect of glycocalyx on nitric oxide production *in vivo*.

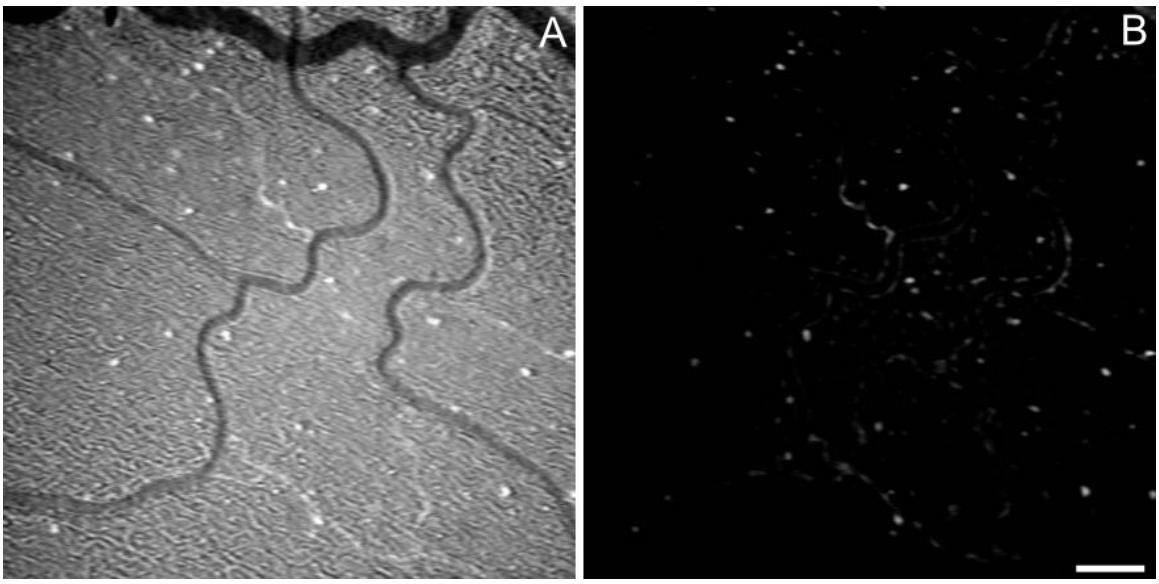

Figure 4.11: NO production was assessed following pre-treatment with heparinase for 5 minutes to degrade the glycocalyx. In vessels that received heparinase solution (A), the corresponding epi-illuminated image (B)show little DAF uptake and labeling on the vessels. The scale bar reflects 100μm.

4.4 Discussion

4.4.1 Nitric oxide inhibition

Disruption of nitric oxide signaling had a dramatic effect on capillary flow. There was an overall reduction of network velocity that was accompanied by a re-distribution of flow in individual capillaries. In some cases, the capillaries were perfused with velocity faster than prior to nitric oxide inhibition. This modification at the capillary level was adequately captured by network CV as calculated with by-path clustering analysis (k-means manual clustering). This reduction in overall flow can be compared directly with the results from the occlusion study presented in the previous chapter, wherein network velocity was significantly reduced with no concomitant elevation in network CV. This may suggest that capillary vessels require nitric oxide signaling to locally control flow parameters within individual capillaries.

Verification of the nitric oxide inhibition was accomplished with fluorescent intensity measurements. DAF fluorescence intensity is linearly proportional to the presence of nitric oxide *in vitro* [71]. The sensitivity of different NOS enzymes to blockade via L-NAME varies, but the L-NAME concentration utilized for inhibition should be sufficient

to eliminate both arteriolar and venular endothelial sources of nitric oxide [71]. Although extravascular levels of nitric oxide availability were not shown to be reduced by DAF labeling measurements, this may be due to the sensitivity of the measurement. The focus of the region-of-interest was on vascular shapes, therefore extravascular labeling was not highlighted by placement of regions-of-interest. A modified intensity measurement may have shown reduced DAF fluorescence.

It should also be noted that nitric oxide inhibition with this particular inhibitor has been well studied in the past. It was shown that leukocyte rolling on post-capillary venules was significantly increased following L-NAME treatment [139]. The effect was also shown to be partially mediated by CD18 upregulation on the leukocytes themselves. The possibility that such a response in leukocytes has a significant contribution to the network CV should also be explored.

4.4.2 Glycocalyx removal

I further showed that capillary velocity is increased following enzymatic removal of the glycocalyx. The impact on capillary network resistance is unknown, since upstream factors may be coupled with the capillary network velocity increase. For example, if the upstream flow to the network is *assumed* to be constant following glycocalyx removal, then the capillary network velocity should be reduced because of more available cross-sectional area in the capillaries themselves. Alternatively, if capillary resistance is reduced by the elevated cross-sectional area, an increased flow for the same nominal pressure drop would also be expected. The impact of active signaling processes is also unknown. Additional studies into the acute response to glycocalyx removal and modifications of capillary hemodynamics are necessary.

The lectin intensity measurements suggest that the heparinase treatment was efficacious for glycocalyx removal. The results from the *in vitro* assay for heparinase activity did not display digestion of heparan sulfate proteoglycan however. The lack of measurable quantities of glucuronic acid in the final reaction volume may have been due to additional dilutions of reagent concentrations. The protocol utilized approximately 100x diluted enzyme and 10x diluted substrate compared with the concentrations suggested by Sigma. With additional time and money, a protocol for an *in vitro* assay for heparinase could be developed based on uronic acid spectroscopy (232–235nm). Other groups have published al-

ternative methods that determine heparinase activity through the use of radiometric [38] or colorimetric electrophoresis [121]. Further, Sigma Diagnostics has made available a kit has been used to measure heparinase activity [1]. Tissue or blood specimens may also be tested for heparinase activity through the use of the latter three measurement methods. The *in vitro* assay I was using would not be able to distinguish between glucuronic acid absorbance and protein absorbance since biological samples absorb ultraviolet light. Future assays of heparinase activity should make use of either the diagnostics kit or an electrophoretic assay.

It has been previously shown that nitric oxide levels are reduced following enzymatic removal of glycocalyx *in vitro* [37], which is supported by my observation of reduced DAF labeling on mesenteric microvessels that had been infused with heparinase for 5 minutes. Reduced NO levels with heparinase treatment would potentially mitigate the effect of lowered vascular resistance. More studies should explore the connection between glycocalyx removal and NO availability *in vivo*. A rhodamine derivative similar to DAF has been generated [76] that would enable concurrent lectin measurements for the glycocalyx and NO availability measurements.

The velocity elevation and CV reduction effects of heparinase treatment may also be transient due to elevated leukocyte adhesion brought on by attenuated glycocalyx. My measurements were made inside a $5 - 10$ minute window immediately following a 10 minute infusion of the enzyme to the muscle. These periods of time were somewhat less than the 20 minute heparinase treatment that achieved maximal ICAM adhesion with antibody-laden microspheres [95]. This suggests that with additional time, the velocity in the capillary network may be reduced by elevated leukocyte-endothelial interactions including white cell rolling, firm adhesion, and eventually capillary plugging [56].

4.4.3 Intravital imaging

There are limitations associated with acquisition and analysis of *in vivo* recorded images in the muscle. Measurements of fluorescence intensity in tortuous muscle capillaries that are three dimensional are dependent on the focal depth. Still images are difficult to obtain while the animal is living. This is a limitation that was overcome in each experiment to varying degrees of success. In the velocity measurements, any tissue motion is additive with motion of fRBC centroids at any instant, which makes detecting the actual cell velocity difficult. Although tissue motion is *linearly* superposed on the blood flow motion, image

alignment methods require a stable fiducial point, so corrections were not available. In retrospect however, inside a single respiratory pulse, the motion of the tissue completes a full loop; therefore, the overall effect on velocity measurements when integrating them over a period of time with several respiratory cycles is zero. The greater effect is on clustering the tracks into the appropriate capillary. If cells are tracked in capillaries that have a degree of motion, the tracks in the final overlay are smudged over a distance of 10–20 microns, instead of centroids overlapping to within 5 microns. This is a difficulty that was overcome, and as my expertise with tissue preparations grew, the difficulty was further reduced.

The actual issue of the third dimension of travel is assumed to be negligible in this study. In reality, it may not be. The path of the cells often dives in and out of focus, making tracking through the whole capillary network uncertain at times. But a true three dimensional model of velocity tracking would have difficulty capturing a whole field of capillaries; with two-photon imaging of brain tissue, one method utilizes a series of line scans to determine the passage of a red cell in a single capillary. The large field of view is required for the current project, despite the two dimensional limitation.

Topical versus intravascular application of lectin

As previously mentioned in the methods section above, fluorescent lectins have been used as a histochemical marker for extravascular domains of microvessels applied topically. I doubted the applicability of topical application of the lectin for one primary reasons. If the lectin can bind extracellular motifs, how would I be able to distinguish between intravascular and extravascular labeling? I found that mast cells in mesentery are good targets for lectin binding, and additionally, a good topical label marker was lymphatic vessels in the mesentery. If a region of tissue showed intense mast cell or lymphatic labeling with the lectin, no vessel images were obtained in that location. In a small number of observations, a number of mast cells directly adjacent to some vessels showed lectin labeling — this was presumably due to vessel leakage. The lectin is approximately 40kDa, a size that would not be excluded by the vasculature, especially if reduced glycocalyx increased permeability.

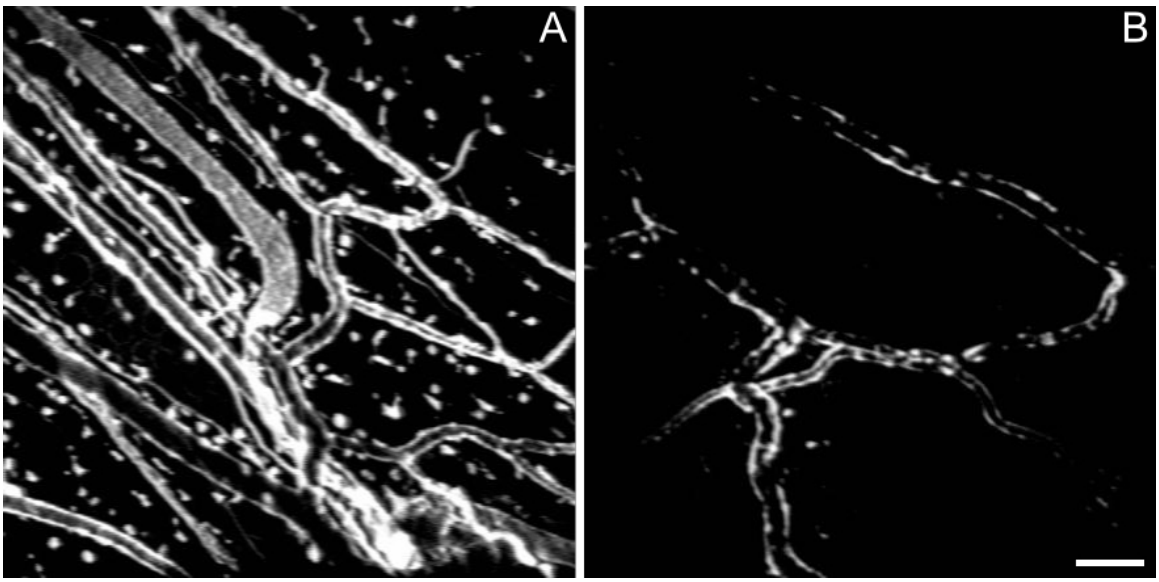

Figure 4.12: The difference between topical superfusion of lectin (A) and intravascular infusion of lectin (B) is captured in the above images. A previously established use of lectins was to topically label microvessels in whole mount immunohistochemistry. This method does not provide insight into the location of intravascular glycoprotein motifs such as the glycocalyx. Using micropipettes to deliver both lectin and heparinase allowed precise intravascular delivery of both reagents, but also strict categorization of topically superfused lectin and infused lectin. There is a stark difference during the experiment: first, mast cells in the interstitium of mesentery are brightly labeled. Second, the intensity of topical labeling is quite intense and often uniform down the length of a vessel. Scale bar is 100 microns.

4.4.4 Interaction of nitric oxide and the glycocalyx

The interaction between the glycocalyx and nitric oxide production has been recently shown through *in vitro* analysis, but has not been fully verified with *in vivo* results. My initial results represent the first attempt to determine the interaction in a living preparation. Further efforts should focus on this interaction, but the groundwork is in place. The preliminary evidence suggests that nitric oxide levels are reduced with an attenuated glycocalyx as previously shown *in vitro* , which supports the theory that the glycocalyx is a mechanotransducer. The mechanical signal could be sensed through GPI-anchored glypicans or cytoskeletal interactions via syndecans [150]. Alternatively, cleavage of the glycocalyx may simply reduce local vascular concentrations of nitric oxide by "washing out" a low-flow exclusion zone. I used topical DAF treatments to ascertain NO levels but did not check NO concentrations with an alternate method as well. Further experiments with enzymes targeted to specific glycocalyx components would allow additional insight

into the connection between the glycocalyx and nitric oxide release.

Work to characterize the impact of NO inhibition with L-NAME on the glycocalyx should also be performed. It has been noted by Suematsu *et al* that L-NAME treatment caused increased white cell rolling and adhesion [140]. As the glycocalyx may serve to shield glycoproteins like selectins and ICAMs from interacting with white cells, shedding the glycocalyx may be the endothelial cells' first response to injury or inflammation [96]. Reduced NO production may be a paracrine signal that the tissue provides to elevate the inflammatory response.

Glycocalyx as hemodynamic impact

Previous application of heparinase for the degradation of the glycocalyx caused a modified hematocrit, but velocity was not increased [19]. This result is not consistent with the finding of nearly two-fold increase in velocity in the results above, although no attempt was made to measure hematocrit concomitantly. The study of red cell flux and hematocrit changes *in vivo*have been used to study oxygenation and nutrient delivery capabilities of the capillary network. While this is a primary capillary function, the present studies have focused on intra-network relationships between capillary velocity. Future improvements to the experimental protocol could focus on the impact of capillary level control on both oxygen delivery and hematocrit. The correlation between hematocrit and number of tracked cells in a capillary could be established. This would allow an estimation of hematocrit and therefore oxygen delivery in the capillary networks.

Glycocalyx as an active signaling structure

Other proteins and structures in the endothelial cell also serve as requisite mediators in the transmission of fluid shear signals. For example, the inclusion of PECAM-1 in mechanotransduction mechanisms has been elucidated. Nitric oxide production and subsequent vasodilation via the endothelium in isolated skeletal muscle arterioles was shown to require functional PECAM-1 *in vivo*through the use of PECAM-$1^{(-/-)}$ mice [5]. This result is strengthened by further evidence of PECAM phosphorylation and downstream extracellular-signal responsive kinase (ERK) signaling in response to both fluid shear stress and non-fluid mechanical stress application [41, 100]. The recent finding that PECAM, cadherin, and VEGFR2 function in concert to transmit the shear stress into the cell in-

terior through PI3K signaling also clarifies a segment of this cascade [162]. But since the PECAM glycoprotein exists inside the glycocalyx structure, the impact of the glycocalyx on mechanosensory mechanisms utilizing PECAM should be examined. The mention of PECAM is especially interesting because platelets also secrete an endogenous heparinase that may allow penetration of glycocalyx or mediate inflammatory responses [39]. Further investigations into this pathway are justified.

The interplay of the glycocalyx with distinct signaling pathways historically has been limited by effective glycocalyx modification and visualization techniques — a limitation that research is currently targeting [90, 122]. The parallel of the glycocalyx interacting directly with the actin cytoskeleton through the syndecan backbone is just an example of current research [148, 149], but clearly the molecular interactions need further elucidation. Furthermore, an exhaustive approach to labeling the glycocalyx may not be possible, due to constant dynamic modification of sulfation patterns on the glycoproteins that comprise the glycocalyx [166].

The glycocalyx remains a dynamic structure that performs multiple functions at the endothelial interface. It constantly modifies the structural components that comprise it, making the use of a single lectin and treatment difficult to conclusively degrade. However, the impact of the functional results found in my research lends further support to the glycocalyx sensing and actuating in a mechanosignal transduction role *in vivo*. Further extension of this work with additional enzymes and molecular probes to determine the response *in vivo* to the reduction of the glycocalyx could be performed. One example would be to solidify the results from heparinase treatments on nitric oxide production that were obtained from a single animal. Additional work could be performed to determine the impact of the glycocalyx removal on PECAM phosphorylation and downstream effects such as vasodilation.

4.4.5 Nitric oxide inhibition as model for hypertension

This final point is an interesting topic that leads into the next chapter. Chronic nitric oxide inhibition (>1wk oral L-NAME treatment) has been shown to cause elevated systemic blood pressure [118]. In addition to the blood pressure elevation, several key mediators of classic hypertension appear to be related, such as endothelin and angiotensin. Nitric oxide is a homeostatic signal for vessels that is also anti-inflammatory, and the interaction

of this nitric oxide signal disruption with glycocalyx in hypertension will be investigated in the next chapter.

4.5 Conclusions

In this chapter, two potential control mechanisms for capillary velocity were manipulated and the impact on the network CV was observed. Interestingly, nitric oxide disruption caused an increase in variation between capillary networks. This may suggest that capillary vessels have intrinsic levels of shear-related signals to control velocity in individual vessels. Nitric oxide signaling is a function that is constitutively present on all microvessels, but differing levels of synthases in different vessels makes the nitric oxide system highly dynamic. Additionally, there is speculation that both hemoglobin and a plasma carrier, S-nitrosothiol, represent a significant, perfused constituent of total nitric oxide availability.

The involvement of the glycocalyx in maintenance of capillary velocity was also examined; when the glycocalyx was removed across the whole network by enzymatic cleavage with heparinase, capillary velocities became elevated with reduced variation as measured by network CV. This suggests that the glycocalyx may function in capillary vessels to maintain capillary perfusion distribution within a network. Whether the method by which the glycocalyx maintains capillary velocity is an active signaling process or a passive hemodynamic response remains unexplored. Hypothetically, since removal of glycocalyx modifies hematocrit, small deviations in glycocalyx production or shedding could modulate hematocrit over longer term — which would affect hemodynamics, shear stresses, and oxygen delivery. Furthermore, the question of elevated permeability should be explored by assessing the effects of other permeabilizing agents on capillary velocity distribution.

4.6 Acknowledgements

The work described in this chapter will be summarized as a portion of a paper in preparation for submission that will be titled “The impact of endothelial mechanotransduction on capillary network perfusion”. The authors include myself, Namgyun Lee, Frank DeLano, and Geert Schmid-Schönbein.

Chapter 5
Dysfunction in hypertension

Hypertensive animals were studied to determine the degree of variation in capillary velocity. Also, the metrics developed to probe nitric oxide signaling pathways and the interaction of the glycocalyx in the previous chapter were utilized to ascertain the contribution of capillary mechanotransduction to dysfunction in hypertension.

5.1 Introduction

Endothelial dysfunction in hypertension has been thoroughly examined, but few conclusions regarding the root cause of pressure elevation have been established. Functional aspects of blood flow in the vasculature in hypertension models were measured on the systemic scale. Systemic blood pressure elevation is attributed to elevated peripheral resistance at the arterial and arteriolar level. Regulation of capillary network perfusion by individual capillaries has not been studied from a functional viewpoint in hypertension.

5.1.1 Microvascular regulation

Microvascular dysfunction in hypertension has been documented with various molecular and biochemical techniques as discussed in recent reviews [34, 138]. Previous ultrastructural research in muscle revealed microvascular networks in hypertensive animals that are very similar [29, 30], but with one minor modification: cross-connections between capillary vessels were reduced in number [133]. The cause of this modification has speculatively been modeled as being due to an attenuated response to pressure, but this result has not been verified experimentally [109]. We hypothesize that modification of the network to remove capillary cross-connections may reduce the capability of the capillary network to

cope with further dysfunctional effects due to injury or illness.

White cell responses are a significant factor in the inflammatory processes elevated in hypertension. When tissue becomes damaged by physical or chemical challenge, the rapid induction of white cell aggregation and adhesion caused the capillary plugging phenomenon, and a concomitant reduction of blood flow in individual vessels of the capillary networks [55]. This may have been due to modified adhesion responses in the white cells themselves [139] or cytoplasmic viscosity alteration [56]. Chronically increased numbers of circulating leukocytes in spontaneously hypertensive rats (SHR) have been associated with elevated capillary resistance [42]. Further, white cells from hypertensive animals have attenuated protective responses to fluid shear stress [42]. Overall reduction of P-selectin expression and elevation of ICAM-1 expression in microvessels due to increased intravascular pressure have been linked to both elevated capillary resistance and compromised immune response [78, 173].

5.1.2 Endothelial dysfunction

The glycocalyx may be a primary mediator in modified endothelial responses in hypertension. The endothelium in hypertensive patients is more permeable [18] which may be an effect of reduced or damaged glycocalyx [60]. An attenuated glycocalyx has been shown in brain tissues from hypertensive rats [163, 164]. The glycocalyx may serve to prevent leukocyte-endothelial interaction of adhesion molecules in healthy microvessels [12, 96]. Furthermore, this component of the endothelial surface layer impacts the shear stress-mediated signal transduction ability of endothelial cells [37, 94] and therefore perform a major role in determining the capillary perfusion in hypertensive animals. As the protective response to shear stress in the endothelium may be nitric oxide production, the reduction of shear responsive signals due to glycocalyx damage or reduction may be an early manifestation of capillary-level dysfunction in hypertension.

5.2 Methods

All animal protocols were developed and approved by UCSD's Animal Care Program, in accordance with AAALAC standards. Wistar-Kyoto (WKY, n=5) and spontaneously hypertensive rats (SHR, n=5) (adults appx. 28 weeks, wt. 300-360g) were restrained under local anesthetic (Xylocaine) and their femoral artery and vein were cannulated with

polyethylene catheters (PE-50, Intramedic). Experiments with age-matched Wistar animals (n=4) were also completed with the same protocols. Mean arterial blood pressure was digitally recorded via strain-gage attached to the arterial catheter (MacLab). After this period, the animal was placed under general anesthesia with sodium pentobarbital (25mg/kg) intravenously with subsequent application as needed (5mg/kg). The spinotrapezius muscle was exteriorized for intravital microscopy as previously discussed (see §2.2.1). A sample (∼2% of total blood volume) of whole blood was obtained via the venous catheter and fluorescently labeled with PKH26 as discussed in previous chapters (§2.2.2). The fluorescently-labeled blood cells (fRBCs) were maintained in heparinized saline (10U/mL of 0.9% saline) at 37°C until the surgical muscle preparation was complete.

5.2.1 Capillary network velocity analysis

The muscle microvasculature was examined via intravital microscopy (Leitz) with a 10x water-immersion objective (NA 0.3). At this magnification, an entire microvascular network comprised of one arteriole - of branching order 3 - a number of capillaries, and one collecting venule - also of branching order 3 - can be visualized in a single field of view. Under brightfield conditions, two to four capillary networks were selected in thin portions of muscle where a single layer of muscle fibers are perfused by single arterioles and venules. Then the sample of fRBCs was returned to the circulation and the networks are then visualized under epifluorescent conditions generated by a mercury lamp (100W). A series of one minute periods of blood flow through different capillary networks were recorded with a SIT camera (MTI-DAGE, Michigan City, IN) and stored on videotape for offline analysis.

The offline analysis was conducted to highlight individual capillary velocities and compare the coefficient of variation between capillaries as mentioned in previous chapters (§2.2.3). The network mean velocity and network coefficient of variation were computed for each of 2–4 networks for 5 animals in each of WKY and SHR strains. The average network mean velocity and network CV were calculated for each animal and each strain. Also, the number of cells in each velocity dataset that exhibit a cell mean velocity less than 75 microns per second was counted for each dataset and compared between WKY and SHR.

5.2.2 Lectin labeling

In select experiments from each animal group, the coverage of the endothelial surface layer of the capillary networks was assessed. Arterioles upstream of the capillary networks of interest were pierced with freshly-fractured micropipettes mounted on a micromanipulator. AlexaFluor488-conjugated lectin (GS-IB_4 lectin at 25μg/ml, Sigma, St. Louis, MO) was infused through the micropipette and labeled the endothelial surface layer in the capillaries of interest. Epi-illuminated images of the lectin-labeled tissue were obtained with both the SIT camera intravitally and also freshly fixed (30 minutes with 10% Formalin) *ex vivo* tissue with a high-resolution still-frame camera (Fuji FinePix S1Pro) and analyzed offline.

5.3 Results

Table 5.1: Blood pressure measurements from WKY and SHR experiments obtained from free-roaming animals.

Group	**Systolic pressure (mmHg)**	**Diastolic pressure mmHg**	**Mean pressure mmHg**	**Heart rate beats/min**
WKY	164 ± 11	105 ± 12	127 ± 11	394 ± 47
SHR†	206 ± 11	134 ± 7	163 ± 8	382 ± 36

†All blood pressure values significantly different between WKY and SHR ($p < 0.05$).

The hypertensive animal, SHR and normotensive control, WKY, have been shown to spontaneously develop elevated systemic blood pressure. The blood pressure was measured at the beginning of each experiment in a free-roaming acquisition period to reduce the effect of anesthesia on blood pressure. The blood pressure information is tabulated in Table 5.1. As expected, the blood pressure is significantly elevated in SHR over WKY ($p < 0.05$). These values are consistent with reported values for WKY and SHR blood pressure recordings.

5.3.1 Network CV in hypertension

A number of velocity recordings from five WKY and five SHR animals were obtained and analyzed; the results are summarized in Figure 5.1. Specifically, 21 networks

in the WKY animals and 15 networks in the SHR animals were utilized for this study. The network mean velocity in the WKY group was slightly higher than that seen in the SHR group, but is insignificant ($p > 0.05$). This difference is seen irrespective of clustering method used. In panel B of the same figure, the network CV from WKY and SHR is shown. A by-path analysis did not show a difference between WKY and SHR animals. But when the same data were analyzed with a by-segment clustering method, the velocity distribution showed increased variation in SHR animals compared to WKY ($p < 0.01$).

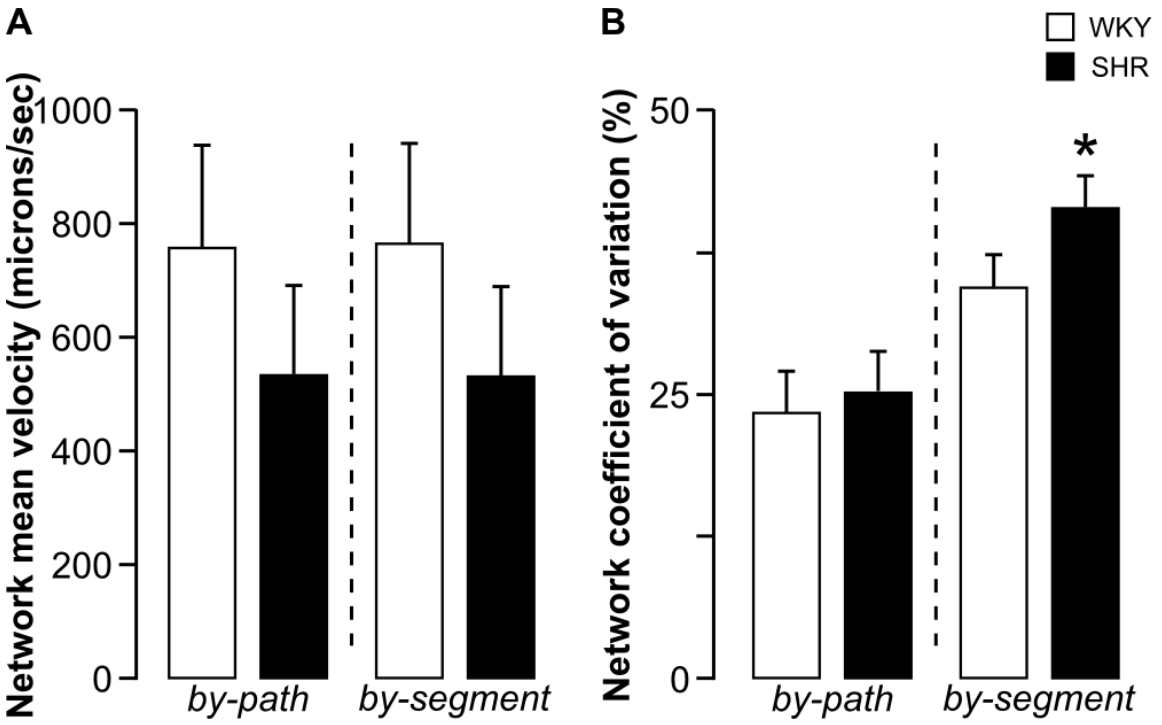

Figure 5.1: The capillary velocity measurements from WKY and SHR experiments are summarized. Network velocity was reduced in SHR compared to WKY, but not significantly ($p > 0.05$). The difference in network velocity is seen despite clustering method utilized. The distribution of the velocity data changes with different clustering algorithms, however. The by-path method shows no difference in capillary velocity distribution as shown by network CV. But when the data is analyzed with by-segment clustering, a significant difference is seen ($p < 0.01$). This may be due to elevated flow observed in cross connections.

Cells were considered to be slow if the cell mean velocity was less than the arbitrarily selected threshold velocity of 75μm/s. An increase in the number of slowly circulating cells was found in SHR compared with WKY rats ($p = 0.07$ from 4 animals each of WKY [10 networks] and SHR [9 networks]). The summary of the results is also shown in Table 5.2. The effect on network CV was investigated for by-path network CV, because the computer program that tallies the number of slow cells and informatically removes them from

Table 5.2: Impact of slow cells on network CV in WKY and SHR

Group	**Average slow cells** (#)	**Network CV with all cells** (%CV)	**Network CV no slow cells** (%CV)
WKY	1.4	27.9 ± 3.1	27.7 ± 3.4‡
SHR	6†	36.3 ± 8.4	35.7 ± 8.7‡

†Slow cells more prominent in SHR animals ($p < 0.05$, one-tailed unpaired t-test). ‡No direct effect on velocity or network CV ($p = 0.92$ for both WKY and SHR network CV with and without slow cells).

the velocity data to recompute network CV was written for by-path clustering as defined in §2.3.2. However, an overall small impact of the slow cells on the re-computed network CV was determined (0.2% reduction for WKY, 0.6% in SHR).

5.3.2 Fluorescent micrographs of lectin in mesentery

Micrographs were obtained from mesenteric tissue that had been infused with fluorescent lectin via micropipette. Example micrographs are displayed in Figure 5.2. The image in Panel A depicts a trans-illuminated field of mesentery from WKY with a number of microvessels; the same field is epi-illuminated in Panel B. The vessels are brightly labeled and little background intensity is present. In Panels C and D, SHR tissue is depicted in the same manner, with the same field displayed under brightfield and darkfield conditions. The SHR microvessels do not label with this lectin as intensely.

A summary of intensity measurements recorded from images of microvessels from 3 WKY and 3 SHR animals is provided in Figure 5.3. In brief, a vascular region of interest was defined on a microvessel segment, and the average intensity was recorded inside this region. Then, that intensity was normalized by the intensity measurement of that same region of interest moved directly adjacent to the vessel. This normalization compensates for leakage of the label and intrinsic background intensity. The natural log-ratio of vascular to extravascular intensity is computed. The average quantity over 50 vessels from the WKY and SHR tissue indicates that the SHR lectin labeling is significantly lower than WKY labeling ($p < 0.05$ by one-tailed t-test).

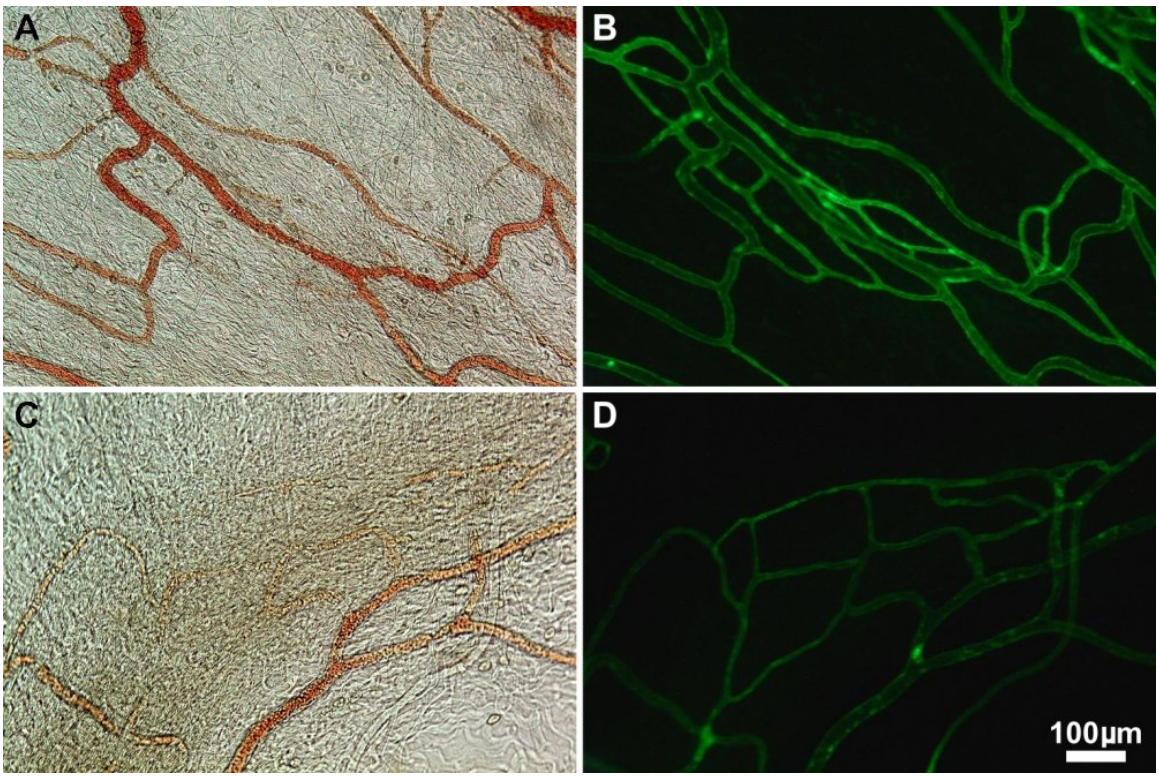

Figure 5.2: Glycocalyx was labeled with fluorescent lectin *in vivo*in normotensive (A, B) and hypertensive animals (C, D). Brightfield microscopy (A, C) show selected microvessels from mesentery preparations in normotensive (WKY) and hypertensive (SHR) animals respectively. Epi-illumination revealed reduced labeling with Alexa488-conjugated *Griffonia simplifolicia-I* B_4-lectin in the SHR vessels (D) compared with WKY vessels (B). Scale bar reflects 100 microns.

5.4 Discussion

The velocity results reveal elevated variation between capillaries perfusing networks in muscle tissue from hypertensive animals. The difference in capillary velocity distribution is apparent only through full consideration of cross-connecting vessels with by-segment clustering analysis. I observed that there was increased flow in cross-connecting vessels in SHR animals compared to WKY (not quantified). This difference in the perfusion of SHR capillary networks may provide insight into the difference in network CV. As previously noted, red blood cells traveling down a single-file capillary in fully-developed flow reach a reduced drag state in the center of the capillary. At bifurcations, this state is disrupted, and the cell must travel axially before the cell might re-assume the reduced-drag state. This situation may not occur down the brief transit length of a cross-connecting capillary. Therefore, the resistance in these vessels may be higher and the cell velocity lower

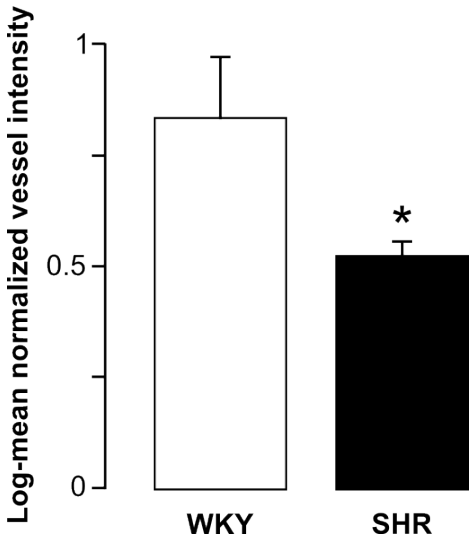

Figure 5.3: Lectin labeling was assessed with an intensity measurement inside the vascular structure. A vessel with both walls in focus was selected and a region-of-interest was constructed for the vessel. The mean intensity inside the vessel was obtained and the ROI was placed in the extravascular region adjacent to the vessel. Another intensity measurement was obtained for the extravascular space. The intravascular intensity is normalized by the extravascular intensity measurement. The data from 3 WKY and 3 SHR experiments was assessed on many vessels, but images of vessels that showed mast cell labeling with lectin were discarded to reduce the impact of topically labeled vessels. $p < 0.05$ by one-tailed Student's t-test.

than their length and dimension would suggest. There must be a fundamental explanation for the increased flow in the cross-connecting vessels in SHR tissue, but at this point, it remains unknown.

The elevated flow in cross-connecting vessels contrasts the reported rarefaction in cross-connecting capillaries [133]. This is an observation that should be further investigated, but some hypotheses may be formed. Elevated cross-connection perfusion may be due to reduced numbers of cross-connecting vessels. But capillary cross-connections offer redundancy in the distribution of blood flow. Since tissue extravasation of leukocytes generally occurs at the level of post-capillary venules, this redundancy may reduce ischemia in tissue microregions during periods where an adherent white cell has blocked a major post-capillary venule. The flow could redistribute through a cross connection to maintain perfusion of the region. A tissue with fewer cross-connections would therefore have reduced capabilities to re-distribute flow around inflamed regions of tissue.

In hypertension, it has also been shown that white cell activity and stiffness are enhanced. Leukocytes respond to fluid shear stress in wild type animals by assuming an anti-inflammatory state: pseudopod retraction and round, pliable shape. This anti-inflammatory state is compromised in SHR leukocytes [42, 43]. This effect may further contribute to a disturbed flow distribution in networks with reduced capillary cross-connections. The elevated white cell activity may cause elevated firm adhesion that would require increased flow redistributions. The impact of white cells on network CV has not been investigated for wild-type, WKY, or SHR capillary networks.

The effect of elevated flow in cross-connections, reduced number of cross-connections, and increased leukocyte resistance may have an effect on reduced velocities as measured by the number of "slow" cells. But the increased number of slow cells in SHR only indicates cell mean velocity that were recorded from the fluorescent cells. The impact of these slow cells on the flow in the rest of the capillary network can only be assumed. Further flow re-distributions may be required due to the slow cells, which could be simulated *in silico* through a predictive analysis of capillary flow.

Mechanisms lowering homogeneity of capillary perfusion may include interactions between blood cells and a smaller glycocalyx — or a glycocalyx with reduced functionality. Duling *et al* showed that a functional glycocalyx may play a role in hematocrit control in capillaries by enzymatic removal of heparan sulfate proteoglycans in wild type animals [19].

In the previous chapter, I showed that acute reduction of glycocalyx caused elevation of velocity in capillary networks with decreased variation between capillaries assessed by network CV. These results suggest that the glycocalyx may be actively maintained within capillary networks to modulate perfusion variation. But the impact of the glycocalyx on capillary perfusion in chronic disease models such as the SHR requires further investigation. The elevation of network CV in the SHR opposes the reduction in network CV by acute glycocalyx degradation. Therefore, an additional factor may be responsible for the elevation of network CV in the SHR hypertension model.

Glycocalyx function as a factor in systemic hypertension would be a fascinating topic of research. An interesting and simple study would be to determine the effect of glycocalyx degradation on systemic hemodynamics such as blood pressure. Since glycocalyx plays both an active or hemodynamic role in maintenance of tissue homeostasis, I hypothesize an elevated systemic blood pressure with systemic removal of glycocalyx .

I did not measure nitric oxide levels concomitantly with the lectin binding. A combination of assays for glycocalyx labeling with concurrent nitric oxide assessment *in vivo* would provide an interesting linkage between the glycocalyx and mechanosignaling in hypertensive animals. As it stands now, the lectin binding was reduced in the SHR animals compared to WKY animals, but no causal links were found. Furthermore, I have showed that the glycocalyx in SHR animals is less intensely labeled with only one particular lectin. Lectin binding to a single constituent of the glycocalyx may not provide sufficient evidence to conclusively state that the functionality of the glycocalyx is compromised in hypertension. A number of lectin binding studies may be required to completely account for the individual glycoproteins that comprise the dynamic structure; but the issue of glycocalyx functionality may never be adequately described in this manner. A balance between feasibility of glycocalyx research and effective probes for functionality of the glycocalyx must be developed.

5.4.1 Metabolic syndrome

A high low-density lipoprotein (LDL) count is often cited as a risk factor for metabolic syndrome — both in diabetes and hypertension. There has been some speculation that oxidized LDL (oxLDL) is also partially responsible for invagination and buildup of fatty acid plaques in atherosclerosis. The impact of LDL and especially oxLDL on the

glycocalyx has also been investigated. It appears that LDL has a particular affinity for highly sulfated groups of proteoglycans in the glycocalyx — primarily heparan sulfated proteoglycans — due to electrostatic interactions [50, 51]. The affinity also increases with oxidation of LDL [89]. Further, oxLDL has been directly applied to rat muscle venules and hematocrit increased in a manner similar to the response to heparinase treatment[11, 19, 169].

The exact repercussions of this affinity on the interaction of the glycocalyx in plaque development and etiology of the metabolic syndrome have not been established. Reactive oxygen species *in vivo*were shown to contribute to reduced bioavailability of NO, which could be a result of glycocalyx damage [58]. The oxidation of LDL may be an initial blood borne factor that either is directly or indirectly responsible for glycocalyx shedding. Potential pathways in the link between LDL and the glycocalyx would be an interesting location for future biochemical research and functional microcirculation studies.

5.5 Conclusions

The genetic model for hypertension offers direct comparison of microvascular control systems in living tissues. I showed that in skeletal muscle capillary networks, the coefficient of variation between capillary velocities is elevated in hypertensive rats. Furthermore, lectin binding assays in the mesentery to determine levels of one particular glycocalyx motif showed differential labeling intensity between WKY and SHR. This test may not directly display attenuated glycocalyx in hypertension, but lectins do provide a functional, intravital assay for the glycocalyx. Furthermore, the binding of this particular lectin in separate Wistar experiments was shown to be reduced following enzymatic cleavage of heparan sulfate proteoglycans. This enzyme treatment was also shown in the literature to reduce mechanosensitive responses in endothelial cell cultures. The acute enzyme treatment differed from the chronic hypertension model with regard to the capillary velocity variation. For this reason, while these data suggest that endothelial dysfunction — in mechanotransduction pathways including the glycocalyx — may contribute to the hypertensive phenotype, additional experiments should be performed to determine the impact of glycocalyx modifications in acute hypertension models.

5.6 Acknowledgements

The work described in this chapter will be summarized as a paper in preparation for submission that will be titled “A Novel Assessment of Capillary Dysfunction in Hypertension”. The authors include myself, Namgyun Lee, Frank DeLano, and Geert Schmid-Schönbein.

Chapter 6
Conclusions and future work

As I finish my experiments examining the impact of endothelial structure and function on capillary perfusion in skeletal muscle, there are several interesting questions that could be posed. Due to the novel nature of my research, the impact of vascular control in capillary networks is also discussed.

6.1 Capillary networks

The results from my thesis work suggest that capillary networks may control perfusion distribution within capillaries with an active mechanism independent of arterioles and venules. Numerical simulations of capillary velocity using a linear conduction model with realistic connectivity, but simplified vascular topology and Newtonian rheology displayed a large velocity distribution between capillaries. The coefficient of variation ranged from 60–120%, depending on the initial pressure conditions selected. This quantity is not confirmed by my experimental results *in vivo*. Capillary networks *in vivo* possess non-uniform topology and non-Newtonian rheology, but the capillary velocity variation assessed by network CV was reduced three-fold from the numerical simulation. This reduction in variation suggests that a control system may actively maintain capillary velocity.

A previous hypothesis was held that passive rheological effects were the source of variation [157]. Some researchers showed that elevation of arteriolar flow decreased variation in capillaries [124]. This result was refuted by other work [14]. My results indicate that elevation of capillary network velocity does not have a significant impact on capillary network CV. This result was shown in control experiments wherein the range of velocity did not correlate with reductions in CV. Also, a series of studies showed no effect on network

CV while arteriolar occlusion reduced flow to the capillary network. Rheological effects were decoupled from topological effects with the occlusion study. Topological effects appear to supply the baseline capillary network velocity variation.

The capillary velocity variation control system may be the effect of endothelial mechanotransduction mechanisms. Nitric oxide signaling was attenuated in the muscle tissue, and capillary network CV was increased. The finding that the removal of the glycocalyx reduced network CV suggests that the glycocalyx may be partially responsible for the maintenance of the network CV. The interplay between nitric oxide and the glycocalyx in microvessels should be further explored.

Finally, the endothelial dysfunction evident in hypertensive animals can be associated with elevated variation in capillary network velocity. Exploration of the glycocalyx in hypertensive animals suggests that modifications to the endothelial surface layer may also be involved. Further work should characterize the impact of nitric oxide and the glycocalyx on elevated capillary network resistance.

The completion of the thesis work has provided a novel exploration of capillary networks as active participants in tissue perfusion. But really, the door is now open for further research into the effects of capillary level control on other biological systems. The impact of capillary level control should continue to be explored.

6.1.1 Effect of shear control on network resistance

A true capillary control system that exists in healthy networks, but may be disrupted in dysfunctional networks, like those I studied in hypertensive animals, may have further impacts on network resistance. Simple computer simulations have provided estimates for network CV, and could produce similar qualitative results for network resistance. Therefore, continuing work should examine the impact of capillary level flow control on network resistance.

In brief, by using the perfusion values previously computed from linear conduction models, a simple resistor model could be developed. Capillary segmental resistances are calculated from a re-ordering of Poiseuille's law as below:

$$-\frac{\Delta P}{\Delta L} = \dot{Q}R, \tag{6.1}$$

where

$$R = \frac{8\mu}{\pi a^4}. \tag{6.2}$$

The parameters a and ΔL are selected from the topological values in the literature [132]. The linear pressure drops ΔP in the model would be compared with experimentally determined pressures in rat muscle microvessels [29–31]. A segmental resistances combination could be performed with respect to series-parallel combinatorial rules from circuit analysis. Then for the schematic topology with Newtonian hemodynamics, the capillary network unit resistance would be found.

As a modification to the above calculations, the putative control hypothesis outlined in equations above could be applied to the same schematic network. Iterative nonlinear solutions would be determined through combination of conservation of mass at each nodal bifurcation with Poiseuille's law.

This study would provide *in silico* support that the network resistance may or may not be effected by capillary level perfusion control. In the past, the question of elevated capillary network resistance in hypertension has been discounted in favor of arteriolar elevation. But with regard to obvious capillary network restructuring in published accounts of rarefaction, modifications to the capillary network are occurring, and the impact on capillary level control should be determined. The final question is whether deranged capillary network control may be partially responsible for the observed rarefaction in hypertension.

6.1.2 O_2 as nutrient under control

Capillary level control would have an impact on oxygen delivery in microvascular networks. Previous results have shown that elevation of superfusate oxygen tension reduces blood flow in the microvasculature [85]. Proper tissue oxygenation relies on efficient distribution of blood to all regions in the capillary network. Metabolic responses to high variation in capillary perfusion could potentially modulate endothelial mechanotransduction. The interaction between nitric oxide and hemoglobin is being actively researched, but less research has focused on the glycocalyx as a factor in oxygen delivery. An expansion of my work on capillary network variation into oxygen delivery could be a future project.

6.1.3 Modeling capillary growth through response to shear stress

The capillary velocity control system reflects a single corollary of the putative capillary dimension control mechanism. The postulate predicts that the fundamental process of capillary growth involves an endothelial shear stress response. By sensing the level of shear,

the capillary network could deduce the need for additional capillaries. This response could be balanced by the tissue response to metabolic needs. Other work to model angiogenesis in capillary networks should account for shear stress as a potential factor.

6.2 Endothelial structure and function

I have shown that the endothelial surface may play a role in determining capillary perfusion for capillary networks. Further investigations into endothelial cell structure and function may elucidate the nature of the glycocalyx function in determining capillary velocity. The interplay between glycocalyx and other signaling molecules continues to be actively researched. But alternative structures in the endothelial cell are also interesting targets for future study.

6.2.1 Blood cell interactions

The impact of white cells on capillary perfusion has been previously investigated by many groups including my laboratory. I speculate that endothelial interactions with leukocytes may be actively limited by the glycocalyx in healthy tissue. An endothelial cell response to inflammatory stimuli may be directed cleavage of the glycocalyx. Injury or inflammation may cause rapid reduction of glycocalyx to enhance leukocyte-endothelial interactions. Alternatively, active degradation of the glycocalyx in inflammation may be a response of the leukocytes themselves. The impact of elevated leukocyte interactions on capillary network CV should be determined.

The glycocalyx reduction response may be controlled by endothelial cells or may be a fundamental mechanical response to high or low shear. In low shear regions, additional plasma associated glycocalyx could be deposited, whereas in high shear regions, the glycocalyx could be stripped of the plasma-derived constituents. The leukocyte-endothelial interactions could be stochastic events that allow the capillary endothelial cell to temporarily reduce velocity locally. Computer simulations of electrochemical and mechanical interactions between the glycocalyx and plasma may provide insight into this possibility.

Additionally, platelets and neutrophils have been shown to constitutively express an enzyme similar to the bacterially-derived heparinase enzyme I utilized for my studies [170]. The neutrophil enzyme cleaves heparan sulfate proteoglycans and other high molecular weight heparins [79]. Other research has shown that a similar enzyme is expressed

on metastatic cancer cells that may help them both enter and exit the bloodstream [7]. The platelet-derived glycocalyx removal is one potential blood cell interaction that should be investigated in future work.

6.2.2 Caveolae

Another endothelial structure that is actively researched as a potential sensor in mechanotransduction mechanisms are the caveolae. Caveolae are a lipid-ordered region of plasma membrane that are characterized as 70-100nm invaginations in many cell types, particularly vascular endothelium, lung epithelium, and smooth and striated muscle [137]. They differ from other vesicular organelles by the structural inclusion of the protein caveolin of which there are three distinct proteins. Caveolae have been functionally implicated in permeability, protein trafficking, and signal transduction. The importance of caveolae in shear signaling has been previously established, so there is precedent to examine caveolae for future examination of endothelial mechanotransduction in capillary network perfusion.

Genetic caveolin-1 variants

Transgenic mice have been developed that either over-express [9] or have knocked-out caveolin-1 [127], [184]. These animals have become well characterized since their emergence, and display several phenotypes of interest to this study. Specifically, the transgenic over-expressing animals display impaired microvascular permeability and reduced levels of Akt and eNOS phosphorylation. The knockout animals display cardiac hypertrophy and microvascular hyperpermeability that suggests that systemic and microvascular resistance may be increased. This effect could be explained, in part, by the inefficiency of deviation from a uniform microvascular shear stress response.

Pilot studies performed during the thesis work outlined above were undertaken to investigate the caveolin-1$^{(-/-)}$ mice that had been developed at UCSD. Several mice were a gift from Dr. Hoshijima. Unfortunately, between a series of practice mice and these mice, no spinotrapezius muscle preparations of sufficient quality were achieved — the small size of even their femoral vessels made a simple mouse cannulation very difficult. The larger vessels in the muscle were often still perfused, but the surgical damage delivered to the tissue typically rendered capillary networks unusable. The focus of the study required high quality perfusion in all the capillaries of a single network, so damaged or otherwise

unperfused tissue made data acquisition impossible.

Caveolae and nitric oxide signaling

Another study that could probe the importance of caveolae function on capillary network perfusion could be performed in rat muscle tissue. This would mitigate all the previously mentioned problems with mouse tissue, but is still a proven functional model for caveolae disruption. Also, the benefit of using a model that is not a genetic variant, but instead a result of an applied inhibitor, would be that the same networks could be probed before and after the application to the tissue. Methyl-β-cyclodextrin and filipin both serve to disrupt lipid-ordered domains in the plasma membrane, and have been used in the literature *in vivo*. The application of these inhibitors have been shown to disrupt the formation and presence of caveolae after the lipid-ordered domain had been modified. Filipin has one advantage too, in that it is also a fluorophore that excites in the UV range, so delivery of the molecule could be easily verified.

There are recent reports that shear stress preconditioning cells enhanced expression levels of mechanosensitive proteins – including eNOS – over static controls, although actual signaling functions that are routed through the caveolae were not examined [120]. Of particular interest is the inhibitory relationship caveolin has with eNOS [48]. eNOS receives a co-translational myristoylation and a post-translational palmitoylation that preferentially targets the enzyme to lipid-ordered regions – either lipid rafts or caveolae – where the activity can be affected [131], [136], [48]. In the case of eNOS, a Ca^{2+}-calmodulin dependent enzyme called acyl protein thioesterase-1 (APT-1) directs de-palmitoylation of eNOS. Upon removal from the caveolae-targeting domain, eNOS upregulation through reduced interaction with caveolin may occur [180]. Caveolin-1 may also play a role in modulation of actin polymerization in response to shear through an integrin-linked Csk-dependent pathway [115]. Therefore, modification of caveolae function in the endothelium would hypothetically reduce the nitric oxide signal, resulting in a capillary network response similar to that seen in §4.1.

6.2.3 Pericyte-endothelial interactions

One interesting capillary component that has not been studied to the same level as the endothelial cell are pericytes. Many accounts suggest that pericytes extend down

the length of the capillary and provide support to the endothelium. They may also be cells responsible for signaling in arterialization of capillaries. They have not been shown to contribute significantly to capillary contractions *in vivo* [116], but they share similar phenotypes with smooth muscle cells. The pericyte does express smooth muscle α-actin but no contractile elements like myosin light chain. Therefore, the question regarding the contraction capabilities of pericytes is unsettled. The overall interaction of pericytes with the endothelium continues to be a topic for active research.

Signaling processes in angiogenesis and vessel stabilization are the topics that have been heavily researched in pericyte-endothelial interaction [172]. Histochemical markers for pericytes include neural-glial cell markers (NG-2) among others [4]. Immunohistochemical assays in mesentery and muscle have shown that NG-2 labeling spans the entire length of capillaries [97]. This extent of pericyte coverage across capillary networks supports the hypothesis that pericyte interactions may control local capillary perfusion. But studies to functionally determine the impact of pericytes in distribution of capillary perfusion have not been attempted to date.

6.3 Tissue selection

The selection of tissues for experimentation was made with the history of the laboratory in mind. *In vivo* methodology established in the lab was taught to me by F.A. DeLano who learned a great deal of the techniques directly from Dr. B.W. Zweifach. So many surgical preparations could have been chosen. The selection of spinotrapezius muscle from three or four muscles previously prepared experimentally was purposeful. First, the spinotrapezius muscle has a large region wherein muscle fibers are aligned in the same direction without much overlap. This simplifies the microcirculation in the area which facilitates imaging and subsequent analysis.

The cremaster preparation is another easily accessible muscle — but the preparation is more destructive to the tissue than the spinotrapezius preparation. The tissue construction is not as simple and the muscle exhibits spontaneous muscle contractions, making one minute long sequence acquisition more difficult. Gracilis muscle, which I have also prepared, is not suitable for transmitted light microscopy without which my application would be impossible. There is the benefit of simplified macrovessels feeding and draining the gracilis, which allows close to total control of the muscle circulation at the macro-level,

as opposed to the microinjection method used primarily above. The mesentery was selected for the obvious reasoning of simple tissue structure and unequaled thin caliber for intravital microscopy.

6.3.1 Analysis in human tissue

The analysis of other tissues would also be of interest. Clearly, expansion of this research into human would be desirable, but non-invasive methods would be required. The retinal microcirculation has been a topic of interest in the past, as it is easily accessible in volunteers [3, 175–177]. Also, the nailfold capillary bed has been examined for many years including the analysis of capillary perfusion [10]. But the development of systems for analysis of vital organs without significant surgical damage also opens new possibilities for capillary perfusion analysis. Furthermore, probing mechanotransduction mechanisms chemically would still be difficult in human subjects.

6.3.2 Two photon laser scanning microscopy

Two photon laser scanning microscopy has been known about in theory for many years. Recent availability of a wide range of fluorophores has allowed an expansion of its use. The technology requires high powered lasers to flood a region of tissue with low intensity (high wavelength) light, such that the probability of multiple (2 or more) photons colliding simultaneously with a fluorophore in a small region becomes realistically achievable. The benefit is that lower intensity light, infrared or higher, has a lower attenuation in tissue, and therefore the signal into the tissue causes less disruption, including tissue fluorescence, heating, and photobleaching. These advantages are outweighed by one more great opportunity that two-photon imaging allows: the lower intensity light penetrates farther into tissue with higher acuity, so deeper tissue regions can be analyzed. There is one group at UCSD that has taken advantage of two-photon imaging to probe capillary blood flow in rat brain tissue [74]. Neurology and brain tissue perfusion could be an exciting future application for analysis of mechanotransduction and the impact of capillary network perfusion.

6.4 Further analysis of vascular dysfunction

Future analysis of vascular dysfunction might include studies of capillary network regulation. I have developed methods by which the impact of capillary networks can be

investigated in different tissues from genetically modified animals or animals in disease models. Two such animal studies that would be interesting would be diabetic animals and animals prone to stroke or atherogenesis. Recent studies have shown that glycocalyx may be removed in response to acute hyperglycemia [186]. The mechanism of action is not clear at this point, but it does provide impetus for further investigation of capillary network velocity in diabetes. Also, the glycocalyx is reduced in response to oxidized lipoproteins. These two responses provide evidence for continuing investigations at the capillary network level for elevated perfusion variation.

Appendix A

Codes for data processing

When I began my thesis work, I wanted to see how things were done by the people who came before me. In many cases, I was developing specialized codes that standardized velocity measurement and calculations. It is for this reason that I include the codes that I produced during my research that enabled me to process incredible amounts of data. I also hope that any students who may come after me would be able to utilize these codes as a resource to jump start their own research.

A.1 Codes for image processing

A.1.1 Subfunction `ImageDownConvert.m`

```
function IND = ImageDownConvert( RGBstring )
%This function accepts the filename of the 1799-framed TIFF movie, and
%converts it to a set of grayscale images, then re-writes it.  This reduces
%the size of one frame from 921KB to 307KB and the whole movie from 1.54GB
%to 520MB.  The additional information has no impact on the image or it's
%quality, so may be removed.

t1 = cputime;
INFO = imfinfo(RGBstring);
frames = length(INFO);
t2 = cputime;
t2-t1

IM = imread(RGBstring, 1);
IND = rgb2gray(IM);
imwrite(IND, ['8bit ' RGBstring], 'Compression', 'none');
for n = 2:frames
    IM = imread(RGBstring, n);
    IND = rgb2gray(IM);
    imwrite(IND, ['8bit ' RGBstring], 'WriteMode', 'append', ...
        'Compression', 'none');
end

t3 = cputime;
t3-t2
```

A.1.2 Image Pro macro

```
Sub iProcess()
'<c><s>F7 (Ctrl + Shft + F7 keyboard shortcut)
'Apply gamma transform of 0.3
ret = IpLutSetAttr(LUT_GAMMA, 30)
ret = IpLutApply()
```

```
'Apply median filter, 7x7 strength, 1 pass
ret = IpFltMedian(7, 1)

'Apply spatial calibration for SIT camera w/ 10x objective
ret = IpSCalSelect("SIT-10x")
ret = IpSCalShowEx(SCAL_DLG_SELECT, SCAL_HIDE)

'Perform object tracking with standard tracking options
ret = IpTrackShow(TRACK_TABLE,TRACK_SHOW)
ret = IpTrackMeas(TM_ADD_AUTO_ALL_TRACKS,0,IpNull)
End Sub
```

A.2 Primary data analysis code: `vProcess`

The MATLAB code `vProcess.m` was a basic skeleton that underwent many revisions to this final point. It was run to input the data and perform many of the basic processing and early analysis functions. Also comments are inserted where necessary to help explain the purpose of minor functions and subfunctions.

```
%vProcess.m
%Nicholas M Scheidler, 26 Jan 2007
%Microcirculation lab, UCSD Bioengineering

%Master script that runs several other scripts to drive data analysis
%Processes object tracking module information from Image-Pro Plus 5.1
%Optionally imports data from a text file or directly from IPP5.

clear all
current = cd;
path(path, current);

%IMPORTANT:  Change with different data files

%DIRECTORY INFORMATION
%HomeDirectory specifies where the .txt file is.
%SummaryDirectory specifies where the .xls file should go.
%BaseExperiment specifies what OVERALL experiment you are running
%Experiment is the ANIMAL code, eg, HGR1 or SD2
%Concatenating string [HomeDirectory  BaseExperiment '\' Experiment] puts
%the Data files in the appropriate place
HomeDirectory = 'D:\Video\';
BaseExperiment = 'Microchannel';
Experiment = '0.058';
Filename = 'transpose 141t';
cd([HomeDirectory BaseExperiment '\' Experiment])
Directory = cd;

%EXPERIMENT INFORMATION
nTracks = 141; %input('Number of object tracks?');
nFrames = 1799; %input('Number of frames?');
ImWidth = 640; %313; %input('Image Width?', 's');
ImHeight = 480; %267; %input('Image Height?', 's');
    Dimensions = [ImWidth ImHeight];

%vProcess CODE START---------------------------------------------
Query = input(['Load data from .mat file: ' Filename ' Data?'], 's');
if Query == 'y'
    load([Filename ' Data.mat'])
else
    Data = InputData([Filename '.txt'], nTracks, nFrames);
    save([Filename ' Data'], 'Data')
end
xData = vertcat(Data.xPos);
yData = vertcat(Data.yPos);
Data = DataInterpolator(Data);
xyData = [xData yData];

FixScatterPlotDimension = input('Fix dimensions on scatter plot?', 's');
if FixScatterPlotDimension == 'y'
    Dimensions = Dimensions * 2.0547;
end
hPlot = PlotCluster(Data, Dimensions, 1);
title('Image Data Overlay: track simulation')
set(hPlot, 'name', 'Image Data Overlay')
xlabel('Horizontal (x)')
ylabel('Vertical (y)')
axis ij

TemporalVD
```

```
pause
closereq

%Run clustering methods and compute final data
%Allow for automatic or manual K-means clustering...
disp('The clustering will be:')
disp('1) automatic by-track K-means method')
disp('2) a manual start K-means method')
disp('3) a correlation-based manual method')
disp('The first 3 methods rely on the number of clusters a priori')
figure(hPlot)
Clusters = input('Into how many capillaries to cluster objects?');

%Automatic clustering methods - requiring only the number of capillaries
KmeansPlots
PlotString = 'aDatar';
[aEnd, aData] = AssignVel(eval(PlotString), Clusters, min([Data(:).length]));
aIdx = CellIndex(aData);
%First for automatic k-means clustering
End = aEnd;
for nE = 1:length(End)
    End(nE).mean = mean(End(nE).vel);
    End(nE).std = std(End(nE).vel);
    End(nE).truncmean = mean(End(nE).trunc);
    End(nE).truncstd = std(End(nE).trunc);
    End(nE).vBarBar = mean(End(nE).vBar);
    End(nE).vBarStd = std(End(nE).vBar);
end
%Auto, Manual, and Correlation replace the old output variables
%(1) is clustered measurements mean velocity
%(2) is clustered measurements standard deviation
%(3) is CV computed from clustered measurements
Auto(1) = mean([End.mean]);
Auto(2) = std([End.mean]);
Auto(3) = Auto(2)/Auto(1);

%(4), (5), (6) are mean, std, and CV from truncated measurements
Auto(4) = mean([End.truncmean]);
Auto(5) = std([End.truncmean]);
Auto(6) = Auto(5)/Auto(4);

%(7), (8), sCV are mean std, and CV from clustered RBC-means
Auto(7) = mean([End.vBarBar]);
Auto(8) = std([End.vBarBar]);
aCV = Auto(8)/Auto(7);

%Input parameters for LimitingTrackNumber
vBarVariance = aCV;
ClusterMethod = 'Auto k-means';
LimitingTrackNumber

TemporalCV
tAuto(1) = Ymeanline;
tAuto(2) = Std;
tAuto(3) = TemporalVariance;

DataCorrelator
aEnd = End;

%Manual input of k-means start points
figure(hPlot)
ManualScript
mIdx = CellIndex(ManualDatar);
End = mEnd;
for nE = 1:length(End)
    End(nE).mean = mean(End(nE).vel);
    End(nE).std = std(End(nE).vel);
    End(nE).truncmean = mean(End(nE).trunc);
    End(nE).truncstd = std(End(nE).trunc);
    End(nE).vBarBar = mean(End(nE).vBar);
    End(nE).vBarStd = std(End(nE).vBar);
end
%(1), (2), (3) is clustered measurements mean, std, CV
Manual(1) = mean([End.mean]);
Manual(2) = std([End.mean]);
Manual(3) = Manual(2)/Manual(1);

%(4), (5), (6) are mean, std, and CV from truncated measurements
Manual(4) = mean([End.truncmean]);
Manual(5) = std([End.truncmean]);
Manual(6) = Manual(5)/Manual(4);

%(7), (8), (9) are mean, std, CV from clustered RBC means
Manual(7) = mean([End.vBarBar]);
Manual(8) = std([End.vBarBar]);
mCV = Manual(8)/Manual(7);

%Input parameters for LimitingTrackNumber
vBarVariance = mCV;
ClusterMethod = 'Manual k-means';
LimitingTrackNumber

TemporalCV
```

```
tManual(1) = Ymeanline;
tManual(2) = Std;
tManual(3) = TemporalVariance;

DataCorrelator
mEnd = End;

%Pooled measurements - mean, std, CV
vData = vertcat(Data.vel);
Pooled(1) = mean(vData);
Pooled(2) = std(vData);
Pooled(3) = Pooled(2)/Pooled(1);

%Pooled RBC means - mean, std, CV
Pooled(4) = mean(vertcat(End.vBar));
Pooled(5) = std(vertcat(End.vBar));
Pooled(6) = Pooled(5)/Pooled(4);

%CORRELATION methods
ClusterMethod = 'Correlation';
ClusterByCorr
vBarVariance = cCV;
LimitingTrackNumber

%Node-to-node definition of tracks
TrackVelocity
tVels = []; tCells = [];
tClusters = length(fieldnames(tVel));
for t = 1:tClusters
    tVels = [tVels; tVel.(['n' num2str(t)]).mean];
    tCells = [tCells; tVel.(['n' num2str(t)]).capvel];
end
tVels = tVels(~isnan(tVels));
tCells = tCells(~isnan(tCells));
nOutput(1) = mean(tVels);
nOutput(2) = std(tVels);
nOutput(3) = std(tVels)/mean(tVels);

nOutput(4) = mean(tCells);
nOutput(5) = std(tCells);
nOutput(6) = std(tCells)/mean(tCells);

oldClusters = Clusters;
Clusters = tClusters;
%ClusterMethod = 'Node-to-node';

%Creates and saves all the output graphs
%For concision, we output only the 'ClusterByCorr' output.
%EndHist
tVelHist
%Export the information from each method to Excel for tabulation
ExportDDE
disp('The data are now in the first row of SUMMARY')%Summary.xls file

Slowness

cd(Directory)
uisave
cd(current)
```

A.2.1 Subfunction `InputData.m`

`InputData` handles the input of tab-delimited data exported from the Image-Pro tracking module. The function requires inputs for the number of frames in the movie and the number of tracked objects in the dataset. It outputs a data structure containing cell centroids, velocity information, and frame placeholders.

```
function Data = InputData(Filename, nTracks, nFrames)
%Export a text file from ImagePro, which can be imported into MATLAB
%through this script

File.vel = dlmread(Filename, '\t', [1 2 nTracks nFrames]);
File.acc = dlmread(Filename, '\t', [1 nFrames+1 nTracks 2*(nFrames-1)]);
File.xPos = dlmread(Filename, '\t', [1 2*nFrames-1 nTracks 3*nFrames-2]);
File.yPos = dlmread(Filename, '\t', [1 3*nFrames-1 nTracks 4*nFrames-2]);
File.vBar = dlmread(Filename, '\t', [1 4*nFrames-1 nTracks 4*nFrames-1]);
File.vStd = dlmread(Filename, '\t', [1 4*nFrames nTracks 4*nFrames]);

File.tMean = dlmread(Filename, '\t', [nTracks+1 2 nTracks+1 nFrames]);
File.tStd = dlmread(Filename, '\t', [nTracks+2 2 nTracks+2 nFrames]);
```

```
for n = 1:1:nTracks
    Data(n).frame = find(File.vel(n, :))';
    if ~isequal(Data(n).frame, [Data(n).frame(1):1:Data(n).frame(end)]')
        disp(['Data ' num2str(n) ' was fixed.'])
        Data(n).frame = [Data(n).frame(1):1:Data(n).frame(end)]'
    end
    Data(n).vel = File.vel(n, Data(n).frame(1):Data(n).frame(end))';
    Data(n).length = length(Data(n).vel);
    Data(n).acc = File.acc(n, find(File.acc(n, :)))';
    Data(n).xPos = File.xPos(n, find(File.xPos(n, :)))';
    Data(n).yPos = File.yPos(n, find(File.yPos(n, :)))';
    Data(n).vBar = File.vBar(n);
    Data(n).vSigma = File.vStd(n);
end

Data(1).tMean = File.tMean;
Data(1).tStd = File.tStd;
```

A.2.2 Subfunction `AssignVel.m`

```
function [Bin, Datar] = AssignVel(Datar, Clusters, Length)
%Based on the index value, velocities are binned into proper capillary

%Initialize a velocity bin object
for C = 1:Clusters
    Bin(C).vel = [];
    Bin(C).frame = [];
    Bin(C).frameBar = [];
    Bin(C).trunc = [];
    Bin(C).vBar = [];
    Bin(C).xPos = [];
    Bin(C).yPos = [];
end

%Use the number of tracks
L = length(Datar)
for m = 1:L
    if isempty(Datar(m).Index)
        continue
    end
    nBin = Datar(m).Index(1);
    Bin(nBin).vel = [Bin(nBin).vel; Datar(m).vel];
    Bin(nBin).xPos = [Bin(nBin).xPos; Datar(m).xPos(1:end-1)];
    Bin(nBin).yPos = [Bin(nBin).yPos; Datar(m).yPos(1:end-1)];
    Bin(nBin).frame = [Bin(nBin).frame; Datar(m).frame];
    Bin(nBin).frameBar = [Bin(nBin).frameBar; Datar(m).frame(1)];
    Bin(nBin).trunc = [Bin(nBin).trunc; Datar(m).vel(1:Length)];
    Bin(nBin).vBar = [Bin(nBin).vBar; Datar(m).vBar];
end
```

A.2.3 Subfunction `ManualCluster.m`

```
function [Datar, yPoints] = ManualCluster(Data, Clusters, Dimensions)

%Give the user the option of creating their own clusters from velocity
%values linked into tracks

ImW = Dimensions(1);
ImH = Dimensions(2);
%ImW = max(get(get(gcf, 'Children'), 'Xlim'));
%ImH = max(get(get(gcf, 'Children'), 'Ylim'));

ManualPlot = figure;
C = colormap;
hold on

% subplot(2,1,1)
for MP = 1:length(Data)
    mColor = C(ceil(64*MP/length(Data)), :);
    PlotData(vertcat(Data(MP).xPos), vertcat(Data(MP).yPos), mColor, ImW, ImH);
end

%Code for input of Y-coord manually or from saved yManual
Reuse = input('Would you like to restore manual cluster points?','s');
if Reuse == 'y'
    disp('Load the data file with the desired cluster points saved.')
    uiload
    yPoints = yManual;
    if length(yManual) ~= Clusters
        disp('Inequality in stated number of capillaries! Must manually enter.')
        [xP, yP] = ginput(Clusters);
        yPoints = yP;
    end
else
    [xP, yP] = ginput(Clusters);
    yPoints = yP;
```

```
end
Points(1:Clusters,1,1) = yPoints';
Points(1:Clusters,1,2) = yPoints';
Points(1:Clusters,1,3) = yPoints';
Points(1:Clusters,1,4) = yPoints';
Points(1:Clusters,1,5) = yPoints';

%Kmeans clusters the average y-vals of each tracks in Data
L = length(Data);
for n = 1:L
    avgY(n) = mean(Data(n).yPos);
end

%Original script (modified: 31Aug2006) had ONE replicate; changed to
%compare 'auto' to 'k-m manual'
idx1 = kmeans(avgY', Clusters, 'dist', 'SqEu', 'replicates', 5, ...
    'emptyaction', 'drop', 'Start', Points);

for n = 1:L
    Data(n).Index = idx1(n) * ones(length(Data(n).yPos), 1);
end

clf
subplot(2,1,1)
for MP = 1:length(Data)
    mColor = C(ceil(64*MP/length(Data)), :);
    PlotData(vertcat(Data(MP).xPos), vertcat(Data(MP).yPos), mColor, ImW, ImH);
end

subplot(2,1,2)
idx = vertcat(Data.Index);
PlotScatter(vertcat(Data.xPos), vertcat(Data.yPos), idx, ImW, ImH);
title('Manual Data (SqEu, 1 rep)')

%pause

Datar = Data;
```

A.2.4 Subfunction DataCorrelator.m

```
%DataCorrelator.m
%Utilizes interpolated positional data to create a correlation score for
%the quality of clustering

%Save the original data
saveData = Data;
Data = DataInterpolator(Data);
clear Output

Output(Clusters).List = [];
%vProcess supplies information for switch navigation
%Generate the cell-capillary index, prime 'Output'
switch ClusterMethod
    case 'Auto k-means'
        for n = 1:length(Data)
            idx = aData(n).Index(1);
            Output(idx).List = [Output(idx).List n];
        end
    case 'Manual k-means'
        for n = 1:length(Data)
            idx = ManualDatar(n).Index(1);
            Output(idx).List = [Output(idx).List n];
        end
    case 'Correlation'
        for n = 1:length(Data)
            idx = cData(n).Index;
            Output(idx).List = [Output(idx).List n];
        end
    otherwise
        disp('What the hell.')
        break
end
WB = waitbar(0, 'Correlating data ...');
%Error handling for ClusterByCorr
for n = 1:Clusters
    if isempty(Output(n).List)
        Answer = questdlg(['Capillary #' num2str(n) ' is empty.  Re-click reference track?'], ...
            'Re-input track?', 'Yes', 'No', 'Yes');
        if strcmp(Answer, 'Yes')
            figure(hCorr)
            cDisp = n;
            InputCluster;
        else
            continue
        end
    end
    Output(n).TheCorr(length(Output(n).List), length(Output(n).List)) = 0;
    for c = 1:length(Output(n).List)
        for r = 1:length(Output(n).List)
            Output(n).TheCorr(c,r) = corr2(Data(Output(n).List(c)).pos, Data(Output(n).List(r)).pos);
```

```
        end
    end
    Output(n).mCorr = mean(mean(Output(n).TheCorr));
    Output(n).cCorr = mean(Output(n).TheCorr, 1);
    Output(n).rCorr = mean(Output(n).TheCorr, 2);
    waitbar(n/Clusters, WB)
end
close(WB)
%Another switch to assign Output to final output variables
switch ClusterMethod
    case 'Auto k-means'
        Output(1).Final = mean([Output.mCorr]);
        aCorrelation = Output(1).Final
    case 'Manual k-means'
        Output(1).Final = mean([Output.mCorr]);
        mCorrelation = Output(1).Final
    case 'Correlation'
        Output(1).Final = mean([Output.mCorr]);
        cCorrelation = Output(1).Final

        %Data output from cluster by correlation
        disp('From "ClusterByCorr" Clustering')
        %Generate cEnd
        cEnd = AssignVel(cData, Clusters, min([cData(:).length]));
        End = cEnd;

        for nE = 1:length(End)
            End(nE).mean = mean(End(nE).vel);
            End(nE).std = std(End(nE).vel);
            End(nE).truncmean = mean(End(nE).trunc);
            End(nE).truncstd = std(End(nE).trunc);
            End(nE).vBarBar = mean(End(nE).vBar);
            End(nE).vBarStd = std(End(nE).vBar);
        end

        %This portion is run in vProcess for other clustering modes
        %Correlation outputs:
        %(1), (2), (3) is clustered measurements mean, std, CV
        Correlation(1) = mean([End.mean]);
        Correlation(2) = std([End.mean]);
        Correlation(3) = Correlation(2)/Correlation(1)

        %(4), (5), (6) are mean, std, and CV from truncated measurements
        Correlation(4) = mean([End.truncmean]);
        Correlation(5) = std([End.truncmean]);
        Correlation(6) = Correlation(5)/Correlation(4);

        %(7), (8), cbcCV are mean std, and CV from clustered RBC-means
        Correlation(7) = mean([End.vBarBar]);
        Correlation(8) = std([End.vBarBar]);
        cCV = Correlation(8)/Correlation(7);

        vBarVariance = cCV;
        ClusterMethod = 'Correlation';
        LimitingTrackNumber

        cEnd = End;
        TemporalCV
        tCorrelation(1) = Ymeanline;
        tCorrelation(2) = Std;
        tCorrelation(3) = TemporalVariance;
    otherwise
        disp('Unknown error.')
        break
end
%Log results in other Data structure
InterpData = Data;
Data = saveData;
```

A.2.5 Subfunction `DataInterpolator.m`

```
function Data = DataInterpolator(Data)
% Parses through the positional (x,y) data for each Track and interpolates
% 100 x,y points for each.  This method allows the treatment of each Track
% as having identical number of data points for correlation comparison

for num = 1:length(Data);
    %num
    frameshort = [Data(num).frame; Data(num).frame(end) + 1];
framelong = frameshort(1):(frameshort(end)-frameshort(1))/99:frameshort(end);

intX = interp1( frameshort, Data(num).xPos, framelong );
intY = interp1( frameshort, Data(num).yPos, framelong );

Data(num).pos = [intX' intY'];
end
```

A.2.6 Subfunction `TrackVelocity.m`

```
%TrackVelocity.m

%Nick Scheidler, 4 Oct 2006

%Builds upon ideas from both ClusterByCorr and PointVelocity.  From image
%overlay, we can generate a previously undetermined number of independent
%capillary vessels.  Unlike before, each vessel will be composed of
%velocity information from track segments, rather than entire track lengths

%Allow recursive action of 'TrackVelocity' button
if ~strcmp(get(gcf, 'Tag'), 'PointVel')
    %Setup figure/GUI
    hTrack = figure;
    set(hTrack, 'Tag', 'PointVel')
    set(hTrack, 'position', [150, 30, 1100, 700])
    set(hTrack, 'name', [Filename ' - TrackVelocity'])
    set(hTrack, 'toolbar', 'figure')

    %Generate overlay and axes
    subplot(1,2,1)
    axTrack = PlotCluster(Data, Dimensions, 0);
    title(['Image Data Overlay for TrackVelocity: FLOW: ' TheFlow])
    xlabel('Horizontal dimension (\mum)')
    ylabel('Vertical dimension (\mum)')
    axis ij

    InputBtn = uicontrol(hTrack, 'position', [150 20 75 20], 'string', ...
        'Track velocity', 'callback', 'TrackVelocity');
    CloseDisp = uicontrol(hTrack, 'String', 'Exit', 'position', [250 20 75 20]);
    Info1 = uicontrol(hTrack, 'style', 'text', 'position', [350 20 400 20]);
    ContinueBtn = uicontrol(hTrack, 'position', [50 20 75 20], 'string', ...
        'Continue', 'callback', 'uiresume', 'enable', 'off');
    set(CloseDisp, 'Callback', 'ExitFigureFcn');
    DropDown = uicontrol(hTrack, 'position', [25 100 50 100], ...
        'string', [{'Circles'} {'Box'}], 'style', 'listbox');

    %Items to initialize only once
    tDisp = 1;
    Radius = 8;%Customize the size of the circle each click allows (in microns)
    C = colormap;
    clear tVel
end

%Click out a single track
Rand = ceil(64*rand(1,1));
set(Info1, 'string', 'Set proper zoom, then click CONTINUE to click points')
set(ContinueBtn, 'enable', 'on')
uiwait(hTrack)
set(Info1, 'string', []);
set(ContinueBtn, 'enable', 'off')

btn = 1;
Xs = []; Ys = [];
if get(DropDown, 'value') == 1
    while btn == 1
        [X,Y,btn] = ginput(1);
        %Indicate where the circle region has been placed
        Rect = rectangle('position', [(X - Radius) (Y - Radius) 2*Radius 2*Radius], ...
            'curvature', [1 1], 'linewidth', 2, 'edgecolor', C(Rand,:));
        Xs = [Xs; X];
        Ys = [Ys; Y];
    end
    Xs = Xs(1:end-1); Ys = Ys(1:end-1); delete(Rect);
elseif get(DropDown, 'value') == 2
    [X,Y] = ginput(2);
    Rect = rectangle('position', [X(1) Y(1) X(2)-X(1) Y(2)-Y(1)], ...
        'linewidth', 2, 'edgecolor', C(Rand,:));
    Xs = [Xs; X];
    Ys = [Ys; Y];
else
    disp('What the hell is wrong with DropDown?')
end

%Calculate and maintain record of distances/points inside circles/box
clear Dist
Dist = sparse(length(Data), max([Data.length]));
if get(DropDown, 'value') == 1
    for x = 1:length(Xs)
        disp(['Next x: ' num2str(x)])
        for R = 1:1:length(Data)
            for L = 1:Data(R).length
                rlDist = sqrt((Data(R).xPos(L)-Xs(x))^2 + (Data(R).yPos(L)-Ys(x))^2);
                Dist(R, L) = Dist(R,L) + (rlDist < Radius);
            end
        end
    end
elseif get(DropDown, 'value') == 2
    for R = 1:1:length(Data)
        for L = 1:Data(R).length
            if Data(R).xPos(L) > Xs(1) & Data(R).xPos(L) < Xs(2) ...
                    & Data(R).yPos(L) > Ys(1) & Data(R).yPos(L) < Ys(2)
```

```
                Dist(R,L) = 1;
            end
        end
    end
else
    disp('What is wrong with DropDown?')
end

%Export data to 'tVel' structure
tVel.(['n' num2str(tDisp)]).vel = [];
tVel.(['n' num2str(tDisp)]).mvel = [];
[r, l] = find(Dist);
RR = unique(r)
subplot(1,2,2), cla
axRR = PlotCluster(Data(RR), Dimensions, 0);
title('Velocity measurements were obtained from the Data below')

%To be included as a Cell, requires Meas >= 3 pts
while ~isempty(RR)
    pts = find(Dist(RR(1),:));
    if length(pts) > 2
        tVel.(['n' num2str(tDisp)]).vel = [tVel.(['n' num2str(tDisp)]).vel; ...
            Data(RR(1)).vel(pts)];
        tVel.(['n' num2str(tDisp)]).mvel = [tVel.(['n' num2str(tDisp)]).mvel; ...
            mean(Data(RR(1)).vel(pts))];
    end
    RR = setdiff(RR, RR(1));
end

%Calculate means, stds, numbers cells/meas
tVel.(['n' num2str(tDisp)]).mean = mean(tVel.(['n' num2str(tDisp)]).vel);
tVel.(['n' num2str(tDisp)]).std = std(tVel.(['n' num2str(tDisp)]).vel);
tVel.(['n' num2str(tDisp)]).meas = length(tVel.(['n' num2str(tDisp)]).vel);

tVel.(['n' num2str(tDisp)]).capvel = mean(tVel.(['n' num2str(tDisp)]).mvel);
tVel.(['n' num2str(tDisp)]).capstd = std(tVel.(['n' num2str(tDisp)]).mvel);
tVel.(['n' num2str(tDisp)]).cells.num = length(tVel.(['n' num2str(tDisp)]).mvel);
tVel.(['n' num2str(tDisp)]).cells.idx = unique(r);
tVel.(['n' num2str(tDisp)]).cells.list = [r l];

set(Info1, 'string', ['#Cells ' num2str(tVel.(['n' num2str(tDisp)]).cells.num) ...
    ' with #measurements ' num2str(tVel.(['n' num2str(tDisp)]).meas) ' found'])

%Increment tDisp for input of next track
tDisp = tDisp + 1;
```

A.2.7 Subfunction `TemporalCV.m`

```
%TemporalCV
%Parses through velocity data and divides the data into one-second pieces;
%the spatial CV is then compared within the pieces to determine temporally
%- averaged spatial variation

BL = 1;
%To allow for the few cases where the movies were 30 seconds
if nFrames > 1000
    T = 60;
else
    T = 30;
end
VasomotorBin = [0:BL:T];

%Parse the data into 'Bins'
for m = 1:length(VasomotorBin)-1
    VelBin(m).vel = [];
    VelBin(m).endvel = [];
    DnFrameBin = VasomotorBin(m)*FPS;
    UpFrameBin = VasomotorBin(m+1)*FPS;
    for n = 1:nTracks
        Frames = find(Data(n).frame > DnFrameBin & Data(n).frame < UpFrameBin);
        VelBin(m).vel = [VelBin(m).vel; Data(n).vel(Frames)];
    end
    for L = 1:Clusters
        Frames = find(End(L).frame > DnFrameBin & End(L).frame < UpFrameBin);
        EndVels = End(L).vel(Frames);
        if ~isempty(EndVels)
            VelBin(m).endvel = [VelBin(m).endvel; mean(EndVels)];
        end
    end
    VelBin(m).mean = mean(VelBin(m).vel);
    VelBin(m).norm = VelBin(m).vel ./ VelBin(m).mean;
    VelBin(m).normmean = mean(VelBin(m).norm);
    VelBin(m).length = length(VelBin(m).vel);
    VelBin(m).std = std(VelBin(m).vel);
    VelBin(m).normstd = std(VelBin(m).norm);
    VelBin(m).variance = VelBin(m).std / VelBin(m).mean;
    VelBin(m).normvariance = VelBin(m).normstd / VelBin(m).normmean;

    VelBin(m).endmean = mean(VelBin(m).endvel);
    VelBin(m).endnorm = VelBin(m).endvel ./ VelBin(m).endmean;
```

```
    VelBin(m).normendmean = mean(VelBin(m).endnorm);
    VelBin(m).endlength = length(VelBin(m).endvel);
    VelBin(m).endstd = std(VelBin(m).endvel);
    VelBin(m).normendstd = std(VelBin(m).endnorm);
    VelBin(m).endvariance = VelBin(m).endstd / VelBin(m).endmean;
    VelBin(m).normendvariance = VelBin(m).normendstd / VelBin(m).normendmean;
end

%Output the plot of temporal variation
figure;
set(gcf, 'name', [Experiment '- ' Filename '- Templot'])
subplot(2,1,1)
plot(0.5:BL:T, [VelBin.endmean])
ylabel('Mean speed (\mum/s)', 'fontsize', 24)
set(gca, 'fontsize', 24, 'xtick', [])
axis([0 T 0 1000])

subplot(2,1,2)
plot(0.5:BL:T, [VelBin.normendvariance]*100)
ylabel('Normalized spatial CV (%)', 'fontsize', 24)
xlabel('Time (s)', 'fontsize', 24)
set(gca, 'fontsize', 24)
axis([0 T 0 100])

Ymeanline = mean([VelBin.normendvariance]);
Std = std([VelBin.normendvariance]);
TemporalVariance = std([VelBin.endmean])/mean([VelBin.endmean]);

hold on, plot([0 T], [Ymeanline*100 Ymeanline*100], 'r--')
hold off
ExitFigureFcn
```

A.2.8 Subfunction `LimitingTrackNumber.m`

```
%LimitingTrackNumber.m
%Examination of the effect of reduced number of tracked objects on the
%stability of the CV calculation; run on first three clustering methods,
%but not on node-to-node because the larger number of capillary segments
%reduces the number of cells per capillary, which has a destabilizing
%effect

clear sCV;
sCV(1) = vBarVariance;
lEnd = End;
SIM = [];

tic
switch ClusterMethod
    case 'Auto k-means'
        TheData = aData;
    case 'Manual k-means'
        TheData = ManualDatar;
    case 'Correlation'
        TheData = cData;
    otherwise
        disp(ClusterMethod)
        return
end

for IND = 1:nTracks
    INDEX(IND) = TheData(IND).Index(1);
end

%Random removal of tracked objects from the dataset
Sim=20; %run 'Sim' number of simulations, compute averages
for S = 1:Sim
    List = [1:nTracks];
    cList = [1:Clusters];
    lEnd = End;
for n = 1:nTracks
        RandomLoss = ceil(length(List)*rand(1));

        lEnd(INDEX(List(RandomLoss))).vBar = ...
            setdiff(lEnd(INDEX(List(RandomLoss))).vBar, ...
            TheData(List(RandomLoss)).vBar);
        if isempty(lEnd(INDEX(List(RandomLoss))).vBar)
            cList = setdiff(cList, INDEX(List(RandomLoss)));
        end
        warning off MATLAB:divideByZero
        lEnd(INDEX(List(RandomLoss))).vBarBar = ...
            mean(lEnd(INDEX(List(RandomLoss))).vBar);

        svBarAvgVel = mean([lEnd(cList).vBarBar]);
        svBarAvgStd = std([lEnd(cList).vBarBar]);
        sCV(n+1) = svBarAvgStd/svBarAvgVel;

        List = setdiff(List, List(RandomLoss));
end
SIM = [SIM; sCV;];
end
```

```
toc

%Generate stability plots
figure, subplot(1,2,1), hold on
set(gcf, 'name', [Experiment ' - ' Filename ' - ' ClusterMethod])
Simul = mean(SIM);
plot([1:nTracks+1], Simul*100, 'r', 'linewidth', 1.75)
plot([1:nTracks+1], max(SIM)*100, 'b')
plot([1:nTracks+1], min(SIM)*100, 'b')
set(gca,'fontsize', 24)
set(gca,'ylim', [0 100])
set(gca,'xlim', [0 nTracks])
xlabel('Number of tracks removed','fontsize',24)
ylabel('Spatial coefficient of variation (%)','fontsize',24)

subplot(1,2,2), plot((max(SIM)-min(SIM))*100)
set(gca, 'fontsize', 24)
set(gca, 'xlim', [0 nTracks])
ylabel('Difference between max/min (%)','fontsize',24)
xlabel('Number of tracks removed ()','fontsize',24)

hgsave(gcf, ['Stability plot-' Filename])
closereq
save(['StabilitySimulation2-' Filename '-' num2str(Sim)],'SIM')

%These parameters are stored for viewing in Excel
%Average CV in simulations for one quarter tracks removed
OneQRem = Simul(floor((nTracks+1)/4)) - Simul(1);

%Average CV in simulations for one quarter tracks removed
HalfRem = Simul(floor((nTracks+1)/2)) - Simul(1);

%Average CV in simulations for one quarter tracks removed
ThreeQRem = Simul(floor(3*(nTracks+1)/4)) - Simul(1);

%Percent removed at CV = CVmax, location of CV = CVmax
[MaxDiffRem, LocMaxDiff] = max(Simul - Simul(1));
PercentMaxDiff = LocMaxDiff/nTracks;
```

A.3 Constructing final output

The graphs and histograms that are standard output for each dataset were generated via the code `EndHist`. The node-to-node clustering schemes were also used for generation of similar output via `tVelHist`. The final cluster plot was generated with `PlotFinal` and allowed visual inspection of the capillary velocities as they relate to the network velocity and network CV.

```
%EndHist.m
%Script that takes End data and displays a series of histograms and
%tabulates means and standard deviations standardly

AxVMax = max(vertcat(End.vel));
AxVBarMax = max(vertcat(End.vBar));

%Sets rows and columns for capillary subplots
nH = length(End);
switch nH
    case 1
        rowH = 1;
        colH = 1;
    case 2
        rowH = 2;
        colH = 1;
    case {3, 4}
        rowH = 2;
        colH = 2;
    case {5, 6}
        rowH = 3;
        colH = 2;
    case {7, 8, 9}
        rowH = 3;
```

```
        colH = 3;
    case {10, 11, 12}
        rowH = 4;
        colH = 3;
    case {13, 14, 15}
        rowH = 5;
        colH = 3;
    case 16
        rowH = 4;
        colH = 4;
    case {17, 18, 19, 20}
        rowH = 5;
        colH = 4;
    case {21, 22, 23, 24, 25}
        rowH = 5;
        colH = 5;
    otherwise
        rowH = input('How many rows in subplot?');
        colH = input('How many columns in subplot?');
end
FS = 24; %Fontsize for figures.

%Distribution of cell number w/ velocity
hRBCvel = figure;
set(hRBCvel, 'name', [Experiment ' - ' Filename ...
' - Erythrocyte Velocity Distribution'])
plot(1:length(Data), sort([Data.vBar]))
xlabel('Cell number', 'fontsize', FS)
ylabel('Mean cell velocity (\mum/s)', 'fontsize', FS)
axis square
FigureScript

%Final display of capillary velocity w/ lines for network CV
PlotFinal
axis square
FigureScript

%Capillary plots - mean velocity histograms
hHist2 = figure;
set(hHist2, 'name', [Experiment ' - ' Filename ...
' - Spatial Mean Velocity Distribution'])
for hH = 1:nH
    subplot(rowH, colH, hH)
    Edges = [0:25:ceil(max(End(SortOrder(hH)).vBar)/50)*50];
    Cnt = histc(End(SortOrder(hH)).vBar, Edges);
    bar(Edges, Cnt/sum(Cnt)*100, 'histc')
    line([End(SortOrder(hH)).vBarBar End(SortOrder(hH)).vBarBar], ...
    [0 20], 'linestyle', '--', 'linewidth', 1)
    line([End(SortOrder(hH)).vBarBar+End(SortOrder(hH)).vBarStd ...
    End(SortOrder(hH)).vBarBar+End(SortOrder(hH)).vBarStd], ...
        [0 20], 'linestyle', '--', 'color', 'r', 'linewidth', 1)
    line([End(SortOrder(hH)).vBarBar-End(SortOrder(hH)).vBarStd ...
    End(SortOrder(hH)).vBarBar-End(SortOrder(hH)).vBarStd], ...
        [0 20], 'linestyle', '--', 'color', 'r', 'linewidth', 1)
    text(0.6*ceil(AxVBarMax/500)*500, 18, ['n=' Len{hH}], 'fontsize', FS-4);
    axis([0 ceil(AxVBarMax/500)*500 0 20])
    set(gca, 'ylim', [0 20])
    if hH < nH - colH + 1
        set(gca, 'xtick', [])
    else
        xlabel('Mean velocity (\mum/s)', 'fontsize', FS)
    end
    if mod(hH, colH) ~= 1
        set(gca, 'ytick', [])
    end
    if hH == 1
            ylabel('Frequency (%)', 'fontsize', FS)
    end
    set(gca, 'fontsize', FS)
end
axis image
FigureScript

%Pooled velocity measurements histogram
clear Edges Cnt
hOverall = figure;
set(hOverall, 'Name', [Experiment ' - ' Filename ...
' - Overall Velocity Distribution'])
Datas = [];
for nN = 1:length(Data)
    Data(nN).frameBar = Data(nN).frame(1);
    Datas = [Datas; Data(nN).vel];
end
Edges = 0:50:ceil(max(Datas)/50)*50;
nDatas = Datas / PooledAvgVel;
hNormOvrl = hist(nDatas, 25);
hOvr1 = hist(Datas, 25);
Cnt = histc(Datas, Edges);
bar(Edges', Cnt/sum(Cnt)*100, 'histc')
ylabel('Frequency (%)', 'fontsize', FS)
xlabel('Velocity (\mum/s)', 'fontsize', FS)
set(gca, 'fontsize', FS)
line([mean(Datas) mean(Datas)], get(gca, 'ylim'), ...
```

```
'linestyle', '--', 'linewidth', 2)
line([mean(Datas)+std(Datas) mean(Datas)+std(Datas)], ...
get(gca, 'ylim'), 'linestyle', '--', 'color', 'r', 'linewidth', 2)
line([mean(Datas)-std(Datas) mean(Datas)-std(Datas)], ...
get(gca, 'ylim'), 'linestyle', '--', 'color', 'r', 'linewidth', 2)
axis square
FigureScript

%Pooled mean velocity histogram
clear Edges Cnt
hOverall2 = figure;
set(hOverall2, 'Name', [Experiment ' - ' Filename ...
' - Overall Mean Velocity Distribution'])
Ends = [];
for nN = 1:length(End)
    Ends = [Ends; End(nN).vBar];
end
nEnds = Ends / AvgVel;
Edges = [0:50:1500];
normEdges = Edges / AvgVel;
hOvr2 = histc(Ends, Edges);
bar(Edges, hOvr2/max(Ends)*100, 'histc')
xlabel('Mean velocity (\mum/s)', 'fontsize', FS)
ylabel('Frequency (%)', 'fontsize', FS)
line([mean(Ends) mean(Ends)], get(gca, 'ylim'), ...
'linestyle', '--', 'linewidth', 2)
line([mean(Ends)+std(Ends) mean(Ends)+std(Ends)], ...
get(gca, 'ylim'), 'linestyle', '--', 'color', 'r', 'linewidth', 2)
line([mean(Ends)-std(Ends) mean(Ends)-std(Ends)], ...
get(gca, 'ylim'), 'linestyle', '--', 'color', 'r', 'linewidth', 2)
set(gca, 'fontsize', FS)
axis square
FigureScript

%Temporal velocity capillary plots
hTemp2 = figure;
set(hTemp2, 'Name', [Experiment ' - ' Filename ...
' -  Temporal Mean Velocity Distribution'])
for hH = 1:nH
    subplot(rowH, colH, hH)
    scatter(End(SortOrder(hH)).frameBar/FPS, ...
    End(SortOrder(hH)).vBar, 5, 'filled')
    set(gca, 'fontsize', FS)
    lMean = line([0 nFrames-1], ...
    [End(SortOrder(hH)).vBarBar End(SortOrder(hH)).vBarBar]);
    set(lMean, 'LineStyle', '--', 'Color', 'k', 'linewidth', 1)
    lLower = line([0 nFrames-1], [(End(SortOrder(hH)).vBarBar - ...
End(SortOrder(hH)).vBarStd) (End(SortOrder(hH)).vBarBar ...
- End(SortOrder(hH)).vBarStd)]);
    set(lLower, 'LineStyle', '-.', 'Color', 'r', 'linewidth', 1)
    lUpper = line([0 nFrames-1], [(End(SortOrder(hH)).vBarBar ...
+ End(SortOrder(hH)).vBarStd) (End(SortOrder(hH)).vBarBar ...
+ End(SortOrder(hH)).vBarStd)]);
    set(lUpper, 'LineStyle', '-.', 'Color', 'r', 'linewidth', 1)
    text(0.6*ceil(nFrames-1)/FPS, 0.9*AxVMax, ['n=' Len{hH}], ...
'fontsize', FS-4);
    axis([0 ceil((nFrames-1)/FPS) 0 AxVMax])
    set(gca, 'xtick', [0 60])
    axis square
    if hH < nH - colH + 1
        set(gca, 'xtick', [])
    else
        xlabel('Time (s)', 'Fontsize', FS)
    end
    if mod(hH, colH) ~= 1
        set(gca, 'ytick', [])
    end
    if hH == 1
        ylabel('Mean velocity (\mum/s)', 'Fontsize', FS)
    end
end
FigureScript

%Velocity versus horizontal position traveled in capillary
hmeanVvsX = figure;
set(hmeanVvsX, 'Name', [Experiment ' - ' Filename ...
' - Mean velocity versus spatial coordinate (x)'])
warning off MATLAB:divideByZero
wBin = 50;
for hH = 1:nH
    subplot(rowH, colH, hH)
    Bounds = [0:wBin:ceil(max(End(SortOrder(hH)).xPos)/wBin)*wBin];
    for B = 1:length(Bounds) - 1
        msV(B) = mean(End(SortOrder(hH)).vel(find(End(SortOrder(hH)).xPos ...
> Bounds(B) & End(SortOrder(hH)).xPos < Bounds(B + 1))));
        ssV(B) = std(End(SortOrder(hH)).vel(find(End(SortOrder(hH)).xPos ...
> Bounds(B) & End(SortOrder(hH)).xPos < Bounds(B + 1))));
        semsV(B) = ssV(B) / sqrt(length(find(End(SortOrder(hH)).xPos ...
> Bounds(B) & End(SortOrder(hH)).xPos < Bounds(B + 1))));
        mid(B) = (Bounds(B) + Bounds(B+1)) / 2;
    end
    hError = errorbar(mid, msV, semsV, 'b');
    for Err = 1:length(hError)
```

```
        set(hError(Err), 'linewidth', 2)
    end
    text(ceil(Dimensions(1)/10)*7, 0.9*AxVBarMax, ['n=' Len{hH}], ...
    'fontsize', FS-4)
    axis([0 ceil(Dimensions(1)/100)*100 0 AxVBarMax])
    axis square
    if hH < nH - colH + 1
        set(gca, 'xtick', [])
    elseif hH == nH
        xlabel('Spatial x-coordinate (\mum)', 'Fontsize', FS)
    end
    if mod(hH, colH) ~= 1
        set(gca, 'ytick', [])
    end
    if hH == 1
        ylabel('Mean velocity (\mum/s)', 'fontsize', FS)
    end
    set(gca, 'fontsize', FS)
end
FigureScript

%Variation in track measurement
clear Vars;
hVarInTrack = figure;
set(hVarInTrack, 'Name', [Experiment ' - ' Filename ...
' - Distribution of Variation in Velocity Measurement'])
for hV = 1:length(Data)
    Vars(hV) = Data(hV).vSigma / Data(hV).vBar * 100;
end
Edges = 0:5:50*ceil(max(Vars)/50);
VarsHist = histc(Vars, Edges);
bar(Edges, VarsHist/sum(VarsHist)*100, 'histc');
set(gca, 'fontsize', FS)
ylabel('Frequency (%)', 'fontsize', FS)
xlabel('Variance in a track (%)', 'fontsize', FS)
axis square
FigureScript
```

A.3.1 SpatialXPlot.m

```
%SpatialXPlot.m
%Plots a spatially-averaged view of the velocity data, vs. horizontal
%position

hmeanVvsX = figure;
set(hmeanVvsX, 'Name', [Experiment ': ' Filename ...
': Mean velocity versus spatial coordinate (x)'])
warning off MATLAB:divideByZero
wBin = 50;
for HH = 1:3%nH
    hH = [3 5 10];
    subplot(3,1,HH)%subplot(rowH, colH, hH)
    Bounds = [0:wBin:ceil(max(End(SortOrder(hH)).xPos)/wBin)*wBin];
    for B = 1:length(Bounds) - 1
        VelB = find(End(SortOrder(hH)).xPos > Bounds(B) & ...
End(SortOrder(hH)).xPos < Bounds(B + 1));
        if length(VelB) < 2
            continue
        end
        msV(B) = mean(End(SortOrder(hH)).vel(VelB))
        ssV(B) = std(End(SortOrder(hH)).vel(VelB))
        semsV(B) = ssV(B) / sqrt(length(VelB))
        mid(B) = (Bounds(B) + Bounds(B+1)) / 2
    end
    mid = mid(find(mid));
    ssV = ssV(find(ssV));
    semsV = semsV(find(semsV));
    msV = msV(find(msV));

    hError = errorbar(mid, msV, semsV, 'b');
    for Err = 1:length(hError)
        set(hError(Err), 'linewidth', 2)
    end
    text(ceil(Dimensions(1)/10)*7, 0.9*AxVBarMax, ...
    ['n=' Len{hH}], 'fontsize', FS-4)
    axis([0 ceil(Dimensions(1)/100)*100 0 AxVBarMax])
    if hH < nH - colH + 1
        set(gca, 'xtick', [])
    elseif hH == nH
        xlabel('Spatial x-coordinate (\mum)', 'Fontsize', FS)
    end
    if mod(hH, colH) ~= 1
        set(gca, 'ytick', [])
    end
    if hH == 1
        ylabel('Mean velocity (\mum/s)', 'fontsize', FS)
    end
    set(gca, 'fontsize', FS)
    clear msV ssV semsV mid
end
```

```
% %for the whole network
hOverallmeanVvsX = figure;
set(hOverallmeanVvsX, 'Name', [Experiment ': ' Filename ...
': Mean velocity versus spatial coordinate, for the network'])
warning off MATLAB:divideByZero
wBin = 0.025;
Bounds = [0:wBin:1];

for B = 1:length(Bounds) - 1
    hV = [];
    for hH = 1:nH
        maxX = max(End(SortOrder(hH)).xPos);
        minX = min(End(SortOrder(hH)).xPos);
        normX = maxX - minX;
        VelB = find((End(SortOrder(hH)).xPos - minX)/normX > Bounds(B) ...
            & (End(SortOrder(hH)).xPos - minX)/normX < Bounds(B + 1));
        hV = vertcat(hV, End(SortOrder(hH)).vel(VelB));
    end
    msV(B) = mean(hV);
    ssV(B) = std(hV);
    semsV(B) = ssV(B) / sqrt(length(VelB));
    mid(B) = (Bounds(B) + Bounds(B+1)) / 2;
end
hError = errorbar(mid, msV, semsV, 'b');
for Err = 1:length(hError)
    set(hError(Err), 'linewidth', 2)
end
text(ceil(Dimensions(1)/10)*7, 0.9*AxVBarMax, ...
['n=' Len{hH}], 'fontsize', FS-4)
axis([0 1 0 AxVBarMax])
xlabel('Spatial x-coordinate (\mum)', 'Fontsize', FS)
ylabel('Mean velocity (\mum/s)', 'fontsize', FS)
set(gca, 'fontsize', FS)
```

A.3.2 PlotFinal.m

```
%SpatialXPlot.m
%Plots a spatially-averaged view of the velocity data, vs. horizontal
%position

hmeanVvsX = figure;
set(hmeanVvsX, 'Name', [Experiment ': ' Filename ...
': Mean velocity versus spatial coordinate (x)'])
warning off MATLAB:divideByZero
wBin = 50;
for HH = 1:3%nH
    hH = [3 5 10];
    subplot(3,1,HH)%subplot(rowH, colH, hH)
    Bounds = [0:wBin:ceil(max(End(SortOrder(hH)).xPos)/wBin)*wBin];
    for B = 1:length(Bounds) - 1
        VelB = find(End(SortOrder(hH)).xPos > Bounds(B) & ...
End(SortOrder(hH)).xPos < Bounds(B + 1));
        if length(VelB) < 2
            continue
        end
        msV(B) = mean(End(SortOrder(hH)).vel(VelB))
        ssV(B) = std(End(SortOrder(hH)).vel(VelB))
        semsV(B) = ssV(B) / sqrt(length(VelB))
        mid(B) = (Bounds(B) + Bounds(B+1)) / 2
    end
    mid = mid(find(mid));
    ssV = ssV(find(ssV));
    semsV = semsV(find(semsV));
    msV = msV(find(msV));

    hError = errorbar(mid, msV, semsV, 'b');
    for Err = 1:length(hError)
        set(hError(Err), 'linewidth', 2)
    end
    text(ceil(Dimensions(1)/10)*7, 0.9*AxVBarMax, ...
    ['n=' Len{hH}], 'fontsize', FS-4)
    axis([0 ceil(Dimensions(1)/100)*100 0 AxVBarMax])
    if hH < nH - colH + 1
        set(gca, 'xtick', [])
    elseif hH == nH
        xlabel('Spatial x-coordinate (\mum)', 'Fontsize', FS)
    end
    if mod(hH, colH) ~= 1
        set(gca, 'ytick', [])
    end
    if hH == 1
        ylabel('Mean velocity (\mum/s)', 'fontsize', FS)
    end
    set(gca, 'fontsize', FS)
    clear msV ssV semsV mid
end

% %for the whole network
hOverallmeanVvsX = figure;
```

```
set(hOverallmeanVvsX, 'Name', [Experiment ': ' Filename ...
': Mean velocity versus spatial coordinate, for the network'])
warning off MATLAB:divideByZero
wBin = 0.025;
Bounds = [0:wBin:1];

for B = 1:length(Bounds) - 1
    hV = [];
    for hH = 1:nH
        maxX = max(End(SortOrder(hH)).xPos);
        minX = min(End(SortOrder(hH)).xPos);
        normX = maxX - minX;
        VelB = find((End(SortOrder(hH)).xPos - minX)/normX > Bounds(B) ...
            & (End(SortOrder(hH)).xPos - minX)/normX < Bounds(B + 1));
        hV = vertcat(hV, End(SortOrder(hH)).vel(VelB));
    end
    msV(B) = mean(hV);
    ssV(B) = std(hV);
    semsV(B) = ssV(B) / sqrt(length(VelB));
    mid(B) = (Bounds(B) + Bounds(B+1)) / 2;
end
hError = errorbar(mid, msV, semsV, 'b');
for Err = 1:length(hError)
    set(hError(Err), 'linewidth', 2)
end
text(ceil(Dimensions(1)/10)*7, 0.9*AxVBarMax, ...
['n=' Len{hH}], 'fontsize', FS-4)
axis([0 1 0 AxVBarMax])
xlabel('Spatial x-coordinate (\mum)', 'Fontsize', FS)
ylabel('Mean velocity (\mum/s)', 'fontsize', FS)
set(gca, 'fontsize', FS)
```

A.4 Post-analysis

The script `Datafiles` was recently written to allow application of any analysis script to the complete list of datafiles I have generated. The bulk of the script was the list of MATLAB datafiles saved in the original video directories. The directory structure and datafiles have been backed up to a database structure and will be available on a Microcirculation Lab website I will create. The velocity data will be accessible then, via `Datafiles` for any analysis from new codes written in the future. As mentioned above at the outset of this chapter, it was my hope that my research could serve as a springboard for another enterprizing graduate student to study and follow in my footsteps. Here is `Datafiles` in it's entirety — complete with the full list of and locations for velocity datafiles I have generated and utilized for my research.

A.4.1 `Datafiles`

A.4.2 `Slowness.m`

```
%Slowness.m
%Requires only to have loaded Data to determine whether there were slow
%individual cells being tracked.

Slow = 0;
SameCell = 0;
SlowDist = [];

SlowCells = find([Data.vBar] < 75);
Slow = length(SlowCells);
if Slow > 0
    for r = 1:Slow
```

```
        SlowX(r) = mean(Data(SlowCells(r)).xPos);
        SlowY(r) = mean(Data(SlowCells(r)).yPos);
    end
    for r = 1:Slow
        SlowDist(r,:) = sqrt((SlowX - SlowX(r)).^2 + (SlowY - SlowY(r)).^2);
    end
    SlowDist = (SlowDist < 10);
    SlowDist = triu(SlowDist - diag(ones(length(SlowDist),1)));
    SameCell = length(find(SlowDist));
    clear SlowDist SlowX SlowY
end
disp([num2str(Slow) ' tracks were very slow.'])
disp(['Of these, ' num2str(SameCell) ' track pairs exist.'])

%Running stand-alone (Filename) or thru Datafiles script (Name)
S = who('Name');
if ~isempty(S) %Datasets
    S = who('-file',Name,'tCells');
else
    S = who('-file',Filename,'tCells');
end

%Account for older data with no nTn clustering / different filenames
if ~isempty(S)
    nTnCV = std(tCells)/mean(tCells);
    disp(['Node-to-node spatial CV is ' num2str(nTnCV)])
else
    nTnCV = std([End.vBarBar])/mean([End.vBarBar]);
    disp(['vBarVariance is ' num2str(vBarVariance)])

    %Basic clustering / manual
    if Slow
        [End, ManualDatar] = ...
            AssignVel(ManualDatar(setdiff([1:length(Data)],SlowCells)), ...
            Clusters, min([ManualDatar.length]));
            for nE = 1:length(End)
                End(nE).mean = mean(End(nE).vel);
                End(nE).std = std(End(nE).vel);
                End(nE).truncmean = mean(End(nE).trunc);
                End(nE).truncstd = std(End(nE).trunc);
                End(nE).vBarBar = mean(End(nE).vBar);
                End(nE).vBarStd = std(End(nE).vBar);
            end
            woSlowCV = std([End.vBarBar])/mean([End.vBarBar]);
    else
        woSlowCV = nTnCV;
        SlowCells = 0;
    end
    Output = [Slow SameCell nTnCV woSlowCV];
    return
end

Fields = fieldnames(tVel);
Segments = length(Fields);
for s = 1:Segments
    CellNumber(s) = tVel.(Fields{s}).cells.num;
end
[SortedCells SegmentOrder] = sort(CellNumber, 'descend');
for s = 1:Segments
    if isempty(tVel.(Fields{SegmentOrder(s)}).mvel)
        SegmentOrd = setdiff(SegmentOrder, SegmentOrder(s));
        SegmentOrder = SegmentOrd;
    end
end
Segments = length(SegmentOrder);
clear End
for s = 1:Segments
    End(s).vel = []; End(s).vBar = []; End(s).xPos = []; End(s).frameBar = [];
    CellRemove = intersect(tVel.(Fields{SegmentOrder(s)}).cells.idx, SlowCells);
    if isempty(CellRemove)
        End(s).vBar = tVel.(Fields{SegmentOrder(s)}).mvel;
        End(s).vel = tVel.(Fields{SegmentOrder(s)}).vel;
        End(s).vBarBar = tVel.(Fields{SegmentOrder(s)}).capvel;
        End(s).vBarStd = tVel.(Fields{SegmentOrder(s)}).capstd;
    else
        CellsInclude = setdiff(tVel.(Fields{SegmentOrder(s)}).cells.idx, CellRemove);
        for c = 1:length(CellsInclude)
            xs = find(tVel.(Fields{SegmentOrder(s)}).cells.list(:,1) == CellsInclude(c));
            if length(xs) > 2
                frames = tVel.(Fields{SegmentOrder(s)}).cells.list(xs,2);
                End(s).vel = [End(s).vel; Data(CellsInclude(c)).vel(frames)];
                End(s).vBar = [End(s).vBar; mean(Data(CellsInclude(c)).vel(frames))];
                End(s).xPos = [End(s).xPos; Data(CellsInclude(c)).xPos(frames)];
                End(s).frameBar = [End(s).frameBar; Data(CellsInclude(c)).frame(frames(1))];
            end
        end
if ~isempty(End(s).vBar)
            End(s).vBarBar = mean(End(s).vBar);
            End(s).vBarStd = std(End(s).vBar);
        else
            End(s).vBarBar = 0;
            End(s).vBarStd = 0;
        end
```

```
    end
end

disp(blanks(1))
vBarBar = End(find([End.vBarBar] > 0).vBarBar);
%sort([End.vBarBar]);
%vBarBar = vBarBar(2:end);
[std(vBarBar) mean(vBarBar)]
woSlowCV = std([vBarBar])/mean([vBarBar]);
disp(['Discounting slow cells, spatial CV is ' num2str(woSlowCV)])
[sort(tCells) sort([End.vBarBar]')]

Output = [Slow SameCell nTnCV woSlowCV];
```

References

[1] Ahn, S. C., Kim, B. Y., Oh, W. K., Park, Y. M., Kim, H. M., and Ahn, J. S., 2006: Colorimetric heparinase assay for alternative anti-metastatic activity. *Life Sci*, **79**(17), 1661–1665. doi:10.1016/j.lfs.2006.05.020.

[2] Ammarguellat, F. Z., Gannon, P. O., Amiri, F., and Schiffrin, E. L., 2002: Fibrosis, matrix metalloproteinases, and inflammation in the heart of doca-salt hypertensive rats: role of et(a) receptors. *Hypertension*, **39**(2 Pt 2), 679–684.

[3] Arend, O., Wolf, S., Jung, F., Bertram, B., Pöstgens, H., Toonen, H., and Reim, M., 1991: Retinal microcirculation in patients with diabetes mellitus: dynamic and morphological analysis of perifoveal capillary network. *Br J Ophthalmol*, **75**(9), 514–518.

[4] Armulik, A., Abramsson, A., and Betsholtz, C., 2005: Endothelial/pericyte interactions. *Circ Res*, **97**(6), 512–523. doi:10.1161/01.RES.0000182903.16652.d7.

[5] Bagi, Z., Frangos, J. A., Yeh, J.-C., White, C. R., Kaley, G., and Koller, A., 2005: Pecam-1 mediates no-dependent dilation of arterioles to high temporal gradients of shear stress. *Arterioscler Thromb Vasc Biol*, **25**(8), 1590–1595. doi:10.1161/01.ATV.0000170136.71970.5f.

[6] Baker, M., and Wayland, H., 1974: On-line volume flow rate and velocity profile measurement for blood in microvessels. *Microvasc Res*, **7**(1), 131–143.

[7] Bar-Ner, M., Kramer, M. D., Schirrmacher, V., Ishai-Michaeli, R., Fuks, Z., and Vlodavsky, I., 1985: Sequential degradation of heparan sulfate in the subendothelial extracellular matrix by highly metastatic lymphoma cells. *Int J Cancer*, **35**(4), 483–491.

[8] Battegay, E. J., de Miguel, L. S., Petrimpol, M., and Humar, R., 2007: Effects of anti-hypertensive drugs on vessel rarefaction. *Curr Opin Pharmacol*. doi:10.1016/j.coph.2006.09.007.

[9] Bauer, P. M., Yu, J., Chen, Y., Hickey, R., Bernatchez, P. N., Looft-Wilson, R., Huang, Y., Giordano, F., Stan, R. V., and Sessa, W. C., 2005: Endothelial-specific expression of caveolin-1 impairs microvascular permeability and angiogenesis. *Proc Natl Acad Sci U S A*, **102**(1), 204–209. doi:10.1073/pnas.0406092102.

[10] Carpentier, P. H., 2001: Current techniques for the clinical evaluation of the microcirculation. *J Mal Vasc*, **26**(2), 142–147.

[11] Constantinescu, A. A., Vink, H., and Spaan, J. A., 2001: Elevated capillary tube hematocrit reflects degradation of endothelial cell glycocalyx by oxidized ldl. *Am J Physiol Heart Circ Physiol*, **280**(3), H1051–H1057.

[12] Constantinescu, A. A., Vink, H., and Spaan, J. A. E., 2003: Endothelial cell glycocalyx modulates immobilization of leukocytes at the endothelial surface. *Arterioscler Thromb Vasc Biol*, **23**(9), 1541–1547. doi:10.1161/01.ATV.0000085630.24353.3D.

[13] Damiano, E. R., 1998: The effect of the endothelial-cell glycocalyx on the motion of red blood cells through capillaries. *Microvasc Res*, **55**(1), 77–91. doi:10.1006/mvre.1997.2052.

[14] Damon, D. H., and Duling, B. R., 1985: Evidence that capillary perfusion heterogeneity is not controlled in striated muscle. *Am J Physiol*, **249**(2 Pt 2), H386–H392.

[15] DeLano, F. A., Balete, R., and Schmid-Schönbein, G. W., 2005: Control of oxidative stress in microcirculation of spontaneously hypertensive rats. *Am J Physiol Heart Circ Physiol*, **288**(2), H805–12. doi:10.1152/ajpheart.00696.2004.

[16] DeLano, F. A., Parks, D. A., Ruedi, J. M., Babior, B. M., and Schmid-Schönbein, G. W., 2006: Microvascular display of xanthine oxidase and nadph oxidase in the spontaneously hypertensive rat. *Microcirculation*, **13**(7), 551–566. doi:10.1080/10739680600885152.

[17] DeLano, F. A., Schmid-Schönbein, G. W., Skalak, T. C., and Zweifach, B. W., 1991: Penetration of the systemic blood pressure into the microvasculature of rat skeletal muscle. *Microvasc Res*, **41**(1), 92–110.

[18] Dell'Omo, G., Penno, G., Pucci, L., Mariani, M., Prato, S. D., and Pedrinelli, R., 2004: Abnormal capillary permeability and endothelial dysfunction in hypertension with comorbid metabolic syndrome. *Atherosclerosis*, **172**(2), 383–389. doi:10.1016/j.atherosclerosis.2003.11.013.

[19] Desjardins, C., and Duling, B. R., 1990: Heparinase treatment suggests a role for the endothelial cell glycocalyx in regulation of capillary hematocrit. *Am J Physiol*, **258**(3 Pt 2), H647–H654.

[20] Dewey, C. F., Bussolari, S. R., Gimbrone, M. A., and Davies, P. F., 1981: The dynamic response of vascular endothelial cells to fluid shear stress. *J Biomech Eng*, **103**(3), 177–185.

[21] Dietrich, H. H., 1989: Effect of locally applied epinephrine and norepinephrine on blood flow and diameter in capillaries of rat mesentery. *Microvasc Res*, **38**(2), 125–135.

[22] Dietrich, H. H., and Tyml, K., 1992: Microvascular flow response to localized application of norepinephrine on capillaries in rat and frog skeletal muscle. *Microvasc Res*, **43**(1), 73–86.

[23] Dintenfass, L., 1967: Inversion of the fahraeus-lindqvist phenomenon in blood flow through capillaries of diminishing radius. *Nature*, **215(5105)**, 1099–100.

[24] Dixon, J. B., Zawieja, D. C., Gashev, A. A., and Cot, G. L., 2005: Measuring microlymphatic flow using fast video microscopy. *J Biomed Opt*, **10**(6), 064016. doi: 10.1117/1.2135791.

[25] Dora, K. A., Xia, J., and Duling, B. R., 2003: Endothelial cell signaling during conducted vasomotor responses. *Am J Physiol Heart Circ Physiol*, **285**(1), H119–H126. doi:10.1152/ajpheart.00643.2002.

[26] Dusserre, N., L'Heureux, N., Bell, K. S., Stevens, H. Y., Yeh, J., Otte, L. A., Loufrani, L., and Frangos, J. A., 2004: Pecam-1 interacts with nitric oxide synthase in human endothelial cells: implication for flow-induced nitric oxide synthase activation. *Arterioscler Thromb Vasc Biol*, **24**(10), 1796–1802. doi:10.1161/01.ATV.0000141133.32496.41.

[27] Eden, E., Waisman, D., Rudzsky, M., Bitterman, H., Brod, V., and Rivlin, E., 2005: An automated method for analysis of flow characteristics of circulating particles from in vivo video microscopy. *IEEE Trans Med Imaging*, **24**(8), 1011–1024.

[28] Ellis, C. G., Wrigley, S. M., and Groom, A. C., 1994: Heterogeneity of red blood cell perfusion in capillary networks supplied by a single arteriole in resting skeletal muscle. *Circ Res*, **75**(2), 357–368.

[29] Engelson, E. T., Schmid-Schönbein, G. W., and Zweifach, B. W., 1985: The microvasculature in skeletal muscle. iii. venous network anatomy in normotensive and spontaneously hypertensive rats. *Int J Microcirc Clin Exp*, **4**(3), 229–248.

[30] Engelson, E. T., Schmid-Schönbein, G. W., and Zweifach, B. W., 1986: The microvasculature in skeletal muscle. ii. arteriolar network anatomy in normotensive and spontaneously hypertensive rats. *Microvasc Res*, **31**(3), 356–374.

[31] Engelson, E. T., Skalak, T. C., and Schmid-Schönbein, G. W., 1985: The microvasculature in skeletal muscle. i. arteriolar network in rat spinotrapezius muscle. *Microvasc Res*, **30**(1), 29–44.

[32] Fåhræus, R., 1929: The suspension stability of the blood. *Physiological Review*, **9**, 241–274.

[33] Fåhræus, R., and Lindqvist, T., 1931: The viscosity of the blood in narrow capillary tubes. *American Journal of Physiology*, **96**, 562–568.

[34] Félétou, M., and Vanhoutte, P. M., 2006: Endothelial dysfunction: a multifaceted disorder (the wiggers award lecture). *Am J Physiol Heart Circ Physiol*, **291**(3), H985–1002. doi:10.1152/ajpheart.00292.2006.

[35] Fenster, M. A., 1992: *A mathematical hemodynamic model of the microcirculation in skeletal muscle, including passive and active vessel properties, hematocrit, and blood rheology.* Master's thesis, University of California, San Diego.

[36] Ferreira, L. F., Padilla, D. J., Musch, T. I., and Poole, D. C., 2006: Temporal profile of rat skeletal muscle capillary haemodynamics during recovery from contractions. *J Physiol*, **573**(Pt 3), 787–797. doi:10.1113/jphysiol.2006.104802.

[37] Florian, J. A., Kosky, J. R., Ainslie, K., Pang, Z., Dull, R. O., and Tarbell, J. M., 2003: Heparan sulfate proteoglycan is a mechanosensor on endothelial cells. *Circ Res*, **93**(10), e136–e142. doi:10.1161/01.RES.0000101744.47866.D5.

[38] Freeman, C., and Parish, C. R., 1997: A rapid quantitative assay for the detection of mammalian heparanase activity. *Biochem J*, **325 (Pt 1)**, 229–237.

[39] Freeman, C., and Parish, C. R., 1998: Human platelet heparanase: purification, characterization and catalytic activity. *Biochem J*, **330 (Pt 3)**, 1341–1350.

[40] Frisbee, J. C., 2005: Reduced nitric oxide bioavailability contributes to skeletal muscle microvessel rarefaction in the metabolic syndrome. *Am J Physiol Regul Integr Comp Physiol*, **289**(2), R307–R316. doi:10.1152/ajpregu.00114.2005.

[41] Fujiwara, K., 2006: Platelet endothelial cell adhesion molecule-1 and mechanotransduction in vascular endothelial cells. *J Intern Med*, **259**(4), 373–380. doi: 10.1111/j.1365-2796.2006.01623.x.

[42] Fukuda, S., Yasu, T., Kobayashi, N., Ikeda, N., and Schmid-Schönbein, G. W., 2004: Contribution of fluid shear response in leukocytes to hemodynamic resistance in the spontaneously hypertensive rat. *Circ Res*, **95**(1), 100–108. doi: 10.1161/01.RES.0000133677.77465.38.

[43] Fukuda, S., Yasu, T., Predescu, D. N., and Schmid-Schnbein, G. W., 2000: Mechanisms for regulation of fluid shear stress response in circulating leukocytes. *Circ Res*, **86**(1), E13–8.

[44] Fulton, D., Gratton, J. P., McCabe, T. J., Fontana, J., Fujio, Y., Walsh, K., Franke, T. F., Papapetropoulos, A., and Sessa, W. C., 1999: Regulation of endothelium-derived nitric oxide production by the protein kinase akt. *Nature*, **399**(6736), 597–601. doi:10.1038/21218.

[45] Fung, Y. C., 1997: *Biomechanics: Circulation*. Springer-Verlag, New York, 2nd edition.

[46] Funk, W., Endrich, B., Messmer, K., and Intaglietta, M., 1983: Spontaneous arteriolar vasomotion as a determinant of peripheral vascular resistance. *Int J Microcirc Clin Exp*, **2**(1), 11–25.

[47] Galbraith, C. G., Skalak, R., and Chien, S., 1998: Shear stress induces spatial reorganization of the endothelial cell cytoskeleton. *Cell Motil Cytoskeleton*, **40**(4), 317–330. doi:3.0.CO;2-8.

[48] García-Cardeña, G., Martasek, P., Masters, B. S., Skidd, P. M., Couet, J., Li, S., Lisanti, M. P., and Sessa, W. C., 1997: Dissecting the interaction between nitric oxide synthase (nos) and caveolin. functional significance of the nos caveolin binding domain in vivo. *J Biol Chem*, **272**(41), 25437–25440.

[49] Gieson, E. J. V., and Skalak, T. C., 2001: Chronic vasodilation induces matrix metalloproteinase 9 (mmp-9) expression during microvascular remodeling in rat skeletal muscle. *Microcirculation*, **8**(1), 25–31.

[50] Gigli, M., Consonni, A., Ghiselli, G., Rizzo, V., Naggi, A., and Torri, G., 1992: Heparin binding to human plasma low-density lipoproteins: dependence on heparin sulfation degree and chain length. *Biochemistry*, **31**(26), 5996–6003.

[51] Gigli, M., Ghiselli, G., Torri, G., Naggi, A., and Rizzo, V., 1993: A comparative study of low-density lipoprotein interaction with glycosaminoglycans. *Biochim Biophys Acta*, **1167**(2), 211–217.

[52] Gray, S. D., 1973: Rat spinotrapezius muscle preparation for microscopic observation of the terminal vascular bed. *Microvasc Res*, **5**(3), 395–400.

[53] Griendling, K. K., and FitzGerald, G. A., 2003: Oxidative stress and cardiovascular injury: Part i: basic mechanisms and in vivo monitoring of ros. *Circulation*, **108**(16), 1912–1916. doi:10.1161/01.CIR.0000093660.86242.BB.

[54] Hansen-Smith, F. M., Watson, L., Lu, D. Y., and Goldstein, I., 1988: Griffonia simplicifolia i: fluorescent tracer for microcirculatory vessels in nonperfused thin muscles and sectioned muscle. *Microvasc Res*, **36**(3), 199–215.

[55] Harris, A. G., and Skalak, T. C., 1993: Effects of leukocyte activation on capillary hemodynamics in skeletal muscle. *Am J Physiol*, **264**(3 Pt 2), H909–H916.

[56] Harris, A. G., and Skalak, T. C., 1993: Leukocyte cytoskeletal structure determines capillary plugging and network resistance. *Am J Physiol*, **265**(5 Pt 2), H1670–H1675.

[57] Harvey, W., 1628: *An Anatomical Study of the Motion of the Heart and of the Blood in Animals*. in Frankfort (Latin); translated by Robert Willis.

[58] Hayakawa, H., and Raij, L., 1999: Relationship between hypercholesterolaemia, endothelial dysfunction and hypertension. *J Hypertens*, **17**(5), 611–619.

[59] Henry, C. B., and Duling, B. R., 1999: Permeation of the luminal capillary glycocalyx is determined by hyaluronan. *Am J Physiol*, **277**(2 Pt 2), H508–H514.

[60] Hu, X., and Weinbaum, S., 1999: A new view of starling's hypothesis at the microstructural level. *Microvasc Res*, **58**(3), 281–304. doi:10.1006/mvre.1999.2177.

[61] Huang, A., Sun, D., Kaley, G., and Koller, A., 1998: Estrogen preserves regulation of shear stress by nitric oxide in arterioles of female hypertensive rats. *Hypertension*, **31**(1 Pt 2), 309–314.

[62] Huang, A., Sun, D., and Koller, A., 2000: Shear stress-induced release of prostaglandin h(2) in arterioles of hypertensive rats. *Hypertension*, **35**(4), 925–930.

[63] Hudetz, A. G., 1993: Percolation phenomenon: the effect of capillary network rarefaction. *Microvasc Res*, **45**(1), 1–10. doi:10.1006/mvre.1993.1001.

[64] Hudlickà, O., Zweifach, B. W., and Tyler, K. R., 1982: Capillary recruitment and flow velocity in skeletal muscle after contractions. *Microvasc Res*, **23**(2), 201–213.

[65] Igarashi, J., Thatte, H. S., Prabhakar, P., Golan, D. E., and Michel, T., 1999: Calcium-independent activation of endothelial nitric oxide synthase by ceramide. *Proc Natl Acad Sci U S A*, **96**(22), 12583–12588.

[66] Ignarro, L. J., Byrns, R. E., Buga, G. M., and Wood, K. S., 1987: Endothelium-derived relaxing factor from pulmonary artery and vein possesses pharmacologic and chemical properties identical to those of nitric oxide radical. *Circ Res*, **61**(6), 866–879.

[67] Intaglietta, M., 1991: Arteriolar vasomotion: implications for tissue ischemia. *Blood Vessels*, **28 Suppl 1**, 1–7.

[68] Intaglietta, M., Tompkins, W. R., and Richardson, D. R., 1970: Velocity measurements in the microvasculature of the cat omentum by on-line method. *Microvasc Res*, **2**(4), 462–473.

[69] Jesmin, S., Sakuma, I., Togashi, H., Yamaguchi, T., Ueno, K.-I., Yoshioka, M., Hattori, Y., Kitabatake, A., and Miyauchi, T., 2004: Altered expression of endothelin and its receptors in the brain of shr-sp at malignant hypertensive stage. *J Cardiovasc Pharmacol*, **44**, S11–S15.

[70] Johnson, P. C., Burton, K. S., Henrich, H., and Henrich, U., 1976: Effect of occlusion duration on reactive hyperemia in sartorius muscle capillaries. *Am J Physiol*, **230**(3), 715–719.

[71] Kashiwagi, S., Kajimura, M., Yoshimura, Y., and Suematsu, M., 2002: Nonendothelial source of nitric oxide in arterioles but not in venules: alternative source revealed in vivo by diaminofluorescein microfluorography. *Circ Res*, **91**(12), e55–e64.

[72] Katona, E., Settakis, G., Varga, Z., Paragh, G., Bereczki, D., Fülesdi, B., and Páll, D., 2006: Target-organ damage in adolescent hypertension. analysis of potential influencing factors, especially nitric oxide and endothelin-1. *J Neurol Sci*, **247**(2), 138–143. doi:10.1016/j.jns.2006.04.007.

[73] Kiefer, F. N., Misteli, H., Kalak, N., Tschudin, K., Fingerle, J., der Kooij, M. V., Stumm, M., Sumanovski, L. T., Sieber, C. C., and Battegay, E. J., 2002: Inhibition of no biosynthesis, but not elevated blood pressure, reduces angiogenesis in rat models of secondary hypertension. *Blood Press*, **11**(2), 116–124.

[74] Kleinfeld, D., Mitra, P. P., Helmchen, F., and Denk, W., 1998: Fluctuations and stimulus-induced changes in blood flow observed in individual capillaries in layers 2 through 4 of rat neocortex. *Proc Natl Acad Sci U S A*, **95**(26), 15741–15746.

[75] Kobayashi, N., DeLano, F. A., and Schmid-Schönbein, G. W., 2005: Oxidative stress promotes endothelial cell apoptosis and loss of microvessels in the spontaneously hypertensive rats. *Arterioscler Thromb Vasc Biol*, **25**(10), 2114–2121. doi: 10.1161/01.ATV.0000178993.13222.f2.

[76] Kojima, H., Hirotani, M., Nakatsubo, N., Kikuchi, K., Urano, Y., Higuchi, T., Hirata, Y., and Nagano, T., 2001: Bioimaging of nitric oxide with fluorescent indicators based on the rhodamine chromophore. *Anal Chem*, **73**(9), 1967–1973.

[77] Koller, A., and Huang, A., 1994: Impaired nitric oxide-mediated flow-induced dilation in arterioles of spontaneously hypertensive rats. *Circ Res*, **74**(3), 416–421.

[78] Komatsu, S., Panés, J., Russell, J. M., Anderson, D. C., Muzykantov, V. R., Miyasaka, M., and Granger, D. N., 1997: Effects of chronic arterial hypertension on constitutive and induced intercellular adhesion molecule-1 expression in vivo. *Hypertension*, **29**(2), 683–689.

[79] Kosir, M. A., Foley-Loudon, P. A., Finkenauer, R., and Tennenberg, S. D., 2002: Multiple heparanases are expressed in polymorphonuclear cells. *J Surg Res*, **103**(1), 100–108. doi:10.1006/jsre.2001.6337.

[80] Krogh, A., 1919: The supply of oxygen to the tissues and the regulation of the capillary circulation. *J Physiol*, **52**(6), 457–474.

[81] Lee, J., and Schmid-Schönbein, G. W., 1995: Biomechanics of skeletal muscle capillaries: hemodynamic resistance, endothelial distensibility, and pseudopod formation. *Ann Biomed Eng*, **23**(3), 226–246.

[82] Lee, S. Y., and Schmid-Schönbein, G. W., 1990: Pulsatile pressure and flow in the skeletal muscle microcirculation. *J Biomech Eng*, **112**(4), 437–443.

[83] Lee, T. Q., Schmid-Schönbein, G. W., and Zweifach, B. W., 1983: The application of an improved dual-slit photometric analyzer for volumetric flow rate measurements in microvessels. *Microvasc Res*, **26**(3), 351–361.

[84] Levesque, M. J., and Nerem, R. M., 1985: The elongation and orientation of cultured endothelial cells in response to shear stress. *J Biomech Eng*, **107**(4), 341–347.

[85] Lindén, M., Sirsjö, A., Lindbom, L., Nilsson, G., and Gidlöf, A., 1995: Laser-doppler perfusion imaging of microvascular blood flow in rabbit tenuissimus muscle. *Am J Physiol*, **269**(4 Pt 2), H1496–H1500.

[86] Lipowsky, H. H., Usami, S., and Chien, S., 1980: In vivo measurements of "apparent viscosity" and microvessel hematocrit in the mesentery of the cat. *Microvasc Res*, **19**(3), 297–319.

[87] Lipowsky, H. H., Usami, S., Chien, S., and Pittman, R. N., 1980: Hematocrit determination in small bowel bore tubes from optical density measurements under white light illumination. *Microvasc Res*, **20**(1), 51–70.

[88] Looft-Wilson, R. C., Payne, G. W., and Segal, S. S., 2004: Connexin expression and conducted vasodilation along arteriolar endothelium in mouse skeletal muscle. *J Appl Physiol*, **97**(3), 1152–1158. doi:10.1152/japplphysiol.00133.2004.

[89] Makoveichuk, E., Lookene, A., and Olivecrona, G., 1998: Mild oxidation of lipoproteins increases their affinity for surfaces covered by heparan sulfate and lipoprotein lipase. *Biochem Biophys Res Commun*, **252**(3), 703–710. doi:10.1006/bbrc.1998.9596.

[90] Mazzetti, S., Librizzi, L., Frigerio, S., de Curtis, M., and Vitellaro-Zuccarello, L., 2004: Molecular anatomy of the cerebral microvessels in the isolated guinea-pig brain. *Brain Res*, **999**(1), 81–90.

[91] Mazzoni, M. C., Warnke, K. C., Arfors, K. E., and Skalak, T. C., 1994: Capillary hemodynamics in hemorrhagic shock and reperfusion: in vivo and model analysis. *Am J Physiol Heart Circ Physiol*, **267**(5), H1928–1935.

[92] Mitchell, D. J., Yu, J., and Tyml, K., 1998: Local l-name decreases blood flow and increases leukocyte adhesion via cd18. *Am J Physiol*, **274**(4 Pt 2), H1264–H1268.

[93] Mochizuki, S., Vink, H., Hiramatsu, O., Kajita, T., Shigeto, F., Spaan, J. A. E., and Kajiya, F., 2003: Role of hyaluronic acid glycosaminoglycans in shear-induced endothelium-derived nitric oxide release. *Am J Physiol Heart Circ Physiol*, **285**(2), H722–H726. doi:10.1152/ajpheart.00691.2002.

[94] Moon, J. J., Matsumoto, M., Patel, S., Lee, L., Guan, J.-L., and Li, S., 2005: Role of cell surface heparan sulfate proteoglycans in endothelial cell migration and mechanotransduction. *J Cell Physiol*, **203**(1), 166–176. doi:10.1002/jcp.20220.

[95] Mulivor, A. W., and Lipowsky, H. H., 2002: Role of glycocalyx in leukocyte-endothelial cell adhesion. *Am J Physiol Heart Circ Physiol*, **283**(4), H1282–H1291. doi:10.1152/ajpheart.00117.2002.

[96] Mulivor, A. W., and Lipowsky, H. H., 2004: Inflammation- and ischemia-induced shedding of venular glycocalyx. *Am J Physiol Heart Circ Physiol*, **286**(5), H1672–H1680. doi:10.1152/ajpheart.00832.2003.

[97] Murfee, W. L., Skalak, T. C., and Peirce, S. M., 2005: Differential arterial/venous expression of ng2 proteoglycan in perivascular cells along microvessels: identifying a venule-specific phenotype. *Microcirculation*, **12**(2), 151–160. doi:10.1080/10739680590904955.

[98] Murray, C. D., 1926: The physiological principle of minimum work: I. the vascular system and the cost of blood volume. *Proc Natl Acad Sci U S A*, **12**(3), 207–214.

[99] Noria, S., Xu, F., McCue, S., Jones, M., Gotlieb, A. I., and Langille, B. L., 2004: Assembly and reorientation of stress fibers drives morphological changes to endothelial cells exposed to shear stress. *Am J Pathol*, **164**(4), 1211–1223.

[100] Osawa, M., Masuda, M., ichi Kusano, K., and Fujiwara, K., 2002: Evidence for a role of platelet endothelial cell adhesion molecule-1 in endothelial cell mechanosignal transduction: is it a mechanoresponsive molecule? *J Cell Biol*, **158**(4), 773–785. doi:10.1083/jcb.200205049.

[101] O'Tierney, P. F., Angelis, E., Tse, M. Y., Pang, J. J., Adams, M. A., and Pang, S. C., 2005: A potential role for the endothelin eta receptor in salt-sensitive hypertension of the proanp gene-disrupted mouse. *Mol Cell Biochem*, **275**(1-2), 57–66.

[102] Palmer, R. M., Ferrige, A. G., and Moncada, S., 1987: Nitric oxide release accounts for the biological activity of endothelium-derived relaxing factor. *Nature*, **327**(6122), 524–526. doi:10.1038/327524a0.

[103] Peng, H., Matchkov, V., Ivarsen, A., Aalkjaer, C., and Nilsson, H., 2001: Hypothesis for the initiation of vasomotion. *Circ Res*, **88**(8), 810–815.

[104] Perachio, A. A., and Correia, M. J., 1983: Design for a slender shaft glass micropipette. *J Neurosci Methods*, **9**(4), 287–293.

[105] Pittman, R. N., and Ellsworth, M. L., 1986: Estimation of red cell flow microvessels: consequences of the baker-wayland spatial averaging model. *Microvasc Res*, **32**(3), 371–388.

[106] Platts, S. H., and Duling, B. R., 2004: Adenosine a3 receptor activation modulates the capillary endothelial glycocalyx. *Circ Res*, **94**(1), 77–82. doi:10.1161/01.RES.0000108262.35847.60.

[107] Poole, D. C., Musch, T. I., and Kindig, C. A., 1997: In vivo microvascular structural and functional consequences of muscle length changes. *Am J Physiol*, **272**(5 Pt 2), H2107–H2114.

[108] Pries, A. R., Neuhaus, D., and Gaehtgens, P., 1992: Blood viscosity in tube flow: dependence on diameter and hematocrit. *Am J Physiol*, **263**(6 Pt 2), H1770–H1778.

[109] Pries, A. R., Reglin, B., and Secomb, T. W., 2001: Structural adaptation of vascular networks: role of the pressure response. *Hypertension*, **38**(6), 1476–1479.

[110] Pries, A. R., and Secomb, T. W., 2002: Structural adaptation of microvascular networks and development of hypertension. *Microcirculation*, **9**(4), 305–314. doi:10.1038/sj.mn.7800144.

[111] Pries, A. R., Secomb, T. W., and Gaehtgens, P., 1995: Design principles of vascular beds. *Circ Res*, **77**(5), 1017–1023.

[112] Pries, A. R., Secomb, T. W., and Gaehtgens, P., 1998: Structural adaptation and stability of microvascular networks: theory and simulations. *Am J Physiol*, **275**(2 Pt 2), H349–H360.

[113] Pries, A. R., Secomb, T. W., Gaehtgens, P., and Gross, J. F., 1990: Blood flow in microvascular networks. experiments and simulation. *Circ Res*, **67**(4), 826–834.

[114] Pries, A. R., Secomb, T. W., Jacobs, H., Sperandio, M., Osterloh, K., and Gaehtgens, P., 1997: Microvascular blood flow resistance: role of endothelial surface layer. *Am J Physiol*, **273**(5 Pt 2), H2272–H2279.

[115] Radel, C., and Rizzo, V., 2005: Integrin mechanotransduction stimulates caveolin-1 phosphorylation and recruitment of Csk to mediate actin reorganization. *Am J Physiol Heart Circ Physiol*, **288**(2), H936–H945. doi:10.1152/ajpheart.00519.2004.

[116] Ragan, D. M., Schmidt, E. E., MacDonald, I. C., and Groom, A. C., 1988: Spontaneous cyclic contractions of the capillary wall in vivo, impeding red cell flow: a quantitative analysis. evidence for endothelial contractility. *Microvasc Res*, **36**(1), 13–30.

[117] Reitsma, S., Slaaf, D., Vink, H., van Zandvoort, M., and Egbrink, M. O., 2007: The endothelial glycocalyx: composition, functions, and visualization. *Pflugers Arch*. doi:10.1007/s00424-007-0212-8.

[118] Ribeiro, M. O., Antunes, E., de Nucci, G., Lovisolo, S. M., and Zatz, R., 1992: Chronic inhibition of nitric oxide synthesis. a new model of arterial hypertension. *Hypertension*, **20**(3), 298–303.

[119] Richardson, D. R., Intaglietta, M., and Zweifach, B. W., 1971: Simultaneous pressure and flow velocity measurements in the microcirculation. *Microvasc Res*, **3**(1), 69–71.

[120] Rizzo, V., Morton, C., DePaola, N., Schnitzer, J. E., and Davies, P. F., 2003: Recruitment of endothelial caveolae into mechanotransduction pathways by flow conditioning in vitro. *Am J Physiol Heart Circ Physiol*, **285**(4), H1720–H1729. doi: 10.1152/ajpheart.00344.2002.

[121] Rozenberg, G. I., Espada, J., de Cidre, L. L., Eijn, A. M., Calvo, J. C., and Bertolesi, G. E., 2001: Heparan sulfate, heparin, and heparinase activity detection on polyacrylamide gel electrophoresis using the fluorochrome tris(2,2'-bipyridine) ruthenium (ii). *Electrophoresis*, **22**(1), 3–11. doi:3.0.CO;2-G.

[122] Rubio-Gayosso, I., Barajas-Espinosa, A., Castillo-Hernandez, J., Ramiro-Diaz, J., Ceballos, G., and Rubio, R., 2005: Enzymatic hydrolysis of luminal coronary glycosidic structures uncovers their role in sensing coronary flow. *Front Biosci*, **10**, 1050–1059.

[123] Sakai, H., Hara, H., Tsai, A. G., Tsuchida, E., and Intaglietta, M., 2000: Constriction of resistance arteries determines l-name-induced hypertension in a conscious hamster model. *Microvasc Res*, **60**(1), 21–27. doi:10.1006/mvre.2000.2240.

[124] Sarelius, I. H., 1986: Cell flow path influences transit time through striated muscle capillaries. *Am J Physiol*, **250**(6 Pt 2), H899–H907.

[125] Schmid-Schönbein, G. W., 1999: Biomechanics of microcirculatory blood perfusion. *Annu Rev Biomed Eng*, **1**, 73–102. doi:10.1146/annurev.bioeng.1.1.73.

[126] Schmid-Schönbein, G. W., Skalak, T. C., and Sutton, D. W., 1989: *Microvascular Mechanics*, chapter Bioengineering Analysis of Blood Flow in Resting Skeletal Muscle, 65–99. Springer-Verlag, New York.

[127] Schubert, W., Frank, P. G., Woodman, S. E., Hyogo, H., Cohen, D. E., Chow, C.-W., and Lisanti, M. P., 2002: Microvascular hyperpermeability in caveolin-1 (-/-) knockout mice. treatment with a specific nitric-oxide synthase inhibitor, l-name, restores normal microvascular permeability in cav-1 null mice. *J Biol Chem*, **277**(42), 40091–40098. doi:10.1074/jbc.M205948200.

[128] Searles, C. D., Ide, L., Davis, M. E., Cai, H., and Weber, M., 2004: Actin cytoskeleton organization and posttranscriptional regulation of endothelial nitric oxide synthase during cell growth. *Circ Res*, **95**(5), 488–495. doi:10.1161/01.RES.0000138953.21377.80.

[129] Segal, S. S., and Duling, B. R., 1989: Conduction of vasomotor responses in arterioles: a role for cell-to-cell coupling? *Am J Physiol*, **256**(3 Pt 2), H838–H845.

[130] Sejersted, O. M., Hargens, A. R., Kardel, K. R., Blom, P., Jensen, O., and Hermansen, L., 1984: Intramuscular fluid pressure during isometric contraction of human skeletal muscle. *J Appl Physiol*, **56**(2), 287–295.

[131] Shaul, P. W., Smart, E. J., Robinson, L. J., German, Z., Yuhanna, I. S., Ying, Y., Anderson, R. G., and Michel, T., 1996: Acylation targets emdothelial nitric-oxide synthase to plasmalemmal caveolae. *J Biol Chem*, **271**(11), 6518–6522.

[132] Skalak, T. C., 1984: *A mathematical hemodynamic network model of the microcirculation in skeletal muscle, using measured blood vessel distensibility and topology.* Ph.D. thesis, University of California, San Diego.

[133] Skalak, T. C., and Schmid-Schönbein, G. W., 1986: The microvasculature in skeletal muscle. iv. a model of the capillary network. *Microvasc Res*, **32**(3), 333–347.

[134] Smith, M. L., Long, D. S., Damiano, E. R., and Ley, K., 2003: Near-wall micro-piv reveals a hydrodynamically relevant endothelial surface layer in venules in vivo. *Biophys J*, **85**(1), 637–645.

[135] Song, H., and Tyml, K., 1993: Evidence for sensing and integration of biological signals by the capillary network. *Am J Physiol*, **265**(4 Pt 2), H1235–H1242.

[136] Sowa, G., Liu, J., Papapetropoulos, A., Rex-Haffner, M., Hughes, T. E., and Sessa, W. C., 1999: Trafficking of endothelial nitric-oxide synthase in living cells. quantitative evidence supporting the role of palmitoylation as a kinetic trapping mechanism limiting membrane diffusion. *J Biol Chem*, **274**(32), 22524–22531.

[137] Stan, R.-V., 2002: Structure and function of endothelial caveolae. *Microsc Res Tech*, **57**(5), 350–364. doi:10.1002/jemt.10089.

[138] Suematsu, M., Suzuki, H., Delano, F. A., and Schmid-Schnbein, G. W., 2002: The inflammatory aspect of the microcirculation in hypertension: oxidative stress, leukocytes/endothelial interaction, apoptosis. *Microcirculation*, **9**(4), 259–276. doi: 10.1038/sj.mn.7800141.

[139] Suematsu, M., Suzuki, H., Tamatani, T., Iigou, Y., DeLano, F. A., Miyasaka, M., Forrest, M. J., Kannagi, R., Zweifach, B. W., and Ishimura, Y., 1995: Impairment of selectin-mediated leukocyte adhesion to venular endothelium in spontaneously hypertensive rats. *J Clin Invest*, **96**(4), 2009–2016.

[140] Suematsu, M., Tamatani, T., DeLano, F. A., Miyasaka, M., Forrest, M., Suzuki, H., and Schmid-Schönbein, G. W., 1994: Microvascular oxidative stress preceding leukocyte activation elicited by in vivo nitric oxide suppression. *Am J Physiol*, **266**(6 Pt 2), H2410–H2415.

[141] Sun, C., and Munn, L. L., 2005: Particulate nature of blood determines macroscopic rheology: a 2-d lattice boltzmann analysis. *Biophys J*, **88**(3), 1635–1645. doi:10.1529/biophysj.104.051151.

[142] Sutton, D. W., and Schmid-Schönbein, G. W., 1991: The pressure-flow relation for plasma in whole organ skeletal muscle and its experimental verification. *J Biomech Eng*, **113**(4), 452–457.

[143] Sutton, D. W., and Schmid-Schönbein, G. W., 1992: Elevation of organ resistance due to leukocyte perfusion. *Am J Physiol*, **262**(6 Pt 2), H1646–H1650.

[144] Sutton, D. W., and Schmid-Schönbein, G. W., 1995: The pressure-flow relation in resting rat skeletal muscle perfused with pure erythrocyte suspensions. *Biorheology*, **32**(1), 29–42.

[145] Suzuki, H., DeLano, F. A., Parks, D. A., Jamshidi, N., Granger, D. N., Ishii, H., Suematsu, M., Zweifach, B. W., and Schmid-Schönbein, G. W., 1998: Xanthine oxidase activity associated with arterial blood pressure in spontaneously hypertensive rats. *Proc Natl Acad Sci U S A*, **95**(8), 4754–4759.

[146] Sweeney, T. E., and Sarelius, I. H., 1989: Arteriolar control of capillary cell flow in striated muscle. *Circ Res*, **64**(1), 112–120.

[147] Sylvest, O., and Hvid, N., 1959: Pressure measurements in human striated muscles during contraction. *Acta Rheumatol Scand*, **5**, 216–222.

[148] Tarbell, J. M., Weinbaum, S., and Kamm, R. D., 2005: Cellular fluid mechanics and mechanotransduction. *Ann Biomed Eng*, **33**(12), 1719–1723. doi:10.1007/s10439-005-8775-z.

[149] Thi, M. M., Tarbell, J. M., Weinbaum, S., and Spray, D. C., 2004: The role of the glycocalyx in reorganization of the actin cytoskeleton under fluid shear stress: a "bumper-car" model. *Proc Natl Acad Sci U S A*, **101**(47), 16483–16488. doi:10.1073/pnas.0407474101.

[150] Tkachenko, E., Rhodes, J. M., and Simons, M., 2005: Syndecans: new kids on the signaling block. *Circ Res*, **96**(5), 488–500. doi:10.1161/01.RES.0000159708.71142.c8.

[151] Tsai, A. G., and Intaglietta, M., 1993: Evidence of flowmotion induced changes in local tissue oxygenation. *Int J Microcirc Clin Exp*, **12**(1), 75–88.

[152] Tsoukias, N. M., Kavdia, M., and Popel, A. S., 2004: A theoretical model of nitric oxide transport in arterioles: frequency- vs. amplitude-dependent control of cgmp formation. *Am J Physiol Heart Circ Physiol*, **286**(3), H1043–H1056. doi:10.1152/ajpheart.00525.2003.

[153] Tyml, K., 1986: Capillary recruitment and heterogeneity of microvascular flow in skeletal muscle before and after contraction. *Microvasc Res*, **32**(1), 84–98.

[154] Tyml, K., 1991: Heterogeneity of microvascular flow in rat skeletal muscle is reduced by contraction and by hemodilution. *Int J Microcirc Clin Exp*, **10**(1), 75–86.

[155] Tyml, K., and Cheng, L., 1995: Heterogeneity of red blood cell velocity in skeletal muscle decreases with increased flow. *Microcirculation*, **2**(2), 181–193.

[156] Tyml, K., and Ellis, C. G., 1982: Evaluation of the flying spot technique as a television method for measuring red cell velocity in microvessels. *Int J Microcirc Clin Exp*, **1**(2), 145–155.

[157] Tyml, K., Ellis, C. G., Safranyos, R. G., Fraser, S., and Groom, A. C., 1981: Temporal and spatial distributions of red cell velocity in capillaries of resting skeletal muscle, including estimates of red cell transit times. *Microvasc Res*, **22**(1), 14–31.

[158] Tyml, K., and Groom, A. C., 1980: Fourier transform analysis of periodic variations of red cell velocity in capillaries of resting skeletal muscle in frogs. *Microvasc Res*, **20**(1), 9–18.

[159] Tyml, K., and Groom, A. C., 1980: Regulation of blood flow in individual capillaries of resting skeletal muscle in frogs. *Microvasc Res*, **20**(3), 346–357.

[160] Tyml, K., Mathieu-Costello, O., and Budreau, C. H., 1992: Distribution of red blood cell velocity in capillary network, and endothelial ultrastructure, in aged rat skeletal muscle. *Microvasc Res*, **44**(1), 1–13.

[161] Tyml, K., Song, H., Munoz, P., and Ouellette, Y., 1997: Evidence for k+ channels involvement in capillary sensing and for bidirectionality in capillary communication. *Microvasc Res*, **53**(3), 245–253. doi:10.1006/mvre.1997.2013.

[162] Tzima, E., Irani-Tehrani, M., Kiosses, W. B., Dejana, E., Schultz, D. A., Engelhardt, B., Cao, G., DeLisser, H., and Schwartz, M. A., 2005: A mechanosensory complex that mediates the endothelial cell response to fluid shear stress. *Nature*, **437**(7057), 426–431. doi:10.1038/nature03952.

[163] Ueno, M., Sakamoto, H., Liao, Y.-J., Onodera, M., Huang, C.-L., Miyanaka, H., and Nakagawa, T., 2004: Blood-brain barrier disruption in the hypothalamus of young adult spontaneously hypertensive rats. *Histochem Cell Biol*, **122**(2), 131–137. doi:10.1007/s00418-004-0684-y.

[164] Ueno, M., Sakamoto, H., Tomimoto, H., Akiguchi, I., Onodera, M., Huang, C.-L., and Kanenishi, K., 2004: Blood-brain barrier is impaired in the hippocampus of young adult spontaneously hypertensive rats. *Acta Neuropathol (Berl)*, **107**(6), 532–538. doi:10.1007/s00401-004-0845-z.

[165] van den Berg, B. M., Vink, H., and Spaan, J. A. E., 2003: The endothelial glycocalyx protects against myocardial edema. *Circ Res*, **92**(6), 592–594. doi:10.1161/01.RES.0000065917.53950.75.

[166] Varki, A., 2006: Nothing in glycobiology makes sense, except in the light of evolution. *Cell*, **126**(5), 841–845. doi:10.1016/j.cell.2006.08.022.

[167] Vigne, P., Lund, L., and Frelin, C., 1994: Cross talk among cyclic amp, cyclic gmp, and ca(2+)-dependent intracellular signalling mechanisms in brain capillary endothelial cells. *J Neurochem*, **62**(6), 2269–2274.

[168] Vink, H., and Duling, B. R., 1996: Identification of distinct luminal domains for macromolecules, erythrocytes, and leukocytes within mammalian capillaries. *Circ Res*, **79**(3), 581–589.

[169] Vink, H., and Duling, B. R., 2000: Capillary endothelial surface layer selectively reduces plasma solute distribution volume. *Am J Physiol Heart Circ Physiol*, **278**(1), H285–H289.

[170] Vlodavsky, I., Eldor, A., Haimovitz-Friedman, A., Matzner, Y., Ishai-Michaeli, R., Lider, O., Naparstek, Y., Cohen, I. R., and Fuks, Z., 1992: Expression of heparanase by platelets and circulating cells of the immune system: possible involvement in diapedesis and extravasation. *Invasion Metastasis*, **12**(2), 112–127.

[171] Vogt, C. J., and Schmid-Schönbein, G. W., 2001: Microvascular endothelial cell death and rarefaction in the glucocorticoid-induced hypertensive rat. *Microcirculation*, **8**(2), 129–139.

[172] von Tell, D., Armulik, A., and Betsholtz, C., 2006: Pericytes and vascular stability. *Exp Cell Res*, **312**(5), 623–629. doi:10.1016/j.yexcr.2005.10.019.

[173] Wang, H., Nawata, J., Kakudo, N., Sugimura, K., Suzuki, J., Sakuma, M., Ikeda, J., and Shirato, K., 2004: The upregulation of icam-1 and p-selectin requires high blood pressure but not circulating renin-angiotensin system in vivo. *J Hypertens*, **22**(7), 1323–1332.

[174] Wayland, H., and Johnson, P. C., 1967: Erythrocyte velocity measurement in microvessels by a correlation method. *Bibl Anat*, **9**, 160–163.

[175] Wolf, S., Arend, O., and Reim, M., 1994: Measurement of retinal hemodynamics with scanning laser ophthalmoscopy: reference values and variation. *Surv Ophthalmol*, **38 Suppl**, S95–100.

[176] Wolf, S., Arend, O., Schulte, K., Ittel, T. H., and Reim, M., 1994: Quantification of retinal capillary density and flow velocity in patients with essential hypertension. *Hypertension*, **23**(4), 464–467.

[177] Wolf, S., Arend, O., Toonen, H., Bertram, B., Jung, F., and Reim, M., 1991: Retinal capillary blood flow measurement with a scanning laser ophthalmoscope. preliminary results. *Ophthalmology*, **98**(6), 996–1000.

[178] Xu, J., Nagata, K., Obata, K., Ichihara, S., Izawa, H., Noda, A., Nagasaka, T., Iwase, M., Naoe, T., Murohara, T., and Yokota, M., 2005: Nicorandil promotes myocardial capillary and arteriolar growth in the failing heart of dahl salt-sensitive hypertensive rats. *Hypertension*, **46**(4), 719–724. doi:10.1161/01.HYP.0000185189.46698.15.

[179] Xu, Z., Park, S.-S., Mueller, R. A., Bagnell, R. C., Patterson, C., and Boysen, P. G., 2005: Adenosine produces nitric oxide and prevents mitochondrial oxidant damage in rat cardiomyocytes. *Cardiovasc Res*, **65**(4), 803–812. doi:10.1016/j.cardiores.2004.12.004.

[180] Yeh, D. C., Duncan, J. A., Yamashita, S., and Michel, T., 1999: Depalmitoylation of endothelial nitric-oxide synthase by acyl-protein thioesterase 1 is potentiated by ca(2+)-calmodulin. *J Biol Chem*, **274**(46), 33148–33154.

[181] Yen, R. T., and Fung, Y. C., 1977: Inversion of fahraeus effect and effect of mainstream flow on capillary hematocrit. *J Appl Physiol*, **42**(4), 578–586.

[182] Yen, R. T., and Fung, Y. C., 1978: Effect of velocity of distribution on red cell distribution in capillary blood vessels. *J R Coll Gen Pract Occas Pap*, **235**(2), H251–H257.

[183] Zarda, P. R., Chien, S., and Skalak, R., 1977: Elastic deformations of red blood cells. *J Biomech*, **10**(4), 211–221.

[184] Zhao, Y.-Y., Liu, Y., Stan, R.-V., Fan, L., Gu, Y., Dalton, N., Chu, P.-H., Peterson, K., Ross, J., and Chien, K. R., 2002: Defects in caveolin-1 cause dilated cardiomyopathy and pulmonary hypertension in knockout mice. *Proc Natl Acad Sci U S A*, **99**(17), 11375–11380. doi:10.1073/pnas.172360799.

[185] Zharov, V. P., Galanzha, E. I., Menyaev, Y., and Tuchin, V. V., 2006: In vivo high-speed imaging of individual cells in fast blood flow. *J Biomed Opt*, **11**(5), 054034. doi:10.1117/1.2355666.

[186] Zuurbier, C. J., Demirci, C., Koeman, A., Vink, H., and Ince, C., 2005: Short-term hyperglycemia increases endothelial glycocalyx permeability and acutely decreases lineal density of capillaries with flowing red blood cells. *J Appl Physiol*, **99**(4), 1471–1476. doi:10.1152/japplphysiol.00436.2005.

[187] Zweifach, B. W., 1954: Direct observation of the mesenteric circulation in experimental animals. *Anat Rec*, **120**(1), 277–291.

[188] Zweifach, B. W., and Lipowsky, H. H., 1977: Quantitative studies of microcirculatory structure and function. iii. microvascular hemodynamics of cat mesentery and rabbit omentum. *Circ Res*, **41**(3), 380–390.